

Giant response to weak pumping in quantum systems with approximate symmetries

INAUGURAL-DISSERTATION
ZUR
ERLANGUNG DES DOKTORGRADES
DER MATHEMATISCH-NATURWISSENSCHAFTLICHEN FAKULTÄT
DER UNIVERSITÄT ZU KÖLN

vorgelegt von

FLORIAN LANGE

aus

KÖLN



Köln, 2020

Berichterstatter: Prof. Dr. Achim Rosch
Prof. Dr. Sebastian Diehl
Prof. Dr. Andreas Klümper

Tag der mündlichen Prüfung: 10. Januar 2020

Contents

| | | |
|----------|--|-----------|
| 1 | Introduction | 5 |
| 1.1 | Methods | 5 |
| 1.1.1 | Density matrix formalism | 5 |
| 1.1.2 | Linear response theory | 7 |
| 1.1.3 | Bogoliubov transformation | 10 |
| 1.2 | Closed quantum systems | 12 |
| 1.2.1 | Integrability | 13 |
| 1.2.2 | The XXZ model | 15 |
| 1.2.3 | Thermalization | 17 |
| 1.2.4 | Thermalization in quantum systems | 19 |
| 1.2.5 | Generalized thermalization in quantum systems | 21 |
| 1.3 | Open quantum system | 24 |
| 1.3.1 | Markovian master equation | 26 |
| 1.3.2 | Floquet theory | 28 |
| 1.4 | Phase transitions | 30 |
| 1.4.1 | Equilibrium phase transitions | 30 |
| 1.4.2 | Non-equilibrium phase transitions | 33 |
| 1.5 | Numerical methods | 34 |
| 1.5.1 | Exact diagonalization | 34 |
| 1.5.2 | Numerical integration of stochastic differential equations | 37 |
| 2 | Perturbative approach to weakly driven many-particle systems | 39 |
| 2.1 | The model | 39 |
| 2.2 | Zeroth order: Generalized Gibbs ensemble | 41 |
| 2.2.1 | Periodic driving | 43 |
| 2.2.2 | Projection operators and effective forces | 43 |
| 2.3 | Perturbation theory | 45 |
| 2.3.1 | Markovian perturbation | 45 |
| 2.3.2 | Missing conservation laws | 48 |
| 2.3.3 | Unitary perturbation | 51 |

| | | |
|----------|---|------------|
| 2.4 | Applications | 53 |
| 2.4.1 | Open Boltzmann equation | 53 |
| 2.4.2 | Lindblad dynamics of fermions | 59 |
| 3 | Time-dependent generalized Gibbs ensembles | 61 |
| 3.1 | Numerical verification of the GGE in the steady state | 62 |
| 3.2 | Time evolution of weakly open quantum systems | 64 |
| 3.2.1 | Time-dependent GGE | 64 |
| 3.2.2 | Time-dependent block-diagonal density matrix | 65 |
| 3.3 | Lindblad dynamics I | 66 |
| 3.4 | Lindblad dynamic II: High temperature expansion | 73 |
| 4 | Pumping approximately integrable systems | 79 |
| 4.1 | The model | 80 |
| 4.2 | Steady state | 83 |
| 4.2.1 | Truncated GGE | 84 |
| 4.2.2 | Block-diagonal ansatz | 87 |
| 4.3 | Results | 88 |
| 4.4 | Further experimental setups | 93 |
| 4.4.1 | Detection of GGEs in solids | 93 |
| 4.4.2 | Detection of GGEs in trapped ion systems | 95 |
| 5 | Generalized hydrodynamics and phase transitions in open quantum systems | 101 |
| 5.1 | Space-dependent Lagrange parameters | 103 |
| 5.1.1 | Homogeneous expansion point | 104 |
| 5.1.2 | Gradient expansion | 105 |
| 5.2 | Transitions in weakly open spin chains | 107 |
| 5.2.1 | Symmetric potential | 107 |
| 5.2.2 | Asymmetric potential | 110 |
| 6 | Stability of long range order in a driven $O(3)$ Heisenberg chain | 113 |
| 6.1 | Introduction | 113 |
| 6.1.1 | Motivation | 113 |
| 6.1.2 | Mermin-Wagner theorem | 114 |
| 6.1.3 | Spin wave theory in equilibrium | 115 |
| 6.1.4 | Flocking | 118 |
| 6.2 | Spin current and long range order | 119 |
| 6.2.1 | The model | 119 |
| 6.2.2 | Floquet spin wave theory | 121 |
| 6.2.3 | Floquet-Boltzmann equation | 123 |

| | | |
|----------|--|------------|
| 6.2.4 | Classical simulation | 129 |
| 6.3 | Field theoretical approach and stability analysis | 136 |
| 6.3.1 | Haldane mapping | 136 |
| 6.3.2 | Stability analysis | 138 |
| 7 | Conclusion and Outlook | 143 |
| | Bibliography | 145 |
| | Appendix A Zeroth order expansion point | 153 |
| | Appendix B Thermal state of the weakly open spin chain in the Ising limit | 155 |
| | Appendix C Phase transitions in weakly open spin chains | 157 |
| | Appendix D Equations of motion of the two continuum fields m and ϕ | 161 |
| | Appendix E Dedication and Declaration | 163 |
| E.1 | Dedication | 163 |
| E.2 | Declaration | 164 |
| E.3 | Teilpublikationen | 164 |

Zusammenfassung

Unsere Umgebung und die Natur als Ganzes betrachtet sind grundsätzlich nicht im Gleichgewicht. Die Existenz von Leben auf der Erde ist nur aus diesem Grund möglich. Alltägliche Beispiele für Nichtgleichgewichtsprozesse sind verschiedene Wetterphänomene, die durch Luft- und Wärmeströme angetrieben werden, Staus auf Autobahnen oder das Schwarmverhalten von Tieren in Gruppen. Diese stehen exemplarisch für viele weitere Phänomene und motivieren, ein besseres Verständnis von Nichtgleichgewichtsprozessen - seien sie klassischer oder quantenmechanischer Natur - zu entwickeln.

Im Nichtgleichgewicht sind die bekannten Konzepte für Gleichgewichtssysteme im Allgemeinen nicht oder nur approximativ anwendbar. Zu diesen Konzepten zählt, dass sich alle makroskopischen Ströme im Mittel zu Null addieren und der Gleichgewichtszustand eines Systems nur durch das fundamentale Prinzip der Entropiemaximierung und die vorliegenden Symmetrien bestimmt ist. Nach dem Noether Theorem, einer der grundlegendsten Beziehungen der Physik, ist jede kontinuierliche Symmetrie mit einer zugehörigen Erhaltungsgröße verbunden.

In dieser Arbeit betrachten wir Vielteilchen-Quantensysteme mit Erhaltungsgrößen, von denen ein Teil durch eine schwache äußere Störung verletzt wird. Wir zeigen, dass unter diesen Umständen hochgradige Nichtgleichgewichtszustände erreicht werden können, die sich durch große Ströme auszeichnen. Das Phänomen, dass eine kleine Störung einen sehr großen Effekt haben kann, falls diese Erhaltungsgrößen schwach verletzt, lässt sich zum Beispiel anhand eines Treibhauses veranschaulichen. Im Inneren des Treibhauses ist aufgrund der guten Isolierung die Energie näherungsweise erhalten. Als Konsequenz kann das Innere sogar nur durch schwache Sonnenlichteinstrahlung auf sehr hohe Temperaturen erwärmt werden.

Die Arbeit gliedert sich wie folgt: Im ersten Kapitel führen wir analytische und numerische Methoden sowie grundlegende Konzepte ein, die in der Arbeit verwendet werden oder zum Verständnis der weiteren Ausführungen beitragen.

Im zweiten Kapitel entwickeln wir eine Störungstheorie für den stationären Zustand eines schwach getriebenen Systems mit näherungsweise erhaltenen Erhaltungsgrößen. Dabei verwenden wir als Entwicklungspunkt ein verallgemeinertes Gibbs Ensemble (GGE), das alle approximativen Erhaltungsgrößen des Modells beinhaltet. Definiert ist das GGE im stationären Zustand nur durch die Form der schwachen äußeren Störung, beziehungsweise durch das Gleichgewicht von verallgemeinerten Heiz- und Kühlprozessen. Wir verifizieren die Gültigkeit der Störungstheorie für zwei schwach gestörte fermionische Modelle, in denen jeweils die Teilchenzahl und die Energie approximativ erhalten sind.

Im dritten Kapitel wenden wir unsere Theorie systematisch auf schwach getriebene integrable Systeme an, die eine makroskopische Anzahl von Erhaltungsgrößen besitzen, wobei wir die Analyse auf die nullte Ordnung der Störungstheorie beschränken. Wir zeigen, dass das Konzept von GGEs, gegen frühere Annahmen, auch in Anwesenheit von schwachen integrabilitätsverletzenden Störungen anwendbar ist, falls zusätzlich "in Freiheitsgrade gepumpt wird", die durch approximative Symmetrien näherungsweise geschützt sind. Weiterhin zeigen wir numerisch, dass auch die Zeitentwicklung von schwach gestörten integrablen Systemen durch ein zeitabhängiges GGE beschrieben werden kann.

Im vierten Kapitel schlagen wir verschiedene Methoden vor, wie unsere Theorie experimentell belegt werden könnte. Insbesondere formulieren wir einen Vorschlag für effiziente Spin- und Wärmepumpen. Im fünften Kapitel führen wir das Konzept eines GGEs mit ortsabhängigen Lagrange-Multiplikatoren ein, mit dem sich räumlich inhomogene Zustände beschreiben lassen können. Ferner stellen wir zwei konkrete Beispiele vor, wie solche Inhomogenitäten durch eine homogene Kopplung an ein Bad erzeugt werden können. Diese Formulierung erlaubt es, Phasenübergänge und spontane Symmetriebrechungen zu untersuchen.

Im letzten eigenständigen Kapitel betrachten wir ein periodisch gestörtes $O(3)$ -symmetrisches Heisenberg Modell in einer Dimension, wobei die Störung derart konstruiert ist, dass sie einerseits die Rotationssymmetrie des Modells nicht bricht, aber andererseits in Anwesenheit eines antiferromagnetischen Ordnungsparameters einen endlichen Spinstrom induziert. Wir untersuchen, inwieweit in einem solchen Modell ein Zustand mit langreichweitiger Ordnung stabil ist und es zur spontanen Symmetriebrechung kommen kann.

Summary

Our environment and nature as a whole are fundamentally not in equilibrium. The existence of life on earth is only possible for this reason. Everyday examples of non-equilibrium processes are various weather phenomena driven by air and heat flows, traffic jams on motorways or the swarm behavior of animals in groups. These are just a few examples of many more phenomena and motivate a better understanding of non-equilibrium processes in classical as well as quantum systems.

Non-equilibrium means that the known concepts, which are valid in equilibrium, are generally not or only approximately applicable. In equilibrium, all macroscopic currents add on average up to zero and the configuration of a system is solely determined by the fundamental principle of entropy maximization and the symmetries present in the system. According to the Noether theorem, which represents one of the most fundamental relations in physics, each continuous symmetry is associated with a conservation law.

In this thesis, we consider quantum systems that have a set of conservation laws of which some are weakly violated by an external perturbation. We show that under these circumstances highly non-equilibrium states can be reached which are characterized by large currents. The phenomenon that a small perturbation can have a very large effect if it breaks a conservation law can, for example, be illustrated with a greenhouse. Inside the greenhouse the energy is approximately conserved due to the good insulation. As a consequence, the interior can be heated up to very high temperatures by even weak sunlight.

The work is structured as follows: In the first chapter we introduce analytical and numerical methods as well as basic concepts that are used within this thesis.

In the second chapter we develop a perturbation theory for the stationary state of weakly perturbed many-particle systems with approximate conservation laws. As an expansion point, we use a generalized Gibbs ensemble (GGE), which includes all approximately conserved quantities of the system. In the stationary state, the GGE is only defined by the form of the weak external perturbation or equivalently by the balance of generalized heating and cooling processes. We verify the validity of the perturbation theory for two weakly perturbed fermionic models, in which the particle number and the energy are approximately conserved.

In chapter three we apply our theory systematically to weakly driven integrable systems that have an extensive number of conservation laws where we limit our analysis to zeroth order in perturbation theory. We show that the concept of GGEs can, against previous assumptions, also be applied in

the presence of weak integrability breaking perturbations if one 'additionally pumps into degrees of freedom' that are approximately protected by symmetries. Furthermore, we provide numerical evidence that the time evolution of weakly perturbed integrable systems can be described by a time-dependent GGE. In the fourth chapter we present different suggestions of how our theory can be verified experimentally. In particular, we formulate a proposal for efficient spin and heat pumps based on approximate integrability.

In the fifth chapter, we introduce the concept of GGEs with space-dependent Lagrange parameters that can be used to describe spatially inhomogeneous states. Furthermore, we give two concrete examples of how such inhomogeneities can be generated by a homogeneous coupling to a non-thermal bath. This formulation allows investigating phase transitions and spontaneous symmetry breaking.

In the last chapter we consider a periodically driven antiferromagnetic $O(3)$ Heisenberg model in one-dimension, where the perturbation is constructed in such a way that on the one hand, it does not break the rotation symmetry of the model, and on the other hand, induces a finite spin current in the presence of a finite antiferromagnetic order parameter. We investigate to what extent in such a model a state with long range order is stable and spontaneous symmetry breaking can occur.

Chapter 1

Introduction

1.1 Methods

1.1.1 Density matrix formalism

The configuration of a quantum mechanical system is described by an element in a Hilbert space, the so-called quantum state. The time evolution of an abstract state $|\psi(t)\rangle$ is governed by the Schrödinger equation

$$i\partial_t |\psi(t)\rangle = H |\psi(t)\rangle, \quad (1.1)$$

where H is the Hamiltonian of the system considered. Note that we set \hbar and all other appearing physical constants to one throughout this thesis. The formal solution of Eq. (1.1) for a time-independent Hamiltonian is given by $|\psi(t)\rangle = U(t, t_0) |\psi(t_0)\rangle$ where $U(t, t_0) := e^{-iH(t-t_0)}$ denotes the time evolution operator and $|\psi(t_0)\rangle$ the initial state at $t = t_0$. In the case of a time-dependent Hamiltonian, the time evolution operator needs to be replaced by a time-ordered exponential $U(t, t_0) = \hat{\mathcal{T}} \exp(-i \int_{t_0}^t dt' H(t'))$ where $\hat{\mathcal{T}}$ is the time-ordering operator [1].

Of special interest are the expectation values of physical quantities, also called observables, which can, in principle, be measured in experiments. According to quantum mechanics, physical quantities are described by hermitian operators which act on the underlying Hilbert space. The expectation value of an observable O in a state $|\psi(t)\rangle$ is given by $\langle O \rangle = \langle \psi(t) | O | \psi(t) \rangle$. Using the cyclicity property of the trace this formula can be also written as

$$\langle O(t) \rangle = \text{Tr}[O |\psi(t)\rangle \langle \psi(t)|] = \text{Tr}[O \rho(t)]. \quad (1.2)$$

Eq. (1.2) defines the statistical operator, also called density matrix $\rho(t)$, of a pure state $|\psi(t)\rangle$. If a system is in a pure state, its density matrix is simply a projection onto this state. In general, the

density matrix for a statistical mixture of orthonormal states $\{|\psi_i\rangle\}$ reads

$$\rho(t) = \sum_i p_i |\psi_i(t)\rangle \langle \psi_i(t)|, \quad (1.3)$$

where p_i is the probability that the system is in state $|\psi_i(t)\rangle$. The density matrix has the following properties: $\rho = \rho^\dagger$ (hermicity), $\rho \geq 0$ (positivity) and $\text{Tr}[\rho] = 1$ (normalization). Starting from the Schrödinger equation, one can derive an equation of motion for $\rho(t)$,

$$\frac{d}{dt}\rho(t) = \hat{\mathcal{L}}_0\rho(t), \quad \hat{\mathcal{L}}_0\rho(t) := -i[H_0, \rho(t)] \quad (1.4)$$

which is referred to as *Liouville-von-Neumann equation*. The dynamics of $\rho(t)$ is governed by the so-called Liouville superoperator (*Liouvillian*) $\hat{\mathcal{L}}_0$. The name superoperator originates in the fact that $\hat{\mathcal{L}}_0$ does not act on states but on operators. While states live in a Hilbert space of dimension d , the dimension of the space of operators acting on this d -dimensional Hilbert space is d^2 . In the following, we denote superoperators by letters with hats. However, we will drop the prefix super in some situations to increase readability.

In the presence of dissipation which could, for example, arise due to a coupling to an external bath, the Liouvillian can under certain assumptions be extended by an additional non-unitary superoperator (dissipator) $\hat{\mathcal{D}}$, $\hat{\mathcal{L}}_0 \rightarrow \hat{\mathcal{L}} = \hat{\mathcal{L}}_0 + \hat{\mathcal{D}}$ and Eq. (1.4) is then simply referred to as *Liouville equation*. The formal solution of Eq. (1.4) is given by $\rho(t) = e^{\hat{\mathcal{L}}t}\rho(t_0)$ where $\rho(t_0)$ is the initial density matrix at time $t = t_0$. For a time-dependent Liouvillian the time evolution superoperator again has to be replaced by a time-ordered exponential. The eigenvalues of $\hat{\mathcal{L}}$ are in general complex. Their real parts are less than or equal to zero if the described physical system is stable. While the imaginary parts of the eigenvalues originate in the Hamiltonian dynamics, the real parts are due to dissipation and lead to relaxation [2].

The left $\{|\nu_\alpha\rangle\}$ and right $\{|\mu_\alpha\rangle\}$ eigenvectors of $\hat{\mathcal{L}}$ do in general not form an orthogonal set as the Liouville superoperator is not hermitian in the absence of time-reversal symmetry. The time evolution of the density matrix in terms of right eigenvectors reads

$$\rho(t) = \sum_\alpha c_\alpha e^{\lambda_\alpha(t-t_0)} |\mu_\alpha\rangle, \quad \hat{\mathcal{L}}|\mu_\alpha\rangle = \lambda_\alpha|\mu_\alpha\rangle \quad (1.5)$$

and the steady state density matrix ρ_∞ is defined by $\hat{\mathcal{L}}\rho_\infty = 0$. The conservation of probability guarantees the existence of at least one steady state. The relaxation time, which is the time after which the steady state is reached, is determined by the so-called Liouvillian gap, i.e. $\min_\alpha |\text{Re}(\lambda_\alpha)|$.

For our purpose, it is useful to introduce a projection (super)operator \hat{P} onto the right eigenstates of $\hat{\mathcal{L}}$. In the general case of non-orthogonal eigenstates, \hat{P} can be represented as

$$\hat{P} = \sum_{\alpha,\beta} (\chi^{-1})_{\alpha\beta} |\mu_\alpha\rangle \langle \mu_\beta|, \quad \chi_{\alpha\beta} = (\mu_\alpha | \mu_\beta) \quad (1.6)$$

where density matrices are interpreted as vectors and $(\cdot|\cdot)$ denotes the standard scalar product. The adjoint Liouville superoperator $\hat{\mathcal{L}}^\dagger$ can be defined through the relation $\text{Tr}[O\hat{\mathcal{L}}\rho] = \text{Tr}[(\hat{\mathcal{L}}^\dagger O)\rho]$. In quantum mechanics there are different representations, also referred to as different pictures, to describe the time evolution of states, observables and density matrices, respectively. In the Schrödinger picture that is used in Eq. (1.1), states evolve in time while observables are time-independent where we neglect an explicit time-dependence. In contrast to that, in the Heisenberg picture the time evolution is transferred to the operators under the constraint that expectation values do not change. The time evolution of an observable O in a state $|\psi(t)\rangle$ is given by

$$\begin{aligned}\langle\psi(t)|O|\psi(t)\rangle &= \langle\psi(0)e^{iHt}|O|e^{-iHt}\psi(0)\rangle = \langle\psi(0)|e^{iHt}Oe^{-iH_0t}|\psi(0)\rangle \\ &= \langle\psi(0)|O^{(H)}(t)|\psi(0)\rangle\end{aligned}$$

where we have set $t_0 = 0$ for convenience. Hence, in the Heisenberg picture the time evolution of operators reads $O^{(H)}(t) = e^{iHt}Oe^{-iHt}$. Also commonly used is the interaction picture representation in situations when the Hamiltonian can be split into a free Hamiltonian H_0 and an (time-dependent) interacting part $H_I(t)$ such that $H = H_0 + H_I(t)$. This motivates to introduce the time evolution operators $U_0(t) = \exp(-iH_0t)$ and $U_I(t) = U_0^\dagger(t)U(t)$. Using $U_0(t)$ and $U_I(t)$ the expectation value of $O(t)$ reads

$$\begin{aligned}\langle\psi(t)|O|\psi(t)\rangle &= \langle\psi(0)U^\dagger(t)|O|U(t)\psi(0)\rangle \\ &= \langle\psi(0)U^\dagger(t)U_0(t)|U_0^\dagger(t)OU_0(t)|U_0^\dagger(t)U(t)\psi(0)\rangle \\ &= \langle\psi(0)U_I^\dagger(t)|U_0^\dagger(t)OU_0(t)|U_I\psi(0)\rangle.\end{aligned}$$

The equations of motion for states, operators and density matrices in the different pictures are summarized in table 1.1.

| | Schrödinger | Heisenberg | Interaction |
|------------------|--|--|---|
| states | $\partial_t \psi^{(S)}(t)\rangle = -iH^{(S)} \psi^{(S)}(t)\rangle$ | $\partial_t \psi^{(H)}(t)\rangle = 0$ | $\partial_t \psi^{(I)}(t)\rangle = -iH_I^{(I)}(t) \psi^{(I)}(t)\rangle$ |
| operators | $\partial_t O^{(S)} = 0$ | $\partial_t O^{(H)}(t) = i[H^{(H)}, O^{(H)}(t)]$ | $\partial_t O^{(I)}(t) = i[H_0^{(I)}, O^{(I)}(t)]$ |
| density matrices | $\partial_t \rho^{(S)}(t) = -i[H^{(S)}, \rho^{(S)}(t)]$ | $\partial_t \rho^{(H)}(t) = 0$ | $\partial_t \rho^{(I)}(t) = -i[H_I^{(I)}(t), \rho^{(I)}(t)]$ |

Table 1.1 Time evolution of states, operators and density matrices in the Schrödinger, Heisenberg and Interaction picture.

1.1.2 Linear response theory

In this section, we give a short introduction to *linear response theory* based on the lecture notes of Prof. D. Tong [3].

Linear response theory deals with the response of a system to an external influence which could, for example, be an applied electromagnetic field or a coupling to an external bath. In linear response

theory it is assumed that the external perturbation is small such that the response of the system can be calculated to first order in the perturbation amplitude. Then, the change of the expectation value of an observable O_i due to an external force ϕ_j can be written as

$$\delta\langle O_i(t) \rangle = \int dt' \sum_j \chi_{ij}(t, t') \phi_j(t') \quad (1.7)$$

where χ_{ij} is called *response function*. In the following, we assume that the system considered is invariant under translations in time, hence allowing us to write $\chi_{ij}(t, t') = \chi_{ij}(t - t')$. As Eq. (1.7) then becomes a convolution, its Fourier transformation factorizes

$$\begin{aligned} \delta\langle O_i(\omega) \rangle &= \int dt' \int dt \sum_j e^{i\omega t} \chi_{ij}(t - t') \phi_j(t') \\ &= \int dt' \int dt \sum_j e^{i\omega(t-t')} \chi_{ij}(t - t') e^{i\omega t'} \phi_j(t') \\ &= \sum_j \chi_{ij}(\omega) \phi_j(\omega). \end{aligned}$$

Thus, in a linear approximation, the system responds at the same frequency ω as it is perturbed with. For simplicity, we will drop the indices i, j for the moment. Since the expectation value of an hermitian observable is real, $\chi(t - t')$ must be real as well. (In the general case χ must be a hermitian matrix. However, in the basis where χ is diagonal the problem can be reduced to the case considered here.) As a consequence $\chi'(\omega) := \text{Re}(\chi(\omega))$ is an even and $\chi''(\omega) := \text{Im}(\chi(\omega))$ is an odd function of ω . Likewise, the Fourier transformation of $\chi'(\omega)$ and $\chi''(\omega)$ are even and odd under time reversal, respectively. The imaginary part $\chi''(\omega)$, which is also called *spectral function*, therefore describes dissipative processes. It can be written in terms of $\chi(\omega)$ as $\chi''(\omega) = -\frac{i}{2} [\chi(\omega) - \chi^*(\omega)]$. The response function $\chi(t - t')$ describes how a perturbation at time t' influences some quantity of interest at time t . As the past can not be affected by the future it directly follows that

$$\chi(t - t') = 0 \quad \text{for } t < t',$$

which is referred to as causality property. For a quantum mechanical system whose Hamiltonian $H(t) = H_0 + \theta(t)\Delta H_j(t)$ can be split into a dominant part H_0 and a weak perturbation $\Delta H_j(t)$, the response function can be calculated as follows

$$\begin{aligned} \langle O_i \rangle(t) &= \text{Tr} \left[\rho^{(I)}(t) O_i^{(I)}(t) \right] \\ &= \text{Tr} \left[\rho_0 e^{i \int_0^t \Delta H_j^{(I)}(t') dt'} O_i^{(I)}(t) e^{-i \int_0^t \Delta H_j^{(I)}(t') dt'} \right] \\ &\approx \text{Tr} \left[\rho_0 \left(\mathbb{1} + i \int_0^t \Delta H_j^{(I)}(t') dt' \right) O_i^{(I)}(t) \left(\mathbb{1} - i \int_0^t \Delta H_j^{(I)}(t') dt' \right) \right] \\ &\approx \langle O_i \rangle_0 + \int_0^\infty \chi_{ij}(t - t') dt', \end{aligned}$$

where we have assumed that the system is in a thermal equilibrium state ρ_0 of the unperturbed system at $t < 0$. Moreover, we have set $\langle \cdot \rangle_0 = \text{Tr}[\cdot \rho_0]$ for the corresponding expectation value. The change of the expectation value $\delta \langle O_i \rangle = \langle O_i \rangle - \langle O_i \rangle_0$ due to the perturbation is the integral over

$$\chi_{ij}(t-t') := -i\theta(t-t') \langle [O_i^{(H)}(t), \Delta H_j^{(H)}(t')] \rangle_0. \quad (1.8)$$

This result is known as the *Kubo formula*. From the Kubo formula, we can deduce that the quantum mechanical response function can be written in terms of a two-point correlation function. In general two-point correlation functions are a measure for variances or fluctuations. On the other hand, the imaginary part of the response function encodes the amount of dissipation in a system. This implies that there is a connection between fluctuations and dissipation in quantum systems that can be formulated in terms of the so-called *fluctuation-dissipation theorem* (FDT). In order to find one possible formulation of the FDT we consider the correlation functions

$$\begin{aligned} C_{ij}^>(t) &= \langle O_i(t) O_j(0) \rangle_0, \\ C_{ij}^<(t) &= \langle O_i(0) O_j(t) \rangle_0 \end{aligned} \quad (1.9)$$

and set $\Delta H_j = O_j$. With the help of Eq. (1.9), the imaginary part of the response function can be written as

$$\begin{aligned} \chi_{ij}''(t) &= -\frac{i}{2} (\chi_{ij}(t) - \chi_{ji}(-t)) \\ &= -\frac{1}{2} (\theta(t) [\langle O_i(t) O_j(0) \rangle_0 - \langle O_j(0) O_i(t) \rangle_0] - \theta(-t) [\langle O_j(-t) O_i(0) \rangle_0 - \langle O_i(0) O_j(-t) \rangle_0]) \\ &= \frac{1}{2} (C_{ji}^<(t) - C_{ij}^>(t)), \end{aligned}$$

where we have used $(\chi_{ij}(t))^* = \chi_{ji}(-t)$, $\theta(t) + \theta(-t) = 1$ and the fact that the equilibrium expectation value fulfills $\langle O_i(-t) O_j(0) \rangle_0 = \langle O_i(0) O_j(t) \rangle_0$. Employing the cyclicity property of the trace one can show that the Fourier transformations of $C_{ji}^>(t)$ and $C_{ij}^<(t)$ are connected through

$$C_{ji}^>(\omega) = e^{\beta\omega} C_{ij}^<(\omega), \quad C_{ji}^<(\omega) = e^{-\beta\omega} C_{ij}^>(-\omega). \quad (1.10)$$

With this relation, we arrive at

$$\chi_{ij}''(\omega) = -\frac{1}{2} (1 - e^{-\beta\omega}) C_{ij}^>(\omega). \quad (1.11)$$

While the left side of Eq. (1.11) quantifies the amount of dissipation in the system, the right side captures the fluctuations $C_{ij}^>(\omega)$ in equilibrium. Eq. (1.10) provides an experimental tool to test whether a piece of matter is in thermal equilibrium or not. The response of an experimentally accessible observable could, in principle, be measured in a typical scattering experiment such as Raman scattering at energy differences ω and $-\omega$ of the incoming and outgoing particles. If the

system is in equilibrium, the ratio $C_{ii}^<(-\omega)/C_{ii}^<(\omega)$ is equal to the Boltzmann factor $e^{\beta\omega}$. Away from equilibrium we expect that this relation is violated.

1.1.3 Bogoliubov transformation

The Bogoliubov transformation is a method to diagonalize Hamiltonians that can be written as a sum of bilinear terms while simultaneously preserving the fermionic or bosonic commutation relations of the involved operators. The topic is treated in many textbooks. Here, we mainly follow [4]. As an example, we consider the bosonic case, which appears again later in Ch. 6, for a general Hamiltonian

$$\begin{aligned} H &= \text{const} + \sum_k \varepsilon_k a_k^\dagger a_k + \varepsilon_k a_k a_k^\dagger + \gamma_k a_k^\dagger a_{-k}^\dagger + \gamma_k^* a_k a_{-k} \\ &= \text{const} + \sum_k \begin{pmatrix} a_k^\dagger & a_{-k} \end{pmatrix} \begin{pmatrix} \varepsilon_k & \gamma_k \\ \gamma_k^* & \varepsilon_k \end{pmatrix} \begin{pmatrix} a_k \\ a_{-k}^\dagger \end{pmatrix}, \quad C_k := \begin{pmatrix} \varepsilon_k & \gamma_k \\ \gamma_k^* & \varepsilon_k \end{pmatrix} \end{aligned}$$

with $\varepsilon_k^2 > |\gamma_k|^2$ and $\gamma_k = \gamma_{-k}$. Our aim is to find a transformation T_k that diagonalizes H and preserves $[a_{k'}, a_k^\dagger] = \delta_{k,k'}$ as well as $[a_{k'}, a_k] = [a_{k'}^\dagger, a_k^\dagger] = 0$. We define $\Psi_k^\dagger := (a_k^\dagger, a_{-k})$ and denote the new coordinates by $\tilde{\Psi}_k^\dagger = (\tilde{a}_k^\dagger, \tilde{a}_{-k})$ such that $\tilde{\Psi}_k^\dagger = T_k \Psi_k^\dagger$ where T_k is given by

$$T_k = \begin{pmatrix} u_k & v_k \\ v_{-k}^* & u_{-k}^* \end{pmatrix}.$$

The commutators $[a_{k'}, a_k^\dagger]$ and $[a_{k'}, a_k]$ then transform as

$$\begin{aligned} [\tilde{a}_{k'}, \tilde{a}_k^\dagger] &= [u_{k'} a_{k'} + v_{k'} a_{-k'}^\dagger, u_k^* a_k^\dagger + v_k^* a_{-k}] = (|u_k|^2 - |v_k|^2) [a_{k'}, a_k^\dagger] \stackrel{!}{=} \delta_{kk'} \\ \Rightarrow \quad |u_k|^2 - |v_k|^2 &= 1 \end{aligned} \tag{1.12}$$

$$\begin{aligned} [\tilde{a}_{k'}, \tilde{a}_k] &= [u_{k'} a_{k'} + v_{k'} a_{-k'}^\dagger, u_k a_k + v_k a_{-k}^\dagger] \stackrel{!}{=} 0 \\ \Rightarrow \quad u_{-k} v_k - v_{-k} u_k &= 0. \end{aligned} \tag{1.13}$$

In order to satisfy condition Eq. (1.13) we assume that $u_k = u_{-k}$ and $v_k = v_{-k}$ hold. Moreover, condition Eq. (1.12) is trivially fulfilled if we set

$$u_k = e^{i\phi_{1,k}} \cosh(\theta_k), \quad v_k = e^{i\phi_{2,k}} \sinh(\theta_k).$$

Using relation Eq. (1.12) the inverse transformation from $\tilde{\Psi}_k$ to Ψ_k reads

$$\Psi_k = T_k^{-1} \tilde{\Psi}_k = \begin{pmatrix} u_k^* & -v_k \\ -v_k^* & u_k \end{pmatrix} \tilde{\Psi}_k$$

as $\det(T_k) = |u_k|^2 - |v_k|^2 = 1$. The transformed Hamiltonian becomes

$$\begin{aligned} H &= \sum_k (T_k^{-1} \tilde{\Psi}_k)^\dagger C_k T_k^{-1} \tilde{\Psi}_k \\ &= \sum_k \tilde{\Psi}_k^\dagger \begin{pmatrix} -v_k^* u_k \gamma_k + |u_k|^2 \varepsilon_k - v_k u_k^* \gamma_k^* + \varepsilon_k |v_k|^2 & u_k^2 \gamma_k + v_k^2 \gamma_k^* - 2u_k v_k \varepsilon_k \\ (v_k^*)^2 \gamma_k + (u_k^*)^2 \gamma_k^* - 2\varepsilon_k v_k^* u_k^* & |v_k|^2 \varepsilon_k - v_k^* u_k \gamma_k - v_k u_k^* \gamma_k^* + |u_k|^2 \varepsilon_k \end{pmatrix} \tilde{\Psi}_k. \end{aligned} \quad (1.14)$$

When we parameterize $\gamma_k = |\gamma_k| e^{i\varphi_k}$ by its absolute value $|\gamma_k|$ and argument φ_k , the dependence on φ_k vanishes for $\phi_{1,k} = -\varphi_k/2$ and $\phi_{2,k} = \varphi_k/2$. To diagonalize the Hamiltonian, we define the angle θ_k such that the off-diagonal terms in Eq. (1.14) vanish. For the chosen values for $\phi_{1,k}$ and $\phi_{2,k}$ the two off-diagonal terms are real and identical. This yields the condition

$$\begin{aligned} |\gamma_k| (\sinh^2(\theta_k) + \cosh^2(\theta_k)) - 2\varepsilon_k \cosh(\theta_k) \sinh(\theta_k) &\stackrel{!}{=} 0 \\ \Rightarrow \tanh(2\theta_k) &= \frac{|\gamma_k|}{\varepsilon_k}, \end{aligned}$$

where we have used the identities $\sinh(2\alpha) = 2 \sinh(\alpha) \cosh(\alpha)$ and $\cosh(2\alpha) = \sinh^2(\alpha) + \cosh^2(\alpha)$. With the help of the transformation T_k , we finally arrive at

$$H = \text{const} + \sum_k \omega_k \tilde{a}_k^\dagger \tilde{a}_k,$$

$$\omega_k = (\cosh^2(\theta_k) + \sinh^2(\theta_k)) \varepsilon_k - 2 \cosh(\theta_k) \sinh(\theta_k) |\gamma_k| = \sqrt{\varepsilon_k^2 - |\gamma_k|^2}.$$

Alternatively, the approach outlined above can be reformulated as a pure diagonalization problem. In order to do so, we first write the constraints set by the commutation relations in terms of $[\Psi_{k,i}, \Psi_{k,j}] = \sigma_{ij}^z$ where σ^z denotes the third Pauli matrix. The transformed commutation relations then read

$$\sigma_{ij}^z \stackrel{!}{=} [\tilde{\Psi}_{k,i}, \tilde{\Psi}_{k,j}^\dagger] = [(T_k \Psi_k)_i, (T_k \Psi_k)_j^\dagger] = (T_k \sigma^z T_k^\dagger)_{ij}. \quad (1.15)$$

Multiplying Eq. (1.15) from the right with σ^z yields an expression for the inverse of T_k , $T_k^{-1} = \sigma^z T_k^\dagger \sigma^z$. By setting $\tilde{T}_k := T_k^{-1}$, we obtain

$$H = \text{const} + \sum_k \tilde{\Psi}_k^\dagger \tilde{T}_k^\dagger C_k \tilde{T}_k \tilde{\Psi}_k = \text{const} + \sum_k \tilde{\Psi}_k^\dagger \tilde{C}_k \tilde{\Psi}_k$$

which suggests that \tilde{T}_k has to be chosen such that $\tilde{C}_k := \tilde{T}_k^\dagger C_k \tilde{T}_k$ is diagonal. This is equivalent to diagonalizing the matrix $\sigma^z C_k$ as

$$\sigma^z \tilde{C}_k = \left(\sigma^z \tilde{T}_k^\dagger \sigma^z \right) \sigma^z C_k \tilde{T}_k = \tilde{T}_k^{-1} \sigma^z C_k \tilde{T}_k.$$

In general, $\sigma^z C_k$ is not hermitian and the transformation \tilde{T}_k is not unitary.

1.2 Closed quantum systems

A quantum system is called closed if it is completely isolated from its environment. While the whole universe is expected to represent a closed system, each subsystem of it is even under the best laboratory conditions exposed to external perturbations and therefore not truly isolated. Nevertheless, in some experiments, as in ultracold atom setups, systems can on experimentally relevant timescales to a good extent be considered to be closed [5]. To this end the timescales of decoherence and dissipation have to be much longer than the timescale of the experiment. In typical ultracold atom experiments atoms are cooled down to very low temperatures up to $\sim 10^{-9}K$ and trapped in optical lattices [6]. Using these experimental setups it is possible to realize models known from condensed matter physics like the Hubbard [7] and the Heisenberg model [8], whose coupling parameters and lattice constants can to high precision be manipulated experimentally.

The Hamiltonian H_0 of a closed system is time-independent and its time evolution is unitary. As a consequence energy is conserved at all times. As pointed out above, the time evolution of an initial state $|\psi_0\rangle$ reads

$$|\psi(t)\rangle = e^{-iH_0 t} |\psi_0\rangle. \quad (1.16)$$

The dynamics of $|\psi(t)\rangle$ is completely deterministic. If the state $|\psi(t)\rangle$ is known at some point in time t , the state $|\psi(t')\rangle$ at any other time t' can be deduced from Eq. (1.16). For the state $|\psi(t)\rangle$ the expectation value of an operator O is given by

$$\begin{aligned} \langle O^{(H)}(t) \rangle &= \langle \psi_0 | e^{iH_0 t} O e^{-iH_0 t} | \psi_0 \rangle = \sum_{n,m} c_n c_m^* e^{i(E_m - E_n)t} O_{nm} \\ &= \sum_n |c_n|^2 O_{nn} + \sum_{n \neq m} c_n c_m^* O_{nm} e^{i(E_m - E_n)t}, \end{aligned} \quad (1.17)$$

where we have used the eigenstates $|n\rangle, |m\rangle$ and the corresponding eigenvalues E_n, E_m of H_0 and the notation $O_{nm} := \langle n | O | m \rangle$, $c_n := \langle n | \psi_0 \rangle$. The first term in the second line of Eq. (1.17) is time-independent while the second one shows oscillatory behavior. Observables that commute with H_0 are time-independent and conserved. An observable O is said to equilibrate under the dynamics of the

system if the long-time limit expectation value $\langle O(t) \rangle$ relaxes to the time-averaged value $\langle O^{(H)} \rangle_{eq}$ [9],

$$\langle O^{(H)}(t) \rangle \xrightarrow{t \rightarrow \infty} \langle O^{(H)} \rangle_{eq} := \lim_{T \rightarrow \infty} \frac{1}{T} \int_0^T dt \langle O^{(H)}(t) \rangle. \quad (1.18)$$

In generic systems, without any symmetries, there are no degeneracies in the energy spectrum. As a consequence, the second term in Eq. (1.17) averages to zero, such that

$$\langle O^{(H)} \rangle_{eq} = \sum_n |c_n|^2 O_{nn}. \quad (1.19)$$

Equivalently, Eq. (1.19) can be written as $\langle O^{(H)} \rangle_{eq} = \text{Tr}[O\rho_{DE}]$ where $\rho_{DE} = \sum_n |c_n|^2 |n\rangle\langle n|$ is the so-called *diagonal ensemble* [10]. It is important to note that the second term in Eq. (1.17) only becomes exactly zero in the thermodynamic and long-time limit. For finite systems, there is always the possibility of quantum revivals, meaning that the sum of a finite number of oscillating terms can always come arbitrary close to its initial condition [11, 12]. However, in generic systems, such events happens on very long time scales and can often be neglected.

1.2.1 Integrability

Nature is far too complex to be described in an exact way. Even simplified physical models can, in general, not be solved analytically. Despite that, there is a class of models which have a particularly rich underlying structure that often allows for an analytical solution. These systems are characterized by an extensive set of constants of motion and are referred to as *integrable*. The existence of constants of motion enables one to determine the dynamics of the system by integration. Thus, it is not necessary to find the solution of a set of potentially coupled differential equations, but to solve a system of ordinary equations or integrals. However, that can still be a very challenging task and one might not be able to solve the system completely with the available means.

Classical dynamics is characterized by trajectories in phase space which is spanned by all possible position \mathbf{x} and momentum variables \mathbf{p} . The dynamics of a quantity f that is function of these phase space variables is governed by $\frac{d}{dt}f = \{f, H\}$ where H denotes the Hamiltonian and $\{A, B\} := \sum_k \frac{\partial A}{\partial x_k} \frac{\partial B}{\partial p_k} - \frac{\partial A}{\partial p_k} \frac{\partial B}{\partial x_k}$ the Poisson bracket. In contrast to generic systems, integrable systems do not explore the whole phase space, but are typically limited to certain orbits and often show quasiperiodic behavior in their dynamics [13]. Famous examples of classical integrable systems are the two-body Kepler problem, the classical harmonic oscillator and the Korteweg-de-Vries equation. Integrability is a very fine-tuned and fragile property. If a weak anharmonicity is introduced in the harmonic potential or a light third mass is added in the case of the two-body Kepler problem, integrability is immediately lost.

A mathematical rigorous definition of integrability can be given as follows: A classical system described by a Hamiltonian $H(\mathbf{q}, \mathbf{p})$ with $2f$ degrees of freedom is called *Liouville integrable* if f functionally independent constants of motion C_i exist that commute with the Hamiltonian $\{C_i, H\} = 0$

and also mutually commute with each other $\{C_i, C_j\} = 0$ [14].

The *Liouville-Arnold theorem* states that the Hamiltonian of an integrable system can be mapped to a canonical form which does not depend explicitly on time but only on the new canonical action-angle coordinates being constant or evolving linearly in time [15]. Note that, in principle, in any classical interacting many-particle system, the starting points of all trajectories in phase space are constants of motion as they do not change with time. However, these are not constants of motion in the sense of Liouville integrability. For a given configuration of the system at time $t > t_0$, where t_0 is the initial time, they can, in general, only be determined by solving the coupled equations of motion and then evolving the system backward in time.

It seems natural to define integrability in quantum systems by taking the classical definition and replacing the $2f$ dimensional phase space by a f dimensional Hilbert space, Poisson brackets by commutators and independent functions in phase space by algebraically independent operators

$$[C_i, H] = 0, \quad [C_i, C_j] = 0 \quad \forall i, j.$$

However, in this analogy it is ambiguous how the constants of motion are defined. If C_i commutes with H , any algebraic function $f(C_i)$ commutes with H as well. Moreover, every projection operator $|n\rangle\langle n|$ onto an eigenstate $|n\rangle$ of H commutes with the Hamiltonian and the number of these projection operators is as large as the dimension of the Hilbert space. Hence, according to this definition, each quantum system would be integrable.

Importantly, not all of these constants of motion are relevant in a similar sense as not all initial conditions in a classical many-particle system are constants of motion according to the Liouville theorem. An additional criterion is needed to define integrability in quantum systems. This criterion is locality. For a discrete lattice system with translational symmetry, we can define a local conservation law C_i fulfilling $[C_i, H_0] = 0$ as a translation-invariant sum of local densities $c_{i,j}$ [16],

$$C_i = \sum_{j=1}^N c_{i,j}$$

where $c_{i,j}$ has only non-trivial support on a finite number of adjacent lattice sites, i.e. $c_{i,j,k} = \mathbb{1}$ for $|k - j| > n_i$. The number of local conserved quantities scales linearly with the system size N and not exponentially as the size of the Hilbert space. Throughout this thesis, we refer to constants of motion also as conservation laws, conserved quantities and charges interchangeably.

Quantum integrability can be associated with the existence of an extensive set of local conserved quantities. Another approach is to say that a quantum system is integrable if a classical limit exists in which the corresponding classical system is integrable [17]. There are integrable lattice as well as continuum models, for example, free [18–20] and conformal field theories [21, 22], non-linear sigma models and non-relativistic field theories like the Lieb-Liniger model [23, 24]. Examples of quantum integrable lattice models are the XXZ spin chain [25], the transverse Ising model [26, 27] and the Fermi-Hubbard model [28, 29] in one-dimension.

In nature, only approximately integrable systems exist because any weak integrability breaking perturbation destroys integrability. However, as already mentioned, integrable systems can, up to good precision, be realized in ultracold atom experiments, at least on certain time scales.

Quantum integrable systems can roughly be divided into two classes. Firstly, systems in which local degrees of freedom can be mapped onto non-interacting quasiparticles using a canonical transformation like a Bogoliubov transformation, or bosonization techniques. This is, for example, the case for the spin-1/2 XY and the transverse Ising model. Due to the equivalence to a single (quasi)particle picture, these systems are also called quasifree [16]. Secondly, Yang-Baxter integrable systems in which multi-particle scattering can be separated into two-particle scattering events. Such systems can be diagonalized using so-called Bethe ansatz techniques [30]. Typically, integrable quantum systems are low-dimensional and feature short range interactions. Often, the notion of quantum integrability and solvability is used interchangeably. However, there are also exceptions as reported in [31].

An effective theoretical approach to test whether a finite size system is integrable or not is to investigate its level statistics. While the distances of adjacent eigenvalues in integrable models are Poisson distributed, in generic systems they obey, in the presence of time reversal symmetry, the statistics of the Gaussian orthogonal ensemble (GOE) and feature level repulsion [32, 33].

Transport in integrable systems is characterized by infinite conductivities. If a current j that is protected, or at least partially protected, by conservation laws is driven by a time-dependent perturbation $E(t)$, the response of the system is infinitely strong. In a linear approximation, the current and the perturbation are related through $j(\omega) = \sigma(\omega)E(\omega)$. The real part of the conductivity $\sigma(\omega)$ in frequency space can be written as $\text{Re}(\sigma(\omega)) = \sigma_{reg}(\omega) + D(T)\delta(\omega)$ where $\sigma_{reg}(\omega)$ denotes the regular part of $\sigma(\omega)$ [34, 35]. The temperature-dependent *Drude weight* $D(T)$ is a weight of the non-regular contribution at $\omega = 0$ that is non-zero if the relaxation of currents in the long-time limit is prohibited by conservation laws. In contrast to that, in generic non-integrable systems $D(T)$ is zero. According to the Mazur inequality, a lower bound for the Drude conductivity is given by

$$D(T) = \frac{1}{2LT} \lim_{t \rightarrow \infty} \langle j(t)j(0) \rangle \geq \frac{1}{2LT} \sum_k \frac{\langle j C_k \rangle^2}{\langle C_k^2 \rangle} \quad (1.20)$$

where L denotes the system size and $\{C_k\}$ is a set of orthogonal conserved quantities, $\langle C_k C_l \rangle = \langle C_k^2 \rangle \delta_{kl}$ [36].

1.2.2 The XXZ model

Within this thesis we mainly consider the spin-1/2 XXZ model in one-dimension. The Hamiltonian of the model reads

$$H_{XXZ} = \sum_j \frac{J}{2} \left(S_j^+ S_{j+1}^- + S_j^- S_{j+1}^+ \right) + \Delta S_j^z S_{j+1}^z \quad (1.21)$$

where J denotes the exchange interaction and Δ the anisotropy term. The ladder operators S_j^\pm are defined by $S_j^\pm := \frac{1}{2}(\sigma_j^x \pm i\sigma_j^y)$ and $S_j^z = \frac{1}{2}\sigma_j^z$ where σ^α ($\alpha = x, y, z$) are Pauli matrices. At $\Delta = J$ the XXZ model simplifies to the $SU(2)$ Heisenberg model. The excitation spectrum is gapless in the regime $|\Delta| < |J|$ and gapped otherwise [37].

The local conserved quantities of the model can be calculated recursively using the so-called boost operator $B := -i\sum_j j h_h$, where $h_j = 1/2J(S_j^+ S_{j+1}^- + S_j^- S_{j+1}^+) + \Delta S_j^z S_{j+1}^z$ is the local Hamiltonian density. The conserved quantity C_{i+1} of order $i+1$ can then be obtained with the formula $C_{i+1} = [B, C_i]$ for $i \geq 2$ [25]. The complexity of the charges increases with increasing order. A conserved quantity C_i of order i contains local densities that have non-trivial support on maximal i neighboring sites. The most local charges of the XXZ model are the total spin in z -direction $C_1 = S^z$, the Hamiltonian itself $C_2 = H_{XXZ}$ and the heat current operator

$$C_3 = J_h = J^2 \sum_j (\mathbf{S}'_j \times \mathbf{S}''_{j+1}) \times \mathbf{S}'_{j+2}, \quad (1.22)$$

where we have defined $S_j^{\prime\alpha} = \sqrt{\lambda_\alpha} S_j^\alpha$, $S_j^{\prime\prime\alpha} = \sqrt{\lambda_z/\lambda_\alpha} S_j^\alpha$ for $\lambda_z = \Delta/J$, $\lambda_x = \lambda_y = 1$. The set of local conservation laws can be divided into the sets of even $\{C_{2n}\}$ and odd $\{C_{2n+1}\}$ charges. Odd conservation laws are conserved currents. In contrast to the set of even charges, they are, for example, odd under time reversal and certain spatial reflection symmetries.

Due to the conservation of the heat current, the corresponding Drude weight is finite at all finite temperatures [38]. In contrast to that, the spin current operator

$$J_s = J \sum_j (S_j^x S_{j+1}^y - S_j^y S_{j+1}^x) \quad (1.23)$$

is not conserved, $[H_0, J_s] \neq 0$. As J_s is odd under spin-reversal while all local conservation laws of the XXZ are even under this transformation, one would expect that the spin Drude weight (also called spin stiffness) is zero. However, it was found that the Drude weight of the spin current is non-zero for $|\Delta| < |J|$ [39] which was explained recently by the detection of an additional set of charges [40, 41]. Importantly, these charges cannot be written as a sum of local densities. The corresponding charge densities can rather be considered as quasilocal, meaning that they are local up to exponential tails. In contrast to the local conservation laws, they do not exhibit spin-reversal invariance and have a finite overlap with the spin current at $|\Delta| < |J|$. Among the known quasilocal conservation laws are the families of X and Z charges [16] where the more exotic charges of the Z family even break the $U(1)$ symmetry of the underlying model.

Due to a finite overlap between the spin current and the quasilocal charges at $|\Delta| < |J|$, the spin stiffness is non-zero indicating ballistic transport. Using the set of common eigenstates $\{|n\rangle\}$ of the local conservation laws the conserved part of the spin current can be constructed as

$$J_s^c = \sum_n \langle n | J_s | n \rangle |n\rangle \langle n|. \quad (1.24)$$

1.2.3 Thermalization

One of the major hallmarks of equilibrium statistical physics is the fact that macroscopic systems with many degrees of freedom can be described by only a few parameters like, for example, temperature T and chemical potential μ . Such a coarse-grained description cannot capture all possible microscopical configurations but it can predict the typical behavior of a system on macroscopic scales. Generally, one is not interested in the position and velocities of all molecules in a classical gas or the exact wave function of a quantum many-body system but rather in measurable correlation functions and local observables. The expectation values of these observables, like energy and particle number, define macroscopic states that are compatible with many microstates. The approach of statistical physics is to replace the description of deterministically evolving microstates by a stochastic theory for macrostates.

The existence of stationary equilibrium probability distributions, also called ensembles, originates in the second law of thermodynamics, which states that the entropy increases in (almost) all processes [42, 43]. The thermal equilibrium distribution is then distinguished as the distribution with maximal entropy.

The entropy of a macroscopic state is a measure for the number of microstates that can realize the former. Thus, in equilibrium where by definition each state in configuration space is equally often reached during the time evolution, a closed system tends to be most likely in the macrostates being consistent with the most microstates. As an illustration, we consider a gas of N particles in an isolated box that is virtually divided into two halves (This is a very commonly used example. A similar setup was, for example, also considered in [44]). We assume that all particles are initialized in the left half of the box at time $t = 0$. After a certain equilibration time, the particles fill the whole box uniformly, as this is the macrostate with the most microscopical realizations. The entropy of a macrostate with N_1 particles on the left and $N - N_1$ particles on the right side is

$$\begin{aligned} S(N_1) &= \ln \left[\binom{N}{N_1} \right] = \ln \left[\frac{N!}{N_1!(N-N_1)!} \right] \approx \ln \left[\frac{\sqrt{2\pi N} \left(\frac{N}{e}\right)^N}{\sqrt{4\pi^2 N_1(N-N_1)} \left(\frac{N_1}{e}\right)^{N_1} \left(\frac{N-N_1}{e}\right)^{N-N_1}} \right] \\ &= \text{const} - \frac{1}{2} (\ln[N_1] + \ln[N-N_1]) - N_1 (\ln[N_1] - 1) - (N-N_1) (\ln[N-N_1] - 1), \end{aligned}$$

where we have used the Stirling formula $n! \approx \sqrt{2\pi n} (n/e)^n$ which is valid for $n \gg 1$. The entropy is maximal at $N_1 = N/2$ as

$$\begin{aligned} \left. \frac{\partial S(N_1)}{\partial N_1} \right|_{N_1=N/2} &= \left(\frac{1}{2(N-N_1)} - \frac{1}{2N_1} + \ln[N-N_1] - \ln[N_1] \right) \Big|_{N_1=N/2} = 0, \\ \left. \frac{\partial^2 S(N_1)}{\partial^2 N_1} \right|_{N_1=N/2} &= 4 \left(\frac{1-N}{N^2} \right) < 0. \end{aligned}$$

Hence, in the most likely configuration half of the particles are on the left and the other half on the right side. However, due to fluctuations on the microscopic level there is a chance to measure a

slightly different number of particles. The probability to find $N/2 - M$ particles in one and $N/2 + M$ particles in the other subsystem is

$$P_M = \frac{1}{2^N} \binom{N}{N/2 \pm M} \approx \frac{1}{\sqrt{\frac{\pi}{2}N}} e^{-\frac{2M^2}{N}}, \quad (M \ll N),$$

where 2^N is the total number of macrostates. Fluctuations are Gaussian distributed with variance $\sigma^2 = N/4$. We see that the probability for all particles N being again in the left half of the box is exponentially small in N . The second law of thermodynamics sets a fixed arrow of time towards the equilibrium state. This is referred to as *irreversibility*. The system can go back to its initial low-entropy configuration but the probability for this process is extremely tiny in a macroscopic system.

In the context of thermal equilibrium, it is important to introduce the concept of a thermal bath. A bath is a large thermodynamic system with so many degrees of freedom that its temperature, chemical potential, ... do not change when it is coupled to the actual system of interest. On the contrary, it dictates the intensive parameters of the system and fixes the expectation values of the corresponding extensive quantities. It can serve as an infinite reservoir for heat, particles or other quantities that are conserved in the whole system.

To find the equilibrium distribution for a given bath coupling one can, for example, use an approach from information theory. The *Shannon entropy* of a discrete probability distribution is defined as [45]

$$S[\{p_j\}] = - \sum_{j=1}^N p_j \ln(p_j). \quad (1.25)$$

where p_j is the probability of the system to be in a macrostate labeled by j . We aim to find the probability distribution that maximizes Eq. (1.25) in the presence of possible constraints set by a coupling to an external bath which can be incorporated in terms of Lagrange multipliers. In the case of a closed system, the only constraint is the normalization of the distribution, i.e. $\sum_j p_j = 1$ and the entropy is maximized by a uniform distribution with $p_j = 1/N$. In physics, this is referred to as the *microcanonical ensemble*. If the system is coupled to a heat bath that fixes the expectation value of the energy $E = \sum_j p_j E_j$, the Shannon entropy is maximal for

$$p_j(E) = \frac{1}{Z(E)} e^{-\beta E_j}, \quad Z(E) = \sum_j e^{-\beta E_j},$$

where $\beta = 1/E$ is the inverse temperature and $Z(E)$ the canonical partition sum. This is the so-called *canonical ensemble*. In the case of energy and particle number fluctuations one obtains the *grand canonical ensemble*. These are the most commonly used ensembles in statistical physics. In the thermodynamic limit, when the relative fluctuations of energy and particle number tend to zero (by virtue of the central limit theorem), these ensembles are believed to be equivalent. This has been rigorously proven for systems with short range interactions [46].

Systems in equilibrium are considered to be *ergodic* [47]. Ergodicity means that the whole phase space is filled equally during the time evolution. As a consequence, the time average of physical observables becomes equivalent to the ensemble average which allows us to work only with time-independent probability distributions in equilibrium statistical physics. For a system in equilibrium with N discrete states, ergodicity means that all transition rates $\Gamma_{i \rightarrow j}$ between states i and j are non-zero and therefore all states can be reached during the dynamics. In equilibrium, the detailed balance relation

$$\Gamma_{i \rightarrow j} P_i = \Gamma_{j \rightarrow i} P_j \quad (1.26)$$

holds, which implies that all probability currents vanish. This can be seen as a defining property of thermal equilibrium. Besides ergodicity, thermalization is associated with the concept of *dynamical chaos* [48]. A system is said to be chaotic if its final state, which is reached after some time t , is extremely sensitive to the initial conditions. Even small changes in the starting configuration can lead to a very different final state. The microscopic state of a system in equilibrium might look completely different for slightly different initial conditions. However, at macroscopic scales, the system can in both cases be well described by an equilibrium ensemble.

1.2.4 Thermalization in quantum systems

A natural question to ask is under which circumstances equilibrated observables in isolated quantum systems can be described by ensembles known from statistical physics. A typical experimental as well as theoretical approach to investigate this question are so-called quantum quenches. In a quantum quench, a system is, typically, first prepared in an eigenstate (mostly the ground state) of a Hamiltonian $H(\lambda)$. Then one parameter λ of the initial Hamiltonian is suddenly set to a new value λ' . As a consequence, the initial state is, in general, no eigenstate of $H(\lambda')$ anymore and evolves unitarily under the new Hamiltonian.

In the case of a generic system, the expectation value $\langle O \rangle$ of an observable O is expected to be given by Eq. (1.18) in the long-time limit which can also be formulated in terms of the diagonal ensemble

$$\rho_{DE} = \sum_n |c_n|^2 |n\rangle \langle n| \quad (1.27)$$

as $\langle O \rangle = \text{Tr}[O \rho_{DE}]$. It can be said that an observable O thermalizes if its long-time limit expectation value can be reproduced by an equilibrium density matrix ρ_{eq} depending only on a few parameters T, μ, \dots ,

$$\langle O \rangle = \text{Tr}[O \rho_{DE}] = \text{Tr}[O \rho_{eq}(T, \mu, \dots)]. \quad (1.28)$$

Note that this statement can only be exactly true in the thermodynamic limit. It is again a priori not clear why closed quantum systems should thermalize as their dynamics is completely unitary. This apparent contradiction is in some sense similar to the paradox of thermalization in deterministically

evolving classical systems. In classical statistical mechanics the contradiction can be resolved by the assumption of ergodicity and dynamical chaos.

The question is how thermalization can be explained in quantum mechanics. A thermal state is completely independent of the initial configuration. In contrast to that, in a closed quantum system, the information about the initial conditions remains available for all times. However, it is important to note that information propagates during the time evolution and is after a sufficiently long time only accessible by global measurements. Typically, the speed at which information spreads in quantum systems is limited by the so-called *Lieb-Robinson bound* [49] whose explicit value depends on the details of the system. As most of the relevant physical observables are described by local operators, the information about the initial state is effectively lost as long as local measurements are concerned and ρ_{DE} in Eq. (1.28) might be replaced by an equilibrium distribution. Another way of defining thermalization is the following: An infinitely large system B is considered to be thermal if the reduced density matrix of all possible finite subsystems $A \subset B$ is given by a thermal distribution, i.e.

$$\rho_A = \text{Tr}_{B/A}[\rho] = \rho_{eq}(T, \mu, \dots). \quad (1.29)$$

If this condition is met, it is said that the system serves as its own heat bath. A commonly used explanation to illustrate thermalization in quantum systems is the so-called *Eigenstate Thermalization Hypothesis* (ETH) [50, 51] which is based on two major assumptions: 1) The diagonal matrix elements $O_{nn} = O(E_n)$ of an operator O depend smoothly on the energy and 2) the off-diagonal matrix elements are much smaller than the diagonal ones $O_{mn} \gg O_{nm}$. If we assume that all relevant energies lie within a shell of width ΔE centered around the energy E , we obtain for the expectation value of O in the long-time limit

$$\begin{aligned} \langle O(t) \rangle &\xrightarrow{t \rightarrow \infty} \sum_n |c_n|^2 O_{nn} + \sum_{n \neq m} c_m^* c_n e^{i(E_m - E_n)t} O_{mn} \\ &\stackrel{1),2)}{\approx} \sum_{n, |E - E_n| < \Delta E} |c_n|^2 O(E_n) \approx \frac{1}{\Omega_{\Delta E}(E)} \sum_{n, |E - E_n| < \Delta E} O(E_n) \approx O(E) \end{aligned} \quad (1.30)$$

where the last equality holds if $O(E_n) \approx O(E)$. Moreover, we have assumed that c_n scales as $1/\sqrt{\Omega_{\Delta E}(E)}$ where $\Omega_{\Delta E}(E)$ denotes the total number of states in the energy shell with energy between $E \pm \Delta E$. The result Eq. (1.30) is equivalent to the one predicted by the microcanonical ensemble and, therefore, an equilibrium expectation value.

The energy window can be chosen sufficiently narrow that only one eigenenergy is included within the shell. Then the expectation value of the observable with respect to the corresponding energy eigenstate is equal to the prediction of the microcanonical ensemble. Thus the information, whether a system thermalizes or not is stored in the energy eigenstates itself. This observation allows the interpretation of energy eigenstates as single ensembles [52]. Thermalization of quantum systems has been observed in several studies as in [10, 53]. However, not all systems thermalize.

1.2.5 Generalized thermalization in quantum systems

One famous example of the failure of thermalization are strongly disordered systems. We consider a spin-1/2 Heisenberg model in one-dimension

$$H = \sum_j J \mathbf{S}_j \mathbf{S}_{j+1} + h_i S_j^z \quad (1.31)$$

that is subject to a random magnetic field $h_i \in [-W, W]$. The field h_i is different on all sites and drawn from a uniform distribution. The model was studied in [54, 52]. Here, we repeat some of the main results. The system shows a phase transition from a thermal to a *Many-body localized* (MBL) phase at a critical disorder strength $(W/J)_c \approx 3.5 \pm 1$ for an energy density compatible with a $T = \infty$ thermal state. In the Many-body localized phase, the system fails to equilibrate and its local configuration is at all times set by the initial conditions. This becomes especially apparent in the extreme limit $J \rightarrow 0$ ($W \neq 0$). At $J = 0$ the model is describing isolated spins precessing in a random magnetic field. Their dynamics is completely determined by the initial configuration and the wavefunction of the whole system is simply a product state of the single-particle wavefunctions. Moreover, each operator $\tau_j = S_j^z$ is a local conserved quantity. In the many-body localized phase at $(W/J) > (W/J)_c$ one can still find a set of local conserved quantities $\{\tau_j\}$. They can be constructed by applying a non-local uniform transformation U to the local operators S_i^z [55],

$$\tau_i = US_i^z U^\dagger = S_i^z + \sum_{jk} J_{ijk}^{\alpha\beta} S_j^\alpha S_k^\beta + \dots, \quad (1.32)$$

where the transformation U is chosen such that $U^\dagger H U$ is up to terms of order $(J/W)^n \ll 1$ diagonal in the eigenbasis of S^z . Then all operators τ_i commute with the Hamiltonian and also mutually commute with each other

$$[\tau_i, H] = [US_i^z U^\dagger, H] = U (S_i^z U^\dagger H U - U^\dagger H U S_i^z) U^\dagger \sim \mathcal{O}((J/W)^n),$$

$$[\tau_i, \tau_j] = [US_i^z U^\dagger, US_j^z U^\dagger] = U (S_i^z S_j^z - S_j^z S_i^z) U^\dagger = 0.$$

The expansion in powers of J/W can for sufficiently strong disorder strength be truncated after the first order. The prefactor $J_{ijk}^{\alpha\beta}$ decays exponentially with the distance of the spins S_j, S_k to the central spin S_i where the characteristic length scale for the decay is given by the localization length ξ [56]. Hence, the operators τ_j can be considered as local up to exponential tails. In contrast to the conservation laws of integrable systems (cf. Sec. 1.2.1), these charges are typically robust and simply adjust to small local perturbations. Note that the former statement does not hold in the case of a weak coupling to a thermal bath [57]. Due to the existence of an extensive set of local conserved quantities, a MBL system cannot thermalize to an ensemble that is only described by a few parameters. Further differences between the thermal (ergodic) and the many-body localized phase are listed in

| Therrmal phase | MBL phase |
|---|--|
| <ul style="list-style-type: none"> • Many-body eigenvalue spacing follows GOE/ GUE/ GSE statistics • System is a reservoir for itself • Diffusive transport of energy, spin • ETH is valid • ‘Volume-law’ entanglement | <ul style="list-style-type: none"> • Many-body eigenvalue spacing follows Poissonian statistics • System is not a reservoir for itself • Zero spin and heat conductivity • ETH is invalid • ‘Area-law’ entanglement |

Table 1.2 Comparison between the thermal and the many-body localized phase. The table is reproduced from [52].

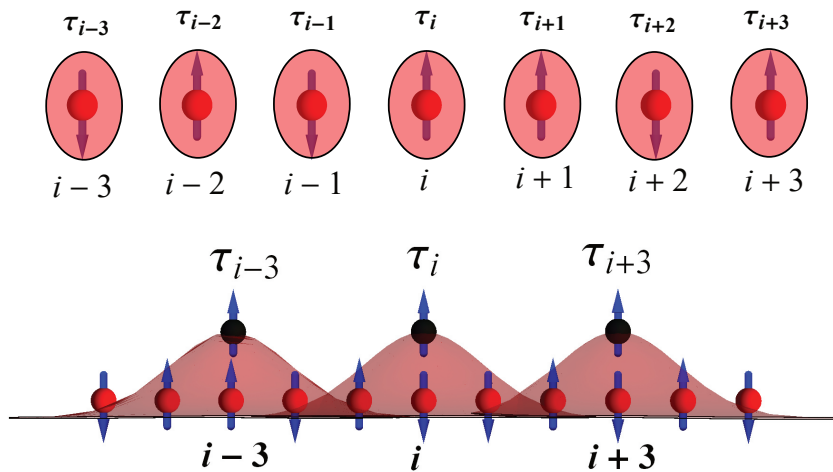


Figure 1.1 In the limit $J \rightarrow 0$ each local operator $\tau_i = S_i^z$ commutes with the Hamiltonian and is therefore conserved (upper figure). For small but finite J ($(W/J) > (W/J)_c$), conserved quantities τ_i can be defined which are local up to exponential tails (lower figure).

table 1.2. Another and related class of systems that fail to thermalize are integrable systems which have been introduced in Sec. 1.2.1. Similarly to MBL, an extensive set of local conserved quantities that constrains the time evolution of the system eventually prevents thermalization.

Experimentally, the failure of thermalization in an integrable system was first observed by Kinoshita et al. [58] in 2006. In their seminal experiment, they found that the momentum distribution of a trapped one-dimensional gas of ^{87}Rb bosons with point-like interaction does not equilibrate even after several thousands of collisions. The experiment can be theoretically described with the integrable Lieb-Liniger model. In a very simplified picture, this observation can be explained with an idealized Newton’s cradle that consists of point like masses moving effectively in one-dimension and colliding

fully elastically. When a ball collides with one of its neighbors, energy and momentum conservation is only satisfied if momenta are exchanged. Such a system can never equilibrate to a thermal state. It has been conjectured that in the thermodynamic limit, the steady state after a quench that preserves integrability can be captured by a *generalized Gibbs ensemble* (GGE) rather than a Gibbs ensemble [59, 26, 60]. At least this is expected to be true as long as the expectation values of local physical observables are considered. A GGE includes all relevant local (and quasilocal) charges of a system with corresponding Lagrange parameters λ_j ,

$$\rho_{GGE} \sim \exp\left(-\sum_j \lambda_j C_j\right) \quad (1.33)$$

and maximizes entropy under the constraints set by the conservation laws. In the case of quenches that break integrability weakly, it was reported that the system eventually thermalizes in the long-time limit. However, on an intermediate timescale, it was found that local observables can be well described by a GGE determined by the initial configurations of the system. This transient regime is called *prethermal* [61, 62]. A further approximation can be made in Eq. (1.33) by including not all conserved quantities but only a finite number N_c which turn out to be most relevant for the case considered. The ensemble is then referred to as a *truncated GGE* (tGGE).

In the case of free models, the local conserved quantities C_j can be replaced by the occupation number operators $\mathcal{S}_k = \alpha_k^\dagger \alpha_k$ where α_k^\dagger and α_k denote the creation and annihilation operators of a quasiparticle state, respectively. The operator \mathcal{S}_k is non-local in position space, but local in momentum space. The values of the Lagrange parameters in the steady (or prethermal) state are determined by the initial conditions,

$$\langle \psi_0 | C_j | \psi_0 \rangle \stackrel{!}{=} \langle C_j \rangle_{GGE}, \quad (1.34)$$

where we have used the notation $\langle C_j \rangle_{GGE} = \text{Tr}[C_j \rho_{GGE}]$. The validity of the GGE ansatz has been shown theoretically for a broad class of free and quasifree models that can be mapped onto free theories [26, 60]. However, there was a long debate about whether a GGE is also able to correctly describe the steady state expectation values of local observables in the presence of interactions. In [63–65], it was observed that a GGE including only local charges cannot capture the exact steady state of a *XXZ* model after a quantum quench. However, it was found later that the GGE ansatz indeed works if all local and quasilocal conservation laws are included [66–68, 65], at least for certain initial conditions [69, 63]. Thus, the exact validity of the GGE ansatz strongly depends on the fact if all relevant conservation laws can be detected and included in the GGE ansatz. Nevertheless, there is the notion that more local conservation laws, included in the tGGE ansatz, have a more substantial impact on the expectation value of local observables than less local ones.

The first experimental verification of the GGE ansatz in an integrable system was given by Langen et al in 2015 [70]. They showed that a degenerate one-dimensional gas of bosonic ^{87}Rb atoms, which is, as already mentioned, to a good extent a realization of the integrable Lieb-Liniger model, relaxes

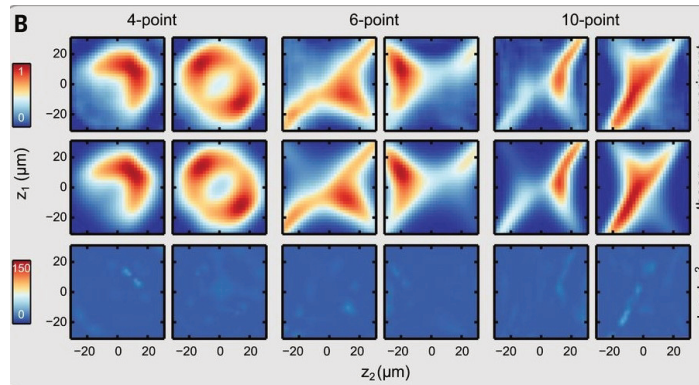


Figure 1.2 Comparison between the experimentally measured 4, 6 and 10-point correlation functions and the theoretical prediction obtained from a tGGE ansatz including 10 conservation laws. The figure is taken from [70].

to a steady state being well captured by a GGE ansatz. By splitting the system into two nominally identical subsystems with approximately the same number of atoms, a quantum quench was performed triggering the non-equilibrium dynamics of the system. To validate the GGE ansatz, they measured n -point correlation functions, using matter-wave interferometry between the two subsystems, and compared their results to theoretical predictions obtained from a truncated GGE ansatz including up to ten conserved quantities. As shown in Fig 1.2 they found a very good agreement between experiment and theory even for higher order correlation functions.

1.3 Open quantum system

A quantum system that is not completely isolated, but subject to external influences and perturbations is referred to as an open quantum system. Such an external influence could, for example, be a coupling to a thermal or non-thermal bath or an applied time-dependent force field.

One convenient approach to deal with the first case is to decompose the Hamiltonian of the whole system into three parts. One part which acts only on the degrees of freedom of the system H_S and the bath H_B and another one H_{SB} describing the system-bath coupling. As one is typically mainly interested in the actual system and not in the bath, the latter one can under certain assumptions be treated as an average influence on a coarse-grained time scale. By tracing out the bath degrees of freedom one can derive an effective non-unitary theory for the dynamics of the reduced system. In the case of time-dependent driving, it is in general difficult to find a simple theory describing the time evolution of the system. Exceptions are situations in which the drive is periodic. Then the so-called *Floquet theory* provides powerful tools to capture the state of the system at stroboscopic times.

Open systems that are not simply coupled to a thermal bath do in general not thermalize in the long-time limit but reach a *non-equilibrium steady state* (NESS). These states can host stationary currents and do not need to be time-independent. For instance, they can show periodic behavior as

limit cycles. In the absence of equilibrium, it is a priori not possible to make an ansatz for a steady state. One rather needs to keep track of the time evolution of the density matrix for given initial conditions or solve $\partial_t \rho = 0$ to determine the steady state.

In the following, we consider a system with a set of possible configurations $C = \{c_n\}$ and an initial probability distribution $P_{t=0}(c_n)$. The equation governing the time propagation of \mathbf{P}_t is called *Master equation*. The most general form of a Master equation reads

$$\frac{\partial}{\partial t} P_t(c_n) = \sum_m \Gamma_{m \rightarrow n} P_t(c_m) - \sum_m \Gamma_{n \rightarrow m} P_t(c_n), \quad (1.35)$$

where $\Gamma_{n \rightarrow m}$ denotes the transition rate from configuration c_n to configuration c_m . The first term in Eq. (1.35) describes gain processes while the second one represents losses. The Master equation preserves the normalization property as $\sum_n \partial_t P_t(c_n) = 0$. Eq. (1.35) can be formulated as a matrix equation

$$\partial_t \mathbf{P}_t = \mathcal{L} \mathbf{P}_t, \quad (1.36)$$

where \mathcal{L} is the Liouville operator (cf. 1.1.1). The entries of \mathbf{P}_t and \mathcal{L} are given by $\mathbf{P}_{t,m} = P_t(c_m)$ and $\mathcal{L}_{nm} = -\Gamma_{n \rightarrow m} + \delta_{nm} \sum_{m'} \Gamma_{m \rightarrow m'}$. The Liouville operator is in general not hermitian. However, it is constrained by the conservation of probability

$$\sum_n \partial_t P_t(c_n) = \sum_m \underbrace{\left(\sum_n \mathcal{L}_{nm} \right)}_{=0} P_t(c_m) = 0$$

meaning that the sum over each column of \mathcal{L} is zero. Moreover, the real parts of all right eigenvalues of \mathcal{L} have to be smaller or equal to zero to ensure stability. That can easily be seen if one decomposes P_t using the right eigenstates of \mathcal{L} . A positive eigenvalue leads to an exponential growing term that, in turn, violates the normalization condition. Also due to the conservation of probability, the Master equation guarantees the existence of at least one stationary probability distribution \mathbf{P}_∞ that fulfills $\mathcal{L} \mathbf{P}_\infty = 0$.

In equilibrium, \mathbf{P}_∞ can, potentially under constraints set by conservation laws, be directly deduced from the principle of entropy maximization. In practice, an equilibrium distribution can be generated with an update scheme that satisfies detailed balance, i.e. $\Gamma_{n \rightarrow m} P_t(c_n) = \Gamma_{m \rightarrow n} P_t(c_m)$, in each evolution step. The precise details of the implementation might not be important as long as detailed balance is fulfilled. That is why, for example, in the case of the Ising model, different numerical methods like the Metropolis algorithm or the Glauber update scheme lead to the correct equilibrium distribution. The physical statement of the detailed balance relation is that all probability currents vanish. This is a hallmark of equilibrium. In contrast to that, out of equilibrium, detailed balance is in general not valid and steady states with stationary probability currents exist. In fact, one class of stationary non-equilibrium systems are characterized by the compensation of fluxes (heat, particle, ...) that are driven

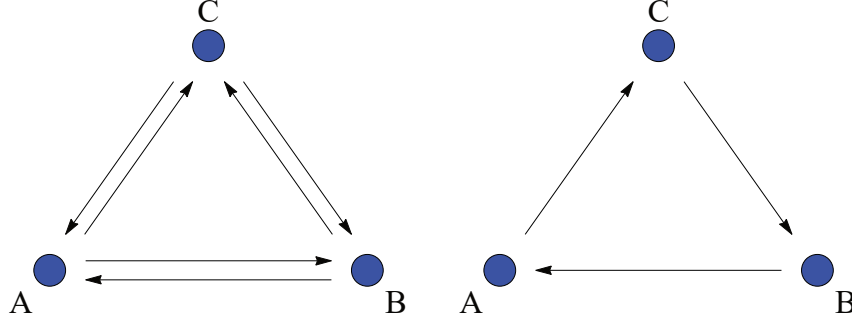


Figure 1.3 Schematic sketch of a $0+1$ dimensional system with three possible states A, B, C . Left: all transition rates are equal and detailed balance is fulfilled leading to a thermal state in which no currents are present. Right: detailed balance is violated and a steady state with non-vanishing currents establishes.

by dissipation and external pumping. As an example we consider the situation depicted in Fig. 1.3 which was, for example, also presented in [71]. Transitions between three possible states A, B and C with rates $\Gamma_{A \rightarrow B} = \Gamma_{B \rightarrow A}$, $\Gamma_{B \rightarrow C} = \Gamma_{C \rightarrow B}$, $\Gamma_{C \rightarrow A} = \Gamma_{A \rightarrow C} = \Gamma$ (left) and $\Gamma_{B \rightarrow A} = \Gamma_{A \rightarrow C} = \Gamma_{C \rightarrow B} = \Gamma$ (right) are given. In both situations the stationary probability distribution is $p_A = p_B = p_C = 1/3$. However, in the first case, detailed balance is fulfilled meaning that an equilibrium configuration is reached while the second case lacks detailed balance leading to a steady state with a stationary current $|J_{AB}| = |J_{BC}| = |J_{CA}| = \Gamma/3$ between two states.

1.3.1 Markovian master equation

In this section, we review briefly how to derive an effective description for the time evolution of an open subsystem S coupled to an environment B . We mainly follow reference [2] which gives a very detailed introduction to the topic. Firstly, we assume that the whole system is closed and its dynamics is unitary. Moreover, we split the Hamiltonian H of the system into one part acting on the system of interest S , one acting on the bath B and one that couples the degrees of freedom of S and B

$$H = H_S + H_B + H_{SB}. \quad (1.37)$$

The time evolution of the density matrix is governed by the von Neumann equation $\partial_t \rho(t) = -i[H, \rho(t)]$. To derive an effective description for the time evolution of the reduced density matrix ρ_S , we trace out the bath degrees of freedom yielding

$$\begin{aligned} \partial_t \rho_S(t) &= -i \text{Tr}_B [[H_{SB}, \rho(t)]] \\ &= - \int_0^t ds \text{Tr}_B [[H_{SB}(t), [H_{SB}(s), \rho(s)]]] \end{aligned} \quad (1.38)$$

where we have used the interaction picture representation and the assumption $\text{Tr}_B[H_{SB}(t), \rho(0)] = 0$. This expressions can be simplified if the following three approximations are made.

- The *Born approximation* assumes that the influence of the system on the bath is small. As a result, the density matrix of the bath ρ_B is only weakly affected by the interaction with the reduced system and the total density matrix factorizes $\rho(t) = \rho_S(t) \otimes \rho_B$.
- The *Rotating-wave (secular) approximation* assumes that highly oscillating terms in Eq. (1.38) that change on a timescale $\tau_s \sim 1/|\omega - \omega'|$, where ω, ω' ($\omega \neq \omega'$) are typical energy scales of the system S , can be neglected. This is justified if the timescale τ_s is much smaller than the typical relaxation time scale of the reduced open system τ_R .
- The *Markov approximation* assumes that environmental excitations decay fast on a time scale τ_B compared to the timescale τ_R on which the reduced open system varies significantly. Thus, in a coarse-grained picture, the bath does not keep any memory of the configuration of the system. As a consequence of this approximation, the time evolution of the reduced system is not unitary anymore but only Markovian, i.e. the dynamics depends only on the current configuration and not on the past.

Using these approximations the *Markovian master equation (Lindblad equation)* finally reads in the Schrödinger picture

$$\partial_t \rho_S(t) = \mathcal{L} \rho_S(t) = -i[H, \rho_S(t)] + \hat{\mathcal{D}}[\rho_S(t)], \quad (1.39)$$

$$\hat{\mathcal{D}}[\rho_S(t)] = \sum_{\alpha} L_{\alpha} \rho_S(t) L_{\alpha}^{\dagger} - \frac{1}{2} \{L_{\alpha}^{\dagger} L_{\alpha}, \rho_S(t)\},$$

where the coupling to the bath is encoded in the so-called *Lindblad operators* L_{α} . The Liouville superoperator $\hat{\mathcal{D}}$ (*Lindbladian*, Lindblad dissipator) preserves hermicity, positivity and the trace of $\rho(t)$ at all times. It describes dissipative processes. The dynamics generated by $\hat{\mathcal{D}}$ can be viewed as those governed by an anti-hermitian Hamiltonian $H^{-} := -\frac{i}{2} \sum_{\alpha} L_{\alpha}^{\dagger} L_{\alpha}$. If we decompose the total Hamiltonian into $H_{tot} = H + H^{-}$, we obtain with $\rho_S(t) = e^{-i(H+H^{-})t} \rho_S(0) e^{i(H-H^{-})t}$,

$$\begin{aligned} \partial_t \rho_S(t) &= -i [(H + H^{-}) \rho_S(t) - \rho_S(t) (H - H^{-})] \\ &= -i[H, \rho_S(t)] - i\{H^{-}, \rho_S(t)\} \\ &= -i[H, \rho_S(t)] - \frac{1}{2} \sum_{\alpha} \{L_{\alpha}^{\dagger} L_{\alpha}, \rho_S(t)\} \end{aligned}$$

which is identical to Eq. (1.39) up to the term $\sum_{\alpha} L_{\alpha} \rho(t) L_{\alpha}^{\dagger}$ that has to be added to ensure conservation of probability. In the following, we drop the index S and denote the density matrix of the reduced system simply by ρ .

1.3.2 Floquet theory

Floquet theory deals with the dynamics of periodically driven systems whose Hamiltonians $H(t)$ fulfill

$$H(t) = H(t+T), \quad T = \frac{2\pi}{\Omega} \quad (1.40)$$

where Ω is the driving frequency. In analogy to the Bloch theorem for systems with a discrete spatial translation symmetry, the Floquet theorem specifies the form of the eigenvalues and eigenstates of a Hamiltonian in the presence of a discrete translational symmetry in time. Here, we present some of the basic ideas of Floquet theory. Note that this section is based on [72, 73]. In order to derive the Floquet theorem, we start from the Schrödinger equation, Eq. (1.1) that is formally solved by $|\psi(t)\rangle = U(t)|\psi(0)\rangle$. It is convenient to introduce the so-called *Floquet Hamiltonian*

$$H^F(t) = H(t) - i\partial_t$$

which is also a hermitian operator and periodic in time. The Floquet Hamiltonian commutes with the so-called *Floquet operator* $U^F(t) := U(t+T)$ that translate a state by one period T ,

$$U^F(t)H^F(t) = U^F(t)H^F(t)(U^F(t))^{-1}U^F(t) = H^F(t+T)U^F(t) = H^F(t)U^F(t).$$

Therefore, one can find a common eigenbasis $\{|\psi_\nu(t)\rangle\}$ of $H^F(t)$ and $U^F(T)$, where ν labels all possible quantum numbers of the state $|\psi_\nu\rangle$. As $U^F(t)$ is a unitary operator, the corresponding eigenvalue equations are of the form

$$U^F(t)|\psi_\nu(t)\rangle = e^{-i\phi_\nu(T)}|\psi_\nu(t)\rangle. \quad (1.41)$$

Due to Eq. (1.40), the Floquet operator satisfies $U^F(nT) = (U^F(T))^n$. Hence, the eigenvalues of $U^F(t)$ fulfill the relation $e^{-i\phi_\nu(nT)} = (e^{-i\phi_\nu(T)})^n$. It follows that the phase $\phi_\nu(T)$ is linear in T and can be written as $\phi_\nu(T) = \varepsilon_\nu T$ where $\varepsilon_\nu \in \mathbb{R}$ is called *quasienergy*. The quasienergies are only defined up to integer multiples of Ω . By diagonalizing the Floquet operators at all times, Eq. (1.41) can formally be solved. However, it turns out that this is in most cases not really practical due to the time-ordering operator $\hat{\mathcal{T}}$ appearing in the formula of $U^F(t)$. An alternative approach is the following: The eigenstates of the Floquet operator can be rewritten as

$$|\psi_\nu(t)\rangle = e^{-i\varepsilon_\nu t}|\phi_\nu(t)\rangle, \quad (1.42)$$

where the so-called *Floquet states* $|\phi_\nu(t)\rangle$ are periodic in time,

$$|\phi_\nu(t+T)\rangle = e^{i\varepsilon_\nu(t+T)}|\psi_\nu(t+T)\rangle = e^{i\varepsilon_\nu(t+T)}U^F(t)|\psi_\nu(t)\rangle = e^{i\varepsilon_\nu t}|\psi_\nu(t)\rangle = |\phi_\nu(t)\rangle.$$

Inserting the Floquet state Eq. (1.42) into the Schrödinger equation yields the eigenvalue equation

$$H^F(t) |\phi_\nu(t)\rangle = \varepsilon_\nu |\phi_\nu(t)\rangle. \quad (1.43)$$

The advantage of Eq. (1.43) is that the eigenvalues ε_ν are time-independent while the Floquet states $|\phi_\nu(t)\rangle$ are periodic in time with period T . For a given solution $|\psi_\nu(t)\rangle$ with Floquet state $|\phi_\nu(t)\rangle$ and quasienergy ε_ν an identical solution $|\psi_{\nu'}(t)\rangle = |\psi_\nu(t)\rangle$ with $|\phi_{\nu'}(t)\rangle = e^{-in\Omega t} |\phi_\nu(t)\rangle$ ($n \in \mathbb{Z}$) can be found where the corresponding quasienergy $\varepsilon_{\nu'} = \varepsilon_\nu - n\Omega$ is shifted by $n\Omega$. Thus, for each solution with quantum number ν an infinite set of Floquet copies exists.

Similar to the dispersion relation in systems with a discrete translation symmetry, the quasienergy spectrum consists of bands in different Floquet sectors which we label by n . The band structure within one sector repeats when shifted by an integer multiple of Ω . For convenience one can choose the sector with $-\Omega/2 < \varepsilon_\nu < \Omega/2$ as a physical reference. Even though there is an analogy between a translation symmetry in space and time, there is also a crucial difference. While the space coordinate is an operator in quantum mechanics, time is not. In lattice systems that have a discrete translational symmetry in space, one finds an infinite number of physical electronic bands. In contrast to that, the number of physical bands in Floquet systems is finite with an infinite number of replicas.

Generally, any quantum state $|\Psi(t)\rangle$ can be written as a linear combination of Floquet eigenstates

$$|\Psi(t)\rangle = \sum_{\nu} c_{\nu} e^{-i\varepsilon_{\nu} t} |\phi_{\nu}(t)\rangle = \sum_{\nu, n} c_{\nu} e^{-i(\varepsilon_{\nu} + n\Omega)t} |\phi_{\nu}^n\rangle$$

where we have defined $c_{\nu} = \langle \phi_{\nu}(0) | \Psi(0) \rangle$ and used the Fourier decomposition $|\phi_{\nu}(t)\rangle = \sum_n e^{-in\Omega t} |\phi_{\nu}^n\rangle$. Often, it is convenient to interpret the states $|\phi_{\nu}^n\rangle$ as components of an infinitely large vector $|\phi_{\nu}\rangle = (\dots, |\phi_{\nu}^{-1}\rangle, |\phi_{\nu}^0\rangle, |\phi_{\nu}^1\rangle, \dots)^T$ that lives in the extended Hilbert space $\mathcal{F} = \mathcal{H} \otimes \mathcal{T}$. Here, \mathcal{H} is the physical Hilbert space and \mathcal{T} denotes the Hilbert space of all square-integrable periodic functions with period T . A scalar product in the extended Hilbert space \mathcal{F} can be defined through

$$\langle\langle \phi | \psi \rangle\rangle := \frac{1}{T} \int_0^T \langle \phi(t) | \psi(t) \rangle dt. \quad (1.44)$$

The components of an operators $\tilde{O} : \mathcal{F} \rightarrow \mathcal{F}$ are given by

$$\tilde{O}_{nm} = \frac{1}{T} \int_0^T e^{in\Omega t} O(t) e^{-im\Omega t}, \quad (1.45)$$

where \tilde{O}_{nm} and $O(t)$ act on the physical Hilbert space \mathcal{H} . For the Floquet Hamiltonian $\tilde{H}^F : \mathcal{F} \rightarrow \mathcal{F}$ we obtain

$$\begin{aligned} \tilde{H}_{nm}^F &= \frac{1}{T} \int_0^T dt e^{in\Omega t} (H(t) - i\partial_t) e^{-im\Omega t} \\ &= H_{n-m} - m\Omega \delta_{nm} \mathbb{1} \end{aligned} \quad (1.46)$$

with

$$H_n = \frac{1}{T} \int_0^T dt e^{in\Omega t} H(t) = H_{-n}^\dagger. \quad (1.47)$$

The Hilbert space \mathcal{F} is infinite dimensional. However, for practical purposes, the number of Floquet zones $2N_f + 1$ can be truncated if the condition $\Omega N_f \gg E_{max}$ is met guaranteeing the validity of the Floquet ansatz [74]. Here, E_{max} denotes the energy scale of the unperturbed Hamiltonian H_0 when using the decomposition $H(t) = H_0 + \Delta H(t)$ ($\Delta H(t+T) = \Delta H(t)$). By diagonalizing the truncated matrix \tilde{H}^F for $n \in \{-N_f, \dots, 0, \dots, N_f\}$ one obtains the quasienergies ε_ν and eigenstates $|\phi_\nu^n\rangle$ which can then, in turn, be used to determine $|\phi_\nu(t)\rangle$ and $|\psi_\nu(t)\rangle$.

Due to periodic driving, the expectation value of the Hamiltonian $\langle H(t) \rangle_\psi$ acquires an explicit time dependence. It is important to note that energy is only conserved when the Hamiltonian commutes with itself at different times, $[H(t), H(t')] = 0$. Consequently, if this condition is not met, the steady state that maximizes entropy without any constraints set by conservation laws is expected to be the trivial state. The more physical picture is that in the presence of interactions, periodic driving provides a channel through which the system can constantly absorb energy. Therefore, it is commonly believed that generic interacting quantum systems, which are periodically driven and not coupled to a thermal bath, heat up to an infinite temperature state in the long-time limit $t \rightarrow \infty$ [75, 76].

This observation can again be explained with the help of the ETH. We consider the case that the typical magnitude of the driving term δ_d is much larger than the width of the Floquet zone such that a broadband of eigenstates $|n\rangle$ of the bare Hamiltonian H_0 contribute to each Floquet state $|\phi_\nu(t)\rangle$. For the expectation value of an observable $O(t)$, we find using the ETH assumption

$$\begin{aligned} \langle O(t) \rangle &\xrightarrow{t \rightarrow \infty} \sum_\nu |c_\nu|^2 \langle \phi_\nu(t) | O | \phi_\nu(t) \rangle \approx \sum_\nu |c_\nu|^2 \sum_{nn'} \alpha_\nu^n(t) \alpha_\nu^{n'*}(t) \langle n | O | n' \rangle \\ &\approx \sum_\nu |c_\nu|^2 \frac{1}{D_{\mathcal{H}}} \sum_{nn'} e^{i(\varphi_\nu^n(t) - \varphi_\nu^{n'}(t))} \langle n | O | n' \rangle \approx \sum_\nu |c_\nu|^2 \frac{1}{D_{\mathcal{H}}} \sum_n \langle n | O | n \rangle \\ &= \frac{1}{D_{\mathcal{H}}} \sum_n \langle n | O | n \rangle = \frac{1}{D_{\mathcal{H}}} \text{Tr}[O \mathbb{1}]. \end{aligned}$$

where we have used $\sum_\nu |c_\nu|^2 = 1$ and assumed that $\alpha_\nu^n(t) = \langle \phi_\nu(t) | n \rangle \approx 1/\sqrt{D_{\mathcal{H}}} \exp(i\varphi_\nu^n(t))$ with uncorrelated phases $\varphi_\nu^n(t)$. Here, $D_{\mathcal{H}}$ denotes the dimension of the Hilbert space. From this argument we can deduce that the steady state density matrix in the long-time limit is given by the trivial operator $\mathbb{1}$ or the infinite temperature state, thus a thermal state $\sim e^{-\beta H}$ with $\beta = 1/T \rightarrow 0$ ($T \rightarrow \infty$).

1.4 Phase transitions

1.4.1 Equilibrium phase transitions

Matter in equilibrium can exist in different phases depending on an external set of parameters. A real world example is water which exists in a liquid phase at room temperature, is a solid below 0°C and a

gas above 100°C at atmospheric pressure. The existence of different phases can be understood with the help of thermodynamic potentials like the Helmholtz free energy that is defined by

$$F(T, V) = E(T, V) - T S(T, V),$$

where E is the energy, T the temperature, V the volume and S the entropy of the system considered. In equilibrium a system is in a state that minimizes the free energy. At small temperatures, this state can be ascertained by minimizing the energy typically leading to an ordered state in the presence of interactions, while at high temperatures where thermal fluctuations are strong, a large entropy minimizes F , which corresponds to a disordered state. At some critical temperature T_c there is a transition between these two phases.

The presence of phases and the transition between them that occur at a critical point in parameter space can theoretically be described by an order parameter. Typically, the order parameter is zero in one phase and non-zero in the other one. For instance, in the case of the liquid gas transition, the difference between the density of the system and the density in the liquid phase can be used as an order parameter. Transitions between phases can be classified according to the behavior of the order parameter at the critical point. If the order parameter jumps, one speaks of a discontinuous first order phase transition while otherwise the transition is referred to be continuous. In the liquid gas transition, gas droplets can form in the liquid phase when the temperature is close to T_c ($T < T_c$). During the formation (growing, shrinking, nucleation) process of these droplets, the temperature does not increase when more energy is pumped into the system as all of the added latent heat is used to dissolve molecular bonds in the fluid. In a certain parameter regime the fluid and gas phase coexist. The occurrence of such a coexistence regime as well as the exchange of latent heat are both characteristic of a first order phase transition.

At a phase transition the properties of matter can change dramatically. For instance, a fluid has a continuous translation symmetry while a solid is only invariant under discrete translations. One says the continuous translation symmetry of the liquid is spontaneously broken at the transition point. This is an emergent phenomenon that only occurs when many particles come together. A single particle does not undergo a phase transition or show spontaneous symmetry breaking.

A well-known example of an equilibrium phase transitions in magnetic systems is the paramagnet ferromagnet transition of the Ising model in dimensions $d \geq 2$. The model describes spins with two degrees of freedom on a discrete lattice which interact with their nearest neighbors through their relative alignment. The Hamiltonian of the model reads $H = J \sum_{\langle i, j \rangle} S_i^z S_j^z$ where $\langle i, j \rangle$ denotes nearest neighbors. In the ferromagnetic version of the model ($J < 0$), a parallel alignment of adjacent spins is energetically favored while for antiferromagnetic coupling ($J > 0$), neighboring spins are anti-aligned in the ground state. For strong thermal fluctuations, the system is in a disordered paramagnetic phase where the magnetization per site, being the order parameter of this transition, is zero. Below the critical temperature, a finite magnetization builds up and the discrete \mathbb{Z}_2 -symmetry of the model is spontaneously broken as one of the two stable configurations is chosen. Thus, the system is in a

state that has a lower symmetry than the underlying model. The transition is continuous which is characterized by the power-law divergence of the spin-spin correlation length ξ ,

$$\xi \sim |T - T_c|^{-\nu},$$

accompanied by the divergence of further thermodynamic response quantities, for example, specific heat $C_V \sim |T - T_c|^{-\alpha}$ and compressibility $\kappa \sim |T - T_c|^{-\gamma}$. Importantly, for a continuous phase transition, the so-called critical exponents $\alpha, \gamma, \nu, \dots$ are independent of the precise details of the model but are only determined by the symmetries and the dimension of the system. This property is called universal and transitions are classified according to their critical behavior in so-called *universality classes*. For instance, phase transitions having the same critical exponents like the Ising transition are commonly referred to as Ising-like transitions. The reason for universal behavior close to the critical points is the divergence of the correlation length that becomes much larger than all length scales of the system. Therefore, the precise details of the model average out and it is, typically, sufficient to treat a continuous phase transition with an effective approach as Landau theory.

The development of the *Renormalization Group theory* (RG) also allowed to investigate theoretically the dynamics close to a critical point. Considering the relaxation time τ of a time-dependent correlation function one can introduce a further critical exponent z ,

$$\tau \sim \xi^z$$

describing the critical slowing down in the vicinity of the critical point. The classification of the dynamics of classical equilibrium phase transitions goes mainly back to Hohenberg and Halperin [77]. In their classification scheme, a transition is classified according to the number of slow modes coupled to the order parameter and is labeled alphabetically starting from model A for systems with no additional conservation laws.

In quantum mechanical models, equilibrium transitions between different phases can also occur at zero temperature when tuning an intrinsic parameter of the Hamiltonian such as interaction strength across a critical value. At this point, the structure of the energy spectrum changes significantly, i.e. an energy gap closes or opens. Due to the absence of thermal fluctuations at $T = 0$, these transitions are only driven by quantum fluctuations. Generically, the phase diagram of a continuous *quantum phase transition* shows an ordered phase below and a quantum disordered state above the quantum critical point (QCP) [27]. At sufficiently small temperatures where quantum fluctuations are still dominating compared to thermal fluctuations, there is a quantum critical region while at high temperatures, the system is classically disordered. Examples of quantum phase transitions are the Mott insulator superfluid [78] and the superconductor insulator transition [79]. Practically, the $T = 0$ state cannot be reached and therefore a pure quantum phase transition cannot be realized in experiments. However, at low temperatures where quantum fluctuations become relevant, the theory of quantum

phase transitions can still give an insight into the physics of a system at the critical point.

1.4.2 Non-equilibrium phase transitions

So far we only considered phase transitions in equilibrium. However, phase transitions can also occur in non-equilibrium systems. Examples of classical non-equilibrium transitions are traffic jams [80] and morphology transitions in growing surfaces [81]. As continuous phase transitions in equilibrium, continuous non-equilibrium phase transitions can be classified according to their universal behavior at the transition point. However, their classification is much less understood than their equilibrium counterparts. A further complexity arises due to the fact that time is an additional degree of freedom [71].

Comparable to the Ising universality class in equilibrium systems, the so-called class of directed percolation plays a prominent role in the context of non-equilibrium phase transitions. It features transitions to an absorbing state that can be reached by the dynamics but not be left by it. For example, models describing the spreading of diseases in a population, fire in a forest or water in a porous medium fall into this class. In the latter example, water can propagate through small pores modeled by bonds of a lattice. These bonds can be open with a probability p allowing water to pass or closed with probability $1 - p$. In the case of directed percolation, there is an additional force (for example a gravitational force) distinguishing one specific direction. If p is smaller than a critical value p_c , the medium is impermeable for the water. At $p > p_c$ it becomes permeable [71].

In the context of non-equilibrium quantum phase transitions, it is often useful to map the quantum dynamics onto classical stochastic processes [82]. The mapping yields the time evolution of operators or expectation values in terms of solutions of classical *stochastic differential equations* (SDEs). Typically, the stochastic dynamics enters the deterministic Heisenberg equation of motion when integrating out fast bath degrees of freedom for a given coupling to an environment. If there are two or more stable or meta-stable solutions of the SDE, transition can occur. Within this description, they can be detected by determining characteristic changes of the probability distribution P as a function of the noise strength. If these changes are accompanied by true symmetry breaking, the transition is referred to as *noise induced phase transition* [83].

In the context of dynamical systems and non-equilibrium phase transitions, the theory of bifurcations plays a very important role. A bifurcation is a qualitative change in the structure of solutions of a dynamical system at a critical point in parameter space. Such a change could, for example, be the emergence of new stable or meta-stable states or the change of the stability of a given state when, for example, the interaction or the driving strength is tuned across a particular value. Similarly to the closure of the spectral gap in Hamiltonian systems, a non-equilibrium phase transition formulated in the language of Liouvillians is signaled by the closure of the Liouvillian gap.

1.5 Numerical methods

1.5.1 Exact diagonalization

As most of the numerical studies of one-dimensional 1/2-spin chains within this thesis are based on *exact diagonalization* (ED), we give a short overview of the topic that follows closely [84]. ED is a numerical method yielding the eigenstates $\{|n\rangle\}$ and corresponding eigenvalues $\{\lambda_n\}$ of a given Hamiltonian H acting on a finite-dimensional Hilbert space. With this information, any quantity of interest can be calculated. Particularly, the dynamics of an arbitrary initial state $|\psi(0)\rangle$ under the Hamiltonian is determined solely by the eigenvalues λ_n and eigenstates $|n\rangle$,

$$|\psi(t)\rangle = e^{-iHt} |\psi(0)\rangle = \sum_n e^{-iHt} |n\rangle \underbrace{\langle n|\psi(0)\rangle}_{=\alpha_n} = \sum_n \alpha_n e^{-i\lambda_n t} |n\rangle.$$

While ED is numerically exact, it is, on the contrary, also limited to very small systems as the Hilbert space grows exponentially with system size. In order to obtain ground states, excitation energies and correlation functions for larger systems, more sophisticated methods like the Lanczos algorithm or t-DMRG have to be applied. In higher dimensions, thermodynamic quantities can be calculated using Monte Carlo based approaches. However, these methods have their own limitations and do not solve the system completely.

At the beginning of an ED analysis, a basis of the finite size Hilbert space has to be chosen where it is often useful to start with a representation in position space. As an example, we consider a one-dimensional spin-1/2 chain on a lattice with N sites. Each spin can be in a $+1$ ($|\uparrow\rangle$) or -1 ($|\downarrow\rangle$) state with respect to a chosen axis. For convenience, we choose the z -axis as a reference. A basis state in the position basis can then be written as a permutation of N zeros and ones as $|1010\dots 01\rangle$ where 0 or 1 at position i denotes a spin down or spin up state at lattice site i , respectively. For N sites, where we assume N to be even in the following, the size of the Hilbert space is 2^N and therefore exponentially large in N . As a consequence, only very tiny systems of size $N \sim 12 - 14$ can be calculated on conventional computers. This is mainly due to the limitation of memory. To reach bigger system sizes, symmetries of the Hamiltonian have to be exploited. By choosing a convenient basis that takes account of these symmetries, the complexity of the ED method can be reduced significantly. A quantum mechanical system is invariant under a symmetry transformation S , if $SHS^{-1} = H$ holds. In the case of a continuous symmetry transformation, Noether's theorem states that S is associated with a conservation law C which commutes with H , $[H, C] = 0$. Therefore, there is a common eigenbasis of C and H . We have

$$HC|n\rangle = CH|n\rangle = \lambda_n C|n\rangle \quad (1.48)$$

i.e., if $C|n\rangle \neq 0$, $C|n\rangle$ is an eigenstate of H with the same eigenvalue as $|n\rangle$. There are two cases:

- In case λ_n is nondegenerate, we have $C|n\rangle = c|n\rangle$ where c is a constant factor. Thus, $|n\rangle$ is a common eigenstate of H and C .
- In case λ_n is m times degenerate, there are m eigenvectors $\{|n_i\rangle\}$ ($i = 1, \dots, m$) associated with λ_n . Since $C|n_i\rangle$ is an eigenstate with eigenvalue λ_n , it can be written as a linear combination of elements of $\{|n_i\rangle\}$. Therefore, C acts only in the subspace spanned by $\{|n_i\rangle\}$ and does not couple eigenstates of H with different eigenvalues. If one chooses a basis in which the degenerate eigenstates belonging to an eigenvalue λ_n are grouped, the Hamiltonian becomes block-diagonal in this basis.

The most convenient symmetries of a XXZ model with periodic boundary conditions are rotations around the z -axis in spin space as well as discrete translations in real space. Associated with these symmetry transformations are the conservation of the z -component of the total spin as well as the conservation of lattice momentum. While the conservation of lattice momentum directly follows from the discrete translation invariance of the system, the conservation of S^z can be easily read off from Eq. (1.21). The only process in the Hamiltonian that connects different states, flips two adjacent spins if they point in different directions. However, this exchange does not change the total number of spins pointing up and down and therefore conserves S^z . The S^z conservation can be straightforwardly incorporated into the ED analysis by ordering the basis states according to their magnetization in z -direction. Then the Hamiltonian written in this ordered basis decouples into $N + 1$ subblocks that can be diagonalized separately. The size of a block with magnetization M is

$$\frac{N!}{\left(\frac{N+2M}{2}\right)! \left(\frac{N-2M}{2}\right)!} \quad (1.49)$$

which can be much smaller than 2^N . Therefore, by ordering the position basis properly, larger systems with about $N \sim 16 - 18$ sites can be calculated. The numerical effort can be further reduced by decomposing each magnetization subblock into N blocks with fixed momentum. To do so, we introduce the translation operator T that shifts a state by one site. We define T by $(T|\psi\rangle)_i = |\psi\rangle_{i-1}$ where $|\psi\rangle$ is a basis state in position representation and the label i refers to the spin at lattice site i . The eigenstates of the translation operator can be written as

$$|R(k)\rangle = \frac{1}{\sqrt{N_R}} \sum_{j=0}^{N-1} e^{-ikj} T^j |R\rangle, \quad (1.50)$$

where $\sqrt{N_R}$ denotes the normalization constant and $|R\rangle$ is a representative for all position basis states that only differ by translations. A unique way to define the representative $|R\rangle$ is to choose the basis state that corresponds to the smallest binary number when the state is expressed as a permutation of

ones and zeros. The eigenvalues of $|R(k)\rangle$ can be calculated as

$$T|R(k)\rangle = \frac{1}{\sqrt{N_R}} \sum_{j=0}^{N-1} e^{-ikj} T^{j+1}|R\rangle = \frac{1}{\sqrt{N_R}} \sum_{j=1}^N e^{-ik(j-1)} T^j|R\rangle = e^{ik}|R(k)\rangle. \quad (1.51)$$

Since $T^N|R\rangle = |R\rangle$, we can conclude that $e^{-ikN} = 1$. Hence, the possible values of k can be selected as follows

$$k = \frac{2\pi}{N}n \quad (n = 0, \dots, N-1).$$

The allowed momenta and the normalization constant N_R of a representative state $|R\rangle$ depend on its periodicity p_R . If a representative state $|R\rangle$ is periodic with periodicity p_R , it holds $|R\rangle = T^{p_R}|R\rangle$ and the total weight of such a state becomes

$$1 + e^{-ikp_R} + e^{-2ikp_R} + \dots + e^{-ik(N-p_R)}. \quad (1.52)$$

This sum vanishes unless the momentum fulfills the condition $kp_R = 2\pi m$ where m is an integer number. Then the total weight is N/p_R and the normalization constant can be read off

$$\begin{aligned} \langle R(k)|R(k)\rangle &= \frac{1}{N_R} p_R \left(\frac{N}{p_R} \right)^2 \stackrel{!}{=} 1 \\ \Rightarrow \quad N_R &= \frac{N^2}{p_R}. \end{aligned}$$

The general protocol to define the new momentum basis is to first identify all representative states and possible momenta in each magnetization subblock and then order all allowed states $|R(k)\rangle$ according to their momenta. As a consequence, each magnetization subblock decouples again into N subblocks. To calculate the matrix elements within a momentum subblock with momentum k , we apply H onto a momentum eigenstate $|R(k)\rangle$,

$$H|R(k)\rangle = \frac{1}{\sqrt{N_R}} \sum_{r=0}^{N-1} e^{-ikr} T^r H|R\rangle = \frac{1}{\sqrt{N_R}} \sum_{j=0}^{N-1} \sum_{r=0}^{N-1} e^{-ikr} T^r H_j|R\rangle$$

where we have used that $H = \sum_j H_j$ can be written as a sum of local densities and $[H, T] = 0$. The operator H_j maps the state $|R\rangle$ onto a new state that is assumed to be shifted by s_j from a representative

state $|R'_j\rangle$ and proportional to a complex number h_j^R ,

$$H|R(k)\rangle = \frac{1}{\sqrt{N_R}} \sum_{j=0}^{N-1} \sum_{r=0}^{N-1} e^{-ikr} T^{(r-s_j)} h_j^R |R'_j\rangle = \sum_{j=0}^{N-1} \sqrt{\frac{N_{R'_j}}{N_R}} e^{-iks_j} h_j^R |R'_j(k)\rangle$$

$$\Rightarrow \langle R'_j(k)|H|R(k)\rangle = \sqrt{\frac{N_{R'_j}}{N_R}} e^{-iks_j} h_j^R.$$

Using the conservation of the total magnetization in z -direction and the conservation of momentum allows us to calculate systems of size $N \sim 20$.

In this thesis ED is, for example, used to determine the common eigenbasis and corresponding eigenvalues of the spin-1/2 XXZ model $C_2 = H_{XXZ}$ and its mutually commuting local conserved charges C_i . Due to degeneracies in the spectrum of H_0 , the common eigenbasis is not unique and the eigenbasis of $\sum_{i=1}^{N_c} C_i$ ($1 \leq N_c \leq N$) is, in general, not an eigenbasis of all charges C_i . However, we find numerically that diagonalizing $\sum_i \xi_i C_i$ with uniformly distributed random numbers ξ_i instead, indeed yields the desired common eigenbasis.

The limitation of ED becomes even more apparent if one goes from closed to open systems and from unitary to non-unitary dynamics. Then not a Hamiltonian but a Liouville superoperator has to be diagonalized to completely determine the dynamics of the system for given initial conditions. While the Hamiltonian acts on states and has dimension 2^{2N} , the Liouville superoperator acts on density matrices and has dimension 2^{4N} . Thus, in the case of open dissipative systems, only spin chains of size $N \sim 6$ can be treated on conventional computers without employing additional symmetries.

1.5.2 Numerical integration of stochastic differential equations

In this section we review how *stochastic differential equation* can be solved numerically. As a reference we use [85]. We consider a stochastic differential equation of the form

$$\frac{dy_i}{dt} = A_i(\mathbf{y}, t) + \sum_k B_{ik}(\mathbf{y}, t) \xi_k(t), \quad (1.53)$$

where $\mathbf{y} = (y_1, \dots, y_n)$ are the dynamical variables of the system and ξ_k are random variables drawn from a Gaussian white noise distribution that fulfill

$$\langle \xi_i(t) \rangle_{\xi} = 0,$$

$$\langle \xi_i(t) \xi_j(t') \rangle_{\xi} = \sigma^2 \delta_{ij} \delta(t - t').$$

Here, $\langle \cdot \rangle_{\xi}$ denotes an average over noise realizations and the term white refers to the fact that the noise-noise correlation function is frequency and momentum independent. If the function $B_{ik}(\mathbf{y}, t)$ depends on \mathbf{y} , the noise is called multiplicative and otherwise additive. A differential equation of the

form Eq. (1.53) without noise term can be solved directly using a discrete integration scheme with a finite integration step Δt . However, since the noise causes discontinuous jumps in the dynamics, the values of y_i and consequently also of B_{ik} are not defined during single noise kicks. Therefore, it is a priori not clear where the non-smooth function B_{ik} has to be evaluated. There are two prevailing interpretations. Typically, in physics, the Stratonovich interpretation is favored where B_{ik} is evaluated at the mean of $y(t)$ and $y(t + \Delta t)$ leading to

$$y_i(t + \Delta t) = y_i(t) + A_i(\mathbf{y}(t), t) \Delta t + \sum_k B_{ik} \left(\frac{\mathbf{y}(t) + \mathbf{y}(t + \Delta t)}{2}, \frac{t + \Delta t}{2} \right) \int_t^{t + \Delta t} \xi(t') dt'.$$

For Stratonovich integrals, the usual rules of calculus apply. In the Ito interpretation B_{ik} is evaluated at a time t before the jump. This yields

$$y_i(t + \Delta t) = y_i(t) + A_i(\mathbf{y}(t), t) \Delta t + \sum_k B_{ik}(\mathbf{y}(t), t) \int_t^{t + \Delta t} \xi(t') dt'.$$

Note that the Ito interpretation involves transformations that require new rules of calculus referred to as Ito calculus [86]. The choice of the interpretation is not solely a technical question as both methods can lead to different solutions of a stochastic differential equation. One language can be translated into the other one by adding a drift term to Eq. (1.53). In the case of purely additive noise, both interpretations lead to the same results. The simplest choice for a numerical integration method is the *Euler scheme* which reads in the Ito language

$$y_i^{(n+1)} = y_i^{(n)} + A_i(\mathbf{y}^{(n)}, t^{(n)}) (t^{(n+1)} - t^{(n)}) + \sum_k B_{ik}(\mathbf{y}^{(n)}, t^{(n)}) (\xi_k^{(n+1)} - \xi_k^{(n)}),$$

where the random increment $\Delta \xi^n(t) := \xi_k^{(n+1)} - \xi_k^{(n)}$ has the properties

$$\begin{aligned} \langle \Delta \xi_i^{(n)} \rangle_\xi &= 0 \\ \langle (\Delta \xi_i^{(n)})^2 \rangle_\xi &= \sigma^2 \Delta t^{(n)}. \end{aligned}$$

In general, it is difficult to derive higher-order integration schemes for stochastic differential equations. However, the Euler method can be straightforwardly improved by using the mean values of A_i and B_{ik} in the time interval $(t^{(n)}, t^{(n+1)})$,

$$\begin{aligned} y_i^{(n+1)} &= y_i^{(n)} + \frac{1}{2} \left(A_i(\mathbf{y}^{(n)}, t^{(n)}) + A_i(\tilde{\mathbf{y}}^{(n+1)}, t^{(n+1)}) \right) (t^{(n+1)} - t^{(n)}) \\ &\quad + \sum_k \frac{1}{2} \left(B_{ik}(\mathbf{y}^{(n)}, t^{(n)}) + B_{ik}(\tilde{\mathbf{y}}^{(n+1)}, t^{(n+1)}) \right) (\xi_k^{(n+1)} - \xi_k^{(n)}) \end{aligned}$$

where $\tilde{\mathbf{y}}^{(n+1)}$ can be approximately predicted by the Euler method. The integration method above is called *Heun's scheme*. It yields Stratonovich solutions of stochastic differential equations and is of order $\mathcal{O}(\Delta t)$.

Chapter 2

Perturbative approach to weakly driven many-particle systems

2.1 The model

We consider a many-body quantum system described by a Hamiltonian H_0 that has a set of conserved quantities. Importantly, we assume that the system is weakly perturbed, for example, by a periodic drive or a coupling to an external bath that breaks at least one of the conservation laws. The statistics of the system is described by a density matrix ρ whose dynamics is governed by the Liouville equation $\dot{\rho} = \hat{\mathcal{L}}\rho$. Due to the weak perturbation, we split the Liouville superoperator $\hat{\mathcal{L}} = \hat{\mathcal{L}}_0 + \hat{\mathcal{L}}_1$ into two parts where $\hat{\mathcal{L}}_0$ describes the dominant unitary Hamiltonian dynamics and $\hat{\mathcal{L}}_1$ the weak perturbation of strength ε that drives the system out of equilibrium,

$$\hat{\mathcal{L}}_0\rho = -i[H_0, \rho], \quad \hat{\mathcal{L}}_1\rho = \begin{cases} -i[\varepsilon H_1(t), \rho], \\ \varepsilon \hat{\mathcal{D}}\rho. \end{cases} \quad (2.1)$$

The perturbation, which is assumed to be translationally invariant, can in principle be of Markovian Lindblad or unitary form where we consider static as well as time-dependent perturbations. However, we first restrict our analysis to a static $\hat{\mathcal{L}}_1$. Moreover, we consider only cases in which a unique steady state is obtained. Thus, the perturbation has to be chosen such that it breaks sufficiently many symmetries of the bare Hamiltonian H_0 . In case of a Markovian perturbation, the Lindbladian $\hat{\mathcal{D}}$ is defined by

$$\hat{\mathcal{D}}\rho = \sum_{\alpha} (L_{\alpha}\rho L_{\alpha}^{\dagger} - \frac{1}{2}\{L_{\alpha}^{\dagger}L_{\alpha}, \rho\}) \quad (2.2)$$

with Lindblad operators L_{α} (cf. Sec. 1.3.1). We denote the conservation laws of the unperturbed system, which are weakly broken by the perturbation, by C_i , i.e. $[C_i, H_0] = 0$ ($i = 1, \dots, N_c$). Note that in the thermodynamic limit ($N \rightarrow \infty$), the number of approximately conserved quantities N_c

can be infinite in the case of integrable systems. In order to develop a perturbation theory for the non-equilibrium steady state, we split the steady state density matrix ρ_∞ into the zeroth order approximation ρ_0 and corrections $\delta\rho$,

$$\lim_{t \rightarrow \infty} \rho(t) = \rho_\infty = \rho_0 + \delta\rho \quad (2.3)$$

with $\rho_0 = \lim_{\varepsilon \rightarrow 0} \lim_{t \rightarrow \infty} \rho(t)$. It is important to note that the different limits do not commute. In the trivial limit $\lim_{t \rightarrow \infty} \lim_{\varepsilon \rightarrow 0} \rho(t)$, one simply obtains an equilibrium state while in the opposite limit a highly non-equilibrium steady state can be reached. For perturbations that are periodic in time, the steady state density matrix is periodically oscillating as well. However, the formula above can still be used when interpreted in Floquet space (cf. Sec. 2.2.1). The higher order corrections $\delta\rho$ are formally given by

$$\delta\rho = -\hat{\mathcal{L}}^{-1} \hat{\mathcal{L}}_1 \rho_0, \quad \hat{\mathcal{L}}^{-1} \rightarrow \lim_{\eta \rightarrow 0} (\hat{\mathcal{L}} - \eta \hat{\mathbb{1}})^{-1}, \quad (2.4)$$

where we have used $\hat{\mathcal{L}} \rho_\infty = \hat{\mathcal{L}}_1 \rho_0 + \hat{\mathcal{L}} \delta\rho = 0$ and $\hat{\mathcal{L}}_0 \rho_0 = 0$. The inverse $\hat{\mathcal{L}}^{-1}$ should be interpreted with an infinitesimal regularization η , as $\hat{\mathcal{L}}$ has a zero mode $\hat{\mathcal{L}} \rho_\infty = 0$. The regularization also avoids the trivial solution $\rho_0 = -\delta\rho$ which can be deduced from the following argument: We can write $\rho_0 = \sum_\alpha c_\alpha \rho^\alpha$ in terms of the right eigenstates ρ^α of $\hat{\mathcal{L}}$ that fulfill $\hat{\mathcal{L}} \rho^\alpha = \lambda_\alpha \rho^\alpha$. Then

$$\begin{aligned} \delta\rho &= -\lim_{\eta \rightarrow 0} (\hat{\mathcal{L}} - \eta \hat{\mathbb{1}})^{-1} \hat{\mathcal{L}}_1 \rho_0 = -\lim_{\eta \rightarrow 0} (\hat{\mathcal{L}} - \eta \hat{\mathbb{1}})^{-1} \hat{\mathcal{L}} \rho_0 \\ &= -\lim_{\eta \rightarrow 0} (\hat{\mathcal{L}} - \eta \hat{\mathbb{1}})^{-1} \sum_\alpha \lambda_\alpha c_\alpha \rho^\alpha \\ &= -\lim_{\eta \rightarrow 0} \sum_\alpha \frac{\lambda_\alpha}{\lambda_\alpha - \eta} c_\alpha \rho^\alpha = -\sum_{\alpha, \lambda_\alpha \neq 0} c_\alpha \rho^\alpha \end{aligned}$$

does not include a contribution from the zero mode ρ_0 . Moreover, introducing a regularization guarantees $\text{Tr}[\delta\rho] = 0$ as it follows from $\text{Tr}[\dot{\rho}] = \text{Tr}[\hat{\mathcal{L}}\rho] = 0$ that $\text{Tr}[\rho^\alpha] = 0$ for all α with $\lambda_\alpha \neq 0$. Using the expansion of $\delta\rho$ above then yields $\text{Tr}[\delta\rho] = 0$. Here, the regularization has to be chosen with a positive sign as the real parts of all right eigenvalues of $\hat{\mathcal{L}}$ are negative. Due to the conservation laws of H_0 , $\hat{\mathcal{L}}_0 \rho_0 = 0$ has no unique solution. While Eq. (2.4) is formally valid for arbitrary ρ_0 with $\hat{\mathcal{L}}_0 \rho_0 = 0$, the correction $\delta\rho$ will only be small if ρ_0 is chosen correctly which will be discussed in the next section. Note that the following chapter is based on [87] for which Dr. Lenarčič contributed most.

2.2 Zeroth order: Generalized Gibbs ensemble

A closed system, which has a set of conservation laws C_i and is initialized in a state $|\psi_0\rangle$, is assumed to relax to a generalized Gibbs ensemble

$$\rho_{GGE} = \frac{e^{-\sum_i \lambda_i C_i}}{\text{Tr}[e^{-\sum_i \lambda_i C_i}]}, \quad (2.5)$$

in the long-time limit [26, 59, 88, 89]. The Lagrange parameters are defined by the expectation values of the conserved quantities in the initial state, i.e. $\langle C_i \rangle_{GGE} = \langle \psi_0 | C_i | \psi_0 \rangle$. The system might be described by another ensemble, but the GGE ansatz is expected to yield correct results in the thermodynamic limit as long as expectation values of local observables are concerned.

In the presence of a small perturbation that breaks the conservation laws only weakly, we expect that a GGE is still a good approximation for the steady state density matrix. Therefore, we use the GGE as an expansion point for the perturbation theory that will be developed in the following, i.e. $\rho_0 = \rho_{GGE}$. Trivially, the GGE ansatz satisfies $\hat{\mathcal{L}}_0 \rho_0 = 0$ that is the defining equation for ρ_0 by construction for all choices of $\{\lambda_i\}$. Therefore, the perturbation $\hat{\mathcal{L}}_1$ has to fix the Lagrange parameters in the steady state. Due to the perturbation, the charges C_i are only approximately conserved and their expectation values change during the time evolution. Hence, in the case of weakly open systems, the GGE in the long-time limit is not determined by the initial conditions but is completely independent of them. Instead, the steady state Lagrange parameters λ_i or, equivalently, the corresponding expectation values of the charges C_i have to be determined from rate equations governed by $\hat{\mathcal{L}}_1$. One of our main statements will be that even though the perturbation is weak of order $\mathcal{O}(\varepsilon)$, the change of the λ_i can be very strong of order $\mathcal{O}(1)$.

Eventually, the Lagrange parameters in the steady state are determined from the condition that the steady state, projected onto the space of conservation laws, is stationary in combination with the condition that $\delta\rho$ should be small for small values of ε . The first condition leads to $\langle \dot{C}_i \rangle = 0$ which can be evaluated using perturbation theory

$$\begin{aligned} \langle \dot{C}_i \rangle &= \text{Tr}[C_i \hat{\mathcal{L}} \rho_\infty] \\ &= \text{Tr}[C_i \hat{\mathcal{L}}_1 \rho_0] + \text{Tr}[C_i \hat{\mathcal{L}}_0 \delta\rho] \approx \text{Tr}[C_i \hat{\mathcal{L}}_1 \rho_0] \end{aligned} \quad (2.6)$$

for $i = 1, \dots, N_c$. Above we have used that $\text{Tr}[C_i \hat{\mathcal{L}}_0 \delta\rho] = 0$ which holds as $\hat{\mathcal{L}}_0^\dagger C_i = i[H_0, C_i] = 0$, and the fact that $\delta\rho$ is small. We therefore obtain from $\langle \dot{C}_i \rangle = 0$ the condition

$$\text{Tr}[C_i \hat{\mathcal{L}}_1 \rho_0] \stackrel{!}{=} 0 \quad (2.7)$$

that fixes ρ_0 . Hence, the Lagrange parameters in the steady state are defined by a set of N_c linear equations. In the analysis, we have omitted all remaining exact conservation laws to simplify the notation. However, they could simply be incorporated by introducing additional Lagrange parameters

in the GGE that are determined by the expectation values of the exactly conserved quantities in the initial state. For a generic GGE, we would have $\text{Tr}[C_i \hat{\mathcal{L}}_1 \rho_0] \neq 0$ for all $i = 1, \dots, N_c$ and Eq. (2.7) can then be viewed as a set of rate equations which describes the dynamics of the approximate conserved quantities within the subspace of slow modes, cf. Sec. 2.2.2.

Note that the strength ε of the perturbation cancels out in Eq. (2.7). Therefore, the steady state density matrix is determined only by the form of the perturbation and not by its strength as long as the perturbation is weak. As ρ_0 is fixed to order ε^0 , it also induces changes of the approximately conserved quantities of order $\mathcal{O}(1)$.

Typically, the expansion of Eq. (2.6) to first order in ε is sufficient to determine ρ_0 in the case of a generic Markovian perturbation. However, if $\text{Tr}[C_i \hat{\mathcal{L}}_1 \rho_0] = 0$ is fulfilled trivially for all ρ_0 , one has to consider higher-order perturbation theory. For example, an expansion to first order in ε always fails in the case of purely Hamiltonian perturbations where $\hat{\mathcal{L}}_1 \rho_0 = -i[\varepsilon H_1, \rho_0]$, as $\text{Tr}[C_i [H_1, \rho_0]] = \text{Tr}[H_1 [\rho_0, C_i]]$ and $[C_i, \rho_0] = 0$. Therefore, $\langle \dot{C}_i \rangle$ has to be calculated to order ε^2 . This is well-known from Fermi's golden rule transition rates which are always quadratic in the perturbation strength. To expand $\delta\rho$ to order ε^2 , we use Eq. (2.4) and the general relation

$$(X + Y)^{-1} = X^{-1} - (X + Y)^{-1} Y X^{-1}, \quad (2.8)$$

with $X = \hat{\mathcal{L}}_0$ and $Y = \hat{\mathcal{L}}_1$. The inverses are considered to be regularized in the same way as in Eq. (2.4). The correction $\delta\rho$ to second order in ε then reads

$$\begin{aligned} \delta\rho &= \delta\rho^{(I)} + \delta\rho^{(II)} \\ &= -\hat{\mathcal{L}}_0^{-1} \hat{\mathcal{L}}_1 \rho_0 + \hat{\mathcal{L}}_0^{-1} \hat{\mathcal{L}}_1 \hat{\mathcal{L}}_0^{-1} \hat{\mathcal{L}}_1 \rho_0. \end{aligned} \quad (2.9)$$

It can be argued that the contribution of the second term $\delta\rho^{(II)}$ vanishes in $\langle \dot{C}_i \rangle$. As this argument is a bit cumbersome and requires the definition of projection operators that will be introduced later in Sec. 2.2.2, it is shifted to App. A. Assuming that $\text{Tr}[C_i \hat{\mathcal{L}}_1 \delta\rho^{(II)}] = 0$, ρ_0 is determined by

$$\text{Tr}[C_i \hat{\mathcal{L}}_1 \hat{\mathcal{L}}_0^{-1} \hat{\mathcal{L}}_1 \rho_0] \stackrel{!}{=} 0 \quad (2.10)$$

in situations where $\text{Tr}[C_i \hat{\mathcal{L}}_1 \rho_0] = 0$ trivially holds. As before, the precise strength ε cancels out in Eq. (2.10) and ρ_0 is fixed to order ε^0 . For a combination of Markovian and unitary perturbations, the two conditions Eq. (2.7) and Eq. (2.10) have to be satisfied simultaneously. The order of the perturbation that fixes ρ_0 can be deduced from the scaling behavior of the Liouvillian gap that can be calculated numerically on small system sizes. If the gap scales as $\sim \varepsilon^k$, ρ_0 is determined by the condition of order ε^k .

2.2.1 Periodic driving

In the last chapter, we have discussed time-independent Liouvillians that lead to static steady states in the long-time limit. However, the formalism can be easily extended to perturbations that are periodic in time with period T , i.e. $\hat{\mathcal{L}}_1(t) = \hat{\mathcal{L}}_1(t+T)$ while we take $\hat{\mathcal{L}}_0$ and the conservation laws C_i to be time-independent. In the limit $t \rightarrow \infty$, the steady state density matrix can be written in terms of oscillating Floquet components,

$$\rho(t) = \sum_n e^{-in\omega t} \rho^{(n)}(t), \quad n \in \mathbb{Z} \quad (2.11)$$

where $\rho^{(-n)} = \rho^{(n)\dagger}$ and $\omega = 2\pi/T$. In the stationary state the Floquet components become time-independent and for $\varepsilon \rightarrow 0$ the zeroth order term ρ_0 is simply given by the Floquet component $\rho^{(0)}$. In the spirit of Floquet theory, one can introduce an extended Hilbert space and interpret the Floquet components as elements of an infinitely large vector $\boldsymbol{\rho} = (\dots, \rho^{(-1)}, \rho^{(0)}, \rho^{(1)}, \dots)$. Then the Liouvillian becomes a static matrix in Floquet space

$$\begin{aligned} \hat{\mathcal{L}} &= \hat{\mathcal{L}}_0 + \hat{\mathcal{L}}_1, \\ \hat{\mathcal{L}}_1^{nm} &= \hat{\mathcal{L}}_1^{n-m} = \frac{1}{T} \int_0^T \hat{\mathcal{L}}_1(t) e^{i\omega(n-m)t} dt, \\ \hat{\mathcal{L}}_0^{nm} &= (in\omega + \hat{\mathcal{L}}_0) \delta_{nm}. \end{aligned} \quad (2.12)$$

The rate equations Eq. (2.7) for Markovian and Eq. (2.10) for unitary perturbations that determine ρ_0 are still valid if the superoperators $\hat{\mathcal{L}}_0, \hat{\mathcal{L}}_1$ are replaced by matrices and C_i, ρ_0 by vectors in Floquet space. Moreover, stationarity of conserved quantities has to be understood on the level of time-averaged expectation values. As C_i and ρ_0 are time-independent their only non-zero Floquet entry is the $n=0$ component. The matrix $\hat{\mathcal{L}}_0$ contains only diagonal terms while $\hat{\mathcal{L}}_1$ has off-diagonal terms due to periodic driving and diagonal contributions in the case of static perturbations. The additional terms $in\omega$ in the diagonal entries of $\hat{\mathcal{L}}_0$ originate in the explicit time dependence of $\rho(t)$, i.e. $\dot{\rho} = \sum_n e^{-in\omega t} (-in\omega \rho^{(n)} + \dot{\rho}^{(n)})$.

2.2.2 Projection operators and effective forces

Before elaborating a perturbative expansion around ρ_0 , it is worth noting that there is a crucial difference between corrections $\delta\rho_{\parallel}$ parallel and $\delta\rho_{\perp}$ perpendicular to the subspace of slow modes that is defined through $\hat{\mathcal{L}}_0 \delta\rho_{\parallel} = 0$. While the dynamics of slow modes is governed by the weak perturbation $\hat{\mathcal{L}}_1$ on a time scale $\sim 1/\varepsilon^k \gg 1$, the elements $\delta\rho_{\perp}$ ($\hat{\mathcal{L}}_0 \delta\rho_{\perp} \neq 0$) from the perpendicular subspace evolve on a much faster time scale of order one. Due to the separation of time scales, it is reasonable to treat the subspaces of slow and fast modes separately. To this end, we introduce a (super)projection operator \hat{P}_{ρ_0} which projects onto the tangential space at ρ_0 . In the following, we omit the argument ρ_0 for brevity and set $\hat{P} = \hat{P}_{\rho_0}$. The tangential space is spanned by the vectors

$\partial\rho_0/\partial\lambda_i$. Therefore, the projection operator \hat{P} and the projection operator \hat{Q} onto the orthogonal subspace can be defined by

$$\hat{P}X \equiv -\sum_{i,j} \frac{\partial\rho_0}{\partial\lambda_i} (\chi^{-1})_{ij} \text{Tr}[C_j X], \quad (2.13)$$

$$\hat{Q}X \equiv (\hat{1} - \hat{P})X = X - \hat{P}X, \quad (2.14)$$

where we have set $\chi_{ij} = -\text{Tr}[C_i \partial\rho_0/\partial\lambda_j] = \langle C_i C_j \rangle_{0,c}$. The matrix of generalized susceptibilities χ_{ij} guarantees the properties $\hat{P}^2 = \hat{P}$, $\hat{Q}^2 = \hat{Q}$ and $\hat{P}\hat{Q} = \hat{Q}\hat{P} = 0$ that are required for a projection operator. Moreover, we write for connected correlation functions $\langle AB \rangle_{0,c} = \langle AB \rangle_0 - \langle A \rangle_0 \langle B \rangle_0$. According to our definition, we have in general $\hat{P}\rho_0 \neq \rho_0$. The projection operator projects on the tangential space that is spanned at ρ_0 and not on the subspace of GGEs. However, the definition can be adapted to obtain this property by adding an additional term [90]. The method of projection operators is frequently used in the context of open systems [91–95, 2].

The adjoint projection operator \hat{P}^\dagger that acts on operators and not on density matrices is defined through $\text{Tr}[(\hat{P}^\dagger A)\rho] = \text{Tr}[A(\hat{P}\rho)]$. Using the definition of \hat{P} yields

$$\hat{P}^\dagger A = -\sum_{ij} C_i (\chi^{-1})_{ji} \text{Tr} \left[A \frac{\partial\rho_0}{\partial\lambda_j} \right]. \quad (2.15)$$

The adjoint superoperator projects operators onto the space of conservation laws. Thus, if the dynamics is only governed by $\hat{\mathcal{L}}_0$, $(\hat{P}^\dagger A)$ is conserved and its expectation value does not change during the time evolution. The adjoint superoperator \hat{P}^\dagger is a very natural object in the context of conservation laws and also appears in the memory matrix formalism [96, 97]. It can also be used to express the Drude weight $D(T)$ in systems in which the decay of a current J is prohibited by conservation laws, i.e. $D(T) = \frac{\beta}{L} \langle (\hat{P}^\dagger J) J \rangle_c$ where L denotes the system size [98, 99].

The projection operator Eq. (2.13) can also be used to quantify the changes of the Lagrange parameter during the time evolution. We project $\dot{\rho}$ onto the space of slow modes which yields the relevant part of the dynamics in the long-time limit. Here, we assume that the density matrix of the system relaxes after a short time of order $\hat{\mathcal{O}}(1)$ to the subspace of GGEs. Within this subspace the system can then approximately be described by $\rho_0(t)$ parameterized by time-dependent Lagrange parameters $\lambda_i(t)$, i.e.

$$\begin{aligned} \hat{P}\dot{\rho} &\approx \sum_i \frac{\partial\rho_0}{\partial\lambda_i} \frac{\partial\lambda_i}{\partial t} = \sum_i \frac{\partial\rho_0}{\partial\lambda_i} F_i, \\ \dot{\lambda}_i = F_i &\approx -\sum_j (\chi^{-1})_{ij} \text{Tr}[C_j \dot{\rho}] = -\sum_j (\chi^{-1})_{ij} \langle \dot{C}_j \rangle. \end{aligned} \quad (2.16)$$

In Eq. (2.16) we have introduced the generalized force F_i governing the dynamics of the λ_i in the space of Lagrange parameters. For a Markovian perturbation the generalized force F_i is to leading order in ε given by $F_i = -\sum_j (\chi^{-1})_{ij} \text{Tr}[C_j \hat{\mathcal{L}}_1 \rho_0]$. To begin with, we restrict our analysis to the steady state where ρ_0 is defined by the vanishing of all generalized forces $F_i = 0 \forall i$. The time evolution

within the subspace of slow modes will be addressed later in Ch. 3. Using the projection superoperator \hat{P} the stationarity condition Eq. (2.7) can be written as

$$\hat{P}(\hat{\mathcal{L}}_1 \rho_0) = 0. \quad (2.17)$$

Similarly, we obtain for unitary perturbations

$$\hat{P}(\hat{\mathcal{L}}_1 \hat{\mathcal{L}}_0^{-1} \hat{\mathcal{L}}_1 \rho_0) = 0. \quad (2.18)$$

The geometrical meaning of Eq. (2.17) and Eq. (2.18) is that in the steady state, the generalized force governing the dynamics of the system in the whole space of density matrices has to be perpendicular to the subspace of slow modes. Hence, the part \mathbf{F} of the force projected on the subspace of slow modes vanishes. In the case of periodic driving, \hat{P} has to be interpreted as a projection operator on the $n = 0$ Floquet sector.

2.3 Perturbation theory

In this section, we present a well-behaved expansion of $\delta\rho$ to all orders of ε . We choose as an expansion point ρ_0 a GGE determined by condition Eq. (2.17) or Eq. (2.18) depending on the form of the perturbation. In order to remove possible singularities in $\hat{\mathcal{L}}^{-1}$, it is necessary to distinguish between the subspaces of slow and fast modes and carefully separate different orders $\hat{\mathcal{O}}(\varepsilon^n)$ within these subspaces. As in the previous section, we denote the component in the image of \hat{P} and \hat{Q} by \parallel and \perp and write

$$\delta\rho = \hat{P}\delta\rho + \hat{Q}\delta\rho = \delta\rho_{\parallel} + \delta\rho_{\perp}.$$

If one is only interested in the expectation values of conserved quantities, the perpendicular component $\delta\rho_{\perp}$ can be neglected, as $\hat{Q}^\dagger C_i = 0$ for $[C_i, H_0] = 0$. However, $\delta\rho_{\perp}$ affects the steady state expectation values of observables that are not conserved.

2.3.1 Markovian perturbation

First, we consider the case where the perturbation breaks all relevant symmetries of the bare Hamiltonian H_0 already to linear order in ε such that $\hat{P}\hat{\mathcal{L}}_1\hat{P}$ has no zero mode. We can then expand the correction

$$\delta\rho = -\hat{\mathcal{L}}^{-1}\hat{Q}\hat{\mathcal{L}}_1\rho_0,$$

where ρ_0 is defined through the condition $\hat{P}\hat{\mathcal{L}}_1\rho_0 = 0$ around $\hat{\mathcal{L}}_0 + \hat{P}\hat{\mathcal{L}}_1\hat{P}$. The second term regularizes possible singularities of $\hat{\mathcal{L}}_0^{-1}$ which are due to conservation laws. We use $\hat{\mathcal{L}}_1 = (\hat{P} + \hat{Q})\hat{\mathcal{L}}_1(\hat{P} + \hat{Q})$

and the fact that $\hat{P}\hat{\mathcal{L}}_1\hat{P}$ is invertible to write

$$\begin{aligned}\mathcal{L}^{-1}\hat{Q} &= (\mathcal{L}_0 + \mathcal{L}_1)^{-1}\hat{Q} \\ &= \left[\left(1 + \left(\hat{P}\hat{\mathcal{L}}_1\hat{Q} + \hat{Q}\hat{\mathcal{L}}_1\hat{P} + \hat{Q}\hat{\mathcal{L}}_1\hat{Q} \right) \left(\mathcal{L}_0 + \hat{P}\hat{\mathcal{L}}_1\hat{P} \right)^{-1} \right) \left(\mathcal{L}_0 + \hat{P}\hat{\mathcal{L}}_1\hat{P} \right) \right]^{-1} \hat{Q} \\ &= \left(\mathcal{L}_0 + \hat{P}\hat{\mathcal{L}}_1\hat{P} \right)^{-1} \sum_{n=0}^{\infty} \left[- \left(\hat{P}\hat{\mathcal{L}}_1\hat{Q} + \hat{Q}\hat{\mathcal{L}}_1\hat{P} + \hat{Q}\hat{\mathcal{L}}_1\hat{Q} \right) \left(\mathcal{L}_0 + \hat{P}\hat{\mathcal{L}}_1\hat{P} \right)^{-1} \right]^n \hat{Q}.\end{aligned}\quad (2.19)$$

In Eq. (2.19) we have utilized the expansion $(1+A)^{-1} = \sum_{n=0}^{\infty} (-1)^n A^n$ and the relation $(AB)^{-1} = B^{-1}A^{-1}$. For power counting in ε , we note that

$$\begin{aligned}\left(\mathcal{L}_0 + \hat{P}\hat{\mathcal{L}}_1\hat{P} \right)^{-1}\hat{P} &= \left(\hat{P}\hat{\mathcal{L}}_1\hat{P} \right)^{-1}\hat{P} \sim \mathcal{O}(1/\varepsilon), \\ \left(\mathcal{L}_0 + \hat{P}\hat{\mathcal{L}}_1\hat{P} \right)^{-1}\hat{Q} &= \left(\hat{Q}\hat{\mathcal{L}}_0\hat{Q} \right)^{-1}\hat{Q} \sim \mathcal{O}(1),\end{aligned}\quad (2.20)$$

where we have used $\hat{P}\hat{\mathcal{L}}_0 = \hat{\mathcal{L}}_0\hat{P} = 0$. While $\hat{\mathcal{L}}_0$ is not invertible, the inverse $\left(\hat{Q}\hat{\mathcal{L}}_0\hat{Q} \right)^{-1}$ within the subspace is well-behaved. Eq. (2.20) is consistent with the condition $\hat{P}\hat{\mathcal{L}}_1\rho_0 = 0$ that fixes ρ_0 . If the condition is not met, it holds $\delta\rho \sim \hat{\mathcal{L}}^{-1}\hat{P}\hat{\mathcal{L}}_1\rho_0 \sim \mathcal{O}(1)$ which contradicts the assumption $\lim_{\varepsilon \rightarrow 0} \delta\rho = 0$.

Using Eq. (2.19) and the scaling relation Eq. (2.20) for correct power counting we can directly obtain an expansion of $\delta\rho_{\perp}$ and $\delta\rho_{\parallel}$ in ε . It is important to note that the structure of the perturbation theory is different in the parallel and the perpendicular subspace. For example, to calculate the first order correction $\delta\rho_{\parallel}$ in ε , one has to expand Eq. (2.19) to second order in $\hat{\mathcal{L}}_1$ while in the perpendicular space an expansion to first order in $\hat{\mathcal{L}}_1$ is sufficient. We obtain $\delta\rho = \delta\rho_{1,\parallel} + \delta\rho_{1,\perp} + \mathcal{O}(\varepsilon^2)$ with

$$\begin{aligned}\delta\rho_{1,\parallel} &= \left(\hat{P}\hat{\mathcal{L}}_1\hat{P} \right)^{-1} \left(\hat{P}\hat{\mathcal{L}}_1\hat{Q} \right) \left(\hat{Q}\hat{\mathcal{L}}_0\hat{Q} \right)^{-1} \hat{Q}\hat{\mathcal{L}}_1\rho_0, \\ \delta\rho_{1,\perp} &= -\hat{\mathcal{L}}_0^{-1}\hat{Q}\hat{\mathcal{L}}_1\rho_0.\end{aligned}\quad (2.21)$$

In the parallel subspace the two superoperators $\hat{\mathcal{L}}_1$ contribute together a factor ε^2 while the inverse $\left(\hat{P}\hat{\mathcal{L}}_1\hat{P} \right)^{-1}$ yields a factor $1/\varepsilon$. Thus, the first non-vanishing term is proportional to $\varepsilon^2/\varepsilon = \varepsilon$. In contrast to that, in the case of $\delta\rho_{1,\perp}$, a straightforward expansion to first order in $\hat{\mathcal{L}}_1$ gives the leading order term in ε . The effect of the weak perturbation to order ε is schematically sketched in Fig. 2.1. With the help of Eq. (2.21), the change of $\langle C_i \rangle$ to linear order in ε can be calculated yielding

$$\langle C_i \rangle_1 = \text{Tr} \left[C_i \left(\hat{P}\hat{\mathcal{L}}_1\hat{P} \right)^{-1} \hat{P}\hat{\mathcal{L}}_1\hat{Q}\hat{\mathcal{L}}_0^{-1}\hat{Q}\hat{\mathcal{L}}_1\rho_0 \right].\quad (2.22)$$

In Fig. 2.2 a graphical illustration of the perturbative expansion up to third order in ε is shown where we distinguish between the parallel (left panel) and the perpendicular (right panel) components. We represent the inverses $\left(\hat{Q}\hat{\mathcal{L}}_0\hat{Q} \right)^{-1}$ and $\left(\hat{P}\hat{\mathcal{L}}_1\hat{P} \right)^{-1}$ as black and white circles, respectively. Different circles are connected by links substituting the superoperators $\hat{Q}\hat{\mathcal{L}}_1^{-1}\hat{Q}$ (black-black), $\hat{P}\hat{\mathcal{L}}_1^{-1}\hat{Q}$

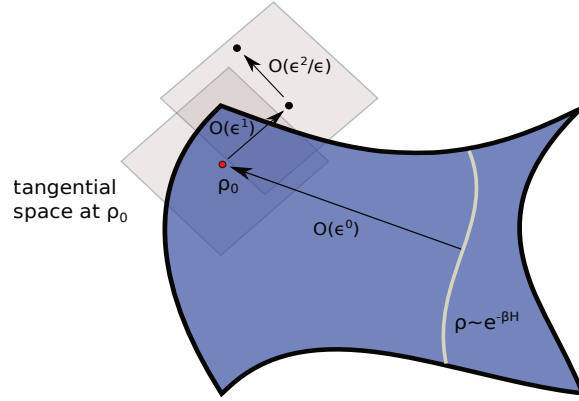


Figure 2.1 The figure illustrates the effect of weak pumping on an approximately integrable system, which is weakly coupled to a thermal bath, schematically. Starting from a thermal state, driving leads to a shift of the steady state density within the subspace of GGEs to ρ_{GGE} where the changes of the Lagrange multipliers parameterizing the GGE are of order ϵ^0 . Corrections parallel and perpendicular to the tangential space at ρ_{GGE} are of order ϵ^2/ϵ and ϵ , respectively.

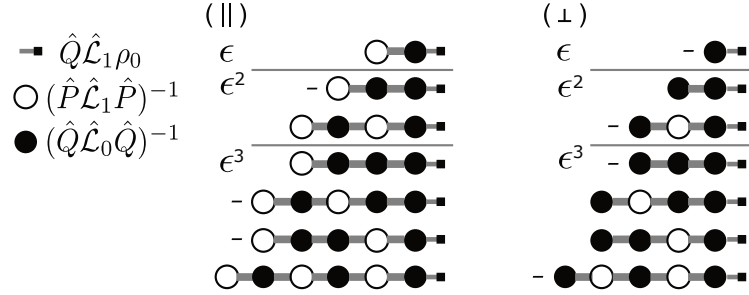


Figure 2.2 Diagrammatic depiction of the structure of corrections to the zeroth order density matrix ρ_0 . The order of the diagram is given by the number of black circles, the sign by the total number of lines. The number of terms to order ϵ^n is given by 2^n . Note that the corrections to order n in the perpendicular and parallel sector are simply related by the relation $\delta\rho_{n,\parallel} = -(\hat{P}\hat{\mathcal{L}}_1\hat{P})^{-1}(\hat{P}\hat{\mathcal{L}}_1\hat{Q})\delta\rho_{n,\perp}$. The caption is partially taken from [87]

(white-black) and $\hat{Q}\hat{\mathcal{L}}_1^{-1}\hat{P}$ (black-white) which follows from $\hat{P}\hat{Q} = \hat{Q}\hat{P} = 0$. There cannot be two neighboring white circles as $\hat{P}\hat{\mathcal{L}}_1\hat{P}$ is used in the expansion point $\hat{\mathcal{L}}_0 + \hat{P}\hat{\mathcal{L}}_1\hat{P}$. The diagram can be read from right to the left where the little square with the thin line represents $\hat{Q}\hat{\mathcal{L}}_1\rho_0$. Due to the \hat{Q} projection operator, the second circle from the right has to be black. The last circle on the left determines whether the diagram contributes to the parallel (white) or the perpendicular subspace (black). All circles in between can be chosen under the condition that neighboring white circles are forbidden. The order $\mathcal{O}(n)$ of a diagram is set by the number of lines minus the number of white circles due to $(\hat{P}\hat{\mathcal{L}}_1\hat{P})^{-1} \sim 1/\epsilon$. The sign of a term is given by $(-1)^{N_L}$ where N_L is the number of lines.

situations in which not all conservation laws are known or it is simply not feasible to include them all. This could, for example, be the case when the thermodynamic limit of integrable systems is considered in which an infinite amount of local conservation laws exists.

In other situations, one might deliberately restrict the number of conservation laws to reduce the complexity of the problem. This is a valid approach if not all charges affect equally strongly the quantities of interest calculated from the GGE. We will show in Ch. 3 that locality can serve as a selection rule for a hierarchy of conservation laws within the GGE ansatz. In such cases it is convenient to approximate ρ_0 by a truncated GGE

$$\rho_0^{[t]} = \frac{\exp\left(-\sum_j \lambda_j^{[t]} C_j^{[t]}\right)}{\text{Tr}\left[\exp\left(-\sum_j \lambda_j^{[t]} C_j^{[t]}\right)\right]} \quad (2.27)$$

with a finite subset of conserved quantities denoted by the label $[t]$. A projection operator \hat{P}_t onto the corresponding slow modes $\partial\rho_0/\partial\lambda_j^{[k]}$ can be introduced as in Eq. (2.13) with $\chi^{[tr]}$ defined for the subset. We denote the missing charges which are not included in the GGE by $C_i^{[m]}$ and set $\chi_{ij}^{[mm]} = \langle C_i^{[m]} C_j^{[m]} \rangle_{0,c}$ and $\chi_{ij}^{[mt]} = \langle C_i^{[m]} C_j^{[t]} \rangle_{0,c}$ where $\langle \cdot \rangle_0$ is an expectation value with respect to $\rho_0^{[t]}$. We aim to address the question of how the effect of the missing charges on zeroth order expectation values can be calculated perturbatively and which signals due to the incorrect expansion point develop in the perturbation theory around ρ_0 . For simplicity, we assume that the missing charges are perpendicular to the $C_i^{[t]}$. This assumption can always be guaranteed by redefining $C_i^{[m]} \rightarrow \hat{Q}_t^\dagger C_i^{[m]}$ where $\hat{Q}_t = 1 - \hat{P}_t$. We define the projection operator \hat{P}_m on the subspace of the tangential space that is spanned by $\partial\rho_0/\partial\lambda_j^{[m]}$ through

$$\hat{P}_m X = -\sum_{i,j} \frac{\partial\rho_0}{\partial\lambda_i^{[m]}} \Big|_{\rho_0^{[t]}} ((\chi^{[mm]})^{-1})_{ij} \text{Tr}[C_j^{[m]} X] \quad (2.28)$$

with $(\partial\rho_0/\partial\lambda_i^{[m]})|_{\rho_0^{[t]}} = -(C_i^{[m]} - \langle C_i^{[m]} \rangle) \rho_0^{[t]}$. The projection operator \hat{P} on the whole tangential space is then given by $\hat{P} = \hat{P}_m + \hat{P}_t$. Under the assumption that the missing conservation laws affect the Langrange parameters in Eq. (2.27) only weakly, we can expand $\rho_0 = \rho_0^{[t]} + \delta\rho_0$ with

$$\delta\rho_0 = \sum_k \frac{\partial\rho_0}{\partial\lambda_k} \Big|_{\rho_0^{[t]}} \delta\lambda_k = -\rho_0^{[t]} \sum_k \bar{C}_k \delta\lambda_k, \quad \bar{C}_k := C_k - \langle C_k \rangle_0 \quad (2.29)$$

in $\delta\lambda_k = \lambda_k - \lambda_k^{[t]}$ where the index k runs over the included and missing conservation laws. Using Eq. (2.7) we obtain the linear approximation $A\delta\lambda = \mathbf{a}$ which is solved by

$$\begin{aligned} \begin{pmatrix} \delta\lambda^{[t]} \\ \delta\lambda^{[m]} \end{pmatrix} &= \begin{pmatrix} A^{[tt]} & A^{[tm]} \\ A^{[mt]} & A^{[mm]} \end{pmatrix}^{-1} \begin{pmatrix} 0 \\ \mathbf{a}^{[m]} \end{pmatrix}, \\ (\mathbf{a}^{[m]})_i &= \text{Tr}[C_i^{[m]} \hat{\mathcal{L}}_1 \rho_0^{[t]}] = \langle \dot{C}_i^{[m]} \rangle_0, \\ A_{ij}^{[tJ]} &= \text{Tr}[C_i^{[t]} \hat{\mathcal{L}}_1 (\bar{C}_j^{[J]} \rho_0^{[t]})] = \langle \dot{C}_i^{[t]} \bar{C}_j^{[J]} \rangle_{0,c}. \end{aligned} \quad (2.30)$$

This result can be used to calculate the change of the expectation value $\langle C_i^{[t]} \rangle$ due to the missing charges,

$$\begin{aligned} \langle \delta C_i^{[t]} \rangle_0 &= - \left(\chi^{[tt]} (A^{-1})^{[tm]} \mathbf{a}^{[m]} \right)_i \\ &\approx \left(\chi^{[tt]} (A^{[tt]})^{-1} A^{[tm]} (A^{[mm]})^{-1} \mathbf{a}^{[m]} \right)_i. \end{aligned} \quad (2.31)$$

In the second step we have assumed that the matrix elements $A^{[tm]}$ between the missing and included charges are small allowing us to expand A^{-1} in $A^{[tm]}$. The physical picture of this assumption is that small changes of the Lagrange parameters $\lambda_j^{[m]}$ induce only small changes of $\langle \dot{C}_i^{[t]} \rangle$. We can deduce that the effect of the missing conservation laws is small if either $\langle \dot{C}_i^{[m]} \rangle_0$ or the dynamical coupling $A_{ij}^{[tm]} = \langle C_i^{[t]} \bar{C}_j^{[m]} \rangle_{0,c}$ is small. Equivalently, Eq. (2.31) can also be expressed in terms of the projection operators \hat{P}_t and \hat{P}_m yielding

$$\begin{aligned} \langle \delta C_i^{[t]} \rangle_0 &= -\text{Tr} \left[C_i^{[t]} \hat{P}_t (\hat{P} \hat{\mathcal{L}}_1 \hat{P})^{-1} \hat{P}_m \hat{\mathcal{L}}_1 \rho_0^{[t]} \right] \\ &\approx \text{Tr} \left[C_i^{[t]} (\hat{P}_t \hat{\mathcal{L}}_1 \hat{P}_t)^{-1} (\hat{P}_t \hat{\mathcal{L}}_1 \hat{P}_m) (\hat{P}_m \hat{\mathcal{L}}_1 \hat{P}_m)^{-1} \hat{P}_m \hat{\mathcal{L}}_1 \rho_0^{[t]} \right], \end{aligned} \quad (2.32)$$

where we have expanded $(\hat{P} \hat{\mathcal{L}}_1 \hat{P})^{-1}$ in $(\hat{P}_t \hat{\mathcal{L}}_1 \hat{P}_m)$. We expect that for a well-considered choice of included charges, the effect of the missing conservation laws is small as long as zeroth order results are considered. On the contrary, their influence on higher order corrections can be very strong. If an expansion point is not correctly determined to order $\mathcal{O}(\varepsilon^0)$, a perturbative expansion around this point typically leads to divergencies. In the linear approximation of $\langle \delta C_i^{[t]} \rangle$, Eq. (2.22), the term $\hat{Q}_t (\hat{Q}_t \hat{\mathcal{L}}_0 \hat{Q}_t)^{-1} \hat{Q}_t$ can for a finite subset of conservation laws be identified as a possible origin of a divergence. If the image of $\rho_0^{[t]}$ under $\hat{\mathcal{L}}_1$ has a component in the subspace spanned by $(\partial \rho_0 / \partial \lambda_i^{[m]})$, we obtain a diverging contribution in the limit $\eta \rightarrow 0$ where η is the regulator of the inverse $\hat{\mathcal{L}}_0^{-1}$. With the projection operator \hat{P}_m , we can write

$$\hat{Q}_t (\hat{Q}_t \hat{\mathcal{L}}_0 \hat{Q}_t)^{-1} \hat{Q}_t = -\frac{\hat{P}_m}{\eta} + \mathcal{O}(\eta^0). \quad (2.33)$$

Inserting Eq. (2.33) into Eq. (2.22) yields

$$\langle \delta C_i^{[t]} \rangle \approx -\text{Tr} \left[C_i^{[t]} (\hat{P}_t \hat{\mathcal{L}}_1 \hat{P}_t)^{-1} (\hat{P}_t \hat{\mathcal{L}}_1 \hat{P}_m) \frac{1}{\eta} \hat{P}_m \hat{\mathcal{L}}_1 \rho_0 \right] + O(\eta^0) \quad (2.34)$$

which is of order ε/η . We see that Eq. (2.34) is identical to Eq. (2.32) if we replace $(\hat{P}_m \hat{\mathcal{L}}_1 \hat{P}_m)$ in Eq. (2.34) by $-\eta$. The occurrence of divergencies within perturbation theory in the limit $\eta \rightarrow 0$ at finite value of ε can be used as a signal for missing conservation laws and a wrongly chosen expansion point ρ_0 .

2.3.3 Unitary perturbation

In the previous discussion, we have considered only the case where $\hat{P}(\hat{\mathcal{L}}_1 \rho_0) = 0$ is not trivially fulfilled and $\hat{P} \hat{\mathcal{L}}_1 \hat{P}$ has a well-defined inverse. However, these assumptions are not met for unitary (time-dependent) perturbations H_1 as $\text{Tr}[C_i[H_1, \partial \rho_0 / \partial \lambda_j]] = 0$ is always fulfilled due to the cyclicity property of the trace and the fact that C_i and $\partial \rho_0 / \partial \lambda_j$ commute. In this case, the rate equations $\partial_t \langle C_i \rangle = 0$ have to be expanded to second order in ε which leads to Fermi's golden rule.

As $\hat{P} \hat{\mathcal{L}}_1 \hat{P} = 0$, we need to find an effective Liouvillian $\hat{P} \hat{\mathcal{L}}_2 \hat{P}$ that governs the dynamics within the subspace of slow modes at small values of ε . We will define $\hat{\mathcal{L}}_2$ by $(\hat{P} \hat{\mathcal{L}}_2 \hat{P})^{-1} \approx (\hat{P} \hat{\mathcal{L}}^{-1} \hat{P})$ up to small corrections in powers of epsilon. In order to calculate different projections of the full inverse $(\hat{P} + \hat{Q}) \hat{\mathcal{L}}^{-1} (\hat{P} + \hat{Q})$, we introduce the transformations

$$\begin{aligned} \hat{U} &= \hat{P} + \hat{Q} - (\hat{P} \hat{\mathcal{L}}_1 \hat{Q}) (\hat{Q} \hat{\mathcal{L}} \hat{Q})^{-1} \hat{Q}, \\ \hat{V} &= \hat{P} + \hat{Q} - \hat{Q} (\hat{Q} \hat{\mathcal{L}} \hat{Q})^{-1} \hat{Q} \hat{\mathcal{L}}_1 \hat{P} \end{aligned} \quad (2.35)$$

that is chosen in such a way that $\hat{U} \hat{\mathcal{L}} \hat{V}$ is block-diagonal, i.e.

$$\hat{U} \hat{\mathcal{L}} \hat{V} = \hat{Q} \hat{\mathcal{L}} \hat{Q} - (\hat{P} \hat{\mathcal{L}}_1 \hat{Q}) (\hat{Q} \hat{\mathcal{L}} \hat{Q})^{-1} (\hat{Q} \hat{\mathcal{L}}_1 \hat{P}), \quad (2.36)$$

where we have used $\hat{P} \hat{\mathcal{L}}_1 \hat{P} = 0$. Then the inverse of Eq. (2.36) can be determined by calculating the inverses of the two subblocks,

$$\begin{aligned} \hat{\mathcal{L}}^{-1} &= \hat{V} (\hat{U} \hat{\mathcal{L}} \hat{V})^{-1} \hat{U} \\ &= \hat{V} (\hat{P} \hat{\mathcal{L}}_2 \hat{P})^{-1} \hat{P} + \hat{Q} (\hat{Q} \hat{\mathcal{L}} \hat{Q})^{-1} \hat{Q} \hat{U} \end{aligned} \quad (2.37)$$

where we have defined $\hat{\mathcal{L}}_2 = -\hat{\mathcal{L}}_1 \hat{Q} (\hat{Q} \hat{\mathcal{L}}_1 \hat{Q})^{-1} \hat{Q} \hat{\mathcal{L}}_1$. For $\hat{P} \hat{\mathcal{L}} \hat{P} = 0$, the projected inverse of $\hat{\mathcal{L}}$ reads in the different subspaces

$$\begin{aligned} \hat{P} \hat{\mathcal{L}}^{-1} \hat{P} &= \hat{P} (\hat{P} \hat{\mathcal{L}}_2 \hat{P})^{-1} \hat{P} \sim \frac{1}{\varepsilon^2}, \\ \hat{P} \hat{\mathcal{L}}^{-1} \hat{Q} &= -\hat{P} (\hat{P} \hat{\mathcal{L}}_2 \hat{P})^{-1} (\hat{P} \hat{\mathcal{L}}_1 \hat{Q}) (\hat{Q} \hat{\mathcal{L}}_1 \hat{Q})^{-1} \hat{Q} \sim \frac{1}{\varepsilon}, \\ \hat{Q} \hat{\mathcal{L}}^{-1} \hat{P} &= -\hat{Q} (\hat{Q} \hat{\mathcal{L}}_1 \hat{Q})^{-1} (\hat{Q} \hat{\mathcal{L}}_1 \hat{P}) (\hat{P} \hat{\mathcal{L}}_2 \hat{P})^{-1} \hat{P} \sim \frac{1}{\varepsilon}, \\ \hat{Q} \hat{\mathcal{L}}^{-1} \hat{Q} &= 0. \end{aligned} \quad (2.38)$$

It is important to stress the difference between an inverse within a subspace, e.g. $(\hat{Q} \hat{\mathcal{L}}_1 \hat{Q})^{-1}$ and a projection on a regularized full inverse, e.g. $\hat{Q} \hat{\mathcal{L}}^{-1} \hat{Q}$. While the latter inverse is zero in this example, the former one is finite, even in the limit $\varepsilon \rightarrow 0$. Using the scaling relations Eq. (2.38) we can express the regularized full inverse projected on the space of slow modes as

$$\hat{P} \hat{\mathcal{L}}^{-1} \hat{P} = \hat{P} (\hat{P} \hat{\mathcal{L}}_2 \hat{P})^{-1} \hat{P} \approx (\hat{P} \hat{\mathcal{L}}_2 \hat{P})^{-1} (1 + \mathcal{O}(\varepsilon)). \quad (2.39)$$

with

$$\hat{\mathcal{L}}_2 = -\hat{\mathcal{L}}_1 \hat{Q} (\hat{Q} \hat{\mathcal{L}}_1 \hat{Q})^{-1} \hat{Q} \hat{\mathcal{L}}_1. \quad (2.40)$$

This allow us to identify $(\hat{P} \hat{\mathcal{L}}_2 \hat{P}) \sim \varepsilon^2$ as an effective Liouvillian in the limit $\varepsilon \rightarrow 0$. The condition Eq. (2.7) fixing ρ_0 can then be adapted by replacing $\hat{\mathcal{L}}_1$ by $\hat{\mathcal{L}}_2$, i.e. $\overline{\text{Tr}[C_i \hat{\mathcal{L}}_2 \rho_0]} = 0$ where the line denotes the time average. Similarly, Eq. (2.17) becomes

$$\hat{P} (\hat{\mathcal{L}}_2 \rho_0) = 0 \quad (2.41)$$

which is equivalent to Eq. (2.18). For $\hat{P} \hat{\mathcal{L}}_2 \hat{P} \neq 0$, which is generically the case for unitary perturbations, a perturbative expansion can be developed around $(\hat{\mathcal{L}}_0 + \hat{P} \hat{\mathcal{L}}_2 \hat{P})$. We obtain

$$\begin{aligned} \hat{\mathcal{L}}^{-1} &= (\hat{\mathcal{L}}_0 + \hat{\mathcal{L}}_1)^{-1} = ((\hat{\mathcal{L}}_0 + \hat{P} \hat{\mathcal{L}}_2 \hat{P}) + (\hat{\mathcal{L}}_1 - \hat{P} \hat{\mathcal{L}}_2 \hat{P}))^{-1} \\ &= (\hat{\mathcal{L}}_0 + \hat{P} \hat{\mathcal{L}}_2 \hat{P})^{-1} \sum_n^{\infty} \left[-(\hat{\mathcal{L}}_1 - \hat{P} \hat{\mathcal{L}}_2 \hat{P}) (\hat{\mathcal{L}}_0 + \hat{P} \hat{\mathcal{L}}_2 \hat{P})^{-1} \right]^n, \end{aligned} \quad (2.42)$$

where we have formally expanded the inverse in $(\hat{\mathcal{L}}_1 - \hat{P} \hat{\mathcal{L}}_2 \hat{P})$. A graphical representation of the terms occurring up to order ε^3 in perturbation theory is shown in Fig. 2.3. Note that in comparison to Fig. 2.2, $(\hat{P} \hat{\mathcal{L}}_1 \hat{P})^{-1} \sim \hat{\mathcal{O}}(\varepsilon^{-1})$ is replaced by $(\hat{P} \hat{\mathcal{L}}_2 \hat{P})^{-1} \sim \hat{\mathcal{O}}(\varepsilon^{-2})$ (white circle). The new diagrammatic rules are, (I) two neighboring white circles, (II) the combination white-black-white and finally (III) the combination white-black- ρ_0 are not allowed. Their corresponding contributions vanish or cancel. These rules directly follow from the definition Eq. (2.40) and the condition Eq. (2.41). The order of a

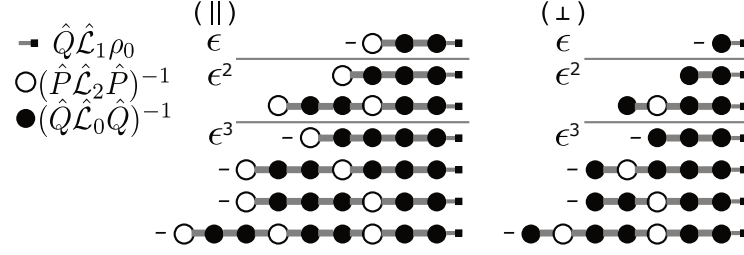


Figure 2.3 Diagrammatic depiction of the corrections $\delta\rho$ to the zeroth order density matrix ρ_0 for cases where $\hat{P}\hat{\mathcal{L}}_1\hat{P} = 0$ (unitary driving). One first draws all possible combinations of white and black circles starting to the right with a black circle connected to ρ_0 (small square). Then one eliminates all diagrams with neighboring white circles, all with the combination white-black-white, and finally also the combination white-black- ρ_0 (small square). The order is given by the number of black minus the number of white circles, the sign by the total number of circles. The number of terms to order ϵ^n is 2^n . Some diagrams do, however, vanish for monochromatic perturbations. The caption is taken from [87].

contribution is given by the number of black minus the number of white circles and the sign by the total number of circles. As before the total number of possible terms to order n is 2^n .

2.4 Applications

2.4.1 Open Boltzmann equation

As a first application of our approach to weakly open quantum systems, we consider a situation in which the unperturbed system has only two local conservation laws, energy and particle number. The concrete model considered describes weakly interacting fermionic quasiparticles with energies e_n whose relaxation to equilibrium is governed by a Boltzmann equation. We assume a constant density of states, which we discretize by L equidistant single-particle states with energies $e_n = n/L$ ($n = 1, \dots, L$) between 0 and 1. We denote the occupation function of a state n by f_{e_n} which is a function of the energy e_n and set $\bar{f}_e = (1 - f_e)$. The Boltzmann equation reads

$$\frac{df_e}{dt} = M[f]_e + \epsilon D[f]_e \quad (2.43)$$

with collision integral

$$\begin{aligned} M[f]_e &= \int_0^1 de_1 de_2 de_3 \delta(e + e_1 - e_2 - e_3) (\bar{f}_e \bar{f}_{e_1} f_{e_2} f_{e_3} - f_e f_{e_1} \bar{f}_{e_2} \bar{f}_{e_3}) \\ &= \frac{1}{L^2} \sum_{i,j,l} (\bar{f}_e \bar{f}_{e_i} f_{e_j} f_{e_l} - f_e f_{e_i} \bar{f}_{e_j} \bar{f}_{e_l}) \delta_{e+e_i, e_j+e_l}. \end{aligned}$$

The Kronecker delta and the delta function ensure conservation of energy during each collision event. To simplify the model we have set all transition rates equal to unity.

We assume that the system is weakly coupled to a bath which allows for particle exchange. Thus, there are additional loss and gain processes which we describe by

$$D[f]_e = -l_e f_e + g_e \bar{f}_e. \quad (2.44)$$

Here, l_e and g_e denote particle loss (cooling) and gain (heating) rates, respectively. In the steady state, the temperature and chemical potential of the system are determined by the ration l_e/g_e . Both of them are independent of the exact strength of the perturbation as long as ε is small. Note that in the presence of Eq. (2.44), the total energy $E = \sum_n e_n f_{e_n}$ and the total particle number $N = \sum_n f_n$ are only approximately conserved.

The perturbation theory for the steady states formulated in the language of Liouvillians can in a one-to-one correspondence be translated to the case of the open Boltzmann equation. Instead of a GGE, we expand around a Fermi-Dirac distribution

$$f_e^0(\beta, \mu) = \frac{1}{1 + e^{\beta(e-\mu)}} \quad (2.45)$$

as $M[f^0] = 0$ holds for any β and μ . This ansatz is equivalent to the choice of a GGE ($\rho_0 = \rho_{GGE}$) that always fulfills $\mathcal{L}_0 \rho_0 = 0$ in the formulation of the previous discussion. In the steady state the Lagrange parameters β for the energy and $-\beta\mu$ for the particle number are determined by Eq. (2.7). For the open Boltzmann equation these condition read in the thermodynamic limit

$$\int de c_i(e) D[f^0]_e = 0, \quad (2.46)$$

where we have denoted the conserved quantities by $c_1(e) = e$ and $c_2(e) = 1$. For our explicit choice of the perturbation, we obtain the following equations

$$\begin{aligned} \frac{1}{L} \frac{dE}{dt} &\approx \varepsilon \int de e (-l_e f_e^0 + g_e (1 - f_e^0)) \stackrel{!}{=} 0, \\ \frac{1}{L} \frac{dN}{dt} &\approx \varepsilon \int de (-l_e f_e^0 + g_e (1 - f_e^0)) \stackrel{!}{=} 0. \end{aligned} \quad (2.47)$$

These conditions can again be formulated with the help of a projection operator \hat{P} that projects on the tangential space at f_e^0 which is spanned by the slow modes $q_i^{\beta, \mu}$,

$$q_1^{\beta, \mu}(e) = \frac{\partial f_e^0}{\partial \beta}, \quad q_2^{\beta, \mu}(e) = \frac{\partial f_e^0}{\partial (-\beta\mu)}. \quad (2.48)$$

In analogy to Eq. (2.13) the projection operator \hat{P} can be defined by

$$\hat{P}[X] = - \sum_{i,j=1}^2 q_i^{\beta,\mu}(e) (\chi^{-1})_{ij} \int de (c_j(e) X(e)), \quad (2.49)$$

$$\chi_{ij}(\beta, \mu) = - \int de c_i(e) q_j^{\beta,\mu}(e).$$

Using this definition, condition Eq. (2.46) can be written as

$$\hat{P}[D[f^0]] = 0$$

which is the analogue of Eq. (2.17). We expect that after a short relaxation time, a Fermi-Dirac distribution is a good approximation to the state of the system. Thus, after a few collision processes the system can be described by a pair of time-dependent parameters $\{\beta(t), \mu(t)\}$. The generalized force governing the dynamics of the Lagrange parameters is according to Eq. (2.16) and Eq. (2.49) given by

$$F_i(\beta, \mu) = -(\chi^{-1})_{ij} \int de c_j(e) \varepsilon D[f^0]_e. \quad (2.50)$$

As the system has only two conservation laws, the generalized force has likewise only two components. The equations of motion of the Lagrange parameter read to leading order in ε

$$\frac{d\beta}{dt}(t) = F_1(t), \quad \frac{d(-\beta\mu)}{dt}(t) = F_2(t). \quad (2.51)$$

A complete comparison between the perturbation theory in the Liouvillian and the open Boltzmann case can be found in table 2.1 at the end of this section.

In order to investigate the relaxation dynamics numerically, we initialize the system at $t = 0$ in a non-equilibrium state with $f_{e_n} = 0$ for odd and $f_{e_n} = 1$ for even n . Thus, in the thermodynamic limit the total number of particles and the total energy are initially $N = L/2$ and $E = L^2/4$. This corresponds to a Fermi-Dirac distribution with $\beta(t=0) = 0$ and $\beta(t=0)\mu(t=0) = 0$. As parameters we take $g_e = 1/4$, $l_e = e$ and set $\varepsilon = 0.01$, $L = 41$. It is reasonable to assume that particles with higher energies leave the system with a higher probability while the gain rate is fixed by the environment. In Fig 2.4 the resulting generalized force field and the trajectory for the chosen initial conditions are plotted within the space of Lagrange parameters. In the steady state we find $\beta = 2.328$ and $\mu = 0.288$. A comparison between the dynamics of the exact occupation functions and the time-dependent Fermi-Dirac distributions for a few levels is shown in Fig. 2.5. After a short time $\tau_0 \sim 5$, which we find to be independent of ε for small ε , collision processes have relaxed the system to a thermal state. The subsequent dynamics is governed by the perturbation and can be qualitatively described by Eq. (2.51). This can be seen in Fig. 2.5 by comparing dots (time-dependent Fermi-Dirac distribution) and solid lines (exact time evolution). However, there are deviations for finite values of ε . Similarly to the

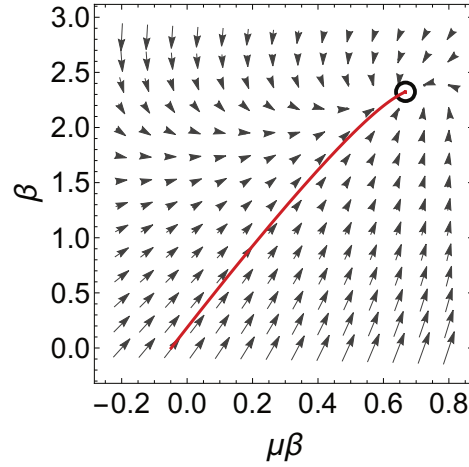


Figure 2.4 Generalized force field calculated with Eq. (2.50) for $L = 41$. The force determines the time evolution of the Lagrange parameters according to Eq. (2.51). The red solid line shows the trajectory for the chosen initial conditions where the unique stationary state is indicated by a black circle. The caption is partially taken from [87].

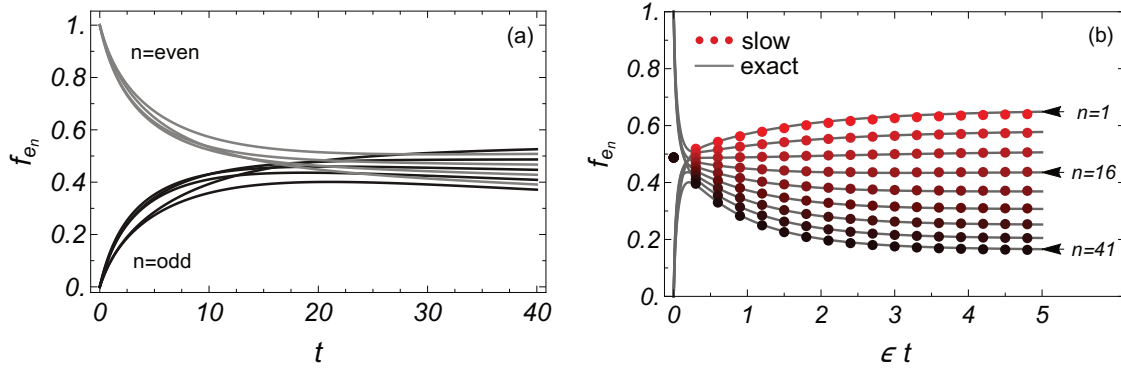


Figure 2.5 Time evolution of the occupation function f_{e_n} shown for $n = 1, 6, 11, \dots, 41$ ($L = 41$) and $\varepsilon = 0.01$ starting from an initial state with $f_{e_n} = 1$ ($f_{e_n} = 0$) for states with even (odd) n , respectively. Left: on short time scales the system relaxes towards a state with $\beta \approx 0$ and equal occupation of all levels. Right: the time evolution toward the steady state occurs on a time scale set by $1/\varepsilon$ and therefore the time axis has been rescaled by a factor ε . The points are obtained by solving the time evolution of the Lagrange parameters using Eq. (2.51) which then determine a Fermi distribution function. The comparison with the exact solution of the Boltzmann equation (lines) shows that this allows for a quantitative description of the slow dynamics for small ε . The caption is partially taken from [87].

Liouvillian case, we therefore expand the steady state occupation function

$$f_e(t \rightarrow \infty) = \sum_m \varepsilon^m f_e^m \quad (2.52)$$

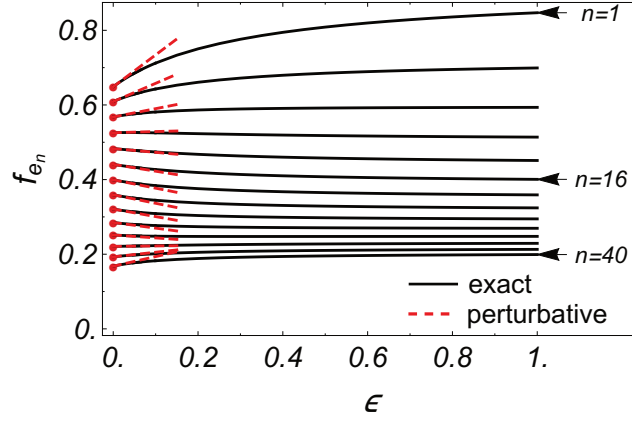


Figure 2.6 Level occupation f_{e_n} as a function of perturbation strength ε . Solid lines are obtained from the exact calculation using the Boltzmann equation, Eq. (2.43), while dashed lines are obtained from the perturbative approach, including zeroth and first order in ε . Only every third n is shown for a system with $L = 41$ single-particle states. The caption is partially taken from [87].

in ε . According to Eq. (2.43), $f_e(t \rightarrow \infty)$ fulfills $M[f_e(t \rightarrow \infty)] + \varepsilon D[f_e(t \rightarrow \infty)] = 0$. In a linear approximation $f_e(t \rightarrow \infty) \approx f_e^0 + \varepsilon f_e^1$, this equation reads

$$\begin{aligned} 0 &= \varepsilon(M^{(0)} + \varepsilon D^{(1)})[f^1] + \varepsilon D[f^0] \\ \Leftrightarrow f^1 &= -(M^{(0)} + \varepsilon D^{(1)})^{-1} D[f^0], \end{aligned} \quad (2.53)$$

where the matrices $M^{(0)}$ and $D^{(1)}$ are defined by a Taylor expansion

$$\begin{aligned} M[f_{e_n}] &\approx \varepsilon \sum_{n'} M_{n,n'}^{(0)} f_{e_{n'}}^1, \\ D[f_{e_n}] &\approx D[f^0]_{e_n} + \varepsilon \sum_{n'} D_{n,n'}^{(1)} f_{e_{n'}}^1. \end{aligned} \quad (2.54)$$

For our choice of perturbation, $D^{(1)}$ is simply a diagonal matrix. Note that Eq. (2.53) has the same form as Eq. (2.4). Similarly, the first order correction $\mathbf{f}^1 = (f_{e_1}^1, \dots, f_{e_L}^1)$ has to be evaluated in the parallel and the perpendicular subspaces, respectively. Using Eq. (2.53) the contributions to the first order correction $\mathbf{f}^1 = \mathbf{f}_{\parallel}^1 + \mathbf{f}_{\perp}^1$ are given by

$$\begin{aligned} \mathbf{f}_{\perp}^1 &= -(QM^{(0)}Q)^{-1} D[\mathbf{f}^0], \\ \mathbf{f}_{\parallel}^1 &= (PD^{(1)}P)^{-1} PD^{(1)}Q (QM^{(0)}Q)^{-1} D[\mathbf{f}^0]. \end{aligned}$$

For a concrete calculation, i.e. a finite number of energy levels, the integral in the definition of the projection operator \hat{P} has to be replaced by a sum. Then, \hat{P} , $\hat{Q} = 1 - \hat{P}$, $D^{(1)}$ and $M^{(0)}$ can be expressed in terms of finite matrices.

Fig. 2.6 shows the steady state occupation function f_{e_n} in dependence of ε for 14 different energy

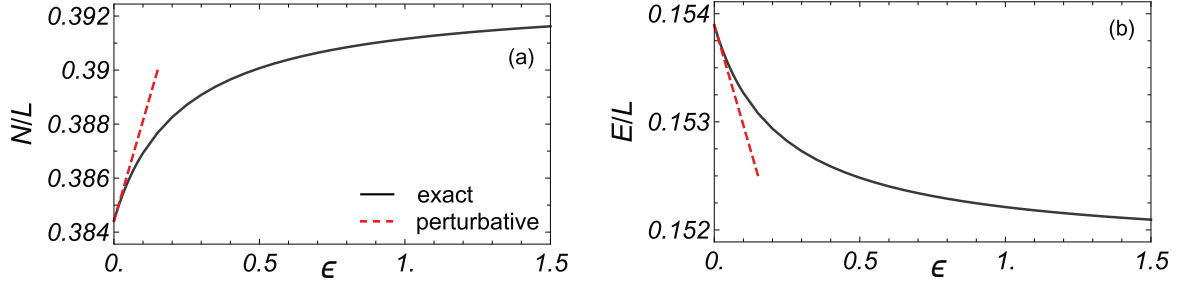


Figure 2.7 Steady state expectation value of (a) particle and (b) energy density as a function of perturbation strength ϵ . The dashed line shows the result obtained from perturbation theory, including zeroth and first order in ϵ while the solid line shows exact results obtained from solving the open Boltzmann equation. The caption is partially taken from [87].

Table 2.1 Comparison of semi-classical open Boltzmann dynamics for level occupation functions and quantum Liouvillian formulation for density matrices.

| Boltzmann | Liouvillian |
|---|---|
| occupation function f_e | density matrix ρ |
| $\frac{df_e}{dt} = M[f]_e + \epsilon D[f]_e$ | $\frac{d\rho}{dt} = \mathcal{L}_0\rho + \mathcal{L}_1\rho$ |
| $f_e(t \rightarrow \infty) = f_e^0 + \delta f_e$ | $\rho(t \rightarrow \infty) = \rho_0 + \delta\rho$ |
| Fermi function: $f_e^0 = \frac{1}{1+e^{\beta(\epsilon-\mu)}}$ | GGE: $\rho_0 = \frac{e^{-\lambda_i C_i}}{\text{Tr}[e^{-\lambda_i C_i}]}$ |
| <i>conservation laws and scalar product</i> | |
| $c_i(e)$ and $q_i^{\beta,\mu}$ | C_i and $\partial\rho_0/\partial\lambda_i$ |
| $\int de c_i(e) f_e$ | $\text{Tr}[C_i\rho] = \langle C_i \rangle$ |
| $\chi_{ij}(\beta, \mu) = -\int de c_i(e) q_j^{\beta,\mu}(e)$ | $\chi_{ij} = -\text{Tr}[C_i \partial\rho_0/\partial\lambda_j]$ |
| <i>zeroth order perturbation theory</i> | |
| $\int de c_i(e) \epsilon D[f^0]_e = 0$ | $\text{Tr}[C_i \mathcal{L}_1\rho_0] = 0$ |
| $\hat{P}[D[f^0]] = 0$ | $\hat{P}(\mathcal{L}_1\rho_0) = 0$ |
| <i>first order corrections</i> | |
| $f_{\perp}^1 = -(QM^{(0)}Q)^{-1}QD[f^0]$ | $\delta\rho_{1,\perp} = -(\hat{Q}\hat{\mathcal{L}}_0\hat{Q})^{-1}\hat{Q}\hat{\mathcal{L}}_1\rho_0$ |
| $f_{\parallel}^1 = (PD^{(1)}P)^{-1}PD^{(1)}Q$ $\times (QM^{(0)}Q)^{-1}QD[f^0]$ | $\delta\rho_{1,\parallel} = (\hat{P}\hat{\mathcal{L}}_1\hat{P})^{-1}\hat{P}\hat{\mathcal{L}}_1\hat{Q}$ $\times \hat{\mathcal{L}}_0^{-1}\hat{Q}\hat{\mathcal{L}}_1\rho_0$ |

levels. We find that in the limit $\epsilon \rightarrow 0$, the slope of $f_{e_n}(\epsilon)$ can be reproduced by the first order correction f^1 .

In Fig. 2.7 the steady state expectation values of the two approximately conserved quantities, energy and particle number, are depicted. Both quantities depend only weakly on ϵ . Nevertheless, we see that an expansion of $f_{e_n}(\epsilon)$ to linear order yields the correct ϵ dependence as long as ϵ is small. Higher order-corrections can be straightforwardly obtained by expanding and solving $M[f_e] + \epsilon D[f_e] = 0$ subsequently in each order of ϵ using the already obtained lower order results.

While the structure of the perturbation theory is the same in the case of the open Boltzmann equation

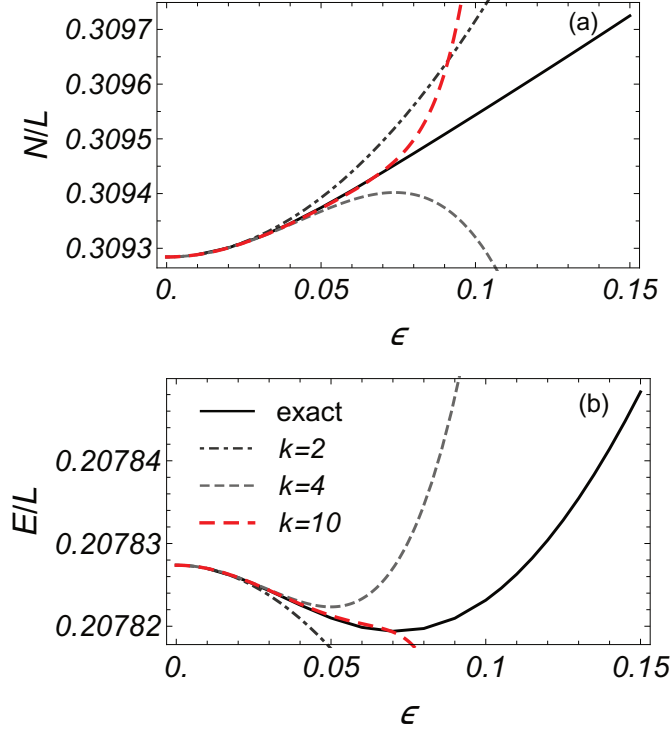


Figure 2.8 Expectation values of (a) particle and (b) energy density as a function of perturbation strength ϵ . We compare perturbative results of order $k = 2, 4, 10$ to the numerically exact values. Parameters: $L = 4$, $U = 0.3$.

and Liouvillian dynamics (separation between the corrections in tangential and perpendicular subspaces), we expect that corrections beyond the linear approximation differ. This is due to the fact that the Liouville equation is a linear while the Boltzmann equation is a non-linear equation.

2.4.2 Lindblad dynamics of fermions

As in the previous example, we consider a fermionic system with L discrete energy levels $e_n = n/L$ ($n = 1, \dots, L$). The Hamiltonian of the system reads

$$H_0 = \sum_{n=1}^L e_n c_n^\dagger c_n + U \sum_{n_1 > n_2, n_3 < n_4} c_{n_1}^\dagger c_{n_2}^\dagger c_{n_3} c_{n_4}, \quad (2.55)$$

where the first term describes the single-particle energies and the second one interactions between fermions in different levels. The full set of local and non-local conservation laws of H_0 is given by the projection operators $|n\rangle \langle n|$ on the many-particle eigenstates $|n\rangle$, $H_0 |n\rangle = \epsilon_n |n\rangle$. A detailed discussion of how these charges can be implemented within the formalism presented above can be found in the next chapter. Here, we briefly present the numerical results we obtain for a small system. We consider again the case that the system is weakly coupled to an environment which allows for particle

exchange. Moreover, it is assumed that this coupling can be captured by a Lindbladian

$$\begin{aligned}
\mathcal{L}_1 &= \varepsilon(\hat{\mathcal{D}}_g + \hat{\mathcal{D}}_l) \quad (\varepsilon \ll 1), \\
\hat{\mathcal{D}}_g &= \sum_n g_n \left(L_n^g \rho L_n^{g\dagger} - \frac{1}{2} \{L_n^{g\dagger} L_n^g, \rho\} \right), \\
\hat{\mathcal{D}}_l &= \sum_n l_n \left(L_n^l \rho L_n^{l\dagger} - \frac{1}{2} \{L_n^{l\dagger} L_n^l, \rho\} \right),
\end{aligned} \tag{2.56}$$

where $\hat{\mathcal{D}}_g$ describes gain processes and $\hat{\mathcal{D}}_l$ particle losses. As Lindblad operators, we simply choose $L_n^g = c_n^\dagger$, $L_n^l = c_n$ and set as above $g_n = 1/4$, $l_n = e_n$. Using the formulas derived in this chapter we can determine the zeroth order of the steady state density matrix and corrections to it in higher orders of ε . In Fig. 2.8 the steady state expectation values of the particle number N/L and energy density E/L are shown as a function of ε for $L = 4$. Similar to Fig. 2.7, the ε dependence of N/L and E/L is very weak. We compare numerically exact values with results obtained from perturbative approximations up to order $k = 0, 2, 4$ and $k = 10$. We find that for the tiny system considered with finite level spacing, perturbation theory works for values of ε which are much smaller than the mean level spacing.

We also observe that in the finite system, corrections linear in ε vanish, cf. Sec. 3.3. It is important to note that there is a crucial difference between perturbation theory in finite and infinite systems. At finite L , the regulator η in Eq. (2.4) needs to be smaller than the mean level spacing ΔE for perturbation theory to be valid. However, in the thermodynamic limit, we are typically in the opposite regime with $\eta \gg \Delta E$. We will address this question in more detail at the end of the following chapter.

Chapter 3

Time-dependent generalized Gibbs ensembles

In the last chapter, we have developed a perturbation theory for the steady state of weakly open quantum systems that have a set of approximate conservation laws. As an expansion point, we use a GGE determined only by the form of the weak perturbation and the approximate symmetries of the system. We have applied our approach to two similar fermionic models which are subject to weak particle losses and gains. In the first example, we have considered the thermodynamic limit of the model and treated the dynamics semi-classically in terms of a weakly open Boltzmann equation where we have included only two local conservation laws in the analysis. In the second example, we have simulated gain and losses through a Markovian Liouvillian in a very small system and have taken all local and non-local conservation laws of the model into account. We have investigated both the validity of the expansion point as well as the effect of higher order corrections by comparing the perturbative results to numerically exact solutions.

In this chapter we focus on weakly perturbed integrable systems that have an extensive set of local and quasilocal approximately conserved quantities. Precisely, we consider the integrable one-dimensional XXZ model that is brought out of equilibrium by a small perturbation. As before, we ask whether a GGE can describe the steady state. Moreover, we are interested in the question of how well a time-dependent GGE can capture the dynamics of the system after a certain prethermalization time. For simplicity, we restrict our analysis to cases with Markovian perturbations where the zeroth order of the steady state density matrix can be determined in first order of \mathcal{L}_1 . The general form of the perturbation, we consider reads

$$\begin{aligned}\mathcal{L}_1 &= \varepsilon \left((1 - \gamma) \hat{\mathcal{D}}^{(1)} + \gamma \hat{\mathcal{D}}^{(2)} \right) \\ \hat{\mathcal{D}}^{(i)} \rho &= \sum_{\alpha} \left(L_{\alpha}^{(i)} \rho L_{\alpha}^{(i)\dagger} - \frac{1}{2} \{ L_{\alpha}^{(i)\dagger} L_{\alpha}^{(i)}, \rho \} \right)\end{aligned}\tag{3.1}$$

where $\hat{\mathcal{D}}^{(i)}$ ($i = 1, 2$) are different Lindblad dissipators and $\varepsilon \ll 1$. We choose the perturbation such that one term, typically, describes heating ($i = 1$) and the other one cooling processes ($i = 2$). Following the arguments of the previous chapter, the steady state is then to zeroth order determined by the balance of heating and cooling (gains and losses) and depends for fixed $\hat{\mathcal{D}}^{(1)}, \hat{\mathcal{D}}^{(2)}$ only on the relative perturbation strength $\gamma \in [0, 1]$. Due to driving (gain processes) compensating for losses, the steady state can be far away from equilibrium even though ε is small. As a measure for the validity of the GGE ansatz, we compare the expectation values of activated local observables O calculated from the GGE ansatz to expectation values obtained from numerically exact solutions. By activated we mean that a non-zero expectation value is, in principle, allowed by symmetry. An observable O is said to be activated if there are no symmetry transformations $\hat{\mathcal{S}}, \hat{\mathcal{S}}'$ that map $\hat{\mathcal{S}} : O\rho_{H_0} \rightarrow -O\rho_{H_0}$ and $\hat{\mathcal{S}}' : \dot{O}\rho_{H_0} \rightarrow -\dot{O}\rho_{H_0}$ where ρ_{H_0} is a statistical operator with the same symmetry properties as the unperturbed Hamiltonian fulfilling $\hat{\mathcal{L}}_0\rho_{H_0} = 0$. If such symmetry transformations exist, we have

$$\begin{aligned}\langle O \rangle_{\rho_{H_0}} &= \text{Tr}[\hat{\mathcal{S}}\hat{\mathcal{S}}^{-1}O\rho_{H_0}] = \text{Tr}[\hat{\mathcal{S}}^{-1}O\rho_{H_0}\hat{\mathcal{S}}] = -\langle O \rangle_{\rho_{H_0}}, \\ \langle \dot{O} \rangle_{\rho_{H_0}} &= \text{Tr}[\hat{\mathcal{S}}'\hat{\mathcal{S}}'^{-1}\dot{O}\hat{\mathcal{L}}\rho_{H_0}] = \text{Tr}[\hat{\mathcal{S}}'^{-1}\dot{O}\hat{\mathcal{L}}\rho_{H_0}\hat{\mathcal{S}}'] = -\langle \dot{O} \rangle_{\rho_{H_0}}\end{aligned}$$

which immediately yields $\langle \dot{O} \rangle_{\rho_{H_0}} = 0$ and $\langle O \rangle_{\rho_{H_0}} = 0$. Particularly, we are interested in cases where conserved currents are activated by external perturbations. For example, in order to activate a current that is odd under time-reversal symmetry (TRS) in a system being invariant under TRS, we have to define Lindblad operators L_α such that they do not simply transform as TRS: $L_\alpha \rightarrow e^{i\phi_\alpha}L_\alpha$ where ϕ_α is a real phase.

The GGE is only a valid concept in the thermodynamic limit if all quasilocal and local conserved quantities are included in the ansatz. However, in the absence of an analytic solution, we are due to numerical restrictions always limited to finite system sizes and finite number of conservation laws. In this chapter, we consider two examples of Markovian driving and address the limits $N \rightarrow \infty$ (system size) and $N_c \rightarrow \infty$ (number of conservation laws included in the GGE) separately.

3.1 Numerical verification of the GGE in the steady state

As pointed out in Sec. 2.2.2, the GGE in the steady state is determined by a set of coupled equations $F_i = 0 \forall i$, where F_i is the generalized force associated with the Lagrange parameter λ_i . To verify the GGE ansatz, we have to compare it to an exact solution.

However, in the numerical simulation of dissipative non-unitary dynamics, we face the problem that we do not deal with Hamiltonians but Liouville operators. While the Hamiltonian of a one-dimensional spin-1/2 system with N lattice sites has dimension 2^{2N} , the dimension of the corresponding Liouville operator is 2^{4N} . Thus, in order to determine the steady state, we have to calculate the kernel of a matrix whose dimension grows exponentially as $\exp(4\log(2)N)$. The complexity restricts the numerically exact calculation to extremely tiny system sizes. On the contrary, we want to use the exact solution to validate the GGE ansatz which is assumed to be only valid in the thermodynamic

limit. Hence, we have to find a way to obtain an exact solution at bigger system sizes. This goal can be achieved by identifying relevant degrees of freedom and replacing the Liouville operator by an effective Liouvillian, which acts only on the subspace of these relevant degrees of freedom.

In the limit $\varepsilon \rightarrow 0$, we can expect that we do not have to consider all components of the Liouville operator but only those describing transitions between approximately conserved quantities. A full set of (quasi)local and non-local, commuting and non-commuting conserved quantities is given by

$$\mathcal{Q} = \{|n\rangle\langle m| \text{ with } E_n^0 = E_m^0\}, \quad (3.2)$$

where $|n\rangle, |m\rangle$ are eigenstates of H_0 with corresponding eigenenergies E_n^0, E_m^0 . In order to obtain a set of hermitian charges, we can replace $|n\rangle\langle m|$ and $|m\rangle\langle n|$ in Eq. (3.2) by $(|n\rangle\langle m| + |m\rangle\langle n|)/2$ and $(|n\rangle\langle m| - |m\rangle\langle n|)/(2i)$ for $n \neq m$. A projection operator $\hat{P}_{\mathcal{Q}}$ on \mathcal{Q} is defined through $\hat{P}_{\mathcal{Q}}X = \hat{P}X + (\text{Tr}[X]/\text{Tr}[\mathbb{1}])\mathbb{1}$. Importantly, any linear combination of elements Q_{nm} of \mathcal{Q} commutes with H_0 . This motivates to introduce the block-diagonal ensemble

$$\rho_{BD} = \sum_{nm} \alpha_{nm} \mathcal{Q}_{nm} \quad (3.3)$$

which is formally a solution of $\hat{\mathcal{L}}_0 \rho_{BD} = 0$ for all possible choices of $\alpha_{nm} \in \mathcal{C}$. Note that we have to require $\alpha_{nn} \in \mathcal{R}_0^+$, $\alpha_{nm} = \alpha_{mn}^*$ and $\sum_n \alpha_{nn} = 1$ for ρ_{BD} to be a well defined statistical operator. In generic systems without any degeneracies, Eq. (3.3) simplifies to the diagonal ensemble. The coefficients α_{nm} in the steady state can be determined by using condition Eq. (2.7) and calculating the kernel of the effective Liouvillian

$$\left(\hat{\mathcal{L}}^{\mathcal{Q}}\right)_{nm}^{n'm'} = \text{Tr}[\mathcal{Q}_{n'm'}^\dagger \hat{\mathcal{L}}_1 \mathcal{Q}_{nm}]. \quad (3.4)$$

If the degree of degeneracy is small, the dimension d ($2^{2N} \leq d \leq 2^{4N}$) of $\hat{\mathcal{L}}^{\mathcal{Q}}$ is much smaller than 2^{4N} . Thus, using the block-diagonal ansatz much larger system sizes can be calculated numerically. Similarly, the effective Liouvillian in the case of unitary perturbations reads

$$\left(\hat{\mathcal{L}}^{\mathcal{Q}}\right)_{nm}^{n'm'} = -\text{Tr}[\mathcal{Q}_{n'm'}^\dagger \hat{\mathcal{L}}_1 \hat{\mathcal{L}}_0^{-1} \hat{\mathcal{L}}_1 \mathcal{Q}_{nm}]. \quad (3.5)$$

We can proceed in two steps to investigate how well a truncated GGE can capture the steady state. Firstly, we validate numerically that the block-diagonal ensemble becomes exact in the limit $\varepsilon \rightarrow 0$ by comparing steady state expectation values of local observables at small system sizes. Secondly, we do the same comparison between the block-diagonal density matrix and a truncated GGE at larger N . Note that the GGE ansatz using maximally $\mathcal{O}(N)$ parameters is much more accessible to numerical studies than the block-diagonal and the numerically exact method using $\mathcal{O}(2^N)$ and $\mathcal{O}(4^N)$ parameters, respectively. The following chapter is partially based on [100].

3.2 Time evolution of weakly open quantum systems

3.2.1 Time-dependent GGE

In Sec. 2.4.1 we have used time-dependent temperatures and chemical potentials to describe the dynamics of fermionic occupation functions in a weakly open system. Here, we address the question whether a translationally invariant many-particle system in the presence of weak integrability breaking perturbations is generically described by a time-dependent generalized Gibbs ensemble

$$\rho_{GGE}(t) = \frac{e^{-\sum_i \lambda_i(t) C_i}}{\text{Tr}[e^{-\sum_i \lambda_i(t) C_i}]}, \quad (3.6)$$

where $\lambda_i(t)$ are time-dependent Lagrange parameters. We assume that the system is initialized in a state $\rho(0)$ and the dynamics is switched on at time $\tau = 0$ where $\tau = J\epsilon t$ is a dimensionless time variable. A description in terms of a time-dependent GGE defined by the form of the perturbation can only be valid for $\tau = \epsilon Jt \gtrsim 1$ and only applies to the expectation values of local observables O , i.e. $\text{Tr}[O\rho(t)] \approx \text{Tr}[O\rho_{GGE}(t)]$.

At small times $\tau \ll 1$, the effect of the weak perturbation can be neglected and the dynamics reduces to a standard quench problem for an integrable system with Lagrange parameters λ_i defined by $\text{Tr}[C_i\rho(\tau \rightarrow 0)] \stackrel{!}{=} \text{Tr}[C_i\rho_{GGE}(\tau \rightarrow 0)]$. In quench protocols the emergence of GGEs has been observed in many studies [101–104], even in the presence of small integrability breaking perturbations [105]. They eventually lead to thermalization on the longest time scales. However, it was found that at intermediate times, on the prethermalization plateau, the system can be well described by a GGE with Lagrange parameters fixed by the initial conditions. The dynamics of weakly open quantum systems at times $\tau \ll 1$ is therefore closely related to the prethermalization regime in quench protocols.

In the following we focus on times $\tau \gtrsim 1$. In this regime, the dynamics of the Lagrange parameters is up to vanishing corrections for small values of ϵ governed by the generalized forces $F_i(t) \approx -\sum_j (\chi(t)^{-1})_{ij} \text{Tr}[C_j \mathcal{L}_1 \rho_{GGE}(t)]$,

$$\dot{\lambda}_i(t) = F_i(\boldsymbol{\lambda}(t)) \quad (3.7)$$

which were introduced in Sec. 2.2.2. Note that in the case of a time-independent perturbation \mathcal{L}_1 , the generalized forces do not depend explicitly on time but only indirectly through the Lagrange parameters. As $F_i(t) \sim \epsilon$ for Markovian perturbations, the time evolution in the subspace of GGEs is slow where the time scale is set by $1/\epsilon$.

Alternatively, Eq. (3.7) can also be derived by projecting the full dynamics onto the subspace of slow modes which separates the slow dynamics within the subspace from the fast dynamics in the perpendicular subspace. As above we set $\rho(t) = \rho_{GGE}(t) + \delta\rho(t)$ with $\rho_{GGE}(t)$ defined such that $\delta\rho(t) \sim \epsilon$ vanishes in the limit $\epsilon \rightarrow 0$. Using the time-dependent version of the projection operator

Eq. (2.13) we obtain

$$\hat{P}(t)(\dot{\rho}_{GGE} + \delta\dot{\rho}) = \hat{P}(t)(\hat{\mathcal{L}}_0 + \hat{\mathcal{L}}_1)(\rho_{GGE} + \delta\rho) \quad (3.8)$$

which simplifies with $\hat{P}(t)\dot{\rho}_{GGE} = \dot{\rho}_{GGE}$, $\hat{\mathcal{L}}_0\rho_{GGE} = 0$, $\hat{P}(t)\hat{\mathcal{L}}_0\delta\rho = 0$ and $\hat{\mathcal{L}}_1\delta\rho \sim \varepsilon^2$ to

$$\hat{P}(t)\delta\dot{\rho} + \dot{\rho}_{GGE} = \hat{P}(t)\hat{\mathcal{L}}_1\rho_{GGE} + \mathcal{O}(\varepsilon^2). \quad (3.9)$$

We can identify $\hat{P}(t)\delta\dot{\rho}$ on the left hand side of Eq. (3.9) with the terms of order ε^2 on the right hand side. This leads to $\dot{\rho}_{GGE} = \hat{P}(t)\hat{\mathcal{L}}_1\rho_{GGE}$ which is equivalent to Eq. (3.7). Hence, we can deduce that the GGE ansatz fulfills the time-evolution equation $\dot{\rho} = \hat{\mathcal{L}}\rho$ projected onto the conservation laws up to corrections of order ε^2 . However, the argument above does not guarantee that the GGE ansatz is a valid description in the long-time limit as small errors might add up leading to wrong predictions. This could, for example, be the case if the steady state we expand around is not unique. In this chapter, we only consider perturbation leading to a unique steady state.

3.2.2 Time-dependent block-diagonal density matrix

In analogy to the time-dependent GGE, we can define a time-dependent block-diagonal density matrix by

$$\rho_{BD}(t) = \sum_{E_n^0=E_m^0} \alpha_{nm}(t) \mathcal{Q}_{nm}, \quad (3.10)$$

where the coefficients α_{nm} at initial time $\tau = 0$ are given by $\alpha_{nm}(0) = \langle n|\rho(0)|m\rangle$. The time evolution of Eq. (3.10) can be determined by demanding $\text{Tr}[|m\rangle\langle n|\dot{\rho}(t)] \stackrel{!}{=} \text{Tr}[|m\rangle\langle n|\dot{\rho}_{BD}(t)]$ up to corrections vanishing for $\varepsilon \rightarrow 0$. By approximating $\dot{\rho}_{BD}(t) \approx \hat{\mathcal{L}}_1\rho_{BD}$ we obtain a set of coupled linear differential equations for $\alpha_{nm}(t)$,

$$\dot{\alpha}_{nm}(t) = \sum_{E_n^0=E_m^0} (\hat{\mathcal{L}}^{\mathcal{Q}})_{nm,n'm'} \alpha_{n'm'}(t), \quad (3.11)$$

where $\hat{\mathcal{L}}^{\mathcal{Q}}$ is the effective Liouville operator which was introduced in the previous section. According to Eq. (3.4), the components of $\hat{\mathcal{L}}^{\mathcal{Q}}$ are given by

$$(\hat{\mathcal{L}}^{\mathcal{Q}})_{nm,n'm'} = \text{Tr}[|m\rangle\langle n|\hat{\mathcal{L}}_1|n'\rangle\langle m'|]. \quad (3.12)$$

Note that, in general, the matrix $\hat{\mathcal{L}}^{\mathcal{Q}}$ is not hermitian and therefore its eigenvectors are not orthogonal. Hence, we have to use the projection operator Eq. (1.6) to project the initial state onto the eigenstates of $\hat{\mathcal{L}}^{\mathcal{Q}}$. We can then employ the decomposition Eq. (1.5) with the right eigenstates of the full Liouvillian replaced by the right eigenstates of $\hat{\mathcal{L}}^{\mathcal{Q}}$ to express the time evolution of $\rho_{BD}(t)$. Similarly to the steady state analysis, the time-dependent block-diagonal density matrix can serve as an exact

comparison to the time-dependent truncated GGE for $\varepsilon \rightarrow 0$ which requires that $\rho_{BD}(t)$ becomes exact in this limit. We can prove this statement by comparing $\rho_{BD}(t)$ to the numerically exact time evolution of $\rho(t)$ which can be obtained by diagonalizing the full Liouvillian and using Eq. (1.5).

3.3 Lindblad dynamics I

We consider the one-dimensional Heisenberg model (XXZ model with $\Delta = J$)

$$H_0 = J \sum_j \mathbf{S}_j \cdot \mathbf{S}_{j+1}$$

which is at initial time $\tau = 0$ described by the statistical operator $\rho(0)$. The dynamics of $\rho(t)$ is governed by the Liouville equation

$$\begin{aligned} \partial_t \rho &= (\mathcal{L}_0 + \mathcal{L}_1) \rho, \\ \mathcal{L}_0 \rho &= -i[H_0, \rho], \quad \mathcal{L}_1 \rho = \varepsilon J \left((1 - \gamma) \hat{\mathcal{D}}^{(1)} + \gamma \hat{\mathcal{D}}^{(2)} \right) \rho, \end{aligned} \quad (3.13)$$

where $\hat{\mathcal{D}}^{(1)}, \hat{\mathcal{D}}^{(2)}$ are Lindblad dissipators. As Lindblad operators we choose

$$L_k^{(1)} = S_k^z \quad \text{and} \quad L_k^{(2)} = \frac{1}{2} (S_k^+ S_{k+1}^- + i S_{k+1}^- S_{k+2}^+). \quad (3.14)$$

The first Lindblad operator $L_k^{(1)}$ represents dephasing and would alone heat the system up to infinite temperature $\rho(t \rightarrow \infty) = \mathbb{1}$. Note that all Lindblad operators L_j fulfilling $[L_j, L_j^\dagger] = 0$ drive a system to the trivial state in the long-time limit. This can easily be seen by inserting $\rho = \mathbb{1}$ into Eq. (3.1). In the case of hermitian Lindblad operators like $L_k^{(1)}$, the condition $[L_j, L_j^\dagger] = 0$ is trivially fulfilled.

The second Lindblad operator $L_k^{(2)}$ is chosen such that it breaks all relevant symmetries up to S^z conservation. Particularly, $L_k^{(2)}$ does not simply transform as $L_k^{(2)} \rightarrow e^{i\phi_k} L_k^{(2)}$ under TRS or spatial mirror symmetries which, in principle, allows for the activation of the odd conservation laws (conserved currents) of the Heisenberg model. Compared to $\hat{\mathcal{D}}^{(1)}$, the second dissipator can be considered as a cooling mechanism. The relative strength of cooling and heating is set by the control parameter $\gamma \in [0, 1]$.

Due to the conservation of S^z , we restrict our numerical analysis to the $S^z = 0$ sector enabling us to treat larger system sizes. This is justified as the $S^z = 0$ sector is the largest and therefore assumed to be the most relevant one in the thermodynamic limit. The steady state can be found by determining the point in the space of Lagrange parameters where the generalized force vanishes. In Fig. 3.1 the generalized force field is shown as a function of the two Lagrange parameters λ_2 (Hamiltonian) and λ_3 (heat current operator). At $\gamma = 0$ the system reaches an infinite temperature state with $\lambda_2 = \lambda_3 = 0$ in the long-time limit while at $\gamma = 1$ the steady state is characterized by a large value of λ_3 corresponding to a large expectation value of the heat current operator.

In Fig. 3.2 the steady state expectation value of the energy and the heat current density are plotted

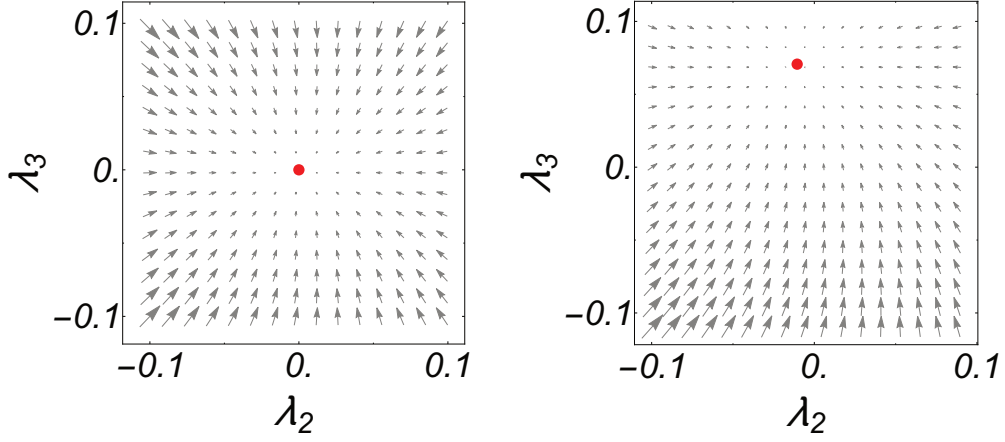


Figure 3.1 Generalized force $\mathbf{F}(\lambda_1, \lambda_2)$ calculated at $\gamma = 0$ (left) and $\gamma = 1$ (right). While at $\gamma = 0$, the infinite temperature state is the unique fixed point of the dynamics, the steady state at $\gamma = 1$ is highly non-thermal with $|\lambda_3| > |\lambda_2|$. Parameters: $N = 8, J = 1$

as a function of γ for $J = 1, N = 8$. The dashed lines show results obtained from the block-diagonal density matrix while the solid lines correspond to numerically exact calculations at different values of ε . We see that the numerically exact results converge towards the ones predicted by ρ_{BD} , when ε goes to zero. This implies that we can consider ρ_{BD} to be exact in the limit $\varepsilon \rightarrow 0$, at least as long as the expectation values of local observables are concerned. Note that this observation is not related to the specific choice of Lindblad operators since we have checked different combinations in Eq. (3.14) as well. Assuming that the block-diagonal ansatz is exact in the limit $\varepsilon \rightarrow 0$, we can use it as a reference for the truncated GGE at larger system sizes.

In Fig. 3.3 we show the steady state expectation values of $C_2 = H_0, C_3, C_4, C_5$ calculated from a tGGE containing $N_C = 4$ conservation laws and from ρ_{BD} at $N = 14$, respectively. We find a good agreement between both methods while the largest deviations can be observed at γ close to 1, when the system is in a highly non-equilibrium state. Even though the GGE is assumed to be only a valid ansatz in the limits of weak perturbations $\varepsilon \rightarrow 0$ and large system sizes $N \rightarrow \infty$, when all symmetry activated local and quasilocal conservation laws are taken into account $N_c \rightarrow \infty$, we find already very good agreement at moderate values of ε, N and N_c .

In Fig. 3.4 we summarize the results obtained from the three methods for the energy and the heat current density in a finite size scaling plot, allowing us to address the question whether the tGGE ansatz is valid in the limit $N \rightarrow \infty$. One of the main statements of Fig. 3.4 is that the truncated GGE becomes more accurate with increasing system size. We also find an improvement when increasing the number of included charges from $N_c = 2$ to $N_c = 4$. However, due to strong finite size effects in the numerically accessible small system sizes, we do not include more or more complex charges. We postpone the analysis of the limit $N_c \rightarrow \infty$ to the following section. At small system sizes $N = 6, 8$,

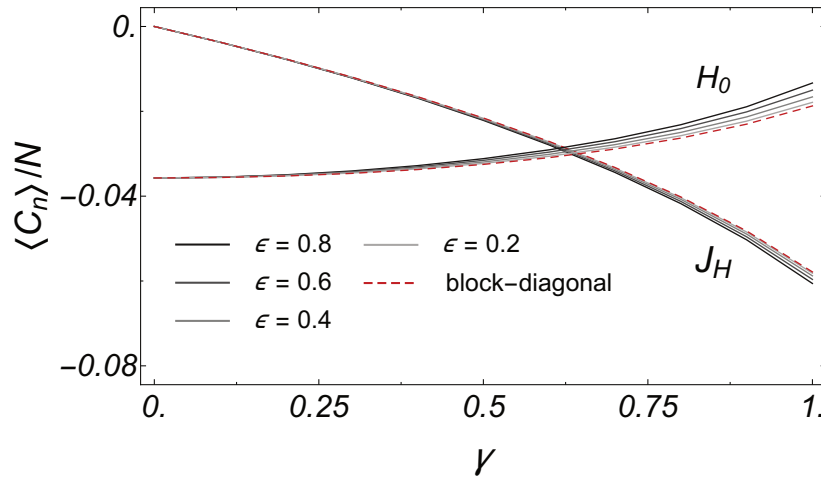


Figure 3.2 Steady state expectation value of the energy and the heat current density as a function of the relative driving strength γ . We compare numerically exact results calculated at different values of ϵ to those predicted by the block-diagonal ansatz which becomes exact in the limit $\epsilon \rightarrow 0$. Parameters: $J = 1, N = 8$.

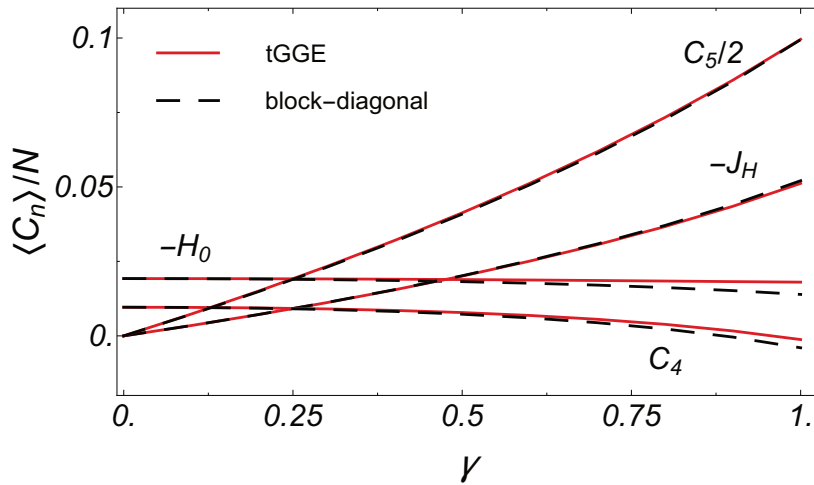


Figure 3.3 Rescaled steady state expectation values of H_0 , J_H , C_4 and C_5 as a function of γ . We find a good agreement between the tGGE ($N_c = 4$) and the block-diagonal ansatz ρ_{BD} . Parameters: $N = 14, J = 1$.

we also compare the block-diagonal and the exact density matrix at $\epsilon = 0.01$ and $\epsilon = 1$. While both methods agree at $\epsilon = 0.01$, we find distinct differences at large ϵ .

In Fig. 3.5 we show the steady state expectation values of the energy and heat current density as a function of the perturbation strength ϵ where we find only a very weak dependence on ϵ . The dashed lines represent the predictions of the block-diagonal density matrix that become exact in the limit $\epsilon \rightarrow 0$. The zeroth order results can be improved using the perturbative expansion for the steady state

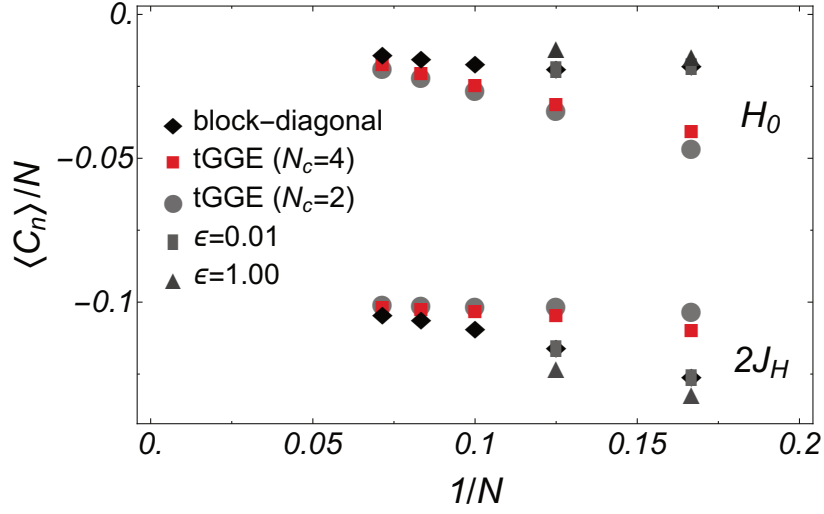


Figure 3.4 Finite size plot for the steady state expectation values of the energy and the heat current density calculated from the numerically exact density matrix ($\epsilon = 0.01, 1.00$), the block-diagonal density matrix and a tGGE ($N_c = 2, 4$).

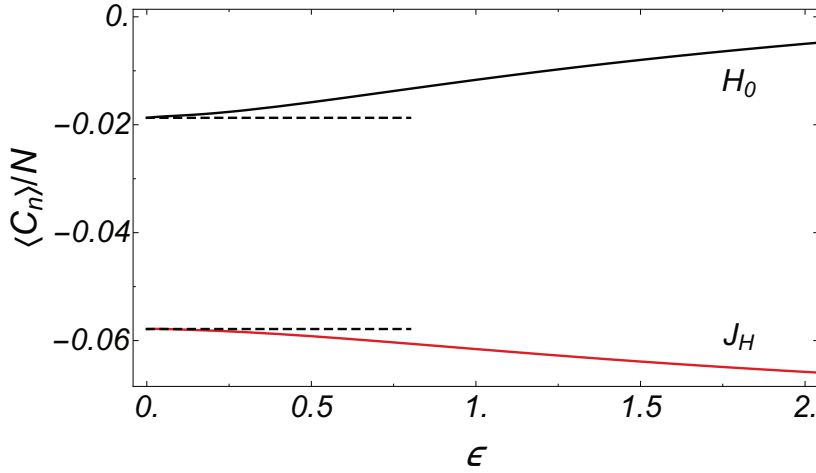


Figure 3.5 Steady state expectation values of the energy and the heat current density as a function of the perturbation strength ϵ . The dashed line shows the zeroth order prediction of the block-diagonal density matrix. Parameters: $N = 8, J = 1, \gamma = 1$.

that was introduced in Ch. 2.

As mentioned in Sec. 2.4.2, there is a distinct difference between perturbation theory in finite systems where ϵ needs to be smaller than the dimensionless level spacing $\delta \sim 1/N$ (or even smaller than the many-particle level spacing 2^{-N}) and infinite systems ($1/N \ll \epsilon \ll 1$) in which we are eventually interested in. In Fig. 3.5 we can indeed identify two regions $\epsilon \lesssim 0.1$ and $0.1 \lesssim \epsilon \lesssim 1$ with qualitatively different behavior. However, for definitive statements the system size considered is too small.

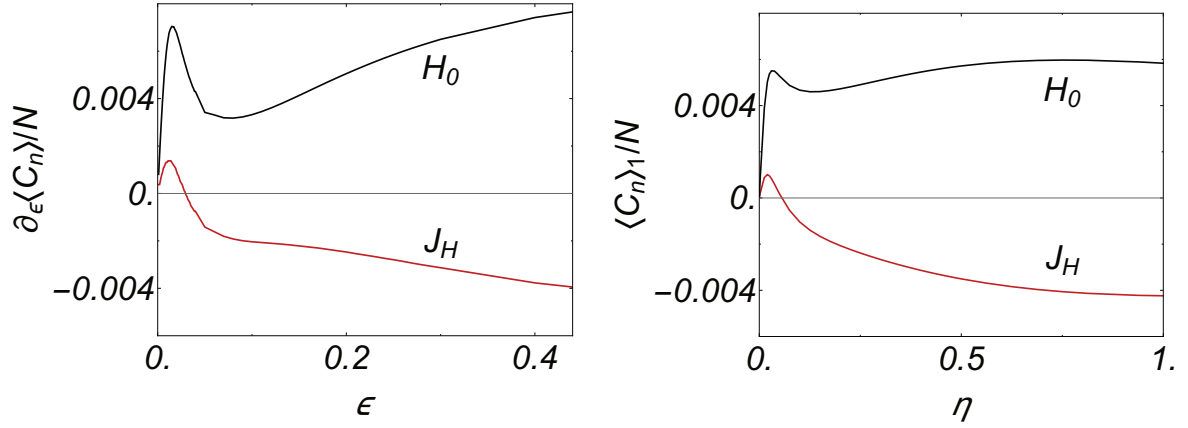


Figure 3.6 Derivative of the energy and heat current density, $\frac{d\langle H_0 \rangle}{d\epsilon}$ and $\frac{d\langle J_H \rangle}{d\epsilon}$ as a function of the perturbation strength ϵ calculated for $\gamma = 1, J = 1, N = 8$ (left). Calculation of the linear correction in ϵ form perturbation theory as a function of broadening η for the same parameters. The caption is taken from [100].

As we are primarily interested in first order corrections, we show in Fig. 3.6 the derivative of the energy and heat current density $d\langle H \rangle/d\epsilon$ and $d\langle J_H \rangle/d\epsilon$ with respect to ϵ (left side). We compare these results to the first order corrections $\langle H_0 \rangle_1$ and $\langle J_H \rangle_1$ calculated with Eq. (2.22) for different broadenings η (right side). While in the thermodynamic limit we typically have $\eta \gg J\delta$, at finite N we choose $\eta \ll J\delta$. Both plots show that the linear slope vanishes in the finite system. This can be easily understood when Eq. (2.22) is written in Lehmann representation. The inverse superoperator $(\mathcal{L}_0 - \eta)^{-1}$ then yields terms proportional to $\text{Im} \left[\frac{1}{E_n^0 - E_m^0 - i\eta} \right]$ ($E_n^0 \neq E_m^0$) which vanish for $\eta \ll J\delta$. Therefore, at finite N the leading order correction in the steady state is $\mathcal{O}(\epsilon^2/\delta)$. We expect that the linear correction does exist in the thermodynamic limit where $\delta \ll \epsilon \ll 1$ and $\delta J \ll \eta \ll J$. However, this regime is difficult to reach in an ED study. Finally, we can deduce from the qualitative agreement between the ϵ and η dependencies that the Lindblad coupling effectively leads to a broadening of levels.

Next, we investigate the time evolution of the weakly open system and address the question whether the dynamics can be described by a time-dependent GGE. As an initial state we choose a classical Néel configuration $|\psi_N\rangle$ with corresponding density operator $\rho(0) = |\psi_N\rangle \langle \psi_N|$. In Fig. 3.7 the time evolution of the nearest-neighbor spin-spin correlation function $\langle \sigma_i^z \sigma_{i+1}^z \rangle$ and the heat current density $\langle J_H \rangle / N$ are shown for $N = 8$. While the heat current is conserved in the unperturbed system, the operator $\sigma_i^z \sigma_{i+1}^z$ does not commute with H_0 . Again we compare the numerically exact results to those obtained from the block-diagonal ansatz. The value of $\langle \sigma_i^z \sigma_{i+1}^z \rangle$ drops from initially -1 to -0.45 on a short time scale of order $1/J = 1$ and then decays on a much longer time scale set by $1/\epsilon$ to its steady state value. At short times we observe rapid oscillations that get damped during the evolution. These oscillations are less pronounced for larger values of ϵ , i.e. stronger damping, and are due

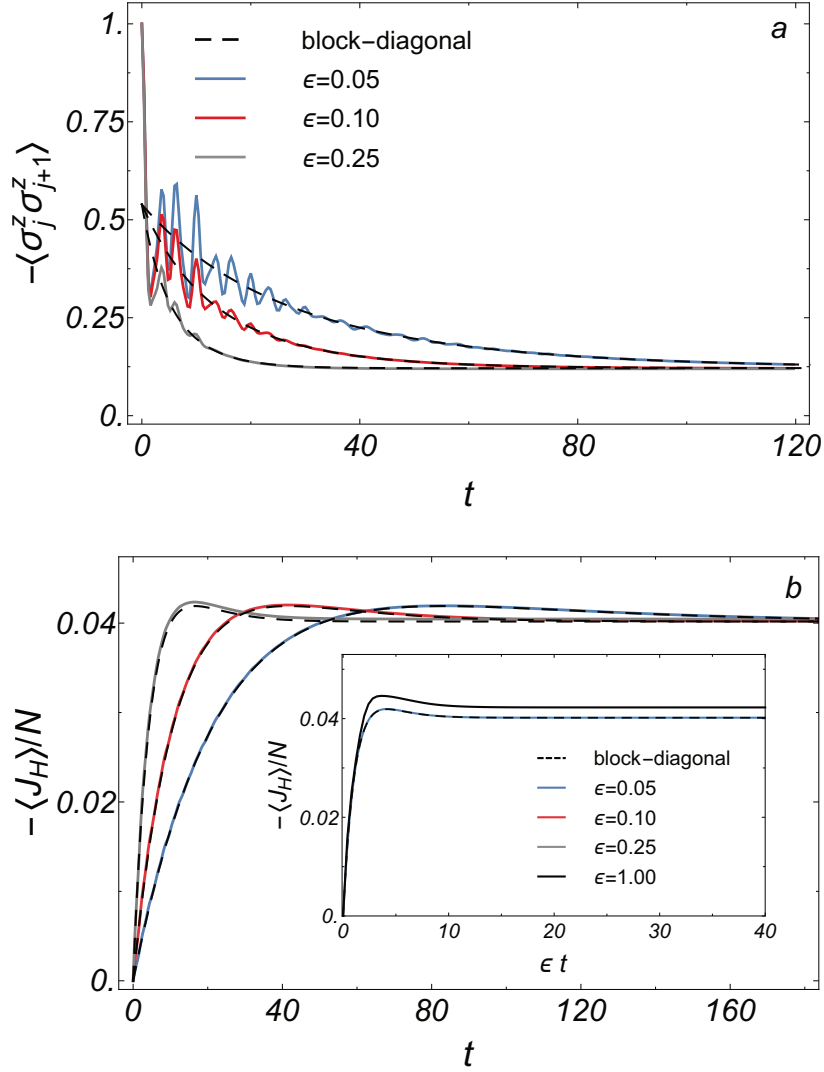


Figure 3.7 Time evolution of the a) spin-spin correlation function $\langle \sigma_j \sigma_{j+1} \rangle$ and the b) heat current density $\langle J_H \rangle / N$ calculated from ρ_∞ ($\epsilon = 0.05, 0.10, 0.25$) and ρ_{BD} .

to the smallness of the system and the fact that $\mathcal{L}_0^\dagger(\sigma_i^z \sigma_{i+1}^z) \neq 0$. We find that the block-diagonal approximation yields the time average of $\langle \sigma_i^z \sigma_{i+1}^z \rangle$ at small values of ϵ which is consistent with Eq. (1.19). Therefore, the block-diagonal ansatz captures the decay of the nearest-neighbor spin-spin correlation function qualitatively.

The time evolution of the heat current is much smoother as it commutes with H_0 . Initially, $\langle J_H \rangle$ is zero in the classical Néel configuration. Later, however, a large current builds up on a time scale set by $1/\epsilon$. Hence, the system reaches a highly non-equilibrium state in the long-time limit. The steady state value of $\langle J_H \rangle / N$ is approximately independent of the perturbation strength for small values of ϵ . We find that the block-diagonal method becomes exact when $\epsilon \rightarrow 0$. At large values of $\epsilon \sim 1$, we

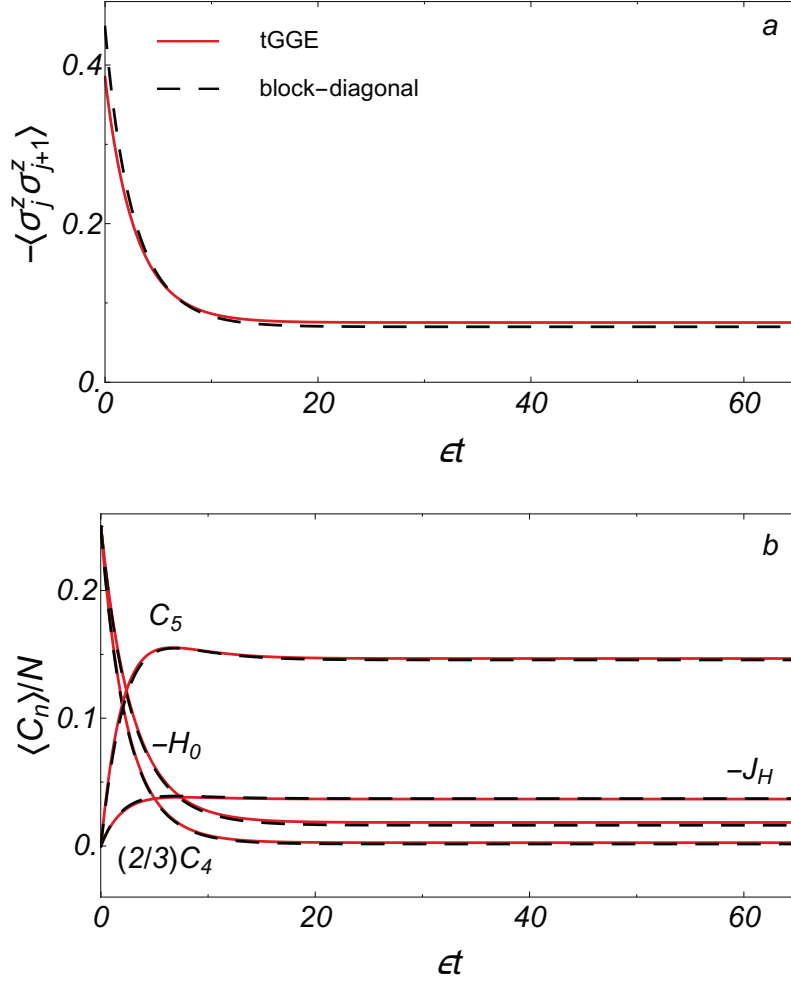


Figure 3.8 Time dependence of the spin-spin correlation function $\langle \sigma_j^z \sigma_{j+1}^z \rangle$ (upper panel) and the charges $C_2 = H_0$, $C_3 = J_H$, C_4 and C_5 (lower panel) calculated from $\rho_{GGE}(t)$ with $N_c = 4$ (solid red line) and from $\rho_{BD}(t)$ (dashed black line).

observe that after a very short time $\tau \sim \mathcal{O}(1)$ errors have accumulated leading to incorrect predictions. We can deduce from our findings that for small values of ϵ the time-dependent block-diagonal density matrix describes the dynamics of the system exactly at times $\tau \gtrsim 1$.

Using these results we can compare the time-dependent tGGE and block-diagonal ansatz at larger system sizes. In Fig 3.8 we show $\langle \sigma_i^z \sigma_{i+1}^z \rangle$ and the expectation values of the approximately conserved quantities $C_2 = H_0$, $C_3 = J_H$, C_4 , C_5 as a function of dimensionless time ϵt . Starting from their prethermalized values, all quantities relax exponentially on a time scale of order $1/\epsilon$ towards their steady state values. In the case of the spin-spin correlation function, the tGGE does not reproduce the correct value in the initial state as $\langle \sigma_i^z \sigma_{i+1}^z \rangle$ was not used to fine-tune $\rho_{GGE}(0)$. However, after a short time of order $\tau \sim 1$, we find that the tGGE gives a qualitatively good description of the time evolution. In contrast to that, the tGGE predicts, by construction, the correct initial values of the approximately

conserved charges included in the tGGE ansatz. It also reproduces accurately the time evolution of the numerically exact ($\varepsilon \rightarrow 0$) results at later times.

3.4 Lindblad dynamic II: High temperature expansion

In the previous section, we have investigated how well a tGGE can predict the time evolution of an integrable system in the presence of weak integrability breaking perturbations. We have found that even with a small number of charges N_c , the tGGE gives an accurate description which improves when increasing the system size N . However, due to strong finite size effects, we have not been able to investigate whether the results obtained from the tGGE converge when systematically increasing the number of conservation laws N_c included in the ansatz. Here, we go to a regime where finite size effects are expected to be small and the limit $N_c \rightarrow \infty$ can be addressed analytically. We consider the XXZ model

$$H_0 = 4 \sum_j J \left(S_j^x S_{j+1}^x + S_j^y S_{j+1}^y \right) + \Delta S_j^z S_{j+1}^z, \quad (3.15)$$

where we have introduced the factor four for later convenience. Similarly to Eq. (3.13), the dynamics of the system is governed by

$$\begin{aligned} \partial_t \rho &= (\mathcal{L}_0 + \mathcal{L}_1) \rho, \\ \mathcal{L}_0 \rho &= -i[H_0, \rho], \quad \mathcal{L}_1 \rho = \varepsilon J \left((1 - \gamma) \hat{\mathcal{D}}^{(1)} + \gamma \hat{\mathcal{D}}^{(2)} \right) \rho, \end{aligned} \quad (3.16)$$

where we choose for the Lindblad operators

$$\begin{aligned} L_k^{(1)} &= 2 \left(S_k^x + i\delta S_{k+1}^x \right), \\ L_k^{(2)} &= \left(\frac{1}{2} + S_k^z \right) S_{k+1}^+ + \left(\frac{1}{2} - S_k^z \right) S_{k+1}^-. \end{aligned} \quad (3.17)$$

Note that we have considered the same example in [106]. While we have designed the Lindblad operators in Eq. (3.14) such that a highly non-equilibrium steady state with large currents is obtained, we focus here on more intuitive Lindblad operators allowing for a better understanding in various limits. The first Lindblad operator fulfills $[L_k^{(1)}, L_k^{(1)\dagger}] = 0$ and therefore $\hat{\mathcal{D}}^{(1)}$ acts as a heating mechanism. Note that for $\delta \neq 0$, the conserved currents of the XXZ model are activated.

The second Lindblad operators flips a spin depending on the orientation of its left neighbor. If the spin at site i points in $+z$ or $-z$ direction, the spin at site $i + 1$ is flipped up or down, respectively. Hence, at $\gamma = 1$ the system tends to be in a superposition of the two fully polarized states, which are eigenstates of H_0 , in the long-time limit.

Both Lindblad operators as well as H_0 (and all other local charges of the XXZ model) are invariant under a rotation by π around the x -axis in spin space $\hat{\mathcal{R}}_{x,\pi}$. Due to $[\hat{\mathcal{R}}_{x,\pi}, \mathcal{L}] = 0$, \mathcal{L} becomes

block-diagonal in the eigenbasis of $\hat{\mathcal{H}}_{x,\pi}$ and decouples into an even-even and an odd-odd parity block. In the following, we restrict our analysis to the even-even sector of $\hat{\mathcal{L}}$ which acts onto the space of density matrices parameterized by local charges. Importantly, the parity-odd quasilocal charges, which have an overlap with the spin current operator at $|\Delta| < |J|$, are not activated by this choice of Lindblad operators.

We consider the case $\gamma \ll 1$ in which the system is approximately in the infinite temperature state at times $\tau \gtrsim 1$. In this regime, we expect that finite size effects are negligible. Moreover, for $\gamma \ll 1$ we can solve the equations, determining the time-evolution of the tGGE, analytically in the thermodynamic limit, at least for a finite number of included charges. For $\rho(t \rightarrow \infty) \approx \mathbb{1}$, the Lagrange parameters λ_j are small allowing us to expand

$$\begin{aligned} \rho_{GGE}(t) &= \frac{e^{-\sum_i \lambda_i(t) C_i}}{\text{Tr}[e^{-\sum_i \lambda_i(t) C_i}]} \\ &\stackrel{\gamma \ll 1}{\approx} \frac{1}{\text{Tr}[\mathbb{1}]} \left(\mathbb{1} - \sum_{i=1}^{N_c} \lambda_i(t) C_i \right) + \mathcal{O}(\lambda^2). \end{aligned} \quad (3.18)$$

where the second line holds for $\text{Tr}[C_i] = 0$. According to Sec. 2.2.2, the dynamics within the subspace of GGEs is governed by a set of rate equations that can be expressed in terms of generalized forces F_i . Using the expansion Eq. (3.18) we obtain to first order in λ_j ,

$$\begin{aligned} F_i(\boldsymbol{\lambda}) &\approx - \sum_j (\chi^{(0)})_{ij}^{-1} c_j \\ &\quad + \sum_k \sum_j \left[(\chi^{(0)})_{ij}^{-1} M_{jk} - \sum_{nm} (\chi^{(0)})_{in}^{-1} \chi_{nmk}^{(1)} (\chi^{(0)})_{mj}^{-1} c_j \right] \lambda_k. \end{aligned} \quad (3.19)$$

where the terms $c_j = \text{Tr}[C_j \hat{\mathcal{L}}_1 \mathbb{1}] / \text{Tr}[\mathbb{1}]$, $M_{ij} = \text{Tr}[C_i \hat{\mathcal{L}}_1 C_j] / \text{Tr}[\mathbb{1}]$, $\chi_{ij}^{(0)} = \text{Tr}[C_i C_j] / \text{Tr}[\mathbb{1}]$ and $\chi_{ijk}^{(1)} = \text{Tr}[C_i C_j C_k] / \text{Tr}[\mathbb{1}]$ can be calculated analytically in terms of Δ, J, δ and γ for a moderate number of charges N_c . In the following, we show that for an arbitrary choice of coupling constants, the steady state expectation values of local observables calculated from a truncated GGE converge to a fixed value, which depends on the parameters, when the number of local conserved quantities N_c is gradually increased. In a second step, we emphasize that this is generically the case at times $\tau \gtrsim 1$. In order to verify that our results are consistent with the exact values in the thermodynamic limit, we compare our findings in the steady state to predictions of a finite size scaling analysis obtained from numerically exact calculations at small system sizes. For simplicity, we set $\delta = 0$ for the time being to avoid even-odd effects. Therefore, only the expectation values of the even charges are non-zero.

First, we take a closer look at the limits $\Delta/J \rightarrow 0$ (free limit) and $\Delta/J \rightarrow \infty$ (Ising limit). In the free limit, the Hamiltonian H_0 can be mapped, with the help of a Jordan-Wigner transformation, onto free fermions hopping on a one-dimensional lattice. In the language of particles, the first Lindblad operator adds or removes a fermion at a site depending on the occupancy. These two processes take place on time scales $1/J$ and $1/(\epsilon J(1 - \gamma))$ and drive the system effectively to a thermal infinite

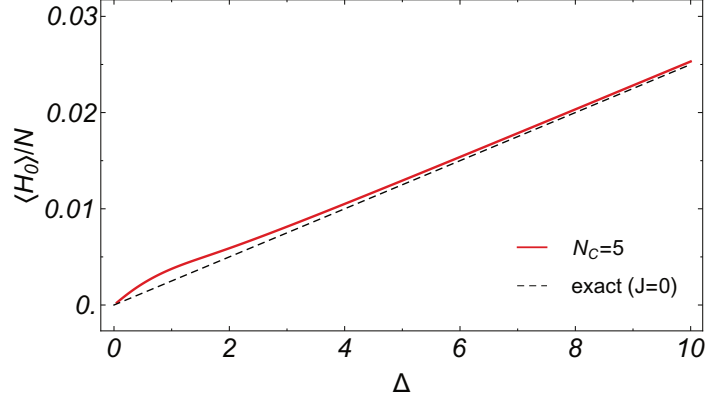


Figure 3.9 Expectation value of the energy density as a function of Δ . The red line shows the result obtained from a truncated GGE with five local conservation laws ($J = 1$). The dashed line displays the slope of the exact solution Eq. (3.20) in the limit $J \rightarrow 0$ where $\langle H_0 \rangle / N \sim \gamma \Delta / 4$. Parameters: $\gamma = 0.01$, $\delta = 0$.

temperature state in which the expectation value of the traceless conserved quantities is zero. The second Lindblad operator adds and removes fermions in dependence on the occupation of the adjacent left site which leads to ordering. However, at $\gamma \ll 1$ this process is negligible and we approximately arrive at $\rho_{GGE}(t \rightarrow \infty) = \mathbb{1}$.

In the Ising limit, it turns out that the steady state density matrix within the GGE manifold, which fulfills the condition $\hat{P}(\hat{\mathcal{L}}_1 \rho_{GGE}) = 0$, can be calculated analytically for arbitrary $\gamma \in [0, 1]$. Surprisingly, the steady state is purely thermal

$$\rho_{GGE}(t \rightarrow \infty) = e^{-\beta(\gamma)H} \quad (3.20)$$

with

$$\beta(\gamma) = \frac{1}{4\Delta} \log(1 - \gamma) \stackrel{\gamma \ll 1}{\approx} -\frac{\gamma}{4\Delta}. \quad (3.21)$$

On the one hand, this result is astonishing as the Ising model has a macroscopic set of local conserved quantities in form of observables containing only σ^z operators. On the other hand, we are in the special situation that the first Lindbladian alone heats the system up to a $T = \infty$ state ($\gamma = 0$) while the second dissipator drives the system to a ground state (or highest energy state) configuration associated with temperature $T = 0$ ($\gamma = 1$). In combination with the fact that in the limit considered both Lindblad operators map eigenstates of H_0 to eigenstates of H_0 it is reasonable to expect that at $0 < \gamma < 1$ a thermal state with temperature $0 < \beta(\gamma) < \infty$ is obtained in the long time limit. Details of the derivation of Eq. (3.21) in one-dimension can be found in the App. B. Unfortunately, this approach can not directly be applied to higher dimensions where a phase transition occurs.

In Fig. 3.9 the expectation value of the energy density calculated from a tGGE with $N_c = 5$ is shown

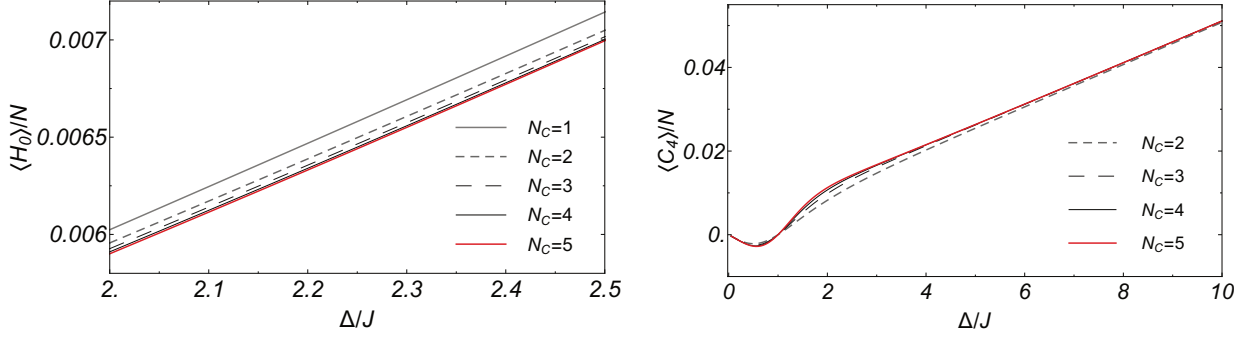


Figure 3.10 Steady state expectation value of the energy and the heat current density as a function of Δ/J calculated from a tGGE containing $N_c = (1, 2, 3, 4, 5)$ charges. Parameters: $\gamma = 0.01$, $\delta = 0$, $J = 1$.

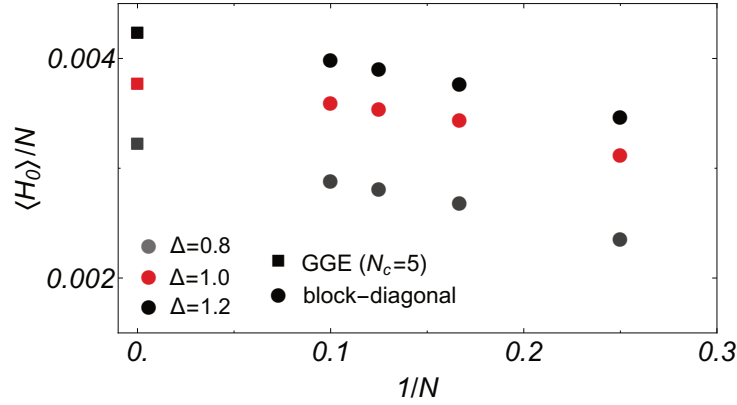


Figure 3.11 Expectation value of the energy density in the steady state calculated numerically with the block-diagonal density matrix for system sizes $N = 4, 6, 8, 10$ and results obtained from a tGGE with $N_c = 5$ in the thermodynamic limit. Parameters: $\gamma = 0.01$, $\delta = 0$, $J = 1$.

as a function of Δ . At $\Delta = 0$ the system is in an infinite temperature state and $\langle H \rangle$ is zero.

At $\Delta \gg J$ the expectation value of the energy density increases linearly where the slope can be extracted from the formula $\langle H_0 \rangle / N \approx -\text{Tr}[H_0^2] \beta(\gamma) / N$, i.e. $\langle H_0 \rangle / N \approx -(\Delta^2 + 2J^2) \beta(\gamma) \approx \Delta \gamma / 4$ for $J = 1$ as long as the expansion Eq. (3.18) is valid. All numbers we present here are small due to the proximity to the infinite temperature state. Fig. 3.10 shows $\langle H_0 \rangle / N$ and $\langle C_4 \rangle / N$ calculated from a tGGE for a different numbers of conserved quantities $N_c = 1, 2, 3, 4, 5$, respectively. We include up to five conservation laws where the most complex charge has maximally non-trivial support on ten neighboring sites. Note that all charges C_i with odd index i are not activated and therefore do not alter the results at $\delta = 0$. We find that the expectation value of local observables calculated from a tGGE converge when N_c is increased. However, so far we do not know whether our results converge to the exact values in the thermodynamic limit. In order to answer this question, we compare the tGGE

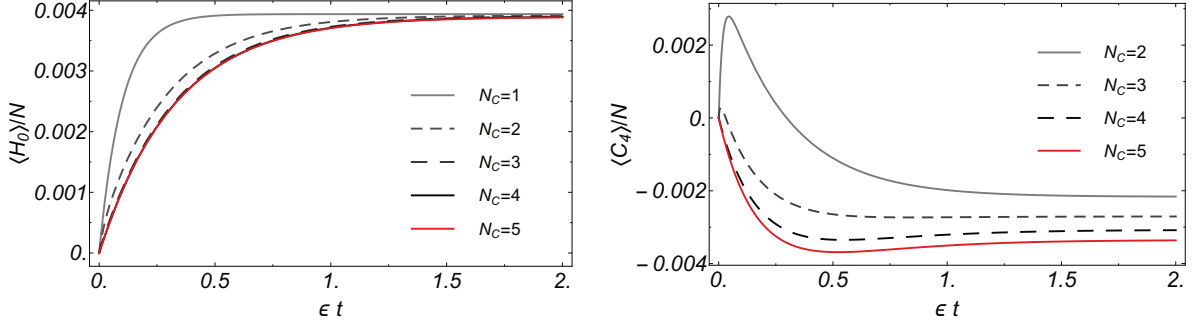


Figure 3.12 Time evolution of (a) $\langle H \rangle / N$ and (b) $\langle C_4 \rangle / N$ calculated from a tGGE with $N_c = (1, 2, 3, 4, 5)$. Parameters: $\Delta = 0.8, J = 1, \delta = 0, \gamma = 0.01$.

results to an extrapolation $N \rightarrow \infty$ of numerically exact calculations at finite system sizes. In Fig. 3.11 $\langle H_0 \rangle / N$ calculated from the block-diagonal steady state density matrix is shown for small system sizes $N = 4, 6, 8, 10$ and $\Delta = 0.8, 1.0, 1.2$. Note again that the block-diagonal ansatz is exact in the limit $\epsilon \rightarrow 0$ and includes all conservation laws of the system. An extrapolation $1/N \rightarrow 0$ of the finite size data agrees well with our findings obtained from a tGGE ansatz with $N_c = 5$ in the thermodynamic limit. This observation suggests that for the calculation of sufficiently local observables, the GGE can be truncated.

In Sec. 3.3 we have given numerical evidence that also the time evolution of weakly open systems can be well described by a time-dependent tGGE at times $\tau \gtrsim 1$. However, due to strong finite size effects we have not been able to analyze the limit $N_c \rightarrow \infty$ rigorously. In the high temperature regime where finite size effects are much smaller, this analysis can be conducted. In Fig. 3.12 the time evolution of $\langle H_0 \rangle / N$ and $\langle C_4 \rangle / N$ are depicted for different values of N_c . In both cases, we observe convergence within the family of local conserved charges. In the case of $\langle H_0 \rangle / N$ results for $N_c = 1, 2, 3, 4, 5$ show rather similar behavior at all times. In contrast to that, a tGGE that only contains C_2 and C_4 ($N_c = 2$) gives a completely wrong prediction of $\langle C_4 \rangle / N$ at short times while the steady state expectation value is qualitatively captured.

Next, we repeat the former analysis for the case $\delta \neq 0$, in which the conserved currents of the XXZ model are activated as well. In the left panel of Fig. 3.13 the expectation value of the heat current density is shown as a function of Δ/J . As above we find that the expectation value converges in the limit $N_c \rightarrow \infty$. In the right panel, we display $\langle J_H \rangle / N$ as a function of N and compare the tGGE ansatz in the thermodynamic limit to the block-diagonal density matrix at finite system sizes. We find that the tGGE ansatz is consistent with an extrapolation $N \rightarrow \infty$. However, we also observe stronger deviations than in Fig. 3.11, especially at $\Delta = 1.2$. This might be the case as J_H is less local than H_0 . Finally, we present $\langle J_H \rangle / N$ as a function of time for different values of $N_c = 2, 4, 6, 8$. Similarly to Fig. 3.12, we find that the results already converge after a short time when N_c is increased.

In this chapter we have considered two different examples of Markovian perturbations. In Sec. 3.3

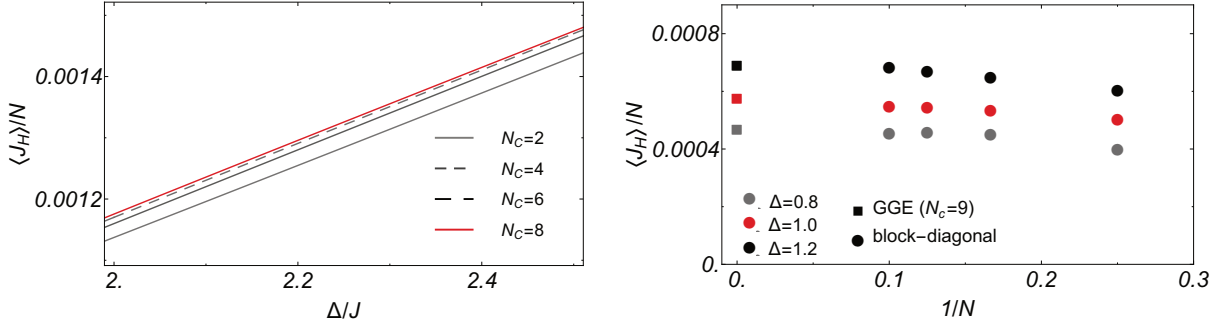


Figure 3.13 The left panel shows the steady state expectation values of the heat current density as a function of Δ/J calculated from a tGGE including $N_c = 2, 4, 6, 8$ charges. In the right panel $\langle J_H \rangle / N$ calculated from the block-diagonal density matrix for system sizes $N = 4, 6, 8, 10$ and results obtained from a tGGE with $N_c = 8$ in the thermodynamic limit are shown. Parameters: $J = 1, \delta = 1, \gamma = 0.01$.

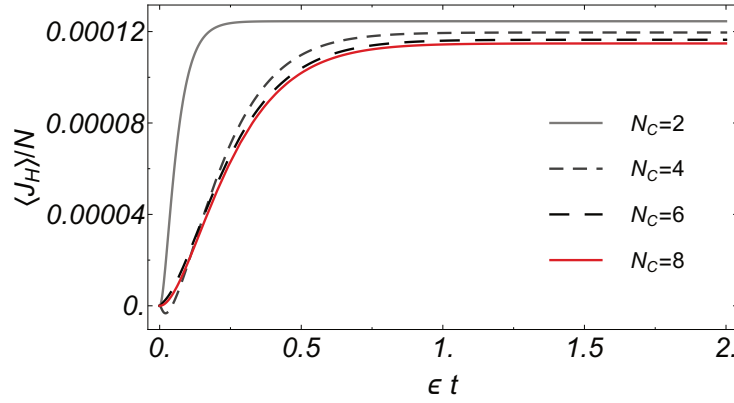


Figure 3.14 Time evolution of the heat current density calculated from a tGGE with $N_c = 2, 4, 6, 8$. Initially, we have set all Lagrange parameters to zero. Parameters: $\Delta = 0.8, J = 1, \delta = 1, \gamma = 0.01$.

we have found numerically that a tGGE with a small number of charges included can describe the dynamics of a weakly open quantum system qualitatively well at times $\tau \gtrsim 1$. Moreover we have observed that the agreement with the exact solution improves when the system size is increased indicating that the GGE is a valid ansatz in the limits $\epsilon \rightarrow 0$ and $N \rightarrow \infty$. In this section, we have considered a Markovian perturbation driving the system into a regime close to the infinite temperature state where the theory developed in Ch. 2 can be applied analytically in the thermodynamic limit. We have found that at times $\tau \gtrsim 1$, the expectation value of local observables converge when the number of local charges included in the tGGE is increased. We have also shown that our findings, obtained from a tGGE in the limits $N \rightarrow \infty$ and $t \rightarrow \infty$, are consistent with numerically exact calculations at finite N , suggesting that a truncated GGE is indeed a valid description in the case considered.

Chapter 4

Pumping approximately integrable systems

The formalism developed in Ch. 2 is based on the principle that a weak symmetry breaking perturbation can drive a system far out of equilibrium to a state that is completely different from the initial one. It is important to note that the occurrence of this effect depends strongly on the form of the chosen perturbation and the symmetries of the system. If a generic closed quantum system is perturbed, for example, in a quench experiment, it typically relaxes on a potentially very long time scale to a thermal Gibbs state [10]. The same is expected to hold in the case of weak integrability breaking quenches for integrable systems [105].

According to the arguments presented above, integrability can be 'revived' and thermalization prevented by weakly pumping into degrees of freedom that are approximately protected by symmetries. This idea is schematically illustrated in Fig. 4.1. A simple example of this effect from classical physics is a greenhouse that is heated by the sun. Due to the good insulation, the energy inside the greenhouse is approximately conserved. Therefore, even weak sunlight can heat the interior to very high temperatures that are much higher than the surrounding temperature. The effect is particularly remarkable in winter. In equilibrium, the temperature inside T_{in} is determined by the balance of the incoming and the outgoing energy flux J_{in} and J_{out} . While J_{in} is approximately constant, the outgoing flux $J_{out} = \alpha(T_{in} - T_{out})$ is to a good approximation proportional to the temperature difference where α denotes the heat conductivity. By setting $|J_{in}| = |J_{out}|$, we obtain $T_{in} = T_{out} + |J_{in}|/\alpha \gg T_{out}$ for $\alpha \ll 1$. This is one manifestation of how a weak perturbation can cause a strong effect in the presence of approximately conserved quantities. Another simple and related example is a fridge whose working principle is also based on insulation and heat transfer/pumping. Further examples that are closer to current research activities are Bose-Einstein condensations of photons, magnons or exciton-polaritons. Due to approximate particle number conservation in the experimental setups, highly occupied states can be engineered by weak laser pumping [107–110].

In Sec. 3.3 we have illustrated the emergence of such strong responses also in weakly open quantum systems that have a macroscopic set of conserved quantities. Precisely, we have considered a

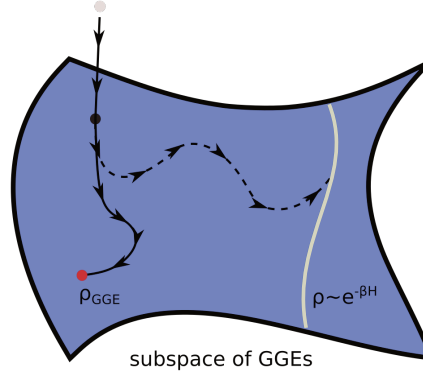


Figure 4.1 Schematic illustration of the effect of weak pumping on an approximately integrable system, which is initialized in an arbitrary initial state (gray dot) and weakly coupled to a thermal bath. After a short time the system relaxes to the subspace of GGEs. Within the subspace the dynamics is governed by the generalized force \mathbf{F} . While the system relaxes to a thermal state (gray line) in the absence of pumping (dashed trajectory), a highly non-equilibrium steady state can be reached if the system is weakly driven (solid trajectory).

Markovian perturbation driving a one-dimensional Heisenberg chain to a very non-thermal state in which a large heat current is present. Here, we consider more realistic models that are potentially more feasible for experimental realizations. Particularly, we suggest a specific setup for efficient integrability based spin and heat pumps in certain spin chain materials. We mainly focus on this application in the following, however, we will present two further experimental proposals for the validation of the phenomenon at the end of the chapter. Note that Sec. 4.1, Sec. 4.2 and Sec. 4.3 are partially based on [111, 106].

4.1 The model

We consider an antiferromagnetic spin chain material that is approximately modeled by an integrable XXZ spin chain

$$H_0 = \sum_j \frac{J}{2} \left(S_j^+ S_{j+1}^- + S_j^- S_{j+1}^+ \right) + \Delta S_j^z S_{j+1}^z - B S_j^z \quad (4.1)$$

possibly placed in a homogeneous magnetic field pointing in z -direction. We are interested in the regime $|\Delta| < |J|$ where the spin current is partially protected by a family of quasilocal conservation laws. To induce currents in the spin chain, we apply a periodic drive modeled by a time-dependent perturbation

$$H_d = \varepsilon_d \sum_j \left((-1)^{j+1} \mathbf{S}_j \cdot \mathbf{S}_{j+1} \sin(\omega t) + (-1)^j S_j^z \cos(\omega t) \right) \quad (4.2)$$

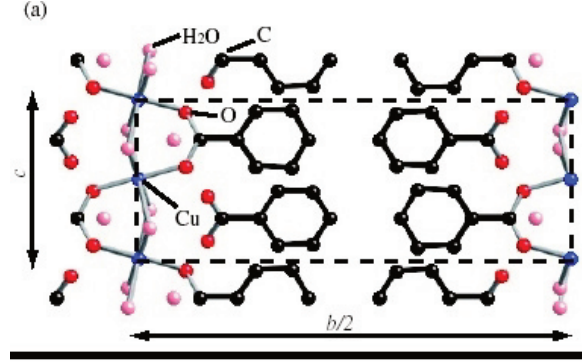


Figure 4.2 Crystal structure of *Cu* Benzoate in the *bc*-plane where the unit cell is depicted in a dashed frame. Oxygen ions are represented by red, copper ions by blue and carbon ions by black balls. The figure is taken from [112].

with driving frequency ω . The driving term is constructed in such a way that its symmetry properties allow for finite spin and heat currents on the one hand and it can be realized experimentally on the other hand. Regarding the first point, the staggered magnetic field and the staggered-bond coupling ensure that all spatial reflection symmetries are broken. Hence, the staggering allows for the existence of currents that flow in a specific direction. Moreover, the staggered magnetic field breaks the symmetries $\hat{\mathcal{R}}_{x,\pi}$ and $\hat{\mathcal{R}}_{y,\pi}$ describing rotations by π around the x - and y -axis in spin space, respectively. This is required for the existence of a finite spin current expectation value as $\hat{\mathcal{R}}_{x,\pi}^{-1} J_s \hat{\mathcal{R}}_{x,\pi} = -J_s$ and $\hat{\mathcal{R}}_{y,\pi}^{-1} J_s \hat{\mathcal{R}}_{y,\pi} = -J_s$. To obtain a finite heat current in second order perturbation theory, the two driving terms in Eq. (4.2) have to be phase shifted. The additional static magnetic field in Eq. (4.1) finally ensures that also the product of $\hat{\mathcal{R}}_{y,\pi}$ with a bond-centered spatial mirror symmetry is broken under which the heat current operator is odd.

While the direction of the spin current depends only on the relative phase shift between the staggered magnetic field and the staggered bond-coupling, the direction of the heat current is set by the phase shift and the direction of the static external magnetic field. We consider Eq. (4.1) together with Eq. (4.2) not as a purely theoretical system but rather a model for certain spin chain materials existing in nature. The staggered exchange coupling and the staggered magnetic field can arise in compounds with two or more magnetic atoms per unit cell, when coupled to a uniform electromagnetic field [113, 114]. For example, in the antiferromagnetic spin chain material *Cu* benzoate, the unexpected magnetic field dependence of a gap opening could be explained with the help of a staggered gyromagnetic g tensor [115, 116]. Effectively, the staggered g tensor gives rise to a staggered magnetic field when an external uniform field is applied. It was suggested that the staggering is due to the existence of two inequivalent *Cu* sites and the low symmetry of the crystal structure [117].

In Fig. 4.2 the crystal structure of *Cu* benzoate is shown. Each *Cu* atom has four *O* atoms of benzoate groups and two *O* atoms of H_2O as ligands that align locally in a structure with an almost tetragonal symmetry. The principal axis for the tetragonal symmetry alternates slightly between neighboring *Cu* atoms which, in turn, is expected to cause an alternating g tensor. The staggered exchange coupling

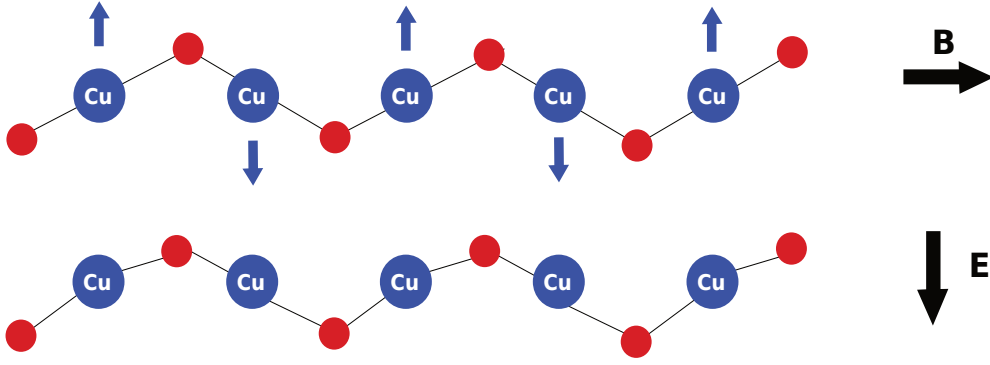


Figure 4.3 Schematic sketch of the effective one-dimensional spin chain in presence of an external magnetic (upper plot) and electric field (lower plot). Due to the existence of two inequivalent *Cu* sites, a staggered g tensor arises that effectively causes a staggered magnetic field when an additional uniform field B is applied. An external electric fields deflects differently charged and oriented ions distinctly causing a staggered bond-coupling.

is generated when a uniform electric field is applied that deflects different ions in a distinct way depending on their charge and orientation in the compound. This makes the angle between an oxygen ion and its two neighboring *Cu* ions alternate and eventually leads to a staggered coupling constant. Schematically, the occurrence of staggering in *Cu* benzoate is depicted in Fig. 4.3. The required time-dependent uniform electric and magnetic field can be provided by shining a laser onto the sample where the laser should typically work in the THz regime to address the relevant energy scales of the spin chain material. Importantly, the power of the laser, which is in our model proportional to ε_d^2 , does not have to be strong to induce currents that are approximately conserved. The relative phase between the two driving terms appearing in Eq. (4.2) can be varied by changing the alignment of the laser with respect to the sample.

Note that $H_d(t)$ alone would drive the system to an infinite temperature state. Thus, an additional cooling mechanism is required in our model. In real solid state systems such a mechanism is, for example, provided by couplings to phonons and ultimately by the coupling to the thermal environment of the experimental setup. These perturbations alone already break integrability weakly. Here, we implement cooling by coupling the spin chain to a thermal bath of Einstein phonons $H_{0,ph} = \omega_{ph} \sum_j a_j^\dagger a_j + \dots$ where the dots indicate further terms which keep the temperature T_{ph} of the bath fixed. We assume that the coupling between bath and spin chain is small such that the total (Floquet) steady state density matrix factorizes into a spin and a phonon part with $\rho_{ph} \sim e^{-H_{0,ph}/T_{ph}}$.

The weak phonon coupling to the bonds is described by

$$H_{ph} = \varepsilon_{ph} \sum_j \left(\mathbf{S}_j \cdot \mathbf{S}_{j+1} (a_j^\dagger + a_j) + \gamma_m \left(S_j^x S_{j+1}^z + S_j^z S_{j+1}^x \right) (a_j^\dagger + a_j) \right). \quad (4.3)$$

We introduce the second term in Eq. (4.3) that mimics relativistic relaxation effects of S_z to break all remaining symmetries in the model. This is essential to obtain a unique Floquet steady state in the long-time limit. Also, in real materials, S^z is not exactly conserved. Besides phonons, there are additional integrability breaking perturbations in real materials, for example, defects that typically dominate at low temperatures [118]. At high temperatures (with T comparable to J) which is the regime we will eventually consider, it is reasonable to assume that the coupling to phonons is the dominant perturbation. Note that the coupling to a thermal bath can be described alternatively in terms of a Markovian Lindblad equation involving a macroscopic set of non-local Lindblad operators $L_{nm} = \exp(-H_0/(2T_{ph})) |m\rangle \langle n|$ where $|n\rangle, |m\rangle$ are eigenstates of H_0 . By inserting L_{nm} into Eq. (1.39), one can directly verify that a steady state solution is given by the thermal density matrix $\rho_{th} = e^{-H_0/T_{ph}}$. The corresponding Liouville superoperator belongs to the class of *Davies generators* modeling thermalization of quantum mechanical systems [119]. Finally, the time evolution equation for the density matrix reads

$$\begin{aligned} \dot{\rho} &= \left(\mathcal{L}_0 + \mathcal{L}_1(t) \right) \rho = \left(\mathcal{L}_0 + \mathcal{L}_{1,ph} + \mathcal{L}_{1,d}(t) \right) \rho, \\ \mathcal{L}_0 \rho &= -i[H_0 + H_{0,ph}, \rho], \quad \mathcal{L}_{1,ph} \rho = -i[H_{ph}, \rho], \quad \mathcal{L}_{1,d}(t) \rho = -i[H_d(t), \rho]. \end{aligned} \quad (4.4)$$

4.2 Steady state

In the presence of a periodic perturbation, we can use the Floquet formalism presented in Sec. 2.2.1 to describe the steady state density matrix in terms of periodically oscillating Floquet components $\rho(t \rightarrow \infty) = \sum_n e^{-i\omega n t} \rho^{(n)}$. Note that in the limit of weak driving $\varepsilon_d \rightarrow 0$, the zeroth order of $\rho(t \rightarrow \infty)$ has only a component in the $n = 0$ Floquet sector, $\rho_0^{(n)} = (\rho_0 \otimes \rho_{ph}) \delta_{n,0}$.

We use two methods to determine the (Floquet) steady state density matrix. Firstly, we parameterize ρ_0 by a small number of local and quasilocal conserved quantities $C_i, i = 1, \dots, N_c$ in terms of a truncated GGE. As we want to investigate the emergence of a finite spin current, we include the diagonal part J_s^c of the spin current operator in the common eigenbasis of the local charges as one conservation law in the tGGE ansatz. By construction J_s^c is a conserved quantity that has a finite overlap with the parity-odd family of quasilocal charges at $|\Delta| < |J|$. However, to reduce the complexity of the problem and avoid stronger finite size effects we include only local conserved quantities apart from J_s^c . Secondly, we calculate the block-diagonal (Floquet) steady state density matrix including all commuting and non-commuting as well as local and non-local conservation laws of H_0 . The second approach becomes numerically exact in the limit $\varepsilon_d, \varepsilon_{ph} \rightarrow 0$ which we explicitly verified in Sec. 3.3 for a Markovian perturbation. We also found for the much simpler model in Sec. 3.3 that a tGGE

with a small number of local charges and the block-diagonal ansatz yield very similar results for the expectation values of local observables.

4.2.1 Truncated GGE

According to Ch. 2, the values of the Lagrange parameters in the steady state are determined by the condition that all generalized forces add up to zero. In the case of a time-dependent unitary perturbation, the force F_i reads

$$F_i = - \sum_j (\chi^{-1})_{ij} \overline{\langle \dot{C}_j \rangle} \quad (4.5)$$

$$\approx \sum_j (\chi^{-1})_{ij} \text{Tr}[\mathbf{C}_j \mathcal{L}_1 \mathcal{L}_0^{-1} \mathcal{L}_1 \rho_0], \quad (4.6)$$

where \mathcal{L}_0 , \mathcal{L}_1 and \mathbf{C}_j , ρ_0 are matrices and vectors in Floquet space, respectively. Equivalently, we can also obtain the long-time limit expectation value $\overline{\langle \dot{C}_j \rangle}$ in a different way by using Green's function methods instead of the expansion introduced in Ch. 2. The solution of the defining equation for the Green's function

$$\left(\partial_t - \hat{\mathcal{L}}_0 \right) \hat{\mathcal{G}}(t) = \delta(t) \mathbb{1} \quad (4.7)$$

is given by $\hat{\mathcal{G}}(t) = \theta(t) e^{\hat{\mathcal{L}}_0 t}$. With the help of $\hat{\mathcal{G}}(t)$ and the ansatz $\rho(t) = \rho_0 + \delta\rho(t)$, we can directly find a solution for the inhomogeneous problem $\left(\partial_t - \hat{\mathcal{L}}_0 \right) \rho(t) = \hat{\mathcal{L}}_1(t) \rho(t)$,

$$\delta\rho(t) = \int_0^t dt' e^{\hat{\mathcal{L}}_0(t-t')} \hat{\mathcal{L}}_1(t') \rho(t') \approx \int_0^t dt' e^{\hat{\mathcal{L}}_0(t-t')} \hat{\mathcal{L}}_1(t') \rho_0, \quad (4.8)$$

where we have used $\hat{\mathcal{L}}_0 \rho_0 = 0$ and have expanded $\rho(t)$ to leading order in ε . Inserting formula Eq. (4.8) into $\text{Tr}[\mathbf{C}_i \hat{\mathcal{L}} \rho(t)]$ then finally yields

$$\overline{\langle \dot{C}_i \rangle} = \lim_{T \rightarrow \infty} \frac{1}{T} \int_0^T dt \int_0^t dt' \text{Tr}[\mathbf{C}_i \hat{\mathcal{L}}_1(t) e^{\hat{\mathcal{L}}_0(t-t')} \hat{\mathcal{L}}_1(t') \rho_0], \quad (4.9)$$

where we have explicitly averaged over time. Note that all contributions in Eq. (4.8) with mixed terms like $\hat{\mathcal{L}}_{1,ph}$, $\hat{\mathcal{L}}_{1,d}(t)$ average to zero as $\hat{\mathcal{L}}_{1,d}(t)$ changes the Floquet sector by ± 1 while $\hat{\mathcal{L}}_{1,ph}$ is time-independent. In order to proceed, we can make use of the fact that $e^{-\hat{\mathcal{L}}_0 t}$ applied to an operator X in Schrödinger picture yields the corresponding Heisenberg representation $X^{(H)}(t)$. That can be shown by decomposing X into $X = \sum_{nm} \alpha_{nm} |n\rangle \langle m|$ where $|n\rangle$, $|m\rangle$ are eigenstates of H_0 and verifying

that $e^{-\mathcal{L}_0 t} |n\rangle \langle m| = e^{i(E_n^0 - E_m^0)t} |n\rangle \langle m|$. Using this relation we obtain

$$\begin{aligned} \overline{\langle \dot{C}_i \rangle} &= + \lim_{T \rightarrow \infty} \frac{1}{T} \int_0^T dt \int_0^t dt' \text{Tr} \left[C_j \hat{\mathcal{L}}_{1,ph} e^{\mathcal{L}_0(t-t')} \hat{\mathcal{L}}_{1,ph} \rho_0 \right] \\ &+ \lim_{T \rightarrow \infty} \frac{1}{T} \int_0^T dt \int_0^t dt' \text{Tr} \left[C_j \hat{\mathcal{L}}_{1,d}(t) e^{\mathcal{L}_0(t-t')} \hat{\mathcal{L}}_{1,d}(t') \rho_0 \right] \\ &= - \lim_{T \rightarrow \infty} \frac{1}{T} \int_0^T dt \int_0^t dt' \text{Tr} \left[C_j [H_{ph}, [H_{ph}^{(H)}(t'-t), \rho_0 \otimes \rho_{ph}]] \right] \\ &- \lim_{T \rightarrow \infty} \frac{1}{T} \int_0^T dt \int_0^t dt' \text{Tr} \left[C_j [H_d(t), [H_d^{(H)}(t'-t), \rho_0]] \right]. \end{aligned} \quad (4.10)$$

Note that $H_d^{(H)}(t'-t)$ in the last line also explicitly depends on t' . Firstly, we consider the contribution of the phonons. As mentioned above, we assume that each bond is coupled to a harmonic oscillator with frequency ω_{ph} and fixed temperature T_{ph} . The total density matrix of the phonon bath reads $\rho_{ph} \sim e^{-H_{0,ph}/T_{ph}}$. Using this assumption we can trace out the phononic degrees of freedom. Naturally, this process yields terms like $\langle a_i^\dagger a_j \rangle_{ph} = n_{ph}(\omega) \delta_{ij}$ and $\langle a_i a_j^\dagger \rangle_{ph} = (1 + n_{ph}(\omega_{ph})) \delta_{ij}$ where $n_{ph}(\omega_\kappa) = 1/(e^{\omega_{ph}/T_{ph}} - 1)$ denotes the equilibrium Bose-Einstein distribution function. We can express Eq. (4.10) in Lehmann representation by inserting identities $\sum_n |n\rangle \langle n|$ and $\sum_m |m\rangle \langle m|$. This formulation allows us to calculate F_i for small system sizes explicitly. With the help of the Dirac identity $\lim_{\eta \rightarrow 0} \frac{1}{x \pm i\eta} = P x \mp i\pi \delta(x)$, the generalized force finally becomes

$$\begin{aligned} F_i^{(ph)} &= 2\pi \varepsilon_{ph}^2 J^2 \sum_{i'} (\chi^{-1})_{ii'} \sum_{m,k} \rho_m (C_{i',m} - C_{i',k}) \\ &\times \left(|\langle k | \mathbf{S}_j \cdot \mathbf{S}_{j+1} | m \rangle|^2 + \gamma_m^2 |\langle k | S_j^x S_{j+1}^z + S_j^z S_{j+1}^x | m \rangle|^2 \right) \\ &\times \left((n_B(E_m^0 - E_k^0) + 1) A^{(ph)}(E_m^0 - E_k^0) + n_B(E_k^0 - E_m^0) A^{(ph)}(E_k^0 - E_m^0) \right) \end{aligned} \quad (4.11)$$

which is, as a typical Fermi's golden rule rate equation, proportional to ε_{ph}^2 . The terms with prefactor n_B describe the absorption while the contributions proportional to $(n_B + 1)$ represent the emission of a phonon which can be induced or spontaneous. Transition processes are weighted with the absolute square of the matrix elements $\langle k | \mathbf{S}_j \cdot \mathbf{S}_{j+1} | m \rangle$ and $\langle k | S_j^x S_{j+1}^z + S_j^z S_{j+1}^x | m \rangle$. Eq. (4.11) is only valid if all charges $\{C_i\}$ mutually commute. Within our numerics, we assume a natural broadened distribution of Einstein phonons using $A^{(ph)}(\omega) = \theta(\omega) \frac{\omega}{\omega_{ph} \eta \sqrt{\pi}} e^{-(\omega - \omega_{ph})/\eta^2}$. This choice of broadening ensures detailed balance which is necessary to obtain a thermal state in the absence of driving as well as positivity of the phonon frequency which guarantees stability. Technically, we average the result obtained from Eq. (4.10) over frequencies using the phonon distribution function $A^{(ph)}(\omega)$ which then yields Eq. (4.11).

Next, we consider the contributions of the periodic drive to F_i . We introduce the notation $H_d(t) = e^{i\omega t} H_d^{(-)} + e^{-i\omega t} H_d^{(+)}$ with $H_d^{(+)\dagger} = H_d^{(-)}$. As in the limit $\varepsilon_d \rightarrow 0$ the GGE ρ_0 and all charges C_i are static in our setup, only transitions from the $n = 0$ to the $n = \pm 1$ Floquet sector and back contribute in

Eq. (4.10) to second order while all other processes average to zero. Hence, the contribution of $H_d(t)$ to the generalized force reads

$$F_i^{(d)} = \frac{2\pi}{N} \varepsilon_d^2 \sum_{i'} (\chi^{-1})_{ii'} \sum_{m,k} \rho_m (C_{i',m} - C_{i',k}) \times \\ \times \left\{ |\langle k | H_d^{(+)} | m \rangle|^2 \delta(E_k^0 - E_m^0 - \omega) + |\langle k | H_d^{(-)} | m \rangle|^2 \delta(E_k^0 - E_m^0 + \omega) \right\}. \quad (4.12)$$

The δ function, which we broaden in our finite size calculation by a Lorentzian $(1/\pi)\eta/(\omega^2 + \eta^2)$, guarantees the conservation of energy.

Note that in the case of unitary perturbations, we can also directly use linear response theory to calculate $\overline{\langle \dot{C}_i \rangle}$ to second order in perturbation strength. We elaborate this in the following for the example of periodic driving. We consider the more general driving term

$$H_d(t) = \cos(\omega t + \phi_1) H_{d,1} + \cos(\omega t + \phi_2) H_{d,2} \quad (4.13)$$

where $H_{d,1}$ and $H_{d,2}$ can be identified with the contribution of the staggered bond-coupling and the staggered magnetic field in Eq. (4.2), respectively. Compared to Eq. (4.2), the phase difference is given by $\pi/2$. To leading order, we obtain for $\langle \dot{C} \rangle$,

$$\partial_t \langle C \rangle = \text{Tr}[C \dot{\rho}] = -i \text{Tr}[C[H_0 + H_d(t), \rho]] \\ \approx -i \text{Tr}[C, H_d(t)] \rho_1 = \langle A \rangle_1, \quad (4.14)$$

where we use the abbreviation $A := -i[C, H_d(t)]$. According to linear response theory, the first order correction to $\langle A \rangle_0$ is given by

$$\langle A \rangle_1 = \int_{t_0}^{\infty} dt' \chi_{AH_d}(t-t') \\ = \int_{t_0}^{\infty} dt' \sum_{i,j=1}^2 \cos(\omega t + \phi_i) \cos(\omega t' + \phi_j) \chi_{A_i H_{d,j}}(t-t') \quad (4.15)$$

with $\chi_{A_i H_{d,j}}(t) = -i\theta(t) \langle [A_i^{(H)}(t), H_{d,j}(0)] \rangle_{GGE}$ and $A_i(t) = -i[C, H_{d,i}(t)]$. Using the Fourier decomposition of $\chi_{A_i H_{d,j}}(t)$ we obtain

$$\langle \dot{C} \rangle \approx \int_{t_0}^{\infty} dt' \chi_{AH_d}(t-t') \quad (4.16) \\ = \frac{1}{2} \sum_{i,j} \cos(\omega t + \phi_i) [\chi_{A_i H_{d,j}}(\omega) e^{-i(\omega t + \phi_j)} + \chi_{A_i H_{d,j}}(-\omega) e^{i(\omega t + \phi_j)}].$$

As we are interested in the zeroth order of the steady state density matrix that lives in the $n = 0$ Floquet sector ($\varepsilon_d \rightarrow 0$), we have to calculate the time-average of Eq. (4.16),

$$\begin{aligned} \overline{\langle \dot{C} \rangle} &\approx \frac{1}{4} \sum_{i,j} (\chi_{A_i H_{d,j}}(\omega) e^{i(\phi_i - \phi_j)} + \chi_{A_i H_{d,j}}(-\omega) e^{-i(\phi_i - \phi_j)}), \\ \chi_{A_i H_{d,j}}(\omega) &= \frac{1}{Z} \sum_{n,m} \frac{1}{\omega + i\varepsilon + (E_n^0 - E_m^0)} \langle n | A_i | m \rangle \langle m | H_{d,j} | n \rangle [e^{-\sum_k \lambda_k C_{k,n}} - e^{-\sum_k \lambda_k C_{k,m}}]. \end{aligned} \quad (4.17)$$

For the response function, the relation $\chi_{A_i H_{d,j}}(\omega) = \chi_{A_j H_{d,i}}^*(-\omega)$ holds. If we insert $A_i = -i[C, H_{d,i}(t)]$ into Eq. (4.17) and use the decomposition $H_d = e^{i\omega t} H_d^{(-)} + e^{-i\omega t} H_d^{(+)}$, we obtain the same expression for $\overline{\langle \dot{C}_i \rangle}$ as in Eq. (4.12). Note that the contribution of the mixed terms in the first line of Eq. (4.17), which break TRS, vanish if the phase difference $\phi_1 - \phi_2$ is an integer multiple of 2π . Technically, we use Newton's method to calculate the root of the generalized force that determines the steady state in which heating and cooling are balanced.

4.2.2 Block-diagonal ansatz

For the block-diagonal ansatz, which becomes exact in the limit $\varepsilon_{ph}, \varepsilon_d \rightarrow 0$, we have to calculate the matrix elements of the effective Liouvillian

$$\left(\hat{\mathcal{L}}^{\mathcal{Q}} \right)_{nm}^{n'm'} = -\text{Tr}[\mathcal{Q}_{n'm'}^\dagger \hat{\mathcal{L}}_1 \hat{\mathcal{L}}_0^{-1} \hat{\mathcal{L}}_1 \mathcal{Q}_{nm}],$$

where $\mathcal{Q}_{nm} = |n\rangle \langle m|$, $\mathcal{Q}_{n'm'} = |n'\rangle \langle m'|$ are elements of the set \mathcal{Q} including all conservation laws. Within our numerics with $\Delta \neq J$ and $B \neq 0$, we find about $2 \cdot 2^N$ elements $\mathcal{Q}_{nm} \in \mathcal{Q}$. Equivalently, the matrix elements can be obtained with the help of Eq. (4.9) if we replace ρ_{GGE} by $\rho_{BD} = \sum_{nm} \alpha_{nm} |n\rangle \langle m|$ and C_i by \mathcal{Q}_{nm} ,

$$\left(\hat{\mathcal{L}}^{\mathcal{Q}} \right)_{nm}^{n'm'} = -\lim_{T \rightarrow \infty} \int_0^T dt \int_0^t dt' \text{Tr}[|m'\rangle \langle n'| \hat{\mathcal{L}}_1(t) e^{\hat{\mathcal{L}}_0(t-t')} \hat{\mathcal{L}}_1(t') (|n\rangle \langle m| \otimes \rho_{ph})]. \quad (4.18)$$

Eq. (4.18) can be explicitly calculated by tracing out the bosonic degrees of freedom and averaging over frequencies using the distribution function $A_{ph}(\omega)$. One can perform several checks to ensure that the matrix obtained from Eq. (4.18) describes a physical Liouvillian. First, the real parts of all eigenvalues of $\hat{\mathcal{L}}^{\mathcal{Q}}$ have to be less than or equal to zero to guarantee stability. Moreover, there has to be at least one right eigenstate with eigenvalue 0 which follows from the conservation of probability. Another consequence of $\text{Tr}[\hat{\mathcal{L}} \rho(t)] = 0$ is that $(1, \dots, 1, 0, \dots, 0)$ is a left eigenvector of $\hat{\mathcal{L}}^{\mathcal{Q}}$ with eigenvalue zero. Here, we have chosen the basis such that the first 2^N components with entry one correspond to projections $|n\rangle \langle n|$ onto common eigenstates of the local charges C_i . In addition to this, $\hat{\mathcal{L}}^{\mathcal{Q}}$ fulfills $\left(\hat{\mathcal{L}}^{\mathcal{Q}} \right)_{nm}^{n'm'} = \left(\hat{\mathcal{L}}^{\mathcal{Q}} \right)_{mn}^{m'n'^*}$ which follows from the cyclicity of the trace and from the property $\text{Tr}[X^\dagger] = \text{Tr}[X]^*$. Note that there are five qualitatively different cases, 1) $n = m = n' = m'$, 2) $n = m \neq n' = m'$, 3) $n \neq m \neq n' \neq m'$, 4) $n = n' \neq m \neq m'$, 5) $n = n' \neq m = m'$ that need to be

considered separately. For more details and concrete formulas one can refer to [106]. To determine the steady state of the dynamics, we calculate the kernel of $\hat{\mathcal{L}}^{\mathcal{Q}}$. As the chosen perturbations break all relevant symmetries, the steady state density matrix ρ_{BD} is the unique solution of $\hat{\mathcal{L}}^{\mathcal{Q}}\rho_{BD} = 0$.

4.3 Results

Within our numerics we consider small values of ε_d and ε_{ph} for which we expect that the steady state is well captured by a tGGE. We validate this assumption by comparing the results obtained from the tGGE ansatz to those calculated from the block-diagonal density matrix. For sufficiently

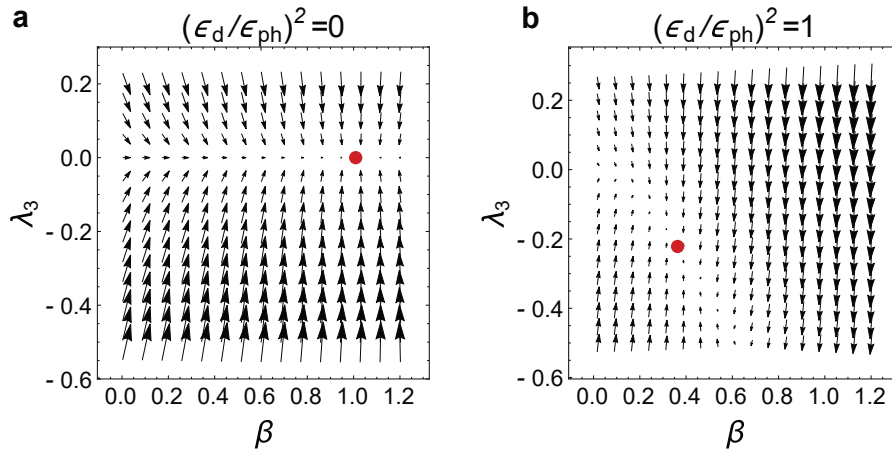


Figure 4.4 Generalized force field as a function of $\beta = \lambda_2$ and λ_3 which are the Lagrange parameters of the Hamiltonian and the heat current operator, respectively. Parameters: $\varepsilon_d/\varepsilon_{ph} = 0$ (left) and $\varepsilon_d/\varepsilon_{ph} = 1$ (right), $J = 1$, $N = 8$.

small values of the perturbation strengths, the steady state depends only on the ratio $(\varepsilon_d/\varepsilon_{ph})^2$. At $(\varepsilon_d/\varepsilon_{ph})^2 = 0$ the system is in a thermal state with a temperature equal to the temperature T_{ph} of the phonon bath. In the opposite limit $(\varepsilon_d/\varepsilon_{ph})^2 \rightarrow \infty$, the system is driven to a thermal infinite temperature state with a finite magnetization, $\rho \sim e^{-\lambda_1 S^z}$. In Fig. 4.4 the generalized force field $\mathbf{F}(\lambda_2, \lambda_3)$ is depicted in the subspace spanned by the two Lagrange parameters $\beta = \lambda_2$ and λ_3 at $(\varepsilon_d/\varepsilon_{ph})^2 = 0$ and $(\varepsilon_d/\varepsilon_{ph})^2 = 1$. For the calculation of \mathbf{F} we use a truncated GGE containing only the Hamiltonian and the heat current operator as charges. In the absence of driving, we obtain a thermal steady state with $\beta = 1/T_{ph}$ and $\lambda_3 = 0$ as all currents vanish in thermal equilibrium. In the limit $(\varepsilon_d/\varepsilon_{ph})^2 \rightarrow \infty$, both Lagrange parameter $\beta = 1/T$ and λ_3 approach zero. Again there are no currents present in the thermal infinite temperature state with finite magnetization. At a finite value of $(\varepsilon_d/\varepsilon_{ph})^2 > 0$ we find a non-zero expectation value of the heat current operator, $\lambda_3 \neq 0$, which reaches its maximal value at $(\varepsilon_d/\varepsilon_{ph})^2 \sim 1$.

In Fig. 4.5 and Fig. 4.6 the expectation values of the energy $\langle H_0 \rangle/N$ and the heat current density $\langle J_H \rangle/N$ are plotted as a functions of $(\varepsilon_d/\varepsilon_{ph})^2$, respectively. Note that in the presence of an external magnetic field, the spin current operators enters the formula for the physical heat current, $J_H =$

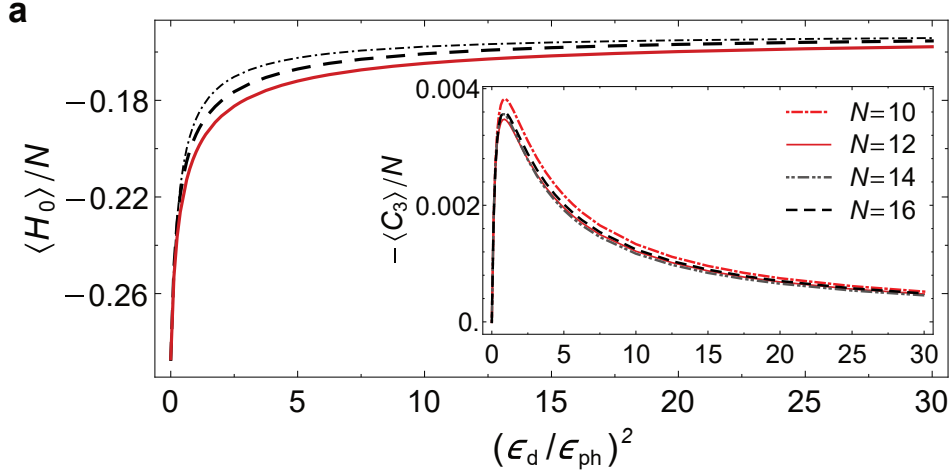


Figure 4.5 a) Expectation value of the energy density in the steady state calculated from the block-diagonal density matrix (solid red line) and a GGE with $N_c = 4$ (dot-dashed black line) and $N_c = 6$ (dashed black line) at $N = 12$. The inset plot shows $\langle C_3 \rangle / N$ calculated for system sizes $N = 10, 12, 14, 16$. Parameters: $J = 1$, $\Delta = 0.8$, $B = -1.0$, $\omega = 1.6\omega_{ph}$, $\omega_{ph} = T_{ph} = 1$.

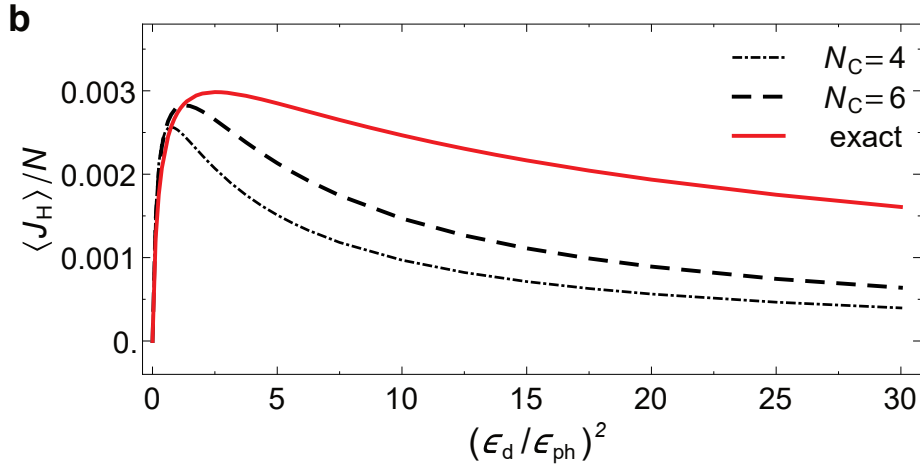


Figure 4.6 b) Expectation value of the heat current density in the steady state, calculated from the block-diagonal density matrix (solid red line) and a GGE with $N_c = 4$ (dot-dashed black line) and $N_c = 6$ (dashed black line) at $N = 12$.

$C_3 - BJ_S$. We compare results obtained from a tGGE ansatz with $N_c = 4$ (dot-dashed black line) and $N_c = 6$ (dashed black line) to numerically exact calculations (red solid line). In the case of the energy density, we find a good agreement between both methods which improves when the number of charges contained in the tGGE is increased from four to six. Note that we only include the most local and simplest charges $S^z, H_0, C_3, (C_4, C_5)$ and the conserved part of the spin current operator. We do not consider more and more complicated conservation laws as we observe strong finite size effects when the maximal support of a conserved quantity becomes larger than $N/2$. In the inset plot of Fig. 4.5, we

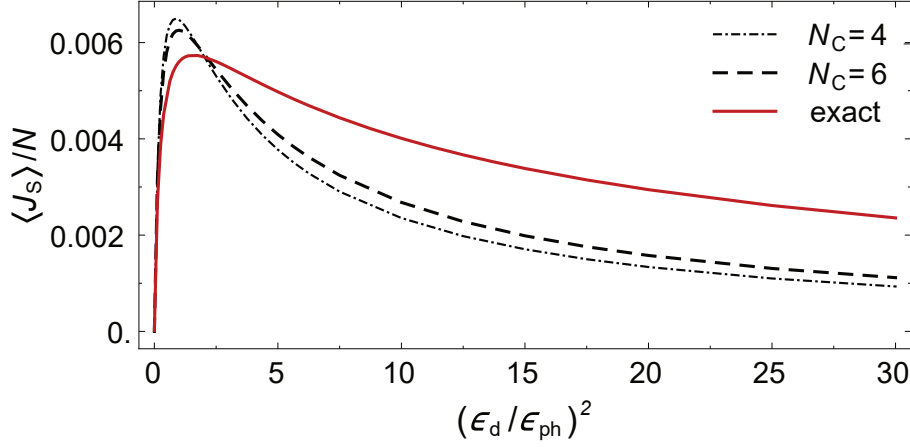


Figure 4.7 Expectation value of the conserved part of the spin current density as a function of the ratio $(\epsilon_d/\epsilon_{ph})^2$ calculated with the block-diagonal density matrix (solid red line) and a GGE with $N_c = 4$ (dot-dashed black line) and $N_c = 6$ (dashed black line) at $N = 12$. Parameters: $J = 1$, $\Delta = 0.8$, $\omega = 1.6\omega_{ph}$, $\omega_{ph} = T_{ph} = 1$.

show $\langle C_3 \rangle / N$ calculated at different system sizes $N = 10, 12, 14, 16$. We see that for a local operator as C_3 finite size effects are small.

The expectation value of the heat current density follows the predicted behavior. In the two limits $(\epsilon_d/\epsilon_{ph})^2 \rightarrow 0$ and $(\epsilon_d/\epsilon_{ph})^2 \rightarrow \infty$, the system is in a thermal state (possibly with finite magnetization) and therefore $\langle J_H \rangle$ is zero. Between these two limits, we find a finite expectation value that reaches a maximum at $\epsilon_d \sim \epsilon_{ph}$. While the tGGE ansatz reproduces the exact results qualitatively, we observe quantitatively strong deviations where a slight improvement can be obtained when N_c is increased by two. Our results suggest that further quasilocal conserved quantities that we do not consider in our study contribute. Similar observation have been made in quench protocols [63, 64].

Note that the external magnetic field B is needed to induce a heat current. The reason for this is that C_3 is odd under the product of a bond-centered rotation by π around the y axis in real and spin space while H_0 is even under this transformation for $B = 0$. In contrast to that, in our model the spin current is also activated at $B = 0$. The steady state expectation value $\langle J_S \rangle / N$ of the spin current density is depicted in Fig. 4.7. We obtain qualitatively similar results as for the heat current. The expectation value $\langle J_S \rangle$ is zero for $(\epsilon_d/\epsilon_{ph})^2 \rightarrow 0$, $(\epsilon_d/\epsilon_{ph})^2 \rightarrow \infty$ and approximately maximal at $\epsilon_d \sim \epsilon_{ph}$. As above we find only qualitative agreement between the numerically exact density matrix ρ_{BD} and the tGGE ansatz ρ_{GGE} .

Another experimentally tunable parameter besides the laser power $\sim \epsilon_d^2$ is the strength of the external magnetic field B . The numerical predictions we obtain for $\langle J_H \rangle / N$, $\langle J_S \rangle / N$ and $\langle C_3 \rangle / N$ at $(\epsilon_d/\epsilon_{ph})^2 = 2.5$ are presented in Fig 4.8. We find that $\langle C_3 \rangle$ and consequently also $\langle J_H \rangle$ are odd functions of B which vanish at $B = 0$ due to symmetry arguments. Thus, by changing the direction of the magnetic field, the direction of the heat current can be reversed. On the contrary, the spin current is an even function of B and depends only weakly on the field. The tGGE can in all cases reproduce the main

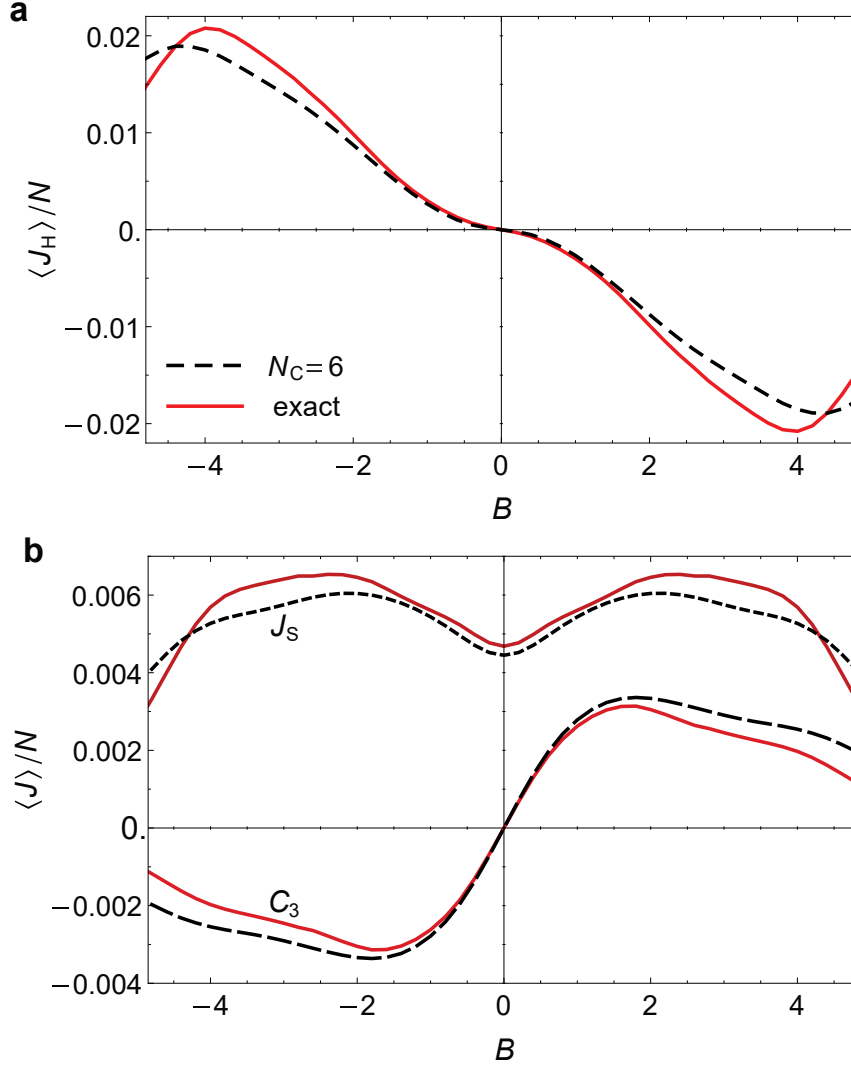


Figure 4.8 Expectation values of a) $\langle J_H \rangle / N$ and b) $\langle C_3 \rangle / N$, $\langle J_s \rangle / N$ as a function of the magnetic field strength B . While J_H and C_3 are odd functions, J_s is even under $B \leftrightarrow -B$.

features of the B -dependence like magnitude and position of extrema semi-quantitatively. We also depict the B -dependence of $\langle H_0 \rangle$ and the expectation value of the more complex charge C_4 in Fig. 4.9 to give further evidence for the claim that the tGGE gives a semi-quantitative description of the weakly open system.

In this section, we have presented an experimental idea of how to realize efficient heat and spin pumps based on integrability. Importantly, exact integrability which is a very fine-tuned property is not required for our approach to work but only the approximate conservation of currents. The precise experimental setup we have in mind is the following: we consider an effectively one-dimensional spin chain material with suitable symmetry properties potentially placed in an external magnetic field. The system is approximately modeled by Eq. (4.1), Eq. (4.2) and Eq. (4.3). Shining a THz laser onto

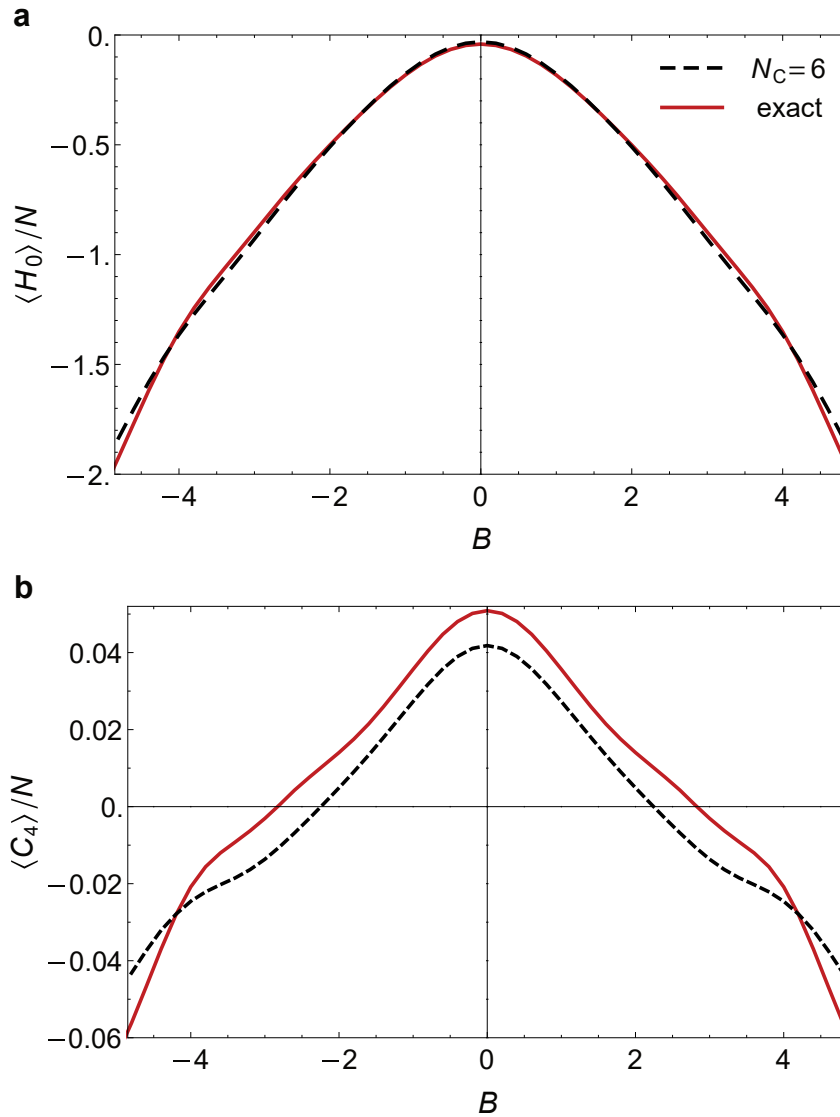


Figure 4.9 Expectation value of a) H_0/N and b) C_4/N as a function of the external magnetic field B calculated from the block-diagonal density matrix (solid red line) and a GGE with $N_c = 6$ (dashed black line) at $N = 12$.

the sample gives rise to an effectively staggered magnetic field and staggered bond-coupling that, in turn, evoke the approximately conserved currents of the system. The direction of the currents can be changed by changing the direction of the static B field in the case of the heat current or by changing the alignment of the laser. As a consequence of a finite heat current, one side of the sample is expected to heat up while the other side cools down which could, in principle, be directly measured.

We claimed that this effect is strong and the proposed heat and spin pump works efficiently, however, the absolute numbers we obtain for $\langle J_H \rangle / N$ and $\langle J_S \rangle / N$ are rather small. Nevertheless, the latter values become very huge when expressed in real physical units. In order to create a heat current of

similar size in a good heat conductor like Cu assuming reasonable values $J \sim k_B \cdot 100K$, $d = 5$ for the distance of the spin chains, and $\kappa_{Cu} \approx 400Wm^{-1}K^{-1}$ one would need a temperature gradient of about 10^5Km^{-1} . Similarly, to create a (transversal) spin current of comparable size in a heavy element like Pt using the spin Hall effect assuming $\rho_{Pt} \approx 10\mu\Omega cm$ and $\alpha_s^{Pt} \approx 10\%$ for the spin Hall angle one needs electric fields of the order of 10^4Vm^{-1} or sizable current densities of the order of $10^{11}Am^{-2}$ [111]. Note that we do not expect to measure such gigantic temperature gradients or fields in an experiment. The comparison above should rather give an impression of how strong the effect is.

In our analysis we neglect the explicit spatial dependence of the problem by using periodic boundary conditions within the numerical simulation. In Ch. 5 we will present an approach on how to describe spatially inhomogeneous states with a GGE parameterized by a set of space-dependent Lagrange parameters.

4.4 Further experimental setups

So far GGEs have been experimentally observed only on time scales where integrability breaking perturbations can be neglected. The experimental suggestion presented above represents a way of detecting the emergence of generalized Gibbs ensembles in weakly open many-body systems. However, our proposal involves a complicated driving term and requires to find a material with suitable symmetry properties, which can be a difficult task. For this reason, we consider here two simpler setups that might be easier implemented experimentally. Note that in contrast to closed systems, GGEs in weakly open systems are completely independent of the initial conditions. They can rather be engineered by the choice of perturbation.

4.4.1 Detection of GGEs in solids

The starting point is the same as before. We consider an effectively one-dimensional spin chain material approximately described by the XXZ model. Similarly, we assume that the dominant relaxation channel is provided by the coupling to phonons that we model by Eq. (4.3). In contrast to the previous setup, we choose a simpler perturbation that only activates the even charges of the XXZ model. The driving term contains one periodic magnetic field in x - and one in y -direction

$$H_d(t) = J\varepsilon_d^2 \sum_j \cos(\omega_d t) B_x S_j^x + \sin(\omega_d t) B_y S_j^y.$$

Note that we need only one magnetic field to activate the even charges of the model. However, we observe numerically that in the presence of a second perpendicular and phase shifted field, the resulting steady state is much further away from equilibrium. As pointed out in Sec 1.1.2, one effective method to test whether a sample is in thermal equilibrium or not is to probe it in a scattering experiment, for example, with inelastic x-ray (RIXS), neutron or Raman scattering. In the following, we consider a Raman scattering experiment and assume that the photons couple through the operator

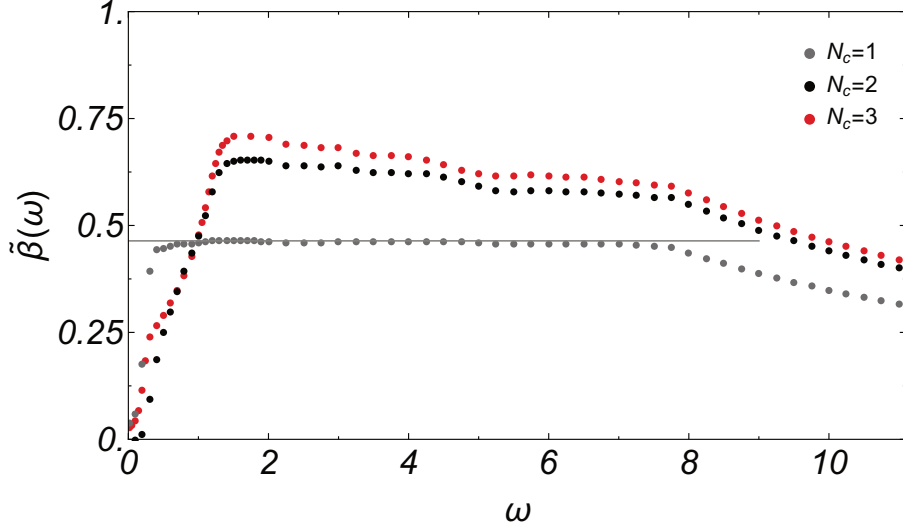


Figure 4.10 Effective inverse temperature $\tilde{\beta}$ as a function of the energy difference ω of the incoming and outgoing photon calculated from a tGGE including $N_c = 1, 2, 3$ conservation laws. The gray solid line shows the inverse temperature of the system which is determined by the balance of heating and cooling. Parameters: $J = 1, B_x = B_y = 1, \omega_d = 1, N = 14$

$A = \sum_j S_j^x S_{j+1}^x$ to the spin degrees of freedom. This is at the moment an arbitrary choice, however, we considered other couplings as well and obtained qualitatively similar results.

According to Sec 1.1.2, the ratio $C_{AA}^<(-\omega)/C_{AA}^<(\omega)$ of the response measured at energy differences ω and $-\omega$ is in thermal equilibrium equal to the Boltzmann weight

$$\frac{C_{AA}^<(-\omega)}{C_{AA}^<(\omega)} = e^{\beta\omega} \quad (4.19)$$

with temperature $T = 1/\beta$. The temperature can also be measured by other means, for example, with a conventional thermometer. A comparison between these values can then be used as a criterion whether the sample is in thermal equilibrium or not. Away from equilibrium, the relation Eq. (4.19) is violated and the new ω dependence of $C_{AA}^<(-\omega)/C_{AA}^<(\omega)$ might be theoretically described by a tGGE ansatz. In Fig. 4.10 we show the effective inverse temperature $\tilde{\beta}(\omega) := \log[C_{AA}^<(-\omega)/C_{AA}^<(\omega)]/\omega$ calculated for a finite system of size $N = 14$. Here, we approximate the steady state density matrix by a tGGE including $N_c = 1, N_c = 2$ and $N_c = 3$ conservation laws, respectively. According to our analysis in Ch. 3, a tGGE including more charges gives a much better description of the true steady state.

At large and small frequencies we observe numerical artifacts due to the smallness of the system and due to the broadening of the delta functions appearing in the correlation functions. For intermediate values of ω , we expect that these effects are considerably smaller and we, therefore, focus on this regime. In the case of a thermal ansatz $N_c = 1$, we simply find the expected relation $\tilde{\beta}(\omega) = \beta$

while for $N_c = 2, N_c = 3$ we observe distinct shifts of $\tilde{\beta}(\omega)$ to higher effective inverse temperatures, respectively. Hence, measuring the effective inverse temperature $\tilde{\beta}(\omega)$ in a weakly driven spin chain material within a Raman scattering experiment and comparing the obtained results to theoretical predictions of a tGGE ansatz might serve as a detection method for GGEs in solids.

4.4.2 Detection of GGEs in trapped ion systems

In the previous two examples of applications we focused on how the emergence of generalized Gibbs ensembles can be detected experimentally in real materials that are brought out of equilibrium. This is an interesting question in its own right. However, another appealing approach is to consider experimental platforms that offer more tuning possibilities allowing to engineer rather specific GGEs in a controlled manner. Naturally, trapped ion systems offer this kind of tunability [120]. In such setups, ions are typically cooled down to $\lesssim K$ using laser cooling techniques and trapped in linear Paul [121] or Penning [122] traps. By freezing out most of the degrees of freedom one can realize models known from many-body physics [123]. Here, we consider an implementation of the XY model in the presence of a magnetic field h based on a trapped ion setup. The Hamiltonian reads

$$H_0 = \sum_j J_x S_j^x S_{j+1}^x + J_y S_j^y S_{j+1}^y + h S_j^z. \quad (4.20)$$

We restrict our analysis to a free model as it can be easier realized experimentally than interacting ones. As a matter of fact in realistic trapped ion setups the coupling decays polynomially with the distance d as $(J/d^\alpha) S_j^{y,x} S_{j+d}^{y,x}$ where $2 \leq \alpha \leq 3$ [122]. Even in the absence of periodic pumping, this is already one weak source of integrability breaking. We assume that the decay is fast enough such that we can only consider the leading order term

$$H_1 = \varepsilon_1 \sum_j J_x S_j^x S_{j+2}^x + J_y S_j^y S_{j+2}^y, \quad \varepsilon_1 = \frac{1}{2\alpha}. \quad (4.21)$$

The perturbation H_1 alone would, potentially after a prethermalization regime, lead to thermalization in the long-time limit. However, a non-equilibrium steady state approximately described by a GGE can be obtained if the system is additionally coupled to a non-thermal bath or driven. Similar to the setup considered in Ch. 3, we model the coupling in terms of two homogeneous Lindbladians $\hat{\mathcal{L}}^{(1)}$ and $\hat{\mathcal{L}}^{(2)}$ with relative strength set by $\gamma \in [0, 1]$. As Lindblad operators we choose

$$\begin{aligned} L_k^{(1)} &= S_{k,x}^-, \\ L_k^{(2)} &= S_{k,x}^+ P_{k+1,x}^\downarrow, \end{aligned}$$

where $P_{k,x}^\downarrow = \frac{1}{2}(1 - \sigma_k^x)$ is a projection onto the state $|\downarrow\rangle_x$ at site k and $S_{k,x}^\pm = \sigma^z \mp i\sigma^y$. The full dynamics is governed by the Liouville superoperator $\hat{\mathcal{L}} = \hat{\mathcal{L}}_0 + \hat{\mathcal{L}}_u + \hat{\mathcal{L}}_1$ with

$$\begin{aligned}\hat{\mathcal{L}}_0\rho &= -i[H_0, \rho], \\ \hat{\mathcal{L}}_u\rho &= -i[H_1, \rho], \\ \hat{\mathcal{L}}_1\rho &= \varepsilon \left((1 - \gamma)\hat{\mathcal{D}}^{(1)} + \gamma\hat{\mathcal{D}}^{(2)} \right) \rho.\end{aligned}$$

A detailed description of how these dynamics can be realized in a trapped ion platform can be found in [124]. In contrast to our previous studies we now consider a combination of unitary and Markovian perturbations. Even though the bare Hamiltonian H_0 is non-interacting, the Lindblad operators being non-local in the language of Jordan-Wigner fermions make the problem effectively interacting. Thus, we cannot give an analytic solution and are limited to finite-size exact diagonalization. We base our analysis of the steady state on the three methods described in Ch. 3. We calculate (I) the exact steady state density matrix ρ_∞ for small values of ε and a tiny system size with $N = 6$, (II) the block-diagonal steady state density matrix at $N = 6, 8, 10$ and (III) a tGGE including a finite number of conservation laws $N_c = 4$ for up to $N = 12$. Our goal is to demonstrate that the steady state is highly non-thermal and can be captured by a tGGE parameterized by a small number of charges. As a measure of how thermal a state is with respect to the expectation value of an observable O , we introduce

$$\eta_O = \frac{\text{Tr}[O\rho_x] - \text{Tr}[O\rho_{th}]}{\text{Tr}[O\rho_{th}]}, \quad (4.22)$$

where ρ_x has to be replaced by ρ_∞ , ρ_{BD} or ρ_{GGE} depending on the chosen method. In the first two cases ρ_{th} is defined by $\text{Tr}[H_0\rho_{th}] = \text{Tr}[H_0\rho_{\infty/BD}]$. For $\rho_x = \rho_{GGE}$, the thermal state is determined from $\langle \dot{H}_0 \rangle_{GE} = 0$ where $\langle \cdot \rangle_{GE}$ is calculated with respect to a Gibbs state that only includes H_0 as a charge. In the following, we focus on the operators $O = H_0, C_4$ that are used to parameterize the tGGE ($N_c = 4$). We expect that operators, which are included in the tGGE ansatz, are most accurately described by ρ_{GGE} . Moreover, both of them can, in principle, be measured experimentally. The explicit expression for C_4 reads

$$C_4 = \sum_j \sum_{\mu=x,y} J_\mu S_j^\mu S_{j+1}^z S_{j+2}^z S_{j+3}^\mu - \frac{1}{2} h J_\mu S_j^\mu S_{j+1}^z S_{j+2}^\mu + \frac{1}{4} J_{\bar{\mu}} S_j^\mu S_{j+1}^\mu, \quad (4.23)$$

where we have introduced the notation $\bar{x} = y, \bar{y} = x$. A rigorous instruction for the calculation of the remaining local conserved quantities of the $XY + h$ model can be found in [25]. First, we compare the three methods presented above and address the question of how relevant the unitary perturbation H_1 is in relation to the dissipative coupling. To this end we show in Fig. 4.11 the expectation values $\langle H_0 \rangle$ and $\langle C_4 \rangle$ per site as a function of the relative driving strength γ at $J_x/J_y = 0.1$ and $J_x/J_y = 2$. We find that the effect of H_1 is weak when comparing the numerically exact calculation with (ρ_∞, NN) and without next-nearest neighbor coupling term (ρ_∞, N) . At $J_x/J_y = 2$ and for $\langle C_4 \rangle$ at $J_x/J_y = 0.1$ results are almost indistinguishable. While H_1 can be straightforwardly incorporated in the numerically exact

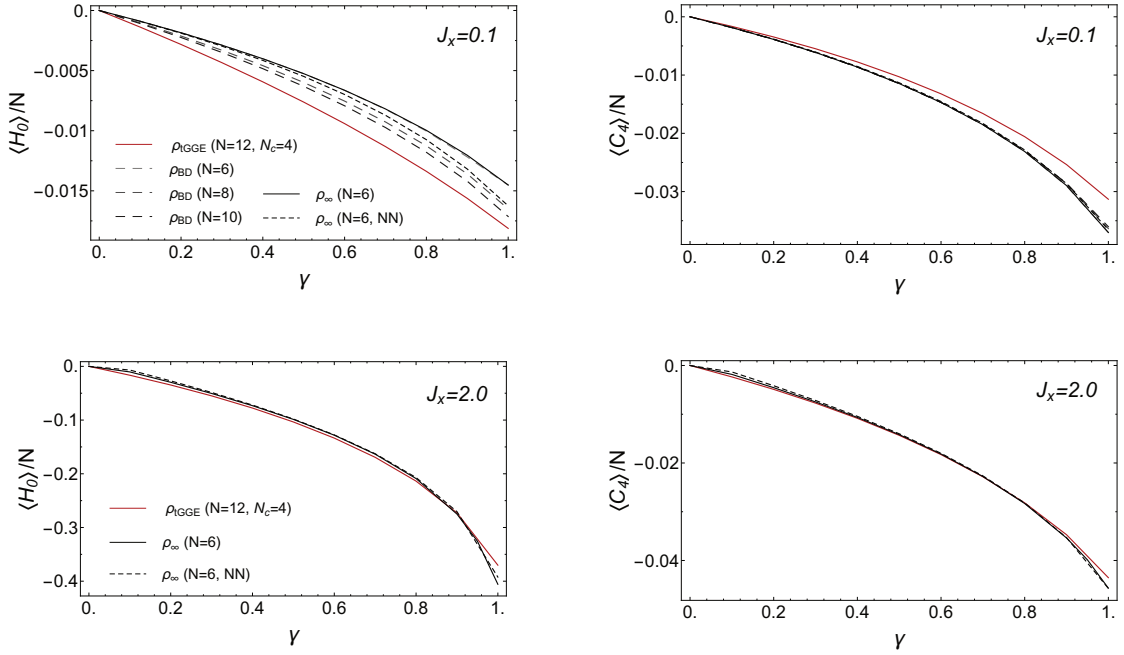


Figure 4.11 Steady state expectation value of H_0 (left) and C_4 (right) calculated from the block-diagonal density matrix for system sizes $N = 6, 8, 10$, from the numerically exact density matrix at $N = 6$ for $\varepsilon_1 = 0.05$ with (dashed black line) and for $\varepsilon_1 = 0$ without (solid black line) next-nearest neighbor coupling, and from a tGGE at $N_c = 4, N = 12$. The upper panel shows results for coupling strength $J_x = 0.1$ and the lower one for $J_x = 2.0$. Parameters: $\gamma = 0.5, \varepsilon = 0.01, J_y = 1$.

calculation, it brings a certain ambiguity into the determination of ρ_{BD} and ρ_{GGE} . This is due to the fact that calculating $\hat{\mathcal{L}}_1 \hat{\mathcal{L}}_0^{-1} \hat{\mathcal{L}}_1$ involves broadening. As the broadening enters only in the calculation of ρ_{BD} and ρ_{GGE} but not ρ_∞ , it makes the comparison between the different methods difficult. Another complication is that suitable broadening is system size dependent and the correct choice for a given N may be ambiguous and not-well defined. Therefore, we use the observation that the next-nearest neighbor coupling does not affect the steady state expectation values of the considered quantities significantly as a justification to omit H_1 in the following calculations.

In Fig. 4.11, we observe that ρ_{GGE} gives the same qualitative result as the exact calculation obtained from ρ_∞ where deviations are most visible at $J_x = 0.1$. We think that this is potentially due to the proximity to the transverse Ising field limit in which new families of charges start to emerge. Partially, deviations can also be explained by finite size effects of the exact and block-diagonal approach as we show by including results obtained from ρ_{BD} as well. In the case of $\langle H_0 \rangle$, ρ_{BD} ($N = 6, 8, 10$) interpolates between the exact ($N = 6$) and the tGGE ($N = 12$) results indicating a better agreement at larger system sizes. For $\langle C_4 \rangle$ we also recognize this interpolation effect but in a much weaker form. In contrast to ρ_{BD} and ρ_∞ , we observe much weaker finite size effects in the case of the GGE ansatz. At larger coupling strength $J_x/J_y = 2$ we find good agreement between all methods at already small

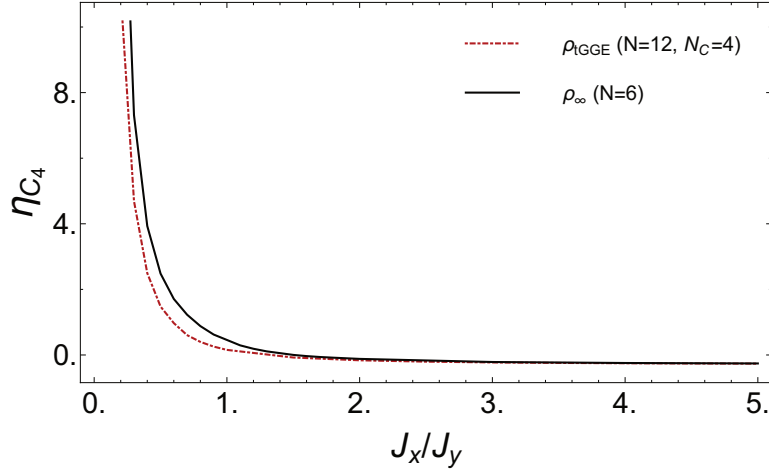


Figure 4.12 The quantity η_{C_4} , which is a measure of how thermal the system is with respect to the operator C_4 , is plotted as a function of the coupling strength J_x . We compare results obtained from the numerically exact density matrix at $N = 6$ to the tGGE results at $N = 12, N_c = 4$. Parameters: $J_y = 1, \varepsilon_1 = 0, \varepsilon = 0.01$.

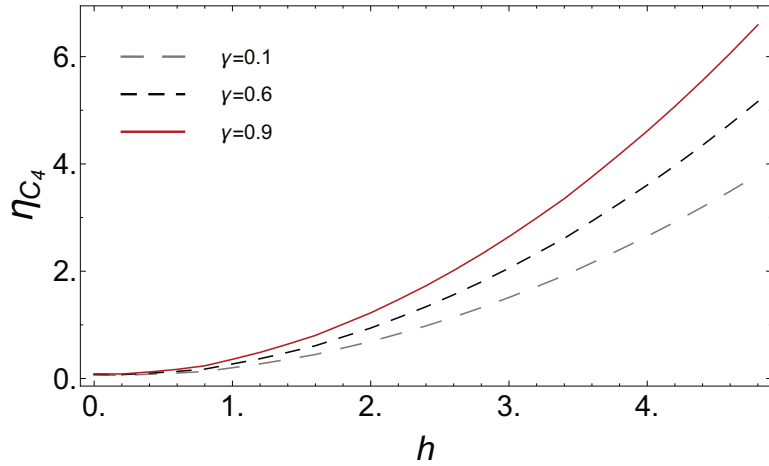


Figure 4.13 The quantity η_{C_4} is plotted as a function of the static field h where we use the tGGE ansatz with $N_c = 4$. Parameters: $J_x = 0.9, J_y = 1, N = 12$.

system sizes. While $|\langle H_0 \rangle| > |\langle C_4 \rangle|$ at $J_x/J_y = 2$, we obtain $|\langle H_0 \rangle| < |\langle C_4 \rangle|$ at $J_x/J_y = 0.1$ showing that the steady state is non-thermal in the regime where the anisotropy is small. In Fig. 4.12, we depict η_{C_4} as a function of J_x/J_y at $h = 1$ and relative coupling strength $\gamma = 0.5$. We find that η_{C_4} becomes very large at small values of J_x where $\langle C_4 \rangle_{th}$ approaches zero, which can be seen in the two left plots of Fig. 4.11. In the opposite limit of large J_x/J_y where $H_0 \approx J_x S_j^x S_{j+1}^x$, we find $\langle C_4 \rangle \approx \langle C_4 \rangle_{th}$. In the Ising limit, the thermal state is a good approximation due to reasons similar to those outlined in Sec. 3.4. Note that the zero crossing varies for different observables and is therefore not a true signal

for a thermal state. Our results suggest that experiments should best be performed in a parameter regime where J_x/J_y is small. However, anisotropy cannot be varied easily in an experiment. Thus, we need another tuning parameter which can be changed with much less effort. For example, the external magnetic field. In Fig 4.13 we show the h dependence of η_{C_4} for $\gamma = 0.1, 0.8, 0.9$ and $J_x = 0.9$. We clearly see that higher field strengths can help to prepare steady states that are further away from equilibrium. In the limit where h becomes larger than all other energy scales in the system, the Hamiltonian reads $H_0 \approx hS_j^z$ and consequently $\langle C_4 \rangle_{th} \approx 0$.

Chapter 5

Generalized hydrodynamics and phase transitions in open quantum systems

Hydrodynamics is the natural framework to describe the dynamics of systems, either classical or quantum, close to equilibrium in the limit of small frequencies $\omega \rightarrow 0$ and small momenta $k \rightarrow 0$. The fundamental assumption of hydrodynamics is based on local entropy maximization or local equilibration [125], meaning that after a short characteristic relaxation time the system is conjectured to locally approach an equilibrium Gibbs state.

Technically, the dynamics is only treated on coarse-grained scales where the system is decomposed into so-called fluid cells that are in local equilibrium and characterized by only a few intensive parameters. Their properties vary only slowly in space and time on scales much larger than all microscopic scales. The fast microscopic dynamics gives, in turn, rise to local equilibration. In the long-time limit, the dynamics of the system is described by a set of coupled, in general, nonlinear differential equations for the expectation values of the conserved quantities, or equivalently, for the corresponding Lagrange parameters. In the presence of conserved currents, the dynamics in frictionless systems is expected to be described by *Euler's equation* while dissipative corrections give rise to *Navier-Stokes equations*.

As an example, we consider a homogeneous Galilean invariant one-dimensional many-body system in which the Hamiltonian H , particle number N and the momentum operator P are conserved. Note that we took this example from [126]. According to hydrodynamics, a system that is close to equilibrium can locally be described by a Gibbs state

$$\rho_{GE,r}(t) \sim e^{-\beta(r,t)(H+\mu(r,t)N+v(r,t)P)} \quad (5.1)$$

which reproduces the expectation values of physical observables $o(r)$, $\langle o(r,t) \rangle \approx \langle o(r,t) \rangle_{GGE,0} = \text{Tr}[o(r)\rho_{GGE,r}(t)]$. On the level of operators, continuity equations hold for the local densities h , n and p

$$\begin{aligned} \partial_t h(r,t) + \partial_r j_h(r,t) &= 0 & \partial_t \langle h(r,t) \rangle_{GGE,0} + \partial_r \langle j_h(r,t) \rangle_{GGE,0} &= 0, \\ \partial_t n(r,t) + \partial_r p(r,t) &= 0 & \rightarrow \partial_t \langle n(r,t) \rangle_{GGE,0} + \partial_r \langle p(r,t) \rangle_{GGE,0} &= 0, \\ \partial_t p(r,t) + \partial_r j_p(r,t) &= 0 & \partial_t \langle p(r,t) \rangle_{GGE,0} + \partial_r \langle j_p(r,t) \rangle_{GGE,0} &= 0, \end{aligned}$$

where j_h , $j_n = p$ and j_p are the corresponding current densities. Note that in this example the particle current j_n itself is conserved.

The general form of a continuity equation $\partial_t \rho(r,t) + \nabla j(r,t) = 0$ is especially intuitive when written in integral form

$$\partial_t \int dV \rho(r,t) = - \int dV \nabla j(r,t) = - \int dA \cdot j(r,t), \quad (5.2)$$

where we have used Gauss' theorem for the last equality. Eq. (5.2) states that the amount of a conserved quantity within a closed volume V can only be changed by a current that flows through the enclosing surface.

The basic approach of hydrodynamics is to perform an expansion in gradients of local densities [127] as

$$\langle p(r,t) \rangle = \langle p(r,t) \rangle_{GGE,0} + A_{pn}^{(1)}(r,t) \partial_r \langle n(r,t) \rangle_{GGE,0} + \dots \quad (5.3)$$

To leading order, the continuity equations for operators directly translate to continuity equations for local expectation values with respect to $\rho_{GGE,r}$. Introducing the velocity field v and using $p = nv$ we obtain from the last two continuity equations

$$\partial_t v + v \partial_r v = - \frac{1}{n} \partial_r P \quad (5.4)$$

which is Euler's equation with pressure $P = j_p - nv^2$. Note that we dropped the brackets $\langle \cdot \rangle_{GGE,0}$ in Eq. (5.4) for brevity.

In the presence of an infinite amount of conservation laws, which is the case in integrable systems, a simple Gibbs state does not suffice to describe the equilibrium steady state. Instead, we expect that these systems relax to a generalized Gibbs state. Recently, a formulation of hydrodynamics for integrable quantum systems referred to as *generalized hydrodynamics* (GHD) was proposed, taking into account an infinite amount of conservation laws [128–130]. In the context of many-body physics, it was shown that the dynamics in certain integrable field theories can be recast into a set of hydrodynamic equations for quasiparticle densities and currents which can be determined using thermodynamic Bethe ansatz techniques [129]. Similar equations were obtained for the Heisenberg model in [130].

Here, we apply the basic idea of GHD to weakly open quantum systems and calculate the hydrody-

dynamic equations to leading order in spatial derivatives in the framework of GGEs with space-dependent Lagrange parameters. For simplicity, we restrict our analysis to perturbations that do not drive any conserved currents. Particularly, we are interested in the emergence of inhomogeneous states with domain walls and non-equilibrium phase transitions that we, however, only treat on phenomenological grounds. Naturally, there are two ways to approach the problem of arising inhomogeneities. Firstly, we could consider explicitly inhomogeneous perturbations $\hat{\mathcal{L}}_1$ that create spatially varying patterns, for example, Lindblad operators acting only on single sites. Secondly, we could define a uniform perturbation which leads to a richer fixed point structure with two or more stable attractors. The system can be in different spatial regions in one of the steady states with transition regions in between. In the following, we will focus on the second approach.

5.1 Space-dependent Lagrange parameters

We consider a system that has a set of conserved quantities $C_j = \int dr c_j(r)$. In the spirit of the previous chapters, we assume that states with weak spatial inhomogeneities can be approximately described by a GGE with space-dependent Lagrange parameters

$$\begin{aligned} \rho_{GGE}(t) &= (Z_{GGE})^{-1} \exp \left(- \sum_j \int dr \lambda_j(r,t) c_j(r) \right), \\ Z_{GGE} &= \text{Tr}[\rho_{GGE}] \end{aligned} \quad (5.5)$$

in the long-time limit where we have replaced the sum appearing in the previous definition of the GGE by an integral. Starting from a discrete quantum model on a lattice, we assume that a continuum limit exists. The GGE is defined through the equations $\langle c_i(r_0, t) \rangle \stackrel{\dagger}{=} \langle c_i(r_0, t) \rangle_{GGE}$ where we use the notation $\langle X \rangle_{GGE} = \text{Tr}[X \rho_{GGE}]$.

First, we neglect the effect of the weak perturbation $\hat{\mathcal{L}}_1$ and write for the total density matrix $\rho(t) = \rho_{GGE}(t) + \delta\rho(t)$. It is important to stress that a GGE with space-dependent Lagrange parameters is no longer a solution of the unperturbed Liouville-von Neumann equation, i.e. $\hat{\mathcal{L}}_0 \rho_{GGE} \neq 0$. The deviation $\delta\rho(t)$ from the exact density matrix is defined through the equation

$$\left(\partial_t - \hat{\mathcal{L}}_0 \right) \delta\rho(t) = - \left(\partial_t - \hat{\mathcal{L}}_0 \right) \rho_{GGE}(t) =: A(t). \quad (5.6)$$

Formally, a solution can be provided with the help of the propagator $\hat{G}(t) = e^{-\hat{\mathcal{L}}_0 t} \theta(t)$ that fulfills $\left(\partial_t - \hat{\mathcal{L}}_0 \right) \hat{G}(t) = \delta(t) \mathbb{1}$. Using $\hat{G}(t)$ we obtain

$$\begin{aligned} \delta\rho(t) &= \int_{t_0}^{\infty} dt' \hat{G}(t-t') A(t') + \hat{G}(t-t_0) \delta\rho(t_0) \\ &= - \int_{t_0}^{\infty} dt' \theta(t-t') e^{-\hat{\mathcal{L}}_0(t-t')} (\partial_{t'} - \hat{\mathcal{L}}_0) \rho_{GGE}(t') + e^{-\hat{\mathcal{L}}_0(t-t_0)} \delta\rho(t_0), \end{aligned} \quad (5.7)$$

where we have denoted the density matrix at initial time t_0 by $\rho(t_0) = \rho_{GGE}(t_0) + \delta\rho(t_0)$. In the following, we assume that the initial conditions can be neglected in the long-time limit.

5.1.1 Homogeneous expansion point

Finally, we want to calculate the expectation values $\langle c_i(r_0, t) \rangle$ of the local charge densities $c_i(r_0)$ to leading order in spatial derivatives and derive a set of hydrodynamic equations for the system. As an expansion point, we choose a homogeneous GGE

$$\rho_{GGE, r_0}(t) = (Z_{GGE, r_0})^{-1} \exp\left(-\sum_j \lambda_j(r_0, t) C_j\right) \quad (5.8)$$

defined at position r_0 . As the terms $\int dr \lambda_j(r, t) c_j(r)$ do not commute with each other for different labels j and explicitly space-dependent Lagrange parameters, we cannot use a straightforward Taylor expansion in Eq. (5.5). However, we can resolve this problem by employing known tools from unitary perturbation theory for Hamiltonian systems $H = H_0 + \Delta H$ that have the property $[H_0, \Delta H] \neq 0$. First, we rewrite the exponential in Eq. (5.5) as

$$\exp\left(-\lambda_2(r_0, t) \left(\sum_j \frac{\lambda_j(r_0, t)}{\lambda_2(r_0, t)} C_j + \sum_j \int dr \left(\frac{\lambda_j(r, t) - \lambda_j(r_0, t)}{\lambda_2(r_0, t)}\right) c_j(r)\right)\right), \quad (5.9)$$

where we assume that $\lambda_2(r_0, t) \neq 0$. In the next step, we define in analogy to a Hamiltonian system

$$H_0 := \sum_j \frac{\lambda_j(r_0, t)}{\lambda_2(r_0, t)} C_j, \quad \Delta H := \sum_j \int dr \left(\frac{\lambda_j(r, t) - \lambda_j(r_0, t)}{\lambda_2(r_0, t)}\right) c_j(r). \quad (5.10)$$

By introducing the imaginary time parameter $\tau \in [0, \lambda_2(r_0, t)]$, we can define the propagation operator

$$U(\tau) := e^{-\tau(H_0 + \Delta H)}$$

that fulfills $\partial_\tau U(\tau) = -(H_0 + \Delta H)U(\tau)$. Note that the initial expression Eq. (5.9) can be recovered if we set $\tau = \lambda_2(r_0, t)$. It is convenient to express the propagator in interaction picture representation, $U^{(I)}(\tau) = e^{\tau H_0} U$. Taking the derivative with respect to τ yields

$$\begin{aligned} \partial_\tau U^{(I)}(\tau) &= H_0 e^{\tau H_0} U(\tau) - e^{\tau H_0} (H_0 + \Delta H) U(\tau) \\ &= -e^{\tau H_0} \Delta H e^{-\tau H_0} U^{(I)}(\tau) = -\Delta H^{(I)}(\tau) U^{(I)}(\tau). \end{aligned} \quad (5.11)$$

In analogy to the time evolution operator for a time-dependent Hamiltonian that does not commute with itself at different times t , we arrive at

$$U^{(I)}(\tau) = \hat{\mathcal{T}} e^{-\int_0^\tau d\tau' \Delta H(\tau')} \quad \Rightarrow \quad U(\tau) = e^{-\tau H_0} \hat{\mathcal{T}} e^{-\int_0^\tau d\tau' \Delta H(\tau')}, \quad (5.12)$$

where $\hat{\mathcal{F}}$ is the (imaginary) time-ordering operator. Eq. (5.12) is equivalent to the thermal density operator $e^{-\beta(H_0+\Delta H)}$ for $\tau = \lambda_2 = \beta$. The great advantage of Eq. (5.12) is the fact that the imaginary time-ordered exponential can be expanded straightforwardly [131] while an expansion of $e^{-\beta(H_0+\Delta H)}$ involves a set of nested commutators which do not vanish for $[H_0, \Delta H] \neq 0$. The price we have to pay to achieve this simplification, is the introduction of the additional parameter τ .

5.1.2 Gradient expansion

We can translate Eq. (5.12) back to the initial problem by inserting H_0 , ΔH and setting $\tau = \lambda_2(r_0, t)$,

$$\begin{aligned} \rho_{GGE}(t) &= Z_{GGE}^{-1} \rho_{GGE, r_0} \hat{\mathcal{F}} e^{-\frac{1}{\lambda_2(r_0, t)} \sum_j \int_0^{\lambda_2(r_0, t)} d\tau \int dr (\lambda_j(r, t) - \lambda_j(r_0, t)) c_j(r, \tau)} \\ &\approx \rho_{GGE, r_0} \left(1 - \sum_j \frac{1}{\lambda_2(r_0, t)} \int_0^{\lambda_2(r_0, t)} d\tau \int dr (\lambda_j(r, t) - \lambda_j(r_0, t)) c_j(r, \tau) \right) \end{aligned} \quad (5.13)$$

where we have expanded the time-ordered exponential to first order in its argument. The truncation is only justified for the calculation of expectation values $\langle o(r_0, t) \rangle$ of local operators $o(r_0)$ if the product of $(\lambda_j(r, t) - \lambda_j(r_0, t))$ and $\text{Tr}[o(r_0) c_j(r, \tau) \rho_{GGE, r_0}(t)]$ is small. For r close to r_0 this is the case for smoothly varying Lagrange parameters that only change significantly on long length scales. At large distances $|r - r_0| \gg 1$, the validity of the expansion is guaranteed if the overlap between the local densities $o(r_0)$ and $c_j(r)$ drops fast on the relevant length scale of the system. Note that the expansion of Z_{GGE}^{-1} to first order can be neglected for the calculation of $\langle \dot{c}_i(r_0, t) \rangle = \text{Tr}[c_i(r_0) \hat{\mathcal{L}}_0 \rho(t)]$ due to $\hat{\mathcal{L}}_0 \rho_{GGE, r_0}(t) = 0$ and symmetry arguments which will be outlined later.

According to our analysis of time-dependent weakly open systems, the time scale on which the density matrix adjusts in the subspace of GGEs is set by $1/\varepsilon$ where ε is the strength of the weak perturbation. For spatial variations we impose the scaling relation $\partial_r \sim \sqrt{\varepsilon}$ which can also be directly obtained by expanding $\partial_t \langle c_i(r_0, t) \rangle$ to leading order in derivatives yielding $\partial_t \sim \partial_r^2 \sim \varepsilon$ in the case where conserved currents are forbidden by symmetry. We obtain for the rate equations of the local densities,

$$\begin{aligned} \partial_t \langle c_i(r_0, t) \rangle &= \text{Tr}[c_i(r_0) \dot{\rho}(t)] = \text{Tr}[c_i(r_0) \dot{\rho}_{GGE}(t)] + \underbrace{\text{Tr}[c_i(r_0) \delta \dot{\rho}(t)]}_{=0} \\ &= \underbrace{\text{Tr}[c_i(r_0) \hat{\mathcal{L}}_0 \rho_{GGE}(t)]}_{=0} + \text{Tr}[c_i(r_0) \hat{\mathcal{L}}_0 \delta \rho(t)]. \end{aligned} \quad (5.14)$$

In the first line of Eq. (5.14) we use $\partial_t \text{Tr}[c_j(r_0) \delta \rho(t)] = 0$ which follows from the definition of ρ_{GGE} . In the second line we employ the definition of the adjoint Liouvillian $\hat{\mathcal{L}}_0^\dagger$, $\text{Tr}[c_i(r_0) \hat{\mathcal{L}}_0 \rho_{GGE}(t)] = \text{Tr}[\hat{\mathcal{L}}_0^\dagger(c_i(r_0)) \rho_{GGE}(t)] = -\partial_{r_0} \text{Tr}[j_i(r_0) \rho_{GGE}(t)] = 0$ and use the fact that odd charges are, by assumption, not activated by $\hat{\mathcal{L}}_1$ and therefore no conserved currents are present in the system. Their corresponding Lagrange parameters are zero. More precisely, as all conserved currents are, for example, odd under time reversal symmetry while all even charges are even under this transformation

we can conclude that $\text{Tr}[j_i(r_0)\rho_{GGE}(t)] = -\text{Tr}[j_i(r_0)\rho_{GGE}(t)] = 0$. The current density j_i is connected to the charge density c_i through a local continuity equation

$$\partial_t c_i(r, t) + \partial_r j_i(r, t) = 0.$$

To motivate the formula $\mathcal{L}_0^\dagger c_i(r_0) = -\partial_{r_0} j_i(r_0)$, we go back to the discrete description of the model. In the Heisenberg picture the time evolution of the local charge density $c_{i,k}$ at lattice site k reads

$$\partial_t c_{i,k} = i[H, c_{i,k}] = \mathcal{L}_0^\dagger c_{i,k} =: -(j_{i,k+1} - j_{i,k})$$

where we use the last equality as a definition for the current density $j_{i,k}$. This is a valid definition as it guarantees the conservation of C_i for periodic boundary conditions

$$\partial_t C_i = \partial_t \sum_k c_{i,k} = -\sum_k (j_{i,k+1} - j_{i,k}) = -\left(\sum_k j_{i,k+1} - \sum_k j_{i,k}\right) = 0.$$

In the last step, we have changed the summation index $k+1 \rightarrow k$ in the first sum. As the difference of a discrete function evaluated at two neighboring sites is equivalent to a discrete derivative in one-dimension, we can conclude that $\mathcal{L}_0^\dagger c_i = -\partial_r j_i$.

Next, we calculate the second term $\text{Tr}[c_i(r_0)\mathcal{L}_0\delta\rho(t)] = -\partial_{r_0}\text{Tr}[j_i(r_0)\delta\rho]$ in the last line of Eq. (5.14) using an expansion of ρ_{GGE} to leading order in derivatives,

$$\begin{aligned} \langle \dot{c}_i(r_0, t) \rangle &\approx -\partial_{r_0}\text{Tr}[j_i(r_0, t)\delta\rho(t_0)] + \partial_{r_0}\text{Tr}\left[j_i(r_0) \int_{t_0}^{\infty} dt' \theta(t-t') e^{-\mathcal{L}_0(t-t')} (\partial_{t'} - \mathcal{L}_0)\rho_{GGE}(t')\right] \\ &\approx \partial_{r_0}\text{Tr}\left[j_i(r_0) \int_{t_0}^{\infty} dt' \theta(t-t') e^{-\mathcal{L}_0(t-t')} (\partial_{t'} - \mathcal{L}_0)\rho_{GGE, r_0}(t') \right. \\ &\quad \left. \left(\mathbb{X} - \sum_j \frac{1}{\lambda_2(r_0, t')} \int_0^{\lambda_2(r_0, t')} d\tau \int dr (\lambda_j(r, t') - \lambda_j(r_0, t')) c_j(r, \tau)\right)\right] \\ &= +\partial_{r_0} \int_{t_0}^t dt' \text{Tr}\left[j_i(r_0, t-t') \sum_j \int_0^{\lambda_2(r_0, t')} d\tau \int dr \frac{\lambda_j(r, t') - \lambda_j(r_0, t')}{\lambda_2(r_0, t')} \rho_{GGE, r_0}(t') \underbrace{\mathcal{L}_0 c_j(r, \tau)}_{=\partial_r j_j(r, \tau)}\right] \\ &= -\partial_{r_0} \int_{t_0 \rightarrow -\infty}^t dt' \int dr \underbrace{\sum_j \frac{1}{\lambda_2(r_0, t')} \int_0^{\lambda_2(r_0, t')} d\tau \text{Tr}\left[j_j(r, \tau) j_i(r_0, t-t') \rho_{GGE, r_0}(t')\right]}_{=: \sigma_{ij}(r, r_0; t, t')} \partial_r \lambda_j(r, t') \\ &= -\partial_{r_0} \sum_j \int dr \int_{-\infty}^t dt' \sigma_{ij}(r, r_0; t, t') \partial_r \lambda_j(r, t') = -\partial_{r_0} \sum_j J_{ij}(r_0, t). \end{aligned}$$

In the first line, we assume that the initial state does not carry any currents, i.e. $\text{Tr}[j_i(r_0, t)\delta\rho(t_0)] = 0$. Moreover, we employ the assumption that the considered perturbation does not activate any conserved currents, which cancels terms proportional to $\text{Tr}[j_i(r_0, t)\rho_{GGE, r_0}(t)]$, $\text{Tr}[j_i(r_0, t)\rho_{GGE, r_0}(t)c_j(r, \tau)]$,

$\text{Tr}[j_i(r_0, t) \partial_t \rho_{GGE, r_0}(t)]$ and $\text{Tr}[j_i(r_0, t) \partial_t \rho_{GGE, r_0}(t) c_j(r, \tau)]$ due to symmetry reasons. In the second last line, the conductivity σ_{ij} , which is a function of r, r_0, t and t' , is introduced, describing the response of $\langle \dot{c}_i(r_0, t) \rangle$ to a spatial variation of the Lagrange parameter λ_j . We can identify the summands in the last line as components of the generalized current $J(r_0, t)$. Expanding $\langle \dot{c}_i(r_0, t) \rangle \approx \langle \dot{c}_i(r_0, t) \rangle_{GGE, 0}$ to leading order and including the weak perturbation in terms of the generalized force \mathbf{F} that acts as a source term in the continuity equation, we finally arrive at

$$\partial_t \langle c_i(r, t) \rangle_{GGE, 0} + \partial_r \sum_j J_{ij}(r, t) = (F_c)_i \langle \mathbf{c}(r, t) \rangle_{GGE, 0} \quad (5.15)$$

where we have defined $(F_c)_i := -\sum_j \chi_{ij} F_j$ (cf. Sec. 2.2.2) and used the notation $\langle \cdot \rangle_{GGE, 0}$ to denote expectation values with respect to a homogeneous GGE. According to our scaling assumption, Eq. (5.15) is of order ε . Equivalently, Eq. (5.15) can be expressed in the space of Lagrange parameters as

$$\partial_t \lambda_i(r, t) - \sum_{j,k} (\chi^{-1})_{ik} \partial_r J_{kj}(r, t) = F_i(\boldsymbol{\lambda}). \quad (5.16)$$

5.2 Transitions in weakly open spin chains

5.2.1 Symmetric potential

We consider a XXZ spin chain which is weakly coupled to a non-thermal bath described by a translational invariant Lindblad superoperator \mathcal{L}_1 . The dynamics of the system is governed by

$$\begin{aligned} \partial_t \rho &= \mathcal{L} \rho = (\mathcal{L}_0 + \mathcal{L}_1) \rho, \\ \mathcal{L}_0 \rho &= -i[H_0, \rho], \quad \mathcal{L}_1 \rho = \varepsilon \left((1 - \gamma) \hat{\mathcal{D}}^{(1)} + \gamma \hat{\mathcal{D}}^{(2)} \right) \rho, \end{aligned} \quad (5.17)$$

where $\hat{\mathcal{D}}^{(1)}$ and $\hat{\mathcal{D}}^{(2)}$ are Lindblad dissipators. We aim to construct the Lindblad coupling such that $\mathcal{L} \rho = 0$ has, in contrast to our previous studies, no unique solution. We are explicitly interested in cases where two or more stable or metastable non-equilibrium steady states exist. This goal can, for example, be achieved by using the Lindblad operators

$$\begin{aligned} L_j^{(1)} &= 2S_j^x, \\ L_j^{(2)} &= P_{j-1}^\uparrow S_j^+ P_{j+1}^\uparrow + P_{j-1}^\downarrow S_j^- P_{j+1}^\downarrow. \end{aligned} \quad (5.18)$$

Note that these operators do not activate the conserved currents of the Heisenberg model. The first Lindblad operator is hermitian and therefore causes dephasing while the second one aligns neighboring spins in $+z$ and $-z$ direction. As $L_j^{(2)}$ is invariant under spin-reversal, none of the two directions is favored. Both of the fully polarized states $|FP, \uparrow\rangle = |\uparrow \dots \uparrow\rangle$, $|FP, \downarrow\rangle = |\downarrow \dots \downarrow\rangle$ are *dark states* of the second Lindblad operator, i.e. $L_j^{(2)} |FP, \uparrow\rangle = L_j^{(2)} |FP, \downarrow\rangle = 0$. Thus, at $\gamma = 1$ one set of steady state

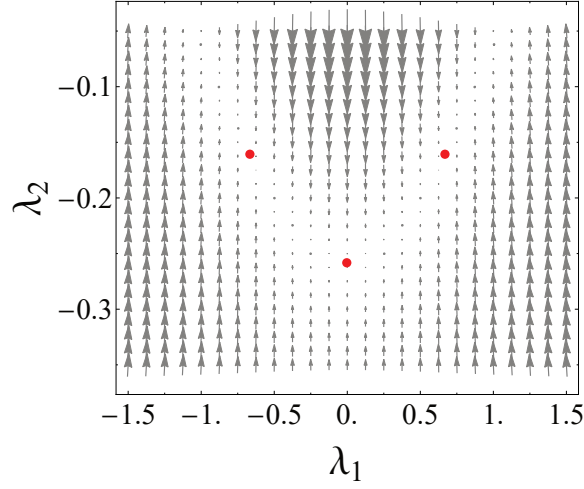


Figure 5.1 Generalized force plotted in the plane spanned by λ_1 and λ_2 at $N = 8$, $\gamma = 0.9$. Two stable fixed points are located at $\lambda_1 = \pm\lambda_1^*$ ($C_1 = S^z$), $\lambda_2 = \lambda_2^*$ ($C_2 = H_0$) with $\lambda_1^* \approx 0.75$ and $\lambda_2^* \approx -0.24$. In addition to this there is an unstable fixed point at $\lambda_1 = 0$, $\lambda_2 \approx -0.26$.

solutions of the full problem is given by

$$\rho_\infty = (\alpha_1 |FP, \uparrow\rangle + \alpha_2 |FP, \downarrow\rangle) (\alpha_1^* \langle FP, \uparrow| + \alpha_2^* \langle FP, \downarrow|) \quad (5.19)$$

with $|\alpha_1|^2 + |\alpha_2|^2 = 1$. As in the previous chapters, we reduce the analysis to the subspace of generalized Gibbs ensembles which is a valid approach in the limit of weak coupling $\varepsilon \ll 1$. The emerging generalized force field $\mathbf{F}(\lambda_1, \lambda_2)$ is depicted in Fig. 5.1 for $\gamma = 0.9$. We find three steady states. Two stable states at $\lambda_1 = \pm\lambda_1^*$, $\lambda_2 = \lambda_2^*$ and an unstable one at $\lambda_1 = \lambda_2 = 0$. To simplify the analysis further, we go over to a mean-field description and approximate the density matrix by $\rho_{MF}(t) \sim \exp(-\lambda_1(t)S^z)$ including only the total magnetization in z -direction S^z as a conserved charge. For the moment we assume that the system is in a homogeneous state.

The projection of Eq. (5.19) onto the space of mean-field density matrices ρ_{MF} yields two stable steady state solutions with magnetization per site and spin $m = \pm 1$ ($\lambda_1 = \mp\infty$) and an unstable one at $m = 0$ ($\lambda_1 = 0$) which are attractive and repulsive fixed points of the map $m \mapsto F_1(m)$, respectively. In the mean-field approximation considered, the simple relation $m(\lambda_1) = -\tanh(\lambda_1/2)$ holds. The fixed point structure can be explained as follows: If the system is in a state with magnetization per site and spin close to one, the first term in $L_j^{(2)}$ is much more efficient than the second one driving the system to the attractive fixed point with $m = 1$. For states with magnetization close to $m = -1$, the argument applies vice versa. As a consequence, the fixed point at $m = 0$ has to be unstable.

Note that the generalized force can be defined with respect to Lagrange parameters $\dot{\lambda}_i = F_i$ or expectation values of local charges $\langle \dot{C}_i \rangle_{GGE,0} = (F_c)_i$ where the transformation between the different formulations is described by the generalized susceptibility χ , cf. Sec. 2.2.2. We can determine the

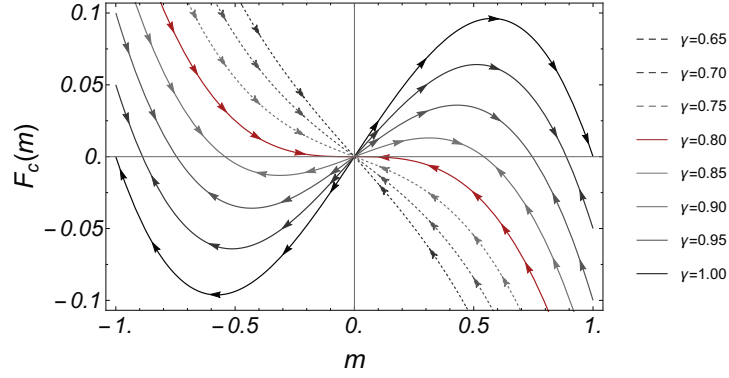


Figure 5.2 Force $F_c(m)$ plotted as a function of the magnetization m per spin and site for $\gamma = 0.65, 0.70, 0.75, 0.80, 0.85, 0.90, 0.95, 1.00$. The critical force with $\gamma = \gamma_c$ is highlighted in red. At $\gamma < \gamma_c$ we find one and at $\gamma > \gamma_c$ three roots.

effective force $(F_c)_i$ by calculating

$$\begin{aligned} \partial_t \langle C_i \rangle &= \sum_{k=1,2} \gamma_k \sum_j \text{Tr} \left[C_i \left(L_j^{(k)} \rho L_j^{(k)\dagger} - \frac{1}{2} \{ L_j^{(k)\dagger} L_j^{(k)}, \rho_{GGE} \} \right) \right] \\ &= \sum_{k=1,2} \gamma_k \sum_j \left\langle L_j^{(k)\dagger} C_i L_j^{(k)} - \frac{1}{2} \left(C_i L_j^{(k)\dagger} L_j^{(k)} + L_j^{(k)\dagger} L_j^{(k)} C_i \right) \right\rangle_{GGE,0}. \end{aligned}$$

For our specific choice of Lindblad operators and $C_i = S^z$ we obtain

$$F_c(m) = m \left(\frac{\gamma}{4} (1 - m^2) - (1 - \gamma) \right).$$

The generalized F_c can be equivalently written as the gradient of a potential $V_c(m)$, $F_c(m) = -\partial_m V_c(m)$ with

$$V_c(m) = \frac{m^2}{16} (8 + \gamma(m^2 - 10)).$$

where we have rescaled $\varepsilon, 2\varepsilon \rightarrow \varepsilon$. In Fig. 5.2 the generalized force is presented for different values of γ . The roots of $F_c(m)$ are located at $m = \pm \sqrt{(5\gamma - 4)/\gamma}$ and $m = 0$ which yields the critical value $\gamma_c = 0.8$ for the relative driving strength. The corresponding force is emphasized by a red trajectory in Fig. 5.2. In the regime $\gamma < \gamma_c$, there is only one real root while $\pm \sqrt{(5\gamma - 4)/\gamma}$ becomes real for $\gamma \geq 0.8$. Starting from $\gamma = 1$, the two stable fixed points approach the unstable one at $m = 0$ when the value of γ is decreased. At $\gamma_c = 0.8$ all three fixed points merge to a single stable one. In Fig. 5.3 the corresponding potential $V_c(m)$ is shown. We find that V_c displays the typical behavior of a continuous transition as a function of γ . For $\gamma < 0.8$ there is only one minimum at $m = 0$. At $\gamma = 0.8$ two new stable minima continuously emerge while the former global minimum at $m = 0$ becomes a maximum. The absolute value of the magnetization per site and spin in the global minimum of $V_c(m)$ is shown in the right panel of Fig. 5.3. Neglecting noise, the order parameter $|m|$ signals

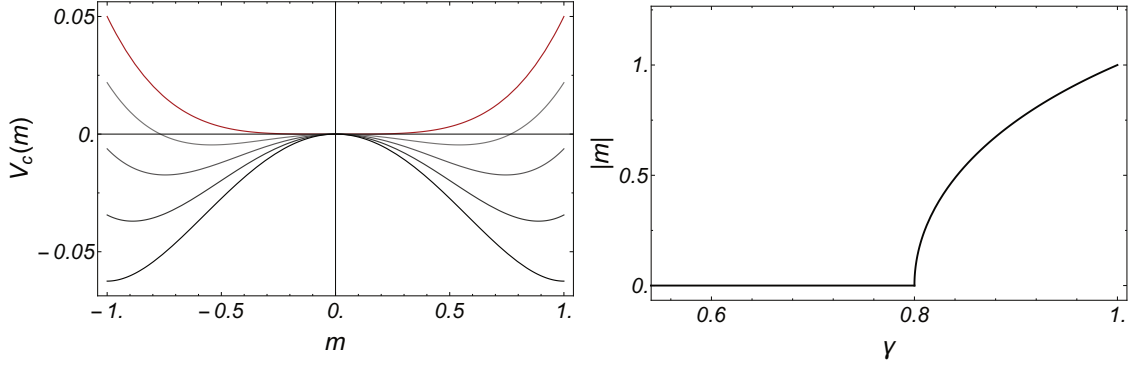


Figure 5.3 Left: the Potential $V_c(m)$ is plotted as a function of the magnetization m per spin and site for $\gamma = 0.80, 0.85, 0.90, 0.95, 1.00$. The critical curve with $\gamma = \gamma_c$ is highlighted in red. At $\gamma < \gamma_c$ we find one minimum and for $\gamma > \gamma_c$ two minima and one maximum. Right: the order parameter $|m|$ is plotted as a function of γ where m is the magnetization per spin and site in the global minimum of the potential V_c .

spontaneous symmetry breaking and a phase transition from the disordered to an ordered state when the control parameter crosses the critical value γ_c . In spatially extended systems, we expect that stable configurations with inhomogeneities exist. Hence, the system can exhibit regions with predominately positive or negative magnetization that are separated by domain walls. Intuitively, we expect that the width of a domain wall scales as $d \sim 1/\sqrt{\epsilon}$ which we can deduce from our scaling assumption. The homogeneous unitary part of the Liouville equation smoothens spatial inhomogeneities. On the contrary, the Markovian Lindblad dynamics favors sharp transitions between different domains. This is due to the fact that the generalized force has no explicit spatial dependence but only depends on the magnetization m , i.e. $F_c(m) > 0$ for $m > 0$ and $F_c(m) < 0$ for $m < 0$. The second Lindbladian, which is the dominant perturbation in the regime considered with $0 \ll \gamma \leq 1$, itself favors sharp transitions, as any state with a clear domain wall like $|\downarrow \dots \downarrow \uparrow \dots \uparrow\rangle$ is a dark state of $L_j^{(2)}$.

In App. C, we consider a non-integrable variation of the XXZ model for which integrability related complexities as finite Drude weights can be neglected and address, phenomenologically, the question of how the formation of domain walls and the emergence of induced transitions can be triggered by fluctuations on short time scales. Note that there is no phase transition in one dimension.

5.2.2 Asymmetric potential

Above we have considered a generalized potential that is symmetric in m , $V_c(m) = V_c(-m)$ and leads to continuous transitions as a function of the driving parameter γ . Here, we design the perturbation such that the corresponding potential is asymmetric which, in principle, allows for discontinuous transitions. To do so, we extend the perturbation \mathcal{L}_1 in Eq. (5.18) by two additional dissipative terms

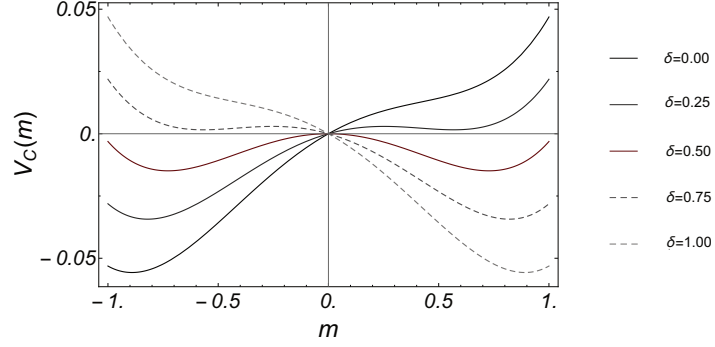


Figure 5.4 The number of local minima of the potential $V_c(m)$ changes when δ crosses the critical values $\delta_{\pm}^*(\gamma, \kappa)$. Parameters: $\gamma = 0.9$, $\kappa = 0.1$.

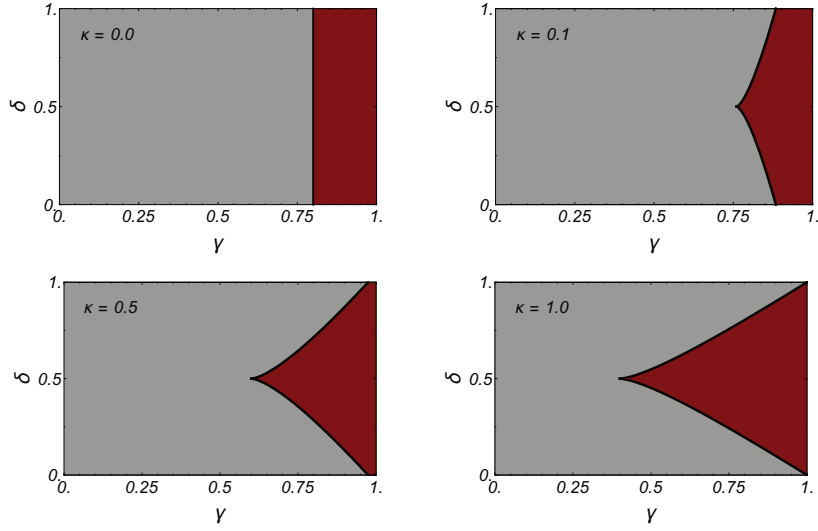


Figure 5.5 Layers of the non-equilibrium phase diagram (γ, δ, κ) for different values of κ . Regions in parameter space where three extrema exist are highlighted in red. In the gray areas, only one stable state can be found.

introducing favoring of one of the two stable states depending on the parameter δ ,

$$\mathcal{L}_1 \rho = \varepsilon \left((1 - \gamma) \hat{\mathcal{D}}^{(1)} + \gamma \hat{\mathcal{D}}^{(2)} + \kappa \left((1 - \delta) \hat{\mathcal{D}}^{(3)} + \delta \hat{\mathcal{D}}^{(4)} \right) \right) \rho, \quad (5.20)$$

where we consider the regime $\kappa, \delta \in [0, 1]$. For the two additional Lindblad operators we simply choose

$$L_j^{(3)} = S_j^-, \quad L_j^{(4)} = S_j^+$$

which yields the following expressions for the generalized force $F_c(m)$ and the potential $V_c(m)$,

$$F_c(m) = m \left(\frac{\gamma}{4}(1 - m^2) - (1 - \gamma) \right) + \frac{\kappa}{2} (\delta(1 - m) - (1 - \delta)(1 + m)),$$

$$V_c(m) = \frac{m}{16} (m(8 + \gamma(m^2 - 10)) + 4\kappa(2 + m - 4\delta)).$$

The potential $V_c(m)$ is sketched in Fig. 5.4 for different values of δ where we fixed all other parameters. For $\delta = 0$, only one minimum exists at $m_-(\delta = 0) = -1$. With increasing value of the relative perturbation strength δ , the position of the minimum is shifted to a larger magnetization $m_-(\delta)$ and the corresponding value of the potential $V_c(m_-(\delta))$ increases. When δ becomes larger than $\delta_-^*(\gamma, \kappa)$, a new local minimum appears at $m_+(\delta)$ which stays metastable in the regime $\delta_-^* < \delta < \delta_c$. At the critical point δ_c , we have $V_c(m_-(\delta_c)) = V_c(m_+(\delta_c))$ marking the center of the coexistence region. In the regime $\delta_c < \delta < \delta_+^*$, we find that $m_+(\delta)$ becomes the global minimum while $m_-(\delta)$ becomes metastable. Beyond δ_+^* only the minimum at $m_+(\delta)$ persists. The potential shows the typical phenomenological behavior of a discontinuous transition as a function of δ .

In Fig. 5.5 layers of the non-equilibrium mean-field phase diagram are shown in the space spanned by γ , δ and κ for $\kappa = 0.0, 0.1, 0.5, 1.0$. Regions in parameter space which exhibit three fixed points are highlighted in red.

Chapter 6

Stability of long range order in a driven $O(3)$ Heisenberg chain

6.1 Introduction

6.1.1 Motivation

It is a well-known fact that in low-dimensional systems with short range interactions, long range order is at any finite temperature unstable if the corresponding broken symmetry is continuous. This statement is rigorously formulated in the so-called *Mermin-Wagner theorem* [132]. It is important to note that the theorem only holds at equilibrium.

In this chapter, we aim to investigate how long range order can possibly be stabilized in a one-dimensional driven system at finite temperature when the order parameter ϕ is coupled to a conservation law m . More precisely, the corresponding current j_s of the conservation law is supposed to have a contribution that is linear in ϕ ,

$$\partial_t m(x,t) + \partial_x j_s(x,t) = 0, \quad (6.1)$$

$$j_s(x,t) = \alpha \phi(x,t) - D \partial_x m(x,t). \quad (6.2)$$

Here, we have assumed that the current has an additional contribution $\sim -\partial_x m(x,t)$ according to Fick's law. As a concrete model, we consider a one-dimensional driven Heisenberg model in which the total magnetization m is conserved which is associated with a $SO(3)$ symmetry ($SU(2)$ in the quantum case) of the spins. We construct the driving term such that it does not break the rotation symmetry as we want to investigate the spontaneous formation of order in the system. However, the perturbation is explicitly designed to allow for a finite spin current in the presence of long range order. The underlying physical intuition is that the spin current, in turn, stiffens the system and prevents aligned spins that are far apart from each other to tilt which would be the case in equilibrium at finite T . Expressed differently, in the case of a homogeneous non-equilibrium steady state that

is characterized by a stationary current $\partial_x j_s = 0$, Eq. (6.2) directly implies that $\phi = \phi_0$ is uniform. However, the former argument does not guarantee that ϕ_0 is finite. The effect would naturally be based on an interplay between the spontaneous emergence of order and the simultaneous evoking of an order stabilizing spin current which eventually requires a self-consistent theory. Note that we consider here the antiferromagnetic version of the Heisenberg model as in the case of ferromagnetic coupling, the relation $j_s \sim \phi$ would cause an unphysical accumulation of an infinite amount of spin at the boundary of two domains.

In order to describe the effect, we first have to define a $SO(3)$ ($SU(2)$) invariant driving term that activates the spin current in the presence of a symmetry breaking order term. We present one possible choice for such a perturbation in Sec. 6.2 and verify that the system indeed hosts a finite spin current in the steady state. Our argument is based on the calculation of the quasiparticle distribution function within the framework of a Floquet-Boltzmann equation.

We give further evidence for the existence of a finite spin current by simulating the corresponding classical equations of motion in Sec. 6.2.4. Even though our model can host a spin current in the presence of a finite order parameter, we do not observe the spontaneous emergence of a current or long range order within our classical simulation. A reason for this could be that the effect requires sensible fine-tuning and we simply do not simulate the dynamics in the correct parameter regime. For example, the time-dependent driving is supposed to drive a spin current in the system which is required for our argument to work. However, on the contrary, pumping also heats the system and is therefore a natural opponent of order.

In Sec. 6.3 we give another explanation, based on a field theoretical ansatz, why we do not observe a steady state with long range order. Our analysis suggests that the term $\alpha\phi$ in Eq.(6.2) leads to an instability of the antiferromagnetically ordered state with respect to its spin-reversed counterpart.

6.1.2 Mermin-Wagner theorem

In condensed matter theory, the Mermin-Wagner theorem states that a continuous symmetry cannot be spontaneously broken in systems with sufficiently short range interactions at non-zero temperature and dimensions $d \leq 2$ [132].

As an example of the concrete consequence of the theorem, we consider the $O(3)$ Heisenberg model with spins of length S . In the symmetry broken phase, neighboring spins are aligned parallel (ferromagnet) or antiparallel (antiferromagnet) to each other and point in a fixed direction representing one of the infinitely many possible symmetry broken states. As rotating or tilting the whole system by an infinitesimal small angle $\Delta\phi$, i.e. exciting a $k = 0$ or a small momentum mode, costs no or only an infinitesimal amount of energy, in low dimensions, the long range ordered state is sensitive to even very small thermal fluctuations at non-zero temperature. The appearance of such low-energy excitations at long-wavelengths, referred to as *Goldstone modes*, is not limited to the Heisenberg model but it is a more general phenomenon in continuous symmetry broken states. Their existence is predicted by the so-called Goldstone theorem [133]. In low dimensions, fluctuations of Goldstone modes destroy

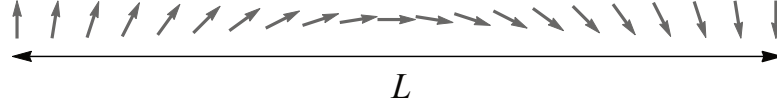


Figure 6.1 Domain wall in a one dimensional spin chain where the angle between two neighboring spins changes uniformly by $\Delta\phi = \pi/(L/a) = \pi/N$.

long range order. However, at higher dimensions, where the number of nearest-neighbor spins and therefore the effect of interactions becomes more important, long range order can be stabilized.

To find the critical dimension at which order becomes unstable in the presence of thermal fluctuations, we consider, for simplicity, the classical $O(2)$ XX-model ($J_x = J_y = J, J_z = 0$) on a d -dimensional square lattice and follow a straightforward domain wall argument. We aim to calculate the energy cost of a domain wall in a one-dimensional row of the d -dimensional hypercube that spreads over the whole system and changes the angle of the spins by π , cf. Fig. 6.1. We assume that the difference of the angle of two neighboring spins is uniform $\Delta\phi = \pi/(L/a) = \pi/N \ll 1$ where a is the lattice spacing, L the edge length of the hypercube and $N = L/a$ the number of spins per row. The energy cost is then given by

$$\Delta E = JS^2 \sum_j \cos(\Delta\phi_j) \approx NJS^2 (\Delta\phi)^2 \sim J \frac{a}{L},$$

where we have used $H = J \sum_j \mathbf{S}_j \mathbf{S}_{j+1} = JS^2 \sum_j \cos(\Delta\phi_j) \approx \eta NJS^2 + JS^2 \sum_j (\Delta\phi_j)^2$ with $\eta = 1$ for the ferro- and $\eta = 0$ for the antiferromagnet. As there are $\sim L^{d-1}$ rows in the system, the total energy cost for a domain wall in the d -dimensional square lattice scales as $\Delta E \sim L^{d-2}$. Thus, the critical dimension is $d_c = 2$. For $d \leq d_c$ the cost of a domain wall does not increase with system size. In the presence of thermal fluctuations, the system can easily go from a given ordered state to one that is tilted with respect to the former. Above d_c the energy barrier grows with N , preventing the system from leaving a spontaneously chosen symmetry broken state.

6.1.3 Spin wave theory in equilibrium

Another way to prove the validity of the Mermin-Wagner theorem is to perform a spin wave expansion around the ordered state and check whether fluctuations diverge or not. From this observation, one can conclude whether the chosen expansion point is invalid or valid. In the following, we consider the antiferromagnetic version of the quantum mechanical $O(3)$ Heisenberg model on a d -dimensional square lattice. Note that the arguments we repeat here can be found in many textbooks and lecture notes, for example, in [4]. As in the classical ground state neighboring spins point in opposite directions, it is convenient to introduce two sublattices A and B . This is useful even though the corresponding quantum mechanical ground state, which is the Néel state, is not identical to its classical counterpart. We can still expect to observe antiferromagnetic patterns in the quantum model,

i.e. spins on sublattice A point predominately in the opposite direction to spins on sublattice B . In *spin wave theory*, excitations above the ground state are modeled by bosonic spin wave excitations that can be formulated in terms of a *Holstein-Primakoff transformation* of the spin operators. The transformation reads

$$\begin{aligned} S_{A,j}^+ &= \sqrt{2S - a_j^\dagger a_j} a_j, & S_{B,j}^+ &= b_j^\dagger \sqrt{2S - b_j^\dagger b_j}, \\ S_{A,j}^- &= a_j^\dagger \sqrt{2S - a_j^\dagger a_j}, & S_{B,j}^- &= \sqrt{2S - b_j^\dagger b_j} b_j, \\ S_{A,j}^z &= S - a_j^\dagger a_j, & S_{B,j}^z &= b_j^\dagger b_j - S, \end{aligned}$$

where a_j^\dagger and b_j^\dagger are bosonic creation operators, acting on the lattice A and B , respectively. Importantly, the spin commutation relations are preserved under this transformation. It is useful to expand the spin operators for large spin in $1/S$. It turns out that even for spin-1/2, the case we are mainly interested in, a truncation after the first order already gives reasonable results in many cases [134, 135]. The physical meaning of this approximation is that interactions between spin waves are neglected. Inserting the transformation into the Hamiltonian yields

$$\begin{aligned} H &= J \sum_{j \in A} \sum_{\boldsymbol{\delta}} \left[S \left(a_j b_{j+\boldsymbol{\delta}} + a_j^\dagger b_{j+\boldsymbol{\delta}}^\dagger \right) + S \left(a_j^\dagger a_j + b_{j+\boldsymbol{\delta}}^\dagger b_{j+\boldsymbol{\delta}} \right) - S^2 \right] \\ &+ J \sum_{j \in B} \sum_{\boldsymbol{\delta}} \left[S \left(b_j a_{j+\boldsymbol{\delta}} + b_j^\dagger a_{j+\boldsymbol{\delta}}^\dagger \right) + S \left(b_j^\dagger b_j + a_{j+\boldsymbol{\delta}}^\dagger a_{j+\boldsymbol{\delta}} \right) - S^2 \right] + \mathcal{O}(S^0), \end{aligned} \quad (6.3)$$

where the index $\boldsymbol{\delta}$ runs over nearest-neighbor sites. Moreover, we assume in the following that the number of lattice sites is even, $N_A = N_B = N/2$. The Hamiltonian can be diagonalized in two steps. First, we calculate the Fourier transformation of Eq. (6.3) where we have to consider that the size of the unit cell in reciprocal space is reduced due to the introduction of the two sublattices in real space. In one dimension the first Brillouin zone can be chosen such that $k \in BZ = [-\pi/2, \pi/2)$ which is half of the size of the original reciprocal unit cell. The Hamiltonian reads in Fourier space with $a_{\mathbf{k}} = \frac{1}{\sqrt{N_A}} \sum_{j \in A} e^{-ikj} a_j$ and $b_{\mathbf{k}} = \frac{1}{\sqrt{N_B}} \sum_{j \in B} e^{-ikj} b_j$,

$$H = -NJS^2 z/2 + JSz \sum_{\mathbf{k}} \left[\gamma_{\mathbf{k}} \left(a_{\mathbf{k}} b_{-\mathbf{k}} + a_{\mathbf{k}}^\dagger b_{-\mathbf{k}}^\dagger \right) + a_{\mathbf{k}}^\dagger a_{\mathbf{k}} + b_{-\mathbf{k}}^\dagger b_{-\mathbf{k}} \right], \quad (6.4)$$

where z denotes the number of nearest-neighbors and $\gamma_{\mathbf{k}}$ is defined as $\gamma_{\mathbf{k}} := \frac{2}{z} \sum_{\boldsymbol{\delta}} \cos(\mathbf{k} \cdot \boldsymbol{\delta})$. The Hamiltonian can then in a second step be diagonalized with the help of a Bogoliubov transformation (cf. Sec. 1.1.3). The ansatz

$$\begin{aligned} \alpha_{\mathbf{k}} &= u_{\mathbf{k}} a_{\mathbf{k}} - v_{\mathbf{k}} b_{-\mathbf{k}}^\dagger \\ \beta_{\mathbf{k}} &= u_{\mathbf{k}} b_{\mathbf{k}} - v_{\mathbf{k}} a_{-\mathbf{k}}^\dagger \end{aligned}$$

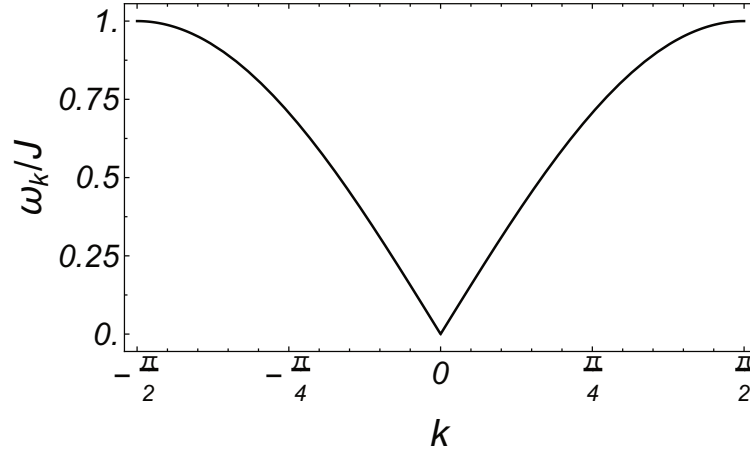


Figure 6.2 Energy dispersion of the antiferromagnet plotted in the magnetic unit cell with $k \in (-\pi/2, \pi/2]$. For small k we find a linear dispersion which confirms the existence of Goldstone modes.

preserves the bosonic commutation relations if $|u_{\mathbf{k}}|^2 - |v_{\mathbf{k}}|^2 = 1$ and $u_{\mathbf{k}}v_{-\mathbf{k}} = u_{-\mathbf{k}}v_{\mathbf{k}}$. These conditions are automatically fulfilled by the parameterization

$$u_{\mathbf{k}} = \cosh(\theta_{\mathbf{k}}), \quad v_{\mathbf{k}} = \sinh(\theta_{\mathbf{k}}) \quad (6.5)$$

for $\theta_{\mathbf{k}} = \theta_{-\mathbf{k}}$. Inserting Eq. (6.5) into Eq. (6.4) and demanding that off-diagonal terms vanish yields the equation $\tanh(2\theta_{\mathbf{k}}) = -\gamma_{\mathbf{k}}$ that determines $\theta_{\mathbf{k}}$. Then the diagonalized Hamiltonian reads in terms of Bogoliubov quasiparticles

$$H = E_0 + \sum_{\mathbf{k}} \omega_{\mathbf{k}} \left(\alpha_{\mathbf{k}}^\dagger \alpha_{\mathbf{k}} + \beta_{\mathbf{k}}^\dagger \beta_{\mathbf{k}} \right), \quad (6.6)$$

where $E_0 = -NJS\frac{z}{2}(S+1) + \sum_{\mathbf{k}} \omega_{\mathbf{k}}$ is a constant. Due to the sublattice symmetry we obtain two quasiparticle species α and β . The dispersion relation of the so-called magnon or spin-wave excitations is given by

$$\begin{aligned} \omega_{\mathbf{k}} &= JSz\sqrt{1 - \gamma_{\mathbf{k}}^2} \\ &\sim |\mathbf{k}| \quad (|\mathbf{k}| \rightarrow 0). \end{aligned} \quad (6.7)$$

The momentum dependence of $\omega_{\mathbf{k}}$ is plotted in Fig. 6.2. At small momenta, Goldstone modes emerge with a dispersion relation $\omega_{\mathbf{k}} \sim |\mathbf{k}|$. Note that the dispersion relation can also be obtained by solving the linearized classical equations of motion of the spins.

The stability of the antiferromagnetic expansion point can be validated by calculating the fluctuations of the sublattice magnetization $\Delta M_{A,B} = M_{A,B} - S$ with respect to the classical value S . As both

sublattices are identical, it does not matter which one we choose. For example, the corrections ΔM_A is given by

$$\begin{aligned}\Delta M_A &= \frac{2}{N} \sum_{\mathbf{k}} \langle a_{\mathbf{k}}^\dagger a_{\mathbf{k}} \rangle \\ &= \frac{2}{N} \sum_{\mathbf{k}} \left[u_{\mathbf{k}}^2 \langle \alpha_{\mathbf{k}}^\dagger \alpha_{\mathbf{k}} \rangle + v_{\mathbf{k}}^2 \langle \beta_{-\mathbf{k}}^\dagger \beta_{-\mathbf{k}} \rangle + u_{\mathbf{k}} v_{\mathbf{k}} \langle \alpha_{\mathbf{k}} \beta_{-\mathbf{k}} + \alpha_{\mathbf{k}}^\dagger \beta_{-\mathbf{k}}^\dagger \rangle \right].\end{aligned}$$

If we assume that the quasiparticle states are thermally occupied, i.e. their occupation follows a Boltzmann distribution $\sim \exp\left(-\beta \sum_{\mathbf{k}} (\alpha_{\mathbf{k}}^\dagger \alpha_{\mathbf{k}} + \beta_{\mathbf{k}}^\dagger \beta_{\mathbf{k}})\right)$ and use $[\beta_{\mathbf{k}}, \beta_{\mathbf{k}}^\dagger] = 1$, we arrive at

$$\begin{aligned}\Delta M_A &= \frac{2}{N} \sum_{\mathbf{k}} \left[u_{\mathbf{k}}^2 \langle \alpha_{\mathbf{k}}^\dagger \alpha_{\mathbf{k}} \rangle + v_{\mathbf{k}}^2 \langle \beta_{-\mathbf{k}}^\dagger \beta_{-\mathbf{k}} \rangle + v_{\mathbf{k}}^2 \right] \\ &= \frac{2}{N} \sum_{\mathbf{k}} \left[n_{\mathbf{k}} \cosh(2\theta_{\mathbf{k}}) + \frac{1}{2} (\cosh(2\theta_{\mathbf{k}}) - 1) \right] \\ &= -\frac{1}{2} + \frac{2}{N} \sum_{\mathbf{k}} \left(n_{\mathbf{k}} + \frac{1}{2} \right) \frac{1}{\sqrt{1 - \gamma_{\mathbf{k}}^2}}\end{aligned}$$

where $\langle \alpha_{\mathbf{k}}^\dagger \alpha_{\mathbf{k}} \rangle = \langle \beta_{-\mathbf{k}}^\dagger \beta_{-\mathbf{k}} \rangle = n_{\mathbf{k}} = 1/(e^{\beta \omega_{\mathbf{k}}} - 1)$ and $\cosh(2\theta_{\mathbf{k}}) = 1/\sqrt{1 - \gamma_{\mathbf{k}}^2}$. In the thermodynamic limit, the sum over the discrete \mathbf{k} values can be replaced by an integral

$$\begin{aligned}\sum_{\mathbf{k}} n_{\mathbf{k}} \frac{1}{\sqrt{1 - \gamma_{\mathbf{k}}^2}} &\sim \lim_{k_0 \rightarrow 0} \int_{k_0}^{\pi/2} dk (e^{\beta \sqrt{1 - \cos^2(ka)}} - 1)^{-1} \frac{k^{d-1}}{\sqrt{1 - \cos^2(ka)}} \\ &\sim \lim_{k_0 \rightarrow 0} \int_{k_0}^{\pi/2} dk k^{d-3}.\end{aligned}$$

For $d \leq d_c = 2$ the integral diverges when k_0 approaches zero while it stays finite for $d > d_c$. Therefore, the divergence of the fluctuations of the order parameter indicates that the expansion about antiferromagnetic order is unstable in dimensions $d \leq 2$ at $T > 0$.

6.1.4 Flocking

One example from nature of long range order in non-equilibrium systems is the dynamics of flocking. Thus, the collective movement of a swarm of many living beings like birds, fish or bacteria. Even though we expect that the motion of a single individual within the swarm only depends on the motions in its direct neighborhood, we observe that the whole swarm moves as an entity.

A simple numerical model to study this behavior is a discrete-time update scheme in which point like birds (point particles) evolve in a d dimensional box. The velocity of a single individual depends in each time step on the averaged velocities of the point particles in its direct environment and on a zero mean noise contribution where the update rule guarantees that the magnitude of the velocities stays constant. In a numerical simulation of the model in two dimensions, it was observed that the

continuous $SO(2)$ symmetry is spontaneously broken and a transition between an ordered phase with a mean velocity of the flock $\langle \mathbf{v} \rangle \neq 0$ and a disordered phase with $\langle \mathbf{v} \rangle = 0$ occurs as the noise strength is increased [136]. In the limit where the magnitude of the velocity goes to zero, the model is very similar to the classical two-dimensional XY model [137]. The normalized velocity can then be identified as a spin which also has a fixed length. However, the classical XY model does not exhibit spontaneous symmetry breaking which is in agreement with the Mermin-Wagner theorem. Stable long range order and the occurrence of spontaneous symmetry breaking is only possible due to the motion of the birds and the non-equilibrium nature of the model.

A field theoretical description of the phenomenon of flocking was given by Toner and Fu in 1995 [138]. They start from the continuum equations of motion for the density ρ and the velocity \mathbf{v} . Importantly, they consider a convective term $(\mathbf{v} \cdot \nabla)\mathbf{v}$ in the momentum equation that does not appear in the theory of the equilibrium XY model and stabilizes long range order. This term is qualitatively similar to the linear coupling of the order parameter to the spin current we consider here. Using RG arguments they showed that fluctuations around an ordered state with non-zero velocity do not diverge, as would be the case in equilibrium.

6.2 Spin current and long range order

6.2.1 The model

We consider a one-dimensional antiferromagnetic quantum Heisenberg model that is periodically driven and weakly coupled to a thermal bath of phonons. The additional bath is necessary as a competing effect to the pumping and prevents the system from heating up to an infinite temperature state. Also in reality, the influence of a thermal environment is expected. The total Hamiltonian reads

$$H(t) = H_0 + H_{0,ph} + \varepsilon_{ph}H_{SB} + H_d(t) \quad (6.8)$$

with constituents

$$\begin{aligned} H_0 &= J \sum_j \mathbf{S}_j \mathbf{S}_{j+1}, \\ H_{0,ph} &= \sum_j \sum_{\kappa} \omega_{\kappa} c_{j,\kappa}^{\dagger} c_{j,\kappa}, \\ H_{SB} &= \sum_{j,\kappa} \mathbf{S}_j \mathbf{S}_{j+1} (c_{j,\kappa} + c_{j,\kappa}^{\dagger}), \\ H_d(t) &= \Delta J_1 \cos(\Omega t) \sum_j (-1)^j \mathbf{S}_j \mathbf{S}_{j+1} + \Delta J_2 \cos(\Omega t + \varphi) \sum_j \mathbf{S}_j \mathbf{S}_{j+2}, \end{aligned} \quad (6.9)$$

where Ω is the driving frequency, φ a phase shift between the two driving terms and ω_{κ} the dispersion relation of the phononic bath. In the following, we denote $H_{d,1}(t) = \cos(\Omega t) \Delta J_1 \sum_j (-1)^j \mathbf{S}_j \mathbf{S}_{j+1}$ and $H_{d,2}(t) = \cos(\Omega t + \varphi) \Delta J_2 \sum_j \mathbf{S}_j \mathbf{S}_{j+2}$. We couple to each bond a bath of phonons which is assumed

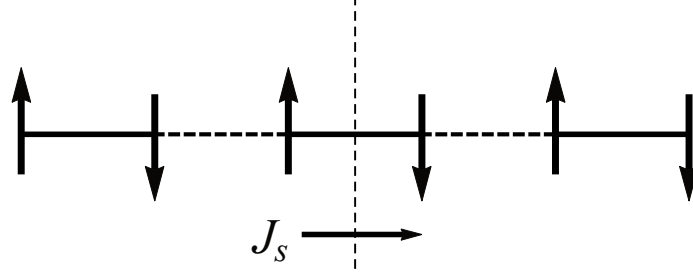


Figure 6.3 Schematic sketch of the system with staggered bond-couplings (solid and dashed lines), established antiferromagnetic order pointing in z -direction (staggered arrows), and a finite spin current (arrow pointing in x -direction) whose direction depends on the sign of the antiferromagnetic order parameter.

to be in a thermal state with a fixed temperature T_{ph} . Note that we consider a weak coupling to the thermal bath in the spirit of the previous chapters. In contrast to that, we expect that the amplitude of the time-dependent perturbation has to be larger than a certain threshold value to induce sufficiently large spin currents which can then, in turn, potentially stabilize long range order.

The total Hamiltonian Eq. (6.8) is invariant under rotations in spin space and, therefore, the total spin is conserved. To investigate the emergence of a spin current, we simulate order within the system by an additional staggered magnetic field term $H_F = -B_{stag} \sum_j (-1)^j S_j^z$, $H(t) \rightarrow H(t) + H_F$ that explicitly breaks the rotation symmetry. Without loss of generality we choose a field pointing in z -direction. This term is not part of the final Hamiltonian describing a system in which order should emerge spontaneously. We only introduce it here to verify whether the spin current operator is activated by the perturbation.

The explicit driving term $H_d(t)$ is constructed such that there is no symmetry transformation that maps J_s to $-J_s$ and simultaneously leaves $H(t) + H_F$ invariant or vice versa. If that were the case, we could deduce from an argument related to the one presented in the introduction of Ch. 3 that $\langle J_s \rangle = 0$. In Fig. 6.3 a schematic sketch of the spin chain in the presence of order (staggered arrows) is shown where solid and dashed lines represent stronger and weaker bond-couplings. The single arrow, labeled by J_s , indicates the direction of the spin current. Note that the direction of J_s eventually depends on the direction of the order parameter field. Examples of symmetries that leave $H(t) + H_F$ invariant are combinations of a rotation by π around the x - or y -axis in spin space $\hat{R}_\pi^{x,y}$ and a bond-centered mirror symmetry in real space or simply a rotation by π around the z -axis in spin space \hat{R}_π^z . One can check easily that the sketch in Fig. 6.3 and, therefore, also the direction of the spin current is invariant under all these symmetry transformations.

Time-reversal symmetry plays a more subtle role. The spin current operator is invariant under TRS while the staggered field H_F is odd. Thus, for a phase difference $\varphi = 0$ between the two driving terms, the product of TRS and $\hat{R}_\pi^{x,y}$ would leave $H(t) + H_F$ invariant and map J_s to $-J_s$ implying that $\langle J_s \rangle = 0$. However, by tracing out the bosonic degrees of freedom under the Markov assumption and

introducing dissipation in the system that breaks time-reversal symmetry explicitly, we expect the activation of the spin current also at $\varphi = 0$ in a full simulation. Nevertheless, we set $\phi = -\pi/2$. Alternatively, as we desire to stabilize the system in the antiferromagnetic staggered state and, therefore, only consider the regime $|\Delta J_1|, |\Delta J_2|, |B_{stag}| < |J|$, we can also refer to a perturbative argument. To obtain a static homogeneous current with $k = 0$, $\omega = 0$ in second order perturbation theory, the driving Hamiltonian has to be made up of two non-commuting contributions. A staggered part $H_{d,1}(t)$ with momentum $|k| = \pi$ and frequency $|\omega| = \Omega$ and a translational invariant part $H_{d,2}(t)$ with $|k| = 0$ and $|\omega| = \Omega$. Before time-averaging, we obtain within the leading order expansion term of $\overline{\langle J_s \rangle}$, contributions of the form

$$(J_s)_{k=0, \omega=0} (H_{d,1}(t))_{|k|=\pi, |\omega|=\Omega} (H_{d,2}(t'))_{k=0, |\omega|=\Omega} (H_F)_{|k|=\pi, \omega=0}$$

which can, in principle, be non-zero and therefore allow by simple power counting for a static and homogeneous spin current in the steady state. Note that we define $H_{d,2}$ with next-nearest neighbor coupling such that $[H_{d,1}, H_{d,2}] \neq 0$ to ensure a finite contribution in second order perturbation theory.

6.2.2 Floquet spin wave theory

As the strength of the drive is not necessarily small, we include $H_d(t)$ into the dominant part of the Hamiltonian $H_0(t) = H_0 + H_F + H_d(t)$ that is treated exactly in our analysis. Similarly to Sec. 6.1.3, we calculate the dispersion relation of the Bogoliubov quasiparticles where we make use of the Floquet ansatz, as $H_0(t)$ is periodic in time. The weak bath coupling will later be used to determine the occupation of the quasiparticle states within a Floquet-Boltzmann equation. For simplicity, we consider a slight variation of Eq. (6.9) and add an additional non-staggered term $\Delta J_1 \cos(\Omega t) \sum_j \mathbf{S}_j \mathbf{S}_{j+1}$ to $H_d(t)$. As a consequence, the sum in the first term $H_{d,1}(t)$ only runs over even sites. Moreover, we set $2\Delta J_1 = \Delta J_2 = \Delta J$ yielding

$$H_d(t) = \Delta J \left(\cos(\Omega t) \sum_{j \in \text{even}} \mathbf{S}_j \mathbf{S}_{j+1} + \sin(\Omega t) \sum_j \mathbf{S}_j \mathbf{S}_{j+2} \right) \quad (6.10)$$

To leading order in the Holstein-Primakoff transformation, we then obtain

$$\begin{aligned} H_0(t) \approx E_0(t) + JS \sum_k \left[\gamma_k (a_k b_{-k} + a_k^\dagger b_{-k}^\dagger) + a_k^\dagger a_k + b_{-k}^\dagger b_{-k} \right] + B_{stag} S \sum_k \left[a_k^\dagger a_k + b_{-k}^\dagger b_{-k} \right] \\ + \cos(\Omega t) \Delta JS \sum_k \left[\left(e^{ika} a_k b_{-k} + e^{-ika} a_k^\dagger b_{-k}^\dagger \right) + a_k^\dagger a_k + b_{-k}^\dagger b_{-k} \right] \\ - 2 \sin(\Omega t) \Delta JS \sum_k (1 - \cos(2ka)) \left(a_k^\dagger a_k + b_{-k}^\dagger b_{-k} \right) + \mathcal{O}(S^0) \end{aligned}$$

with $E_0(t) = -N \left(J + \frac{\Delta J}{2} \cos(\Omega t) - \Delta J \sin(\Omega t) \right) S^2 - N B_{stag} S$. The corresponding Floquet Hamiltonian acting on the extended Hilbert space can be determined using Eq. (1.46) which yields

$\tilde{H}_0^F \approx \text{const} + \sum_k \Psi_k^\dagger \tilde{H}_{0,k}^F \Psi_k - \tilde{\Omega}$ with

$$\Psi_k = \left(\dots, a_k^{(1)}, b_{-k}^{(1)\dagger}, a_k^{(0)}, b_{-k}^{(0)\dagger}, a_k^{(-1)}, b_{-k}^{(-1)\dagger}, \dots \right)^T,$$

$$(\tilde{H}_{0,k}^F)_{nm} = h_{0,k} \delta_{nm} + \Delta h_{0,k} \delta_{n,m-1} + \Delta h_{0,k}^\dagger \delta_{n,m+1}, \quad \tilde{\Omega}_{nm} = n\Omega \mathbb{1} \delta_{nm}.$$

where n, m denote Floquet indices. Above we have approximated $E_0(t)$ by $\overline{E_0(t)}$ as we are mainly interested in the k dependence of the quasiparticle energies. Note that due to the monochromatic driving term, only off-diagonal entries with Floquet indices n, m which differ by ± 1 are non-zero. The matrices $h_{0,k}$ and $\Delta h_{0,k}$ read

$$h_{0,k} = S \begin{pmatrix} J + B_{stag} & J\gamma_k \\ J\gamma_k & J + B_{stag} \end{pmatrix}, \quad \Delta h_{0,k} = \Delta JS \begin{pmatrix} 1 + 2i(\gamma_{2k} - 1) & \delta_k^* \\ \delta_k & 1 + 2i(\gamma_{2k} - 1) \end{pmatrix},$$

where we have set $\delta_k = e^{ika}$. The matrix $\tilde{H}_{0,k}^F$ can be diagonalized using a Bogoliubov transformation. According to Sec. 1.1.3, the Bogoliubov transformation can be recast into a diagonalization problem for the matrix $\tilde{H}_{0,k}^F \tilde{\sigma} - \tilde{\Omega}$ where $\tilde{\sigma}_{nm} = \sigma_z$ encodes the bosonic commutation relations. The eigenvalues of $\tilde{H}_{0,k}^F \tilde{\sigma} - \tilde{\Omega}$ can then, up to a possible sign, be identified as the quasienergies of $H_0^F(t)$.

In Fig. 6.4 we show the quasienergy spectrum within the first Floquet zone with $n = 0$. Note that in the presence of the driving term, the spectrum is still gapless and each branch is twofold degenerate due to the sublattice symmetry. In principle, this degeneracy could be lifted by introducing an additional next-nearest neighbor coupling term in the Hamiltonian that differs on the A and B sublattices. However, this is not relevant for the activation of the spin current and we do not include such a term here.

Our final goal would be to show self-consistently that the spectrum becomes gapped in the presence of a finite expectation value of the spin current operator. Trivially, a gap emerges if we simply set $B_{stag} \neq 0$. In contrast to the static case with $\Delta J = 0$, the dispersion relation is asymmetric for $\Delta J \neq 0$. This is a necessary criterion for the existence of a finite spin current expectation value due to a $k \rightarrow -k$ anti-symmetry of the spin current operator. In the language of bosonic operators, J_s reads in momentum space

$$J_s = i \frac{J}{2} \sum_j \left(S_j^+ S_{j+1}^- - S_j^- S_{j+1}^+ \right)$$

$$\approx JS \sum_k \sin(ka) \begin{pmatrix} a_k^\dagger & b_{-k} \end{pmatrix} \begin{pmatrix} 0 & 1 \\ 1 & 0 \end{pmatrix} \begin{pmatrix} a_k \\ b_{-k}^\dagger \end{pmatrix}.$$

Fig. 6.5 shows the diagonal component $\langle\langle \phi_{s,k} | \tilde{J}_s | \phi_{s,k} \rangle\rangle$ of the spin current operator \tilde{J}_s with respect to the eigenstate $|\phi_{s,k}\rangle$ of the Floquet Hamiltonian \tilde{H}_0^F where $s = 1, 2$ labels the quasiparticle species. We use the same notation as in Sec. 1.3.2. Thus, $|\phi_{s,k}\rangle$ is an element of the extended Hilbert space \mathcal{F} and \tilde{J}_s is an operator which acts on \mathcal{F} . Qualitatively, we again observe that $\langle\langle \phi_{s,k} | \tilde{J}_s | \phi_{s,k} \rangle\rangle$ becomes asymmetric in the presence of the time-dependent perturbation. It is important to mention that the

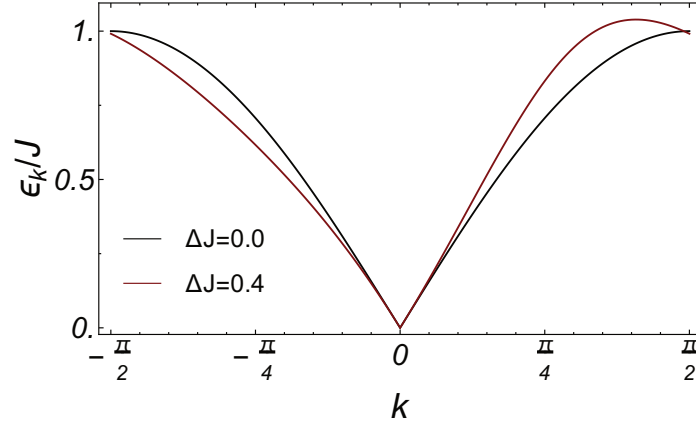


Figure 6.4 Dispersion relation ε_k of the Bogoliubov quasiparticles in presence ($\Delta J = 0.4$, red line) and in absence ($\Delta J = 0.0$, black line) of driving at $\Omega = 0.44$, $J = 1$, $B_{stag} = 0$. The drive breaks the symmetry $\varepsilon_k = \varepsilon_{-k}$ resulting in a tilted dispersion relation.

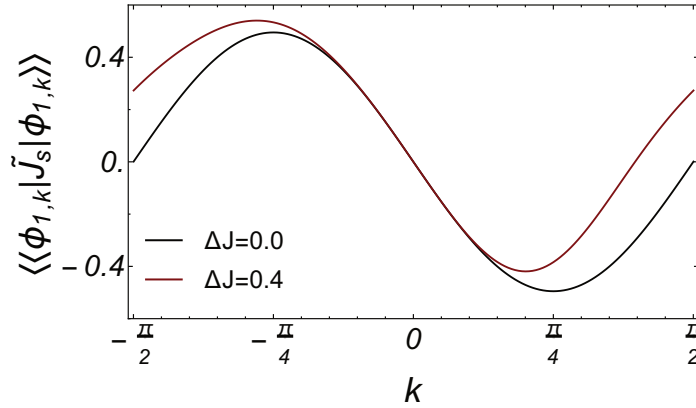


Figure 6.5 Matrix element $\langle\langle\phi_{1,k}|\tilde{J}_s|\phi_{1,k}\rangle\rangle$ of the spin current operator \tilde{J}_s for $\Delta J = 0.4$ (red line) and $\Delta J = 0.0$ (black line) at $\Omega = 0.44$, $J = 1$, $B_{stag} = 0$. In the absence of driving the matrix element is odd under the transformation $k \rightarrow -k$ while the anti-symmetry is broken at $\Delta J \neq 0$.

asymmetric dispersion relation is not a sufficient condition for the existence of a finite spin current in the steady state. If the system were in equilibrium and consequently the quasiparticle eigenstates were thermally occupied, the expectation value of the spin current would still be zero. Only in non-equilibrium, a finite spin current can be evoked.

6.2.3 Floquet-Boltzmann equation

Above we have determined the dispersion relation of the Bogoliubov quasiparticle states but so far we do not know how these states are occupied. Eventually, this information is provided by the weak

coupling to the external thermal bath. Technically, the occupation in the steady state can be determined from a Floquet-Boltzmann equation which simplifies to lowest order in perturbation strength to a set of rate equations. To derive these rate equations, we consider the occupation number operator $n_{s,p}$ of a quasiparticle state and calculate $\overline{\langle \partial_t n_{s,p} \rangle}$ to second order in perturbation theory where p denotes the momentum quantum number and $s \in \{1, 2\}$ the species of the quasiparticle. We assume that the total density matrix factorizes into a thermal phonon part that is held at constant temperature and a spin part that is solely described by the occupation of all quasiparticle states, $\rho(t) = |\{n_q\}\rangle \langle \{n_q\}| \otimes e^{-\beta H_{0,ph}}$. Using Eq. (4.9) we obtain

$$\langle \dot{n}_{s,p} \rangle_{\{n_q\}} = \lim_{t \rightarrow \infty} \frac{-1}{T} \int d\omega \mathcal{N}(\omega) \int_0^T dt \int_0^t dt' \text{Tr} \left[n_{s,p} \left[H_{SB}, [H_{SB}^{(H)}(t-t'), |\{n_q\}\rangle \langle \{n_q\}| \otimes e^{-\beta H_{0,ph}}] \right] \right] \quad (6.11)$$

where we have used the spectral function $\mathcal{N}(\omega) = \sum_{\kappa} \delta(\omega - \omega_{\kappa})$ of the dissipative bath. Later we assume that the bath coupling is ohmic meaning that $\mathcal{N}(\omega)$ can be approximated up to a cut-off frequency Ω_D by a linear function. By tracing out the bath degrees of freedom and using $\text{Tr}[c_{j,\kappa}^{\dagger} c_{j,\kappa} e^{-\beta H_{0,ph}}] = n_B(\omega_{\kappa})$ with Bose-Einstein distribution function n_B , we arrive at

$$\begin{aligned} \langle \dot{n}_{s,p} \rangle_{\{n_q\}} &= \lim_{t \rightarrow \infty} \frac{1}{T} \int d\omega \mathcal{N}(\omega) \int_0^T dt \int_0^t dt' \sum_j \\ &\quad \langle [H_{SB,j}, n_{s,p}] H_{SB,j}^{(H)}(t'-t) \rangle_{\{n_q\}} \left(n_B(\omega) e^{-i\omega(t'-t)} + (1 + n_B(\omega)) e^{+i\omega(t'-t)} \right) \\ &\quad + \langle [(H_{SB,j}, n_{s,p}) H_{SB,j}^{(H)}(t'-t)]^{\dagger} \rangle_{\{n_q\}} \left(n_B(\omega) e^{+i\omega(t'-t)} + (1 + n_B(\omega)) e^{-i\omega(t'-t)} \right). \end{aligned}$$

We can write the local densities $H_{SB,j}^A, H_{SB,j}^B$ in terms of bosonic operators using the Holstein-Primakoff transformation defined above,

$$\begin{aligned} H_{SB,j}^A &= S \left[a_j b_{j+1} + a_j^{\dagger} b_{j+1}^{\dagger} + a_j^{\dagger} a_j + b_{j+1}^{\dagger} b_{j+1} \right] + \mathcal{O}(S^0), \\ H_{SB,j}^B &= S \left[b_j a_{j+1} + b_j^{\dagger} a_{j+1}^{\dagger} + b_j^{\dagger} b_j + a_{j+1}^{\dagger} a_{j+1} \right] + \mathcal{O}(S^0) \end{aligned}$$

for the two sublattices A and B , respectively. In the following, we aim to express Eq. (6.11) entirely in terms of the occupation numbers $n_{p,1} = \langle n_{p,1} \rangle_{\{n_q\}} = \langle f_p^{\dagger} f_p \rangle_{\{n_q\}}$ and $n_{p,2} = \langle n_{p,2} \rangle_{\{n_q\}} = \langle g_p^{\dagger} g_p \rangle_{\{n_q\}}$. The operators $f_k^{\dagger}, g_k^{\dagger}$ create a Floquet eigenstate of $H_0^F(t)$ with momentum k and flavor $s = 1, 2$, $f_k^{\dagger}(t) |0\rangle = |\phi_{k,1}(t)\rangle$ and $g_k^{\dagger}(t) |0\rangle = |\phi_{k,2}(t)\rangle$ from the quasiparticle vacuum $|0\rangle$. In analogy to the Bogoliubov transformation in the static case, we can write

$$\begin{aligned} f_k(t) &= \sum_n e^{-in\Omega t} \left(v_{1,k}^{(n)} a_k + v_{2,k}^{(n)} b_{-k}^{\dagger} \right), \\ g_{-k}^{\dagger}(t) &= \sum_n e^{-in\Omega t} \left(\tilde{v}_{1,k}^{(n)} a_k + \tilde{v}_{2,k}^{(n)} b_{-k}^{\dagger} \right), \end{aligned} \quad (6.12)$$

where n denotes the Floquet component and $(\dots, v_{1,k}^{(0)}, v_{2,k}^{(0)}, \dots)$, $(\dots, \tilde{v}_{1,k}^{(0)}, \tilde{v}_{2,k}^{(0)}, \dots)$ are eigenvectors of the matrix $\tilde{H}_0^F \tilde{\sigma} - \tilde{\Omega}$ with corresponding quasienergies in the first Floquet zone. The Heisenberg representation of f_k and g_k can be obtained by expressing the Hamiltonian $H_0(t)$ in the basis of Floquet states

$$H_0(t) = \sum_{\alpha,\beta} (H_0)_{\alpha\beta}(t) (f_{\alpha}^{\dagger}(t) f_{\beta}(t) + g_{\alpha}^{\dagger}(t) g_{\beta}(t)) \quad (6.13)$$

and calculating, for example, the Heisenberg equation of motion of $f_k(t)$,

$$\frac{d}{dt} \left(f_k^{(H)}(t) \right) = i \left[H_0^{(H)}(t), f_k^{(H)}(t) \right] + \left(\frac{\partial f_k(t)}{\partial t} \right)^{(H)}. \quad (6.14)$$

For the commutator in Eq. (6.14) we obtain $\left[H_0^{(H)}(t), f_k^{(H)}(t) \right] = -\sum_{\beta} (H_0)_{k\beta}(t) f_{\beta}^{(H)}(t)$. Together with the Floquet eigenvalue equation $(H_0(t) - i\partial/\partial t) |\phi_{k,1}(t)\rangle = \varepsilon_k |\phi_{k,1}(t)\rangle$ or equivalently $\partial f_k(t)/\partial t = i\sum_{\beta} ((H_0)_{k\beta}(t) - \varepsilon_{\beta} \delta_{\beta k}) f_{\beta}(t)$, we arrive at the simple differential equation

$$\frac{d}{dt} f_k^{(H)}(t) = -\varepsilon_k f_k^{(H)}(t).$$

Thus, the Heisenberg representation of f_k and g_k is given by

$$f_k^{(H)}(t) = e^{-i\varepsilon_k t} f_k(t), \quad g_k^{(H)}(t) = e^{-i\varepsilon_k t} g_k(t).$$

In order to proceed, we need the inverse transformation of Eq. (6.12) which formally reads in position basis

$$\begin{aligned} a_j &= \sum_k \sum_n e^{-in\Omega t} \left(\mu_{1,k}^n(j) f_k(t) + \mu_{2,k}^n(j) g_{-k}^{\dagger}(t) \right), \\ b_j &= \sum_k \sum_n e^{-in\Omega t} \left(\tilde{\mu}_{1,k}^n(j) f_{-k}^{\dagger}(t) + \tilde{\mu}_{2,k}^n(j) g_k(t) \right). \end{aligned} \quad (6.15)$$

where the spatial dependence of the coefficients is given by $\mu_{1,k}^n(j) = \frac{1}{\sqrt{N/2}} e^{ijk} \mu_{1,k}^n$. Inserting Eq. (6.15) into the formulas for ΔH_j^A , ΔH_j^B and then subsequently into Eq. (6.11) yields

$$\begin{aligned}
\dot{n}_{1,p} = & -2\pi S^2 \frac{N}{2} \int d\omega \mathcal{N}(\omega) \sum_k \sum_{\delta=\pm 1} \sum_{\Delta=-N_f}^{N_f} \quad (6.16) \\
& |V_1(p, k, \delta, \Delta)|^2 \times \\
& \left(\left[n_B \delta ((\varepsilon_k + \varepsilon_p) + \omega + \Delta \Omega) + (1 + n_B) \delta ((\varepsilon_k + \varepsilon_p) - \omega + \Delta \Omega) \right] n_{1,p} n_{2,k} \right. \\
& \left. - \left[n_B \delta ((\varepsilon_p + \varepsilon_k) - \omega + \Delta \Omega) + (1 + n_B) \delta ((\varepsilon_p + \varepsilon_k) + \omega + \Delta \Omega) \right] (1 + n_{1,p})(1 + n_{2,k}) \right) \\
& + |W_1(p, k, \delta, \Delta)|^2 \times \\
& \left(\left[n_B \delta ((\varepsilon_p - \varepsilon_k) + \omega + \Delta \Omega) + (1 + n_B) \delta ((\varepsilon_p - \varepsilon_k) - \omega + \Delta \Omega) \right] n_{1,p}(1 + n_{1,k}) \right. \\
& \left. - \left[n_B \delta ((\varepsilon_k - \varepsilon_p) + \omega - \Delta \Omega) + (1 + n_B) \delta ((\varepsilon_k - \varepsilon_p) - \omega - \Delta \Omega) \right] n_{1,k}(1 + n_{1,p}) \right)
\end{aligned}$$

where we have used the relation $\text{Re}[\lim_{t \rightarrow T} \int_0^T dt \int_0^t dt' E^{i(\Delta E \pm \omega) - \eta}(t-t')] = 2\pi \delta(\Delta E \pm \omega)$. Moreover, we have dropped the frequency argument of $n_B(\omega)$ for brevity. While the first two contributions describe the simultaneous creation or annihilation of two quasiparticles, one of each species, the second two terms take account of processes where one quasiparticle is created and another one of the same species is annihilated.

In principle, infinitely many Floquet bands contribute in Eq. (6.16). However, for practical reasons, we truncate the number of sectors and include only $2N_f + 1$ within our calculation. We find numerically that results obtained from Eq. (6.16) already converge for $N_f \sim \mathcal{O}(1)$ at sufficiently large driving frequencies. The sum over $\delta = \pm 1$ is due to the two sublattices and the prefactors V_1 and W_1 are given by

$$\begin{aligned}
V_1(p, k, \delta, \Delta) = & \sum_n \left(\mu_{2,-k}^{(n)}(j) \tilde{\mu}_{1,-p}^{(\Delta-n)}(j + \delta) + \mu_{1,p}^{(n)*}(j) \tilde{\mu}_{2,k}^{(\Delta-n)*}(j + \delta) \right. \\
& \left. + \mu_{1,p}^{(n)*}(j) \mu_{2,-k}^{(\Delta-n)}(j) + \tilde{\mu}_{2,k}^{(n)*}(j + \delta) \tilde{\mu}_{1,-p}^{(\Delta-n)}(j + \delta) \right) \\
W_1(p, k, \delta, \Delta) = & \sum_n \left(\mu_{1,p}^{(n)}(j) \tilde{\mu}_{1,-k}^{(n-\Delta)}(j + \delta) + \mu_{1,k}^{(n)*}(j) \tilde{\mu}_{1,-p}^{(n+\Delta)*}(j + \delta) \right. \\
& \left. + \mu_{1,k}^{(n)*}(j) \mu_{1,p}^{(n+\Delta)}(j) + \tilde{\mu}_{1,-p}^{(n)*}(j + \delta) \tilde{\mu}_{1,-k}^{(n-\Delta)}(j + \delta) \right)
\end{aligned}$$

where $j \in \{1, \dots, N\}$ is in arbitrary site index. The corresponding equation for $\dot{n}_{2,p}$ can be simply obtained by exchanging all indices 1 and 2 in Eq. (6.16). Note that in the presence of the periodic perturbation, the Boltzmann equation above includes explicitly energy violating processes ($\Delta \neq 0$) that

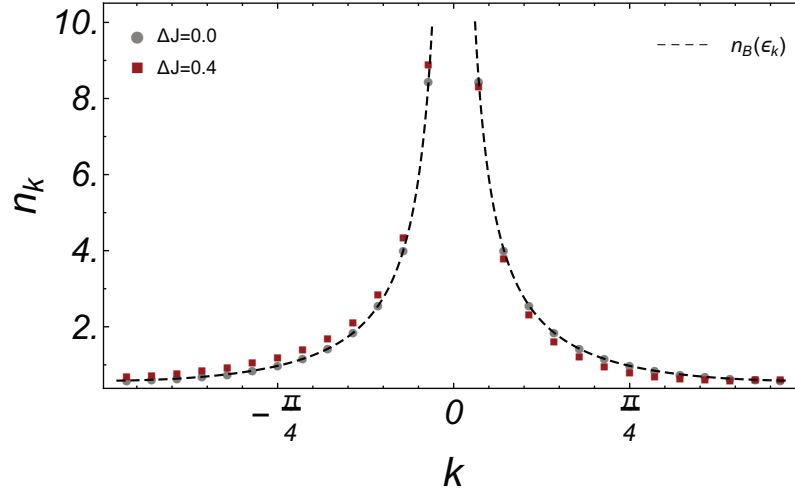


Figure 6.6 Occupation of the quasiparticle states at $\Delta J = 0.0$ (gray circles) and $\Delta J = 0.4$ (red squares). While in the absence of driving the occupation number follows an equilibrium Bose-Einstein distribution, we find an asymmetric distribution at $\Delta J = 0.4$. Parameters: $J = 1$, $\Omega = 4.5$, $T_{ph} = 1$, $B_{stag} = 0$, $N = 26$.

drive the system to a non-thermal state. This is visualized in Fig. 6.6 where we compare the steady state distribution n_k , which is in our setup identical for the two species, at $\Delta J = 0$ and $\Delta J = 0.4$. While in the absence of driving, the occupation follows an equilibrium Bose-Einstein distribution, the distribution becomes asymmetric at $\Delta J \neq 0$ indicating a non-equilibrium state. However, in both cases, n_k diverges when $k \rightarrow 0$ due to the existence of Goldstone modes. Adding a staggered magnetic field term H_F to the Hamiltonian would gap the Goldstone modes out and regulate the divergence of n_k at $k = 0$.

At finite magnetic field strength B_{stag} , we can calculate the spin current expectation value $\langle J_s \rangle_{\{n_q\}}$ as a function of the order parameter $\phi = \langle \sum_j (-1)^j S_j^z \rangle_{\{n_q\}} / N$. Here, the expectation value of an operator X with respect to $\{n_q\}$ is defined as

$$\langle X \rangle_{\{n_q\}} = \sum_k \langle \langle \phi_{1,k} | \tilde{X} | \phi_{1,k} \rangle \rangle n_{1,k} + \langle \langle \phi_{2,k} | \tilde{X} | \phi_{2,k} \rangle \rangle n_{2,k} \quad (6.17)$$

where \tilde{X} is the corresponding operator acting on the extended Hilbert space. As our calculation is based on an expansion around the staggered state in which the order parameter is one, our ansatz breaks down, when $|\phi|$ becomes too small. Therefore, in Fig. 6.7 we plot the spin current density only in the regime $|\phi| \gtrsim 0.2$. We find that for the chosen parameters, which are not optimized yet, the spin current density saturates to a value of $\langle J_s \rangle_{\{n_q\}} / N \approx 0.02$ when ϕ approaches one. At small values of ϕ we find a linear behavior that is extrapolated to zero for $|\phi| \lesssim 0.2$. From this we can deduce the linear coefficient α we have introduced phenomenologically in Eq. (6.2) at the beginning of this

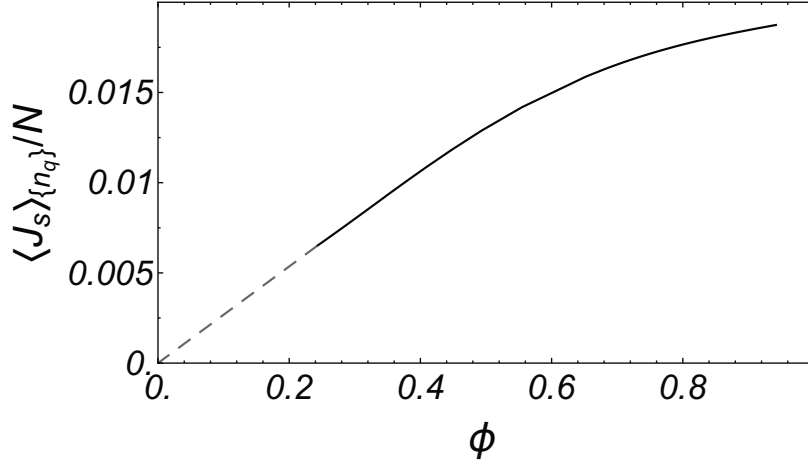


Figure 6.7 Expectation value of the spin current operator calculated with Eq. (6.17) as a function of the order parameter at $J = 1$, $\Delta J = 0.1$, $\Omega = 4.44$, $T_{ph} = 1$. The dashed line shows a linear interpolation in the regime of small values of ϕ where the expansion around a staggered state breaks down.

chapter. As we later simulate the classical analogue of the Hamiltonian Eq. (6.8), it is instructive to consider the classical limit of Eq. (6.16). It is reasonable to expect that at high temperatures $T \gg \epsilon_k$, quantum effects become less relevant and classical physics prevails. In the high temperature regime, $n_{1,p}$, $n_{2,p}$ and n_B are large allowing us to keep only the leading order terms in powers of occupation numbers. As all terms of order three cancel, we arrive at

$$\begin{aligned}
 \dot{n}_{1,p} = & -2\pi S^2 \frac{N}{2} \int d\omega \mathcal{N}(\omega) \sum_k \sum_{\delta=\pm 1} \sum_{\Delta=-N_f}^{N_f} \\
 & |V^{(1)}(p, k, \delta, \Delta)|^2 \times \\
 & \left[n_{1,p} n_{2,k} \delta((\epsilon_k + \epsilon_p) - \omega + \Delta\Omega) - n_B (n_{1,p} + n_{2,k}) \delta((\epsilon_p + \epsilon_k) - \omega + \Delta\Omega) \right. \\
 & \left. - (n_B (n_{1,p} + n_{2,k}) + n_{1,p} n_{2,k}) \delta((\epsilon_p + \epsilon_k) + \omega + \Delta\Omega) \right] \\
 & + |W^{(1)}(p, k, \delta, \Delta)|^2 \times \\
 & \left[n_B n_{1,p} \delta((\epsilon_p - \epsilon_k) + \omega + \Delta\Omega) + (n_{1,p} n_{1,k} + n_B n_{1,p}) \delta((\epsilon_p - \epsilon_k) - \omega + \Delta\Omega) \right] \\
 & - \left[n_B n_{1,k} \delta((\epsilon_k - \epsilon_p) + \omega - \Delta\Omega) + (n_{1,k} n_{1,p} + n_{1,k} n_B) \delta((\epsilon_k - \epsilon_p) - \omega - \Delta\Omega) \right]
 \end{aligned}$$

which is of order two in occupation numbers.

6.2.4 Classical simulation

Above we have shown that the model Eq. (6.8) together with Eq. (6.9) hosts a spin current in the presence of an antiferromagnetic order parameter, which we have simulated by an external staggered magnetic field in the Hamiltonian. However, we have not verified that long range order and a finite spin current, which is conjectured to stabilize the former, emerge spontaneously. To investigate this question, we simulate the classical equations of motion of the model defined in Eq. (6.8) on a one-dimensional lattice. For the derivation, we follow [139]. As a classical analogue to the quantum mechanical Hamiltonian, we consider $H = H_{\text{sys}} + H_{\text{bath}} + H_{\text{int}}$,

$$\begin{aligned} H_{\text{sys}} &= J \sum_{\alpha} \mathbf{S}_{\alpha} \mathbf{S}_{\alpha+1}, \\ H_{\text{bath}} &= \sum_{\alpha, \kappa} \left(\frac{p_{\alpha, \kappa}^2}{2m_{\alpha, \kappa}} + \frac{1}{2} m_{\alpha, \kappa} \omega_{\alpha, \kappa}^2 x_{\alpha, \kappa}^2 \right), \\ H_{\text{int}} &= - \sum_{\alpha, \kappa} F_{\alpha} x_{\alpha, \kappa} + \Delta H \end{aligned}$$

describing interacting classical spins coupled to a bath of harmonic oscillators with frequency $\omega_{\alpha, \kappa}$ and mass $m_{\alpha, \kappa}$. At the moment the force \mathbf{F} is an arbitrary function of the spin degrees of freedom. However, we later set $F_{\alpha} = \mathbf{S}_{\alpha} \mathbf{S}_{\alpha+1}$ to recover the coupling term defined in Eq. (6.9). As canonical variables of the spin degrees of freedom, we choose the angle φ' within the xy -plane and the projection of the spin onto the z -axis S^z [140]. The spin can then be expressed in terms of these canonical variables as

$$\mathbf{S} = \begin{pmatrix} \sqrt{1 - (S^z)^2} \cos \varphi' \\ \sqrt{1 - (S^z)^2} \sin \varphi' \\ S^z \end{pmatrix}.$$

The additional counter term ΔH is introduced in H_{int} to compensate for $F_{\alpha} x_{\alpha}$ and is chosen in such a way that at fixed bath coordinates for which $H_{\text{bath}} + H_{\text{int}}$ is minimal, the minimum of H is only set by the derivatives of H_{sys} with respect to the spin degrees of freedom,

$$\begin{aligned} (i) \quad \frac{\partial H}{\partial x_{\alpha, \kappa}} &= m_{\alpha, \kappa} \omega_{\alpha, \kappa}^2 x_{\alpha, \kappa} - F_{\alpha} \stackrel{!}{=} 0 & \Rightarrow & \quad x_{\alpha, \kappa} = \frac{F_{\alpha}}{m_{\alpha, \kappa} \omega_{\alpha, \kappa}^2}, \\ (ii) \quad \frac{\partial H_{\text{int}}}{\partial \varphi'_{\beta}} &= - \sum_{\alpha, \kappa} \frac{1}{m_{\alpha, \kappa} \omega_{\alpha, \kappa}^2} \frac{\partial F_{\alpha}}{\partial \varphi'_{\beta}} F_{\alpha} + \frac{\partial \Delta H}{\partial \varphi'_{\beta}} \stackrel{!}{=} 0 & \Rightarrow & \quad \Delta H = \sum_{\alpha, \kappa} \frac{1}{2m_{\alpha, \kappa} \omega_{\alpha, \kappa}^2} F_{\alpha}^2, \end{aligned}$$

where the last equality could equivalently be obtained from $\partial H_{\text{int}} / \partial S_{\beta}^z = 0$. Inserting the counter term into H yields

$$H = H_{\text{sys}} + \sum_{\alpha, \kappa} \left(\frac{p_{\alpha, \kappa}^2}{2m_{\alpha, \kappa}} + \frac{1}{2} m_{\alpha, \kappa} \omega_{\alpha, \kappa}^2 \left(x_{\alpha, \kappa} - \frac{F_{\alpha}}{m_{\alpha, \kappa} \omega_{\alpha, \kappa}^2} \right)^2 \right).$$

Eventually, we are interested in the dynamics of quantities \mathbf{A} that are function of the system variables only where the influence of the bath is treated as an average effect on a course-grained time scale. To obtain such a formulation, we firstly calculate Hamilton's equations of the bath coordinates

$$\begin{aligned}\frac{dx_{\alpha,\kappa}}{dt} &= \{x_{\alpha,\kappa}, H_{tot}\} = \frac{p_{\alpha,\kappa}}{m_{\alpha,\kappa}}, \\ \frac{dp_{\alpha,\kappa}}{dt} &= \{p_{\alpha,\kappa}, H_{tot}\} = -m_{\alpha,\kappa}\omega_{\alpha,\kappa}^2 x_{\alpha,\kappa} + F_{\alpha}\end{aligned}\quad (6.18)$$

describing the dynamics of a driven harmonic oscillator. The coupled differential equations Eq. (6.18) can be solved using the Green's functions method

$$x_{\alpha,\kappa}(t) = x_{\alpha,\kappa}^h(t) + \frac{1}{m_{\alpha,\kappa}\omega_{\alpha,\kappa}} \int_{t_0}^t ds \sin(\omega_{\alpha,\kappa}(t-s)) F_{\alpha}(s),$$

where $x_{\alpha,\kappa}^h(t) = x_{\alpha,\kappa}(0) \cos(\omega_{\alpha,\kappa}(t-t_0)) + \frac{p_{\alpha,\kappa}(0)}{m_{\alpha,\kappa}\omega_{\alpha,\kappa}} \sin(\omega_{\alpha,\kappa}(t-t_0))$ denotes the solution of the homogeneous differential equation for $F_{\alpha} = 0$. The latter result can be used to express $\dot{\mathbf{A}}$ as a function of the spin degrees of freedom

$$\begin{aligned}\frac{dA}{dt} &= \{A, H_{sys}\} + \sum_{\alpha,\kappa} \frac{1}{2m_{\alpha,\kappa}\omega_{\alpha,\kappa}^2} \{A, F_{\alpha}^2\} - \sum_{\alpha,\kappa} x_{\alpha,\kappa} \{A, F_{\alpha}\} \\ &= \{A, H_{sys}\} - \sum_{\alpha} \{A, F_{\alpha}\} \left[\xi_{\alpha}(t) - \int_{t_0}^t ds \gamma(t-s) \frac{dF_{\alpha}(s)}{ds} \right].\end{aligned}\quad (6.19)$$

For the second equality, we have performed an integration by parts and introduced

$$\begin{aligned}\xi_{\alpha}(t) &= \sum_{\kappa} \left[x_{\alpha,\kappa}^h(t) - \frac{1}{m_{\alpha,\kappa}\omega_{\alpha,\kappa}^2} F_{\alpha}(t_0) \cos(\omega_{\alpha,\kappa}(t-t_0)) \right], \\ \gamma_{\alpha}(t) &= \sum_{\kappa} \frac{1}{m_{\alpha,\kappa}\omega_{\alpha,\kappa}^2} \cos(\omega_{\alpha,\kappa}t).\end{aligned}$$

The term ξ_{α} contains the initial conditions $x_{\alpha,\kappa}(0)$, $p_{\alpha,\kappa}(0)$ of the bath degrees of freedom which can be considered as independent random variables distributed according to an equilibrium probability distribution $\sim e^{-\beta H}$. By virtue of the central limit theorem, we can expect that ξ_{α} follows, as a sum of many random variables with a finite variance, a Gaussian distribution that is completely defined by its first two moments

$$\langle \xi_{\alpha}(t) \rangle = 0, \quad \langle \xi_{\alpha'}(t) \xi_{\alpha}(t') \rangle = 2k_B T \delta_{\alpha,\alpha'} \gamma(t-t'). \quad (6.20)$$

As a useful quantity, we introduce the spectral density of the bath

$$J(\omega) = \frac{\pi}{2} \sum_{\alpha} \frac{1}{m_{\alpha} \omega_{\alpha}} \delta(\omega - \omega_{\alpha})$$

that we can use to express the damping kernel γ as

$$\gamma(t) = 2 \int_0^{\infty} \frac{d\omega}{\pi} \frac{J(\omega)}{\omega} \cos(\omega t).$$

In case the number of oscillators is large, the spectral density becomes a smooth function of ω . For ohmic damping, i.e. $J(\omega) \approx (\lambda/2)\omega$ below a cutoff frequency Ω_D , the damping kernel is a delta function, $\gamma(t-t') = \lambda \delta(t-t')$.

Next, we consider the specific case $F_{\alpha} = \mathbf{S}_{\alpha} \mathbf{S}_{\alpha+1}$ which is equivalent to the interaction term in Eq. (6.9) and set $\mathbf{A} = \mathbf{S}_j$. With the help of Eq. (6.19), we obtain for the equation of motion of a spin at site j ,

$$\begin{aligned} \left(\frac{d\mathbf{S}_j}{dt} \right)_{\text{Heisen+damp}} &= \{\mathbf{S}_j, H_{\text{sys}}\} - \sum_{\alpha} \{\mathbf{S}_j, F_{\alpha}\} \left[\xi_{\alpha}(t) - \lambda \frac{dF_{\alpha}(t)}{dt} \right] \\ &= -\mathbf{S}_j \times \mathbf{S}_{j+1} \left(J - \xi_j(t) + \lambda \frac{d}{dt} (\mathbf{S}_j \mathbf{S}_{j+1}) \right) \\ &\quad - \mathbf{S}_j \times \mathbf{S}_{j-1} \left(J - \xi_{j-1}(t) + \lambda \frac{d}{dt} (\mathbf{S}_{j-1} \mathbf{S}_j) \right) \end{aligned} \quad (6.21)$$

where we have used $\{\mathbf{S}_j, \mathbf{S}_j \mathbf{S}_{j+1}\} = -\mathbf{S}_j \times \mathbf{S}_{j+1}$ which directly follows from the definition of the Poisson bracket

$$\{\mathbf{S}_j, \mathbf{S}_j \mathbf{S}_{j+1}\} = \frac{\partial \mathbf{S}_j}{\partial \varphi'_j} \frac{\partial (\mathbf{S}_j \mathbf{S}_{j+1})}{\partial S_j^z} - \frac{\partial \mathbf{S}_j}{\partial S_j^z} \frac{\partial (\mathbf{S}_j \mathbf{S}_{j+1})}{\partial \varphi'_j}.$$

Similarly, the driving term in the Hamiltonian Eq. (6.9) leads to an additional contribution

$$\left(\frac{d\mathbf{S}_j}{dt} \right)_{\text{drive}} = -\Delta J_1 (-1)^j \cos(\Omega t) \mathbf{S}_j \times (\mathbf{S}_{j-1} - \mathbf{S}_{j+1}) - \Delta J_2 \sin(\Omega t) \mathbf{S}_j \times (\mathbf{S}_{j-2} + \mathbf{S}_{j+2}) \quad (6.22)$$

in the equations of motion. Before simulating the full dynamics of the system, it is instructive to consider first the mean-field equations of motion in the absence of noise $T = 0$ by setting $\mathbf{S}_j \rightarrow \mathbf{S}_e$ for j even and $\mathbf{S}_j \rightarrow \mathbf{S}_o$ for j odd. Note that the contribution of the time-dependent perturbation as defined in Eq. (6.9), leading to Eq. (6.22), vanishes on mean-field level. This is not the case when the first driving term $H_{d,1}(t)$ is only defined on even or odd sites as in Eq. (6.10). However, we do not include $H_d(t)$ here as damping is absent on mean-field level as well, which is due to the conservation of $\mathbf{S}_e \cdot \mathbf{S}_o$. Therefore, we simply obtain the equations of motion of two coupled classical spins

$$\frac{d}{dt} \mathbf{S}_e = -J (\mathbf{S}_e \times \mathbf{S}_o), \quad \frac{d}{dt} \mathbf{S}_o = -\frac{d}{dt} \mathbf{S}_e. \quad (6.23)$$

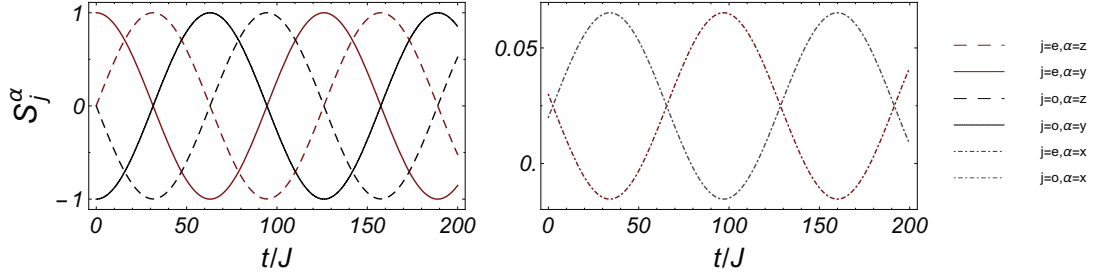


Figure 6.8 Time evolution of the three spin components of the even (red) and the odd (black) spin for initial conditions $\mathbf{S}_e \approx \mathbf{e}_z$, $\mathbf{S}_o \approx -\mathbf{e}_z$. For the chosen initial conditions with total spin $\mathbf{S} \approx \mathbf{0}$, both spins rotate in the yz -plane while staying approximately anti-parallel.

We can solve Eq. (6.23) exactly by introducing the relative coordinates $\mathbf{S}_0 = \mathbf{S}_e - \mathbf{S}_o$. The time derivative of \mathbf{S}_0 can then be written as $\partial \mathbf{S}_0 / \partial t = -\mathbf{S}_0 \times \mathbf{S}$ where $\mathbf{S} = \mathbf{S}_e + \mathbf{S}_o$ is the conserved total spin. Thus, the relative spin precesses around the fixed total spin leading to a precession of the single spins for $\mathbf{S}_e \approx \mathbf{S}_o$. However, for initial conditions that are close to the staggered state with $\mathbf{S} \approx \mathbf{0}$, we observe that both spins oscillate in a plane while staying approximately anti-parallel throughout the time evolution as shown in Fig. 6.8. Therefore, we do not find a stationary stable state we could expand around on mean-field level.

In the following, we consider the full dynamics governed by Eq. (6.21) and Eq. (6.22). The equations of motion cannot be implemented directly in the presence of damping as both sides of the first order ordinary differential equation (ODE) depend explicitly on the time derivatives of the spin degrees of freedom. This kind of differential equation is known as an implicit differential equation [141]. We aim to translate the ODE from an implicit to an explicit form. As already mentioned, an implicit differential equation depends in some numerical discretization scheme on both sides on the future values of the dynamical variable $\mathbf{S}^{(n+1)}$ as

$$\mathbf{S}^{(n+1)} \sim \mathbf{f}(\mathbf{S}^{(n+1)}, \mathbf{S}^{(n)}, t^{(n)})$$

which means that in every time step, one can plug all known values for $\{S_i^{(n)}\}$ into \mathbf{f} to obtain a set of linear equations for the $3N$ unknowns $\{S_i^{(n+1)}\}$ that can be solved using, for example, a Gauss-Jordan algorithm. Therefore, in each time step, a linear system of equations has to be solved. For the stochastic differential equation, we can write

$$\dot{\mathbf{S}} = \mathbf{f}(\mathbf{S}, \dot{\mathbf{S}}, t) + \mathbf{g}(\boldsymbol{\xi}, \mathbf{S}). \quad (6.24)$$

As Eq. (6.21) is linear in $\dot{\mathbf{S}}$, the deterministic contribution is formally given by

$$\mathbf{f}(\mathbf{S}, \dot{\mathbf{S}}, t) = \mathbf{M}(\mathbf{S})\dot{\mathbf{S}} + \mathbf{b}(\mathbf{S}), \quad (6.25)$$

where \mathbf{S} , $\mathbf{g}(\boldsymbol{\xi}, \mathbf{S})$ and $\mathbf{b}(\mathbf{S})$ are vectors with $3N$ components, i.e. $\mathbf{S} = (\mathbf{S}_1, \mathbf{S}_2, \dots, \mathbf{S}_N)$. For the specific example Eq. (6.21) and Eq. (6.22), the contributions read

$$\begin{aligned} \mathbf{b}_j &= -\mathbf{S}_j \times \mathbf{S}_{j+1} (J - (-1)^j \Delta J_1 \cos(\Omega t)) - \mathbf{S}_j \times \mathbf{S}_{j-1} (J + (-1)^j \Delta J_1 \cos(\Omega t)) \\ &\quad - \Delta J_2 \sin(\Omega t) \mathbf{S}_j \times (\mathbf{S}_{j+2} + \mathbf{S}_{j-2}), \\ \mathbf{g}_j &= -\mathbf{S}_j \times (\mathbf{S}_{j-1} \boldsymbol{\xi}_{j-1} + \mathbf{S}_{j+1} \boldsymbol{\xi}_j). \end{aligned}$$

The Jacobian M is formally defined as

$$M(\mathbf{S}) = \begin{pmatrix} \partial f_1 / \partial \dot{S}_1^x & \partial f_1 / \partial \dot{S}_1^y & \dots & \partial f_1 / \partial \dot{S}_N^z \\ \vdots & \vdots & \vdots & \vdots \\ \partial f_{3N} / \partial \dot{S}_1^x & \dots & \dots & \partial f_{3N} / \partial \dot{S}_N^z \end{pmatrix}. \quad (6.26)$$

With the decomposition Eq. (6.25), we can solve for the derivative $\dot{\mathbf{S}}$,

$$\dot{\mathbf{S}} = (\mathbb{1} - M)^{-1} [\mathbf{b}(\mathbf{S}) + \mathbf{g}(\boldsymbol{\xi}, \mathbf{S})] \quad (6.27)$$

which yields an explicit differential equation. The equivalence of Eq. (6.27) and Eq. (6.24) is guaranteed if $(\mathbb{1} - M)$ is invertible which is the case in our example. For the implementation of the discretized stochastic differential equation, we employ Heun's method that is explained in Sec. (1.5.2). The dynamics described by Eq. (6.21) and Eq. (6.22) conserves the length of each spin and also the total magnetization, as the Hamiltonian is invariant under global rotations in spin space. Note that a numerical method that approximates a solution, typically violates the physical conservation laws of the given system. We observe that this violation is especially evident in the presence of noise. Typically, a single time step of the numerical algorithm evolves the solution of the system out of the manifold of conserved quantities G . We can correct for that by projecting the solution back onto the manifold after each time step [142]. Technically, we minimize the Euclidean norm

$$\mathcal{L}_G[\tilde{\mathbf{S}}] = \frac{1}{2} \|\tilde{\mathbf{S}}^{(n+1)} - \mathbf{S}^{(n+1)}\|^2 + \mathbf{g}_c^T(\tilde{\mathbf{S}}^{(n+1)}) \boldsymbol{\lambda}$$

between the solution $\mathbf{S}^{(n+1)} \notin G$ suggested by the numerical scheme and a solution with $\tilde{\mathbf{S}}^{(n+1)} \in G$ under the constraints

$$\begin{aligned} \mathbf{g}_{c,j}(\mathbf{S}) &= (\mathbf{S}_j^x)^2 + (\mathbf{S}_j^y)^2 + (\mathbf{S}_j^z)^2 - 1 = 0, & j \in (1, \dots, N), \\ \mathbf{g}_{c,N+i}(\mathbf{S}) &= \sum_{j=1}^N \mathbf{S}_j^{\alpha_i} = 0, & i \in \{1, 2, 3\}, \alpha_i \in \{x, y, z\}, \end{aligned}$$

where we assume a zero magnetization state. Therefore, in every time step the matrix $(\mathbb{1} - M)$ has to be inverted and the extremization problem $\delta \mathcal{L}_G / \delta S_j^\alpha = 0$ has to be solved. This increases the

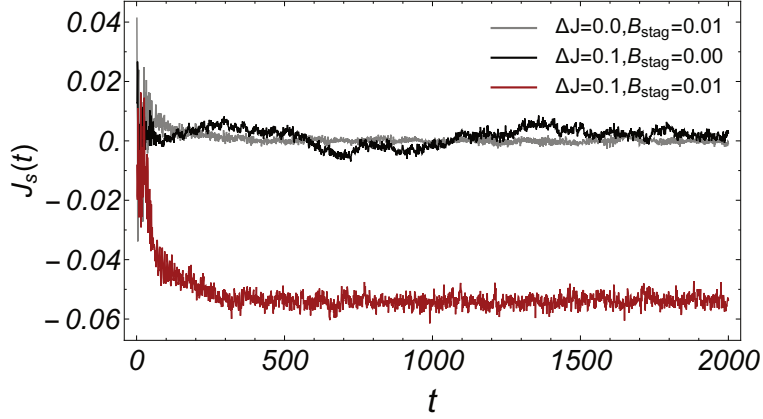


Figure 6.9 Time-dependence of the classical spin current at $\Delta J = 0.0$, $B_{stag}=0.01$ (gray), $\Delta J = 0.1$, $B_{stag} = 0.00$ (black) and $\Delta J = 0.01$, $B_{stag} = 0.01$ (red) averaged over 20 noise realizations. Parameters: $J = 1$, $\lambda = 0.5$, $\Omega = 3$, $T_{ph} = 0.01$, $N = 20$

numerical complexity of the method and restricts the accessible system sizes to about $N \sim \mathcal{O}(10^2)$. We want to verify if the system described by Eq. (6.21) and Eq. (6.22) can, as predicted by our analysis of the corresponding quantum model, host a finite spin current in the steady state when being subject to an additional staggered magnetic field H_F . The field gives rise to an additional term in the equations of motion, namely

$$\left(\frac{d\mathbf{S}_j}{dt}\right)_{staggered} = (-1)^j B_{stag} (\mathbf{S}_j \times \mathbf{e}_z). \quad (6.28)$$

The full equations of motion then read

$$\left(\frac{d\mathbf{S}_j}{dt}\right) = \left(\frac{d\mathbf{S}_j}{dt}\right)_{Heisen+damp} + \left(\frac{d\mathbf{S}_j}{dt}\right)_{drive} + \left(\frac{d\mathbf{S}_j}{dt}\right)_{staggered}. \quad (6.29)$$

Firstly, we initialize the system in a randomly chosen zero magnetization state. In Fig. 6.9 the time evolution of the spin current is shown for $\Delta J = 0.1$ and $\Delta J = 0$ at $B_{stag} = 0.01$ and for $\Delta J = 0.1$ at $B_{stag} = 0$. While in the presence of an external field B_{stag} , the spin current is zero at $\Delta J = 0$, we observe a finite current at $\Delta J = 0.1$ in the long-time limit which is consistent with our symmetry analysis. However, we find that also at $B_{stag} = 0$ but $\Delta J = 0.1$, the spin current is on average zero. Also for a broad range of parameters, we do not observe the emergence of a spin current or the spontaneous formation of long range order without the symmetry breaking term H_F . Instead we find that the heating effect of the periodic pumping is dominant as can be seen in Fig 6.10 where the time-averaged spin-spin correlation $\langle S_1 S_j \rangle$ is shown as a function of the distance j for $\Delta J = 0$ and $\Delta J = 0.1$. Secondly, we choose as an initial condition a state in which all neighboring spins are approximately anti-aligned such that the order parameter is close to its maximal value, i.e. $\phi = (1/N) \sum_j (-1)^j \mathbf{S}_j \approx \phi_0 = \mathbf{e}_z$. According to our analysis so far, we therefore expect to observe

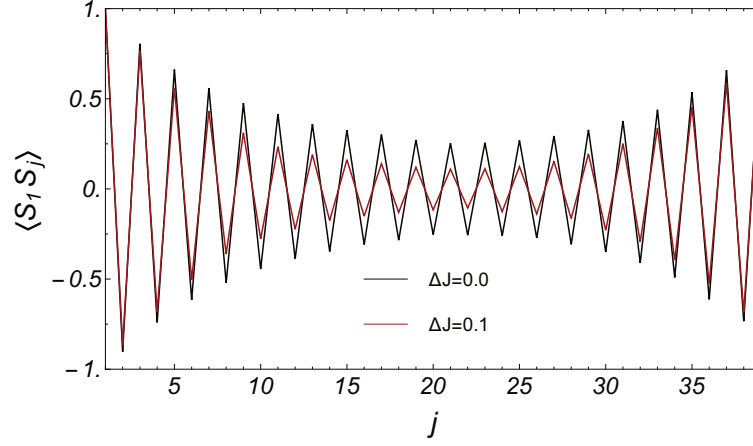


Figure 6.10 The time averaged spin-spin correlation function $\langle S_1 S_j \rangle$ as a function of the distance j between the two spins is shown. We observe that driving leads to a faster decay of $\langle S_1 S_j \rangle$ due to heating effects. Parameters: $J = 1$, $\lambda = 0.5$, $\Omega = 3$, $T = 0.1$, $N = 40$.

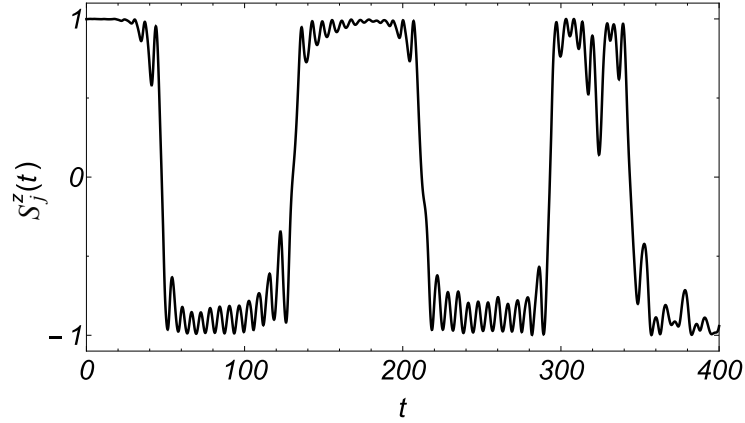


Figure 6.11 The time evolution of the z -component of a single spin is shown. The dynamics of the whole system is governed by the equations of motion Eq. (6.9) at $J = 1$, $\Delta J = 0.1$, $\Omega = 1$, $T = 0$, $\lambda = 1$, $B_{stag} = 0$, $N = 20$. The system is initialized close to a staggered state.

a finite spin current at $\Delta J \neq 0$ in the steady state. Initially, we conjectured that a spin current can stabilize long range order in the system. For our arguments to work, we have to demand that, at least at $T = 0$ but with finite damping, the ordered initial state is stable for $\Delta J \neq 0$ even if $B_{stag} = 0$. However, we find that this is not the case. The staggered configuration is unstable in the presence of the time-dependent perturbation when the system size becomes larger than a critical size L^* . In Fig. 6.11 the time evolution of the z -component of a single spin is plotted for $L > L^*$. The whole system shows successive transitions between the two configurations with $\phi \approx \pm \phi_0$ corresponding to two spin-reversed classical antiferromagnetic states. In the next section, we give an argument based on a field theoretical approach to explain these instabilities.

6.3 Field theoretical approach and stability analysis

6.3.1 Haldane mapping

So far our notion of stabilization of long range order through a spin current is based on the phenomenological equations Eq. (6.1) and Eq. (6.2) that neglect the precise time evolution of the order parameter field ϕ . Here, we derive coupled equations of motion for the staggered and the uniform component of the spins by performing the so-called *Haldane mapping* which is applicable if there is a clear separation between short and long length scales. For the derivation, we make use of [4]. According to the transformation, each spin is related to two continuous vector fields, the order parameter field ϕ and the so-called canting field \mathbf{m} through

$$\begin{aligned}\hat{\Omega}_j &:= \mathbf{S}_j/S = (-1)^j \sqrt{1 - \mathbf{m}_j^2} \phi_j + \mathbf{m}_j \\ &\approx (-1)^j \phi_j + \mathbf{m}_j - \frac{\mathbf{m}_j^2}{2} (-1)^j \phi_j,\end{aligned}$$

where the expansion is valid for small \mathbf{m}_j . To simplify the notations, we have set $\mathbf{m}_j = \mathbf{m}(x_j, t)$. The conservation of the length of the spins is guaranteed by the two constraints

$$\mathbf{m}_j \cdot \phi_j = 0, \quad |\phi_j|^2 = 1 \quad (6.30)$$

that have to be fulfilled at any time. For instance, the transformation is used to map the d dimensional quantum Heisenberg antiferromagnet onto the $d + 1$ dimensional non-linear sigma model. If the system is close to the classical Néel state with small \mathbf{m} and $\phi_j \approx \phi_0$, the total magnetization is given by $\mathbf{M}/S \approx \sum_j ((-1)^j \phi_j + \mathbf{m}_j) \approx \sum_j \mathbf{m}_j$. The canting field can be interpreted as a dynamic magnetization as it is due to temporal variations of ϕ_j [143]. Note that we double the degrees of freedom from two to four when performing the mapping described above, as both fields have together six degrees of freedom that are subject to two constraints. This overdetermination can be cured in reciprocal space by reducing the corresponding volume of the unit cell by a factor two. Equations of motion can be derived by calculating the Euler-Lagrange equations of the Lagrangian density

$$\mathcal{L}[\{\phi_j, \mathbf{m}_j\}] = \sum_j \mathcal{K}[\{\phi_j, \mathbf{m}_j\}] - \mathcal{H}[\{\phi_j, \mathbf{m}_j\}],$$

where \mathcal{H} denotes the Hamiltonian density and \mathcal{K} the kinetic energy term. For a single spin, the kinetic part of the action, which is also called *Berry phase*, is given by $\mathcal{K} = S\omega[\mathbf{\Omega}]$ with $\omega[\mathbf{\Omega}] := \int_0^t dt' \hat{\Omega} \cdot \mathbf{A}(\hat{\Omega})$. Here, $\hat{\Omega} = \mathbf{S}/S$ denotes the unit vector of the spin \mathbf{S} and the vector potential \mathbf{A} fulfills $\partial A^\beta / \partial \hat{\Omega}^\alpha = \varepsilon^{\alpha\beta\gamma} \hat{\Omega}^\gamma$. Geometrically, the Berry phase describes the surface on the S^2 sphere

which is enclosed by the path $\hat{\Omega}(t)$. In order to expand $\omega[\hat{\Omega}]$ in \mathbf{m} , we calculate the first variation

$$\begin{aligned}
\delta\omega[\hat{\Omega}] &= \int_0^t dt' \delta \left(\dot{\hat{\Omega}} \cdot \mathbf{A}(\hat{\Omega}) \right) \\
&= \int_0^t dt' \left[\left[\frac{\partial A^\alpha}{\partial \hat{\Omega}^\beta} \delta \hat{\Omega}^\beta \dot{\hat{\Omega}}^\alpha + A^\alpha \delta \dot{\hat{\Omega}}^\alpha \right] + \left[\frac{\partial A^\alpha}{\partial \hat{\Omega}^\beta} \dot{\hat{\Omega}}^\beta \delta \hat{\Omega}^\alpha - \frac{\partial A^\alpha}{\partial \hat{\Omega}^\beta} \dot{\hat{\Omega}}^\beta \delta \hat{\Omega}^\alpha \right] \right] \\
&= \underbrace{\int_0^t dt' \frac{d}{dt} \left(\mathbf{A} \cdot \delta \hat{\Omega} \right)}_{=0} + \int_0^t dt' \frac{\partial A^\alpha}{\partial \hat{\Omega}^\beta} \underbrace{\left(\delta \hat{\Omega}^\beta \dot{\hat{\Omega}}^\alpha - \dot{\hat{\Omega}}^\beta \delta \hat{\Omega}^\alpha \right)}_{=\varepsilon^{\alpha\beta\gamma} (\hat{\Omega} \times \delta \hat{\Omega})_\gamma} \\
&= - \int_0^t dt' \dot{\hat{\Omega}} \cdot (\hat{\Omega} \times \delta \hat{\Omega}) \quad \Rightarrow \quad \frac{\delta\omega}{\delta \hat{\Omega}} = \dot{\hat{\Omega}} \times \hat{\Omega}.
\end{aligned}$$

We use the gauge freedom of the vector potential to define \mathbf{A} such that $\mathbf{A}(-\hat{\Omega}) = \mathbf{A}(\hat{\Omega})$. One possible choice for \mathbf{A} that guarantees this property is $-\cos(\theta)/\sin(\theta)\hat{\phi}$ where θ is the polar angle and $\hat{\phi}$ the unit vector of the azimuth angle. Moreover, we consider fixed boundary conditions for which the integral over the total derivative above vanishes, $\delta \hat{\Omega}(0) = \delta \hat{\Omega}(t) = 0$. Thus, we obtain $S\omega_j[\mathbf{S}] \approx (-1)^j S\omega_j[\phi_j] + S \mathbf{m}_j \cdot \frac{\delta\omega}{\delta \phi_j} = \Upsilon + S \mathbf{m}_j \cdot (\dot{\phi}_j \times \phi_j)$. The term $\Upsilon = S \sum_j (-1)^j \omega_j[\phi_j]$ is called *topological Berry phase*. It is a topological invariant, meaning that Υ does not change through continuous deformation of ϕ_j . Particularly, Υ/S assumes only integer multiples of 2π . As its variation is zero, it also does not affect the classical equations of motion. However, for half-integer spin the phase $e^{i\Upsilon}$ can be positive or negative which can, for example, lead to strong effects on ground state correlations and excitation spectra [4, 144]. Using the Lagrange density $\mathcal{L} = \int dx S \mathbf{m} \cdot (\dot{\phi} \times \phi) - \mathcal{H}[\{\phi, \mathbf{m}\}]$ we can derive coupled equations of motion for the continuous fields \mathbf{m} and ϕ ,

$$\dot{\phi} = \boldsymbol{\omega}_m \times \phi, \quad (6.31)$$

$$\dot{\mathbf{m}} = \boldsymbol{\omega}_\phi \times \phi + \boldsymbol{\omega}_m \times \mathbf{m}_j, \quad (6.32)$$

where we have defined $\boldsymbol{\omega}_m := -\frac{1}{S} \frac{\delta \mathcal{H}}{\delta \mathbf{m}}$ and $\boldsymbol{\omega}_\phi := -\frac{1}{S} \frac{\delta \mathcal{H}}{\delta \phi}$. By construction Eq. (6.31) and Eq. (6.32) fulfill the constraints Eq. (6.30) which can be verified straightforwardly. Note that the same equations of motion have been derived in [143]. In order to obtain the contribution of the Heisenberg Hamiltonian to the Hamiltonian density \mathcal{H} , we express H_0 in terms of ϕ_j and \mathbf{m}_j and perform an expansion to leading order in ∂_x and \mathbf{m} . A continuum theory can be obtained by replacing discrete differences by derivatives and the total sum by an integral $\sum_j \mathcal{H}_j \rightarrow \int \frac{dx}{a} \mathcal{H}$ where a is the distance between two adjacent spins. Assuming that spatial variations are small we obtain to leading order

$$\mathcal{H} = \frac{A}{2} (\mathbf{m}(x,t))^2 + \frac{B}{2} (\partial_x \phi(x,t))^2, \quad (6.33)$$

where we have set $A = 4JS^2$ and $B = JS^2a^2$. The derivation and a discussion about the validity of Eq. (6.31), Eq. (6.32) and the continuum Hamiltonian density Eq. (6.33) can be found in App. D. The variation of \mathcal{H} with respect to the continuous fields $\boldsymbol{\phi}$ and \mathbf{m} can be calculated with

$$\frac{\delta \mathcal{H}}{\delta \mathbf{m}} = \frac{\partial \mathcal{H}}{\partial \mathbf{m}} - \partial_x \frac{\partial \mathcal{H}}{\partial \partial_x \mathbf{m}} + \partial_x^2 \frac{\partial \mathcal{H}}{\partial \partial_x^2 \mathbf{m}} - \dots \quad (6.34)$$

which yields

$$\frac{\delta \mathcal{H}}{\delta \mathbf{m}} = A \mathbf{m}(x,t), \quad \frac{\delta \mathcal{H}}{\delta \boldsymbol{\phi}} = -B \partial_x^2 \boldsymbol{\phi}(x,t). \quad (6.35)$$

By inserting Eq. (6.35) into Eq. (6.31) and Eq. (6.32), we arrive at

$$\begin{aligned} \dot{\mathbf{m}}(x,t) &= (B/S) \partial_x (\partial_x \boldsymbol{\phi}(x,t) \times \boldsymbol{\phi}(x,t)), \\ \dot{\boldsymbol{\phi}}(x,t) &= (A/S) (\boldsymbol{\phi}(x,t) \times \mathbf{m}(x,t)). \end{aligned} \quad (6.36)$$

Note that we can deduce from second equation that ∂_t scales as \mathbf{m} and consequently from the first one that $\mathbf{m} \sim \partial_x$. Therefore, we treat \mathbf{m} and ∂_x in the expansion on an equal footing. For the canting field \mathbf{m} we obtain a continuity equation as the total magnetization is conserved. To develop a better intuition for the dynamics of the order parameter field, we calculate the second derivative of $\boldsymbol{\phi}$ yielding

$$\ddot{\boldsymbol{\phi}} + C (4|\mathbf{m}|^2 + a^2 (\boldsymbol{\phi} \cdot \partial_x^2 \boldsymbol{\phi})) \boldsymbol{\phi} - Ca^2 \partial_x^2 \boldsymbol{\phi} = 0$$

which is a Klein-Gordon-like equation where we have set $C = 4J^2S^2$. The contribution of the damping term to \mathcal{H} can be calculated in a similar way as in the classical case by integrating out the bath degrees of freedom. However, due to the form of the damping involving four spin operators, its contributions is of order four in \mathbf{m} and ∂_x . In the following, we limit the stability analysis of the staggered state to the leading order contributions where we include damping phenomenologically.

6.3.2 Stability analysis

We consider the equations of motion Eq. (6.36) expanded to leading order in \mathbf{m} and ∂_x in combination with the two phenomenological contributions $\alpha \boldsymbol{\phi}$ and $-D \partial_x \boldsymbol{\phi}$ to the spin current

$$\begin{aligned} \dot{\mathbf{m}} &= JS \partial_x (\partial_x \boldsymbol{\phi} \times \boldsymbol{\phi}) + \alpha \partial_x \boldsymbol{\phi} + D \partial_x^2 \mathbf{m}, \\ \dot{\boldsymbol{\phi}} &= 4JS (\boldsymbol{\phi} \times \mathbf{m}), \end{aligned} \quad (6.37)$$

where we have set $a = 1$. The existence of a contribution to J_s that is linear in $\boldsymbol{\phi}$ has been motivated in Sec. 6.2 while we expect that the diffusion term naturally arises in the dissipative system. Again we choose the coordinate system such that the z -axis points in the direction of the homogeneous order parameter field $\boldsymbol{\phi}_0 = \mathbf{e}_z$ which is together with $\mathbf{m}_0 = \mathbf{0}$ a solution of Eq. (6.37). The stability of

this solution can be analyzed by linearizing the equations of motion with the ansatz $\phi \approx \phi_0 + \delta\phi$, ($\delta\phi \perp \phi_0$) and $\mathbf{m} \approx \mathbf{m}_0 + \delta\mathbf{m}$ around ϕ_0, \mathbf{m}_0 where the constraint $\delta\phi \perp \phi_0$ guarantees that $|\phi|^2 = 1 + \mathcal{O}(\delta\phi^2)$. As $\delta\phi^z$ is time-independent and δm^z not coupled to the other dynamical variables in the linearized theory, we can restrict our analysis to the four components $\delta m^\pm = \delta m^x \pm i\delta m^y$ and $\delta\phi^\pm = \delta\phi^x \pm i\delta\phi^y$,

$$\partial_t \begin{pmatrix} \delta m_k^+ \\ \delta m_k^- \\ \delta\phi_k^+ \\ \delta\phi_k^- \end{pmatrix} = \begin{pmatrix} -Dk^2 & 0 & iJk^2S + i\alpha k & 0 \\ 0 & -Dk^2 & 0 & -iJk^2S + i\alpha k \\ 4iJS & 0 & 0 & 0 \\ 0 & -4iJS & 0 & 0 \end{pmatrix} \begin{pmatrix} \delta m_k^+ \\ \delta m_k^- \\ \delta\phi_k^+ \\ \delta\phi_k^- \end{pmatrix}$$

where the eigenvalues of the stability matrix read

$$\lambda_1^\pm = -\frac{1}{2} \left(Dk^2 \pm \sqrt{D^2k^4 - 16JSk(JkS + \alpha)} \right),$$

$$\lambda_2^\pm = -\frac{1}{2} \left(Dk^2 \pm \sqrt{D^2k^4 - 16JSk(JkS - \alpha)} \right).$$

For $D = 0$ and $\alpha = 0$ we obtain a linear dispersion $\varepsilon_k = 2JSk$ which is consistent with Eq. (6.7). We find that for $\alpha \neq 0$ and small values of k an instability arises at $k^* = \frac{\alpha}{JS}$ or equivalently at a critical system size $L^* = \frac{2\pi JS}{\alpha}$ when the real part of one eigenvalue becomes positive. To visualize this instability, we simulate the equations of motion Eq. (6.37) numerically for a spin chain of length $L > L^*$ that is initially prepared in a configuration with $\phi(x, 0) = \tilde{\phi}_0(x)$ where $|\tilde{\phi}_0(x) - \phi_0| \ll 1$ for all x . In Fig. 6.12 we show the time evolution of the field component $\phi^z(x_0, t)$ at a fixed point x_0 . We find that $\phi^z(x_0, t)$ stays first approximately constant. However, after a time of order one, $\phi^z(x_0, t)$ suddenly changes its sign and starts to oscillate around the configuration with $\phi \approx -\phi_0$ where oscillations are damped by the diffusion term in Eq. (6.37). After being sufficiently damped into the state with $\phi(x, t) \approx -\phi_0$, the instability manifests itself by another sign change. This process is then repeated in an approximately periodic manner.

Note that $\phi^z(x_0, t)$ shows a very similar behavior as the spin component $S_j^z(t)$, cf. Fig. 6.11, whose dynamics is governed by the full equations of motion Eq. (6.28) at temperature $T = 0$. Therefore, the field theory Eq. (6.37) reproduces one of the main features of the noiseless dynamics which are periodic transitions between two classical Néel configurations.

In Fig. 6.13, the spatial dependence of $\phi(x, t_0)$ and $\mathbf{m}(x, t_0)$ is depicted at a time t_0 before, approximately at and after a transition showing that the whole system undergoes these transitions and not only single spins. In the following we give an analytic solution for the equations of motion in the long-wavelength limit $k \rightarrow 0$ where Eq. (6.37) simplifies to

$$\dot{\mathbf{m}} \approx \alpha \partial_x \phi, \tag{6.38}$$

$$\dot{\phi} \approx 4JS (\phi_j \times \mathbf{m}_j).$$

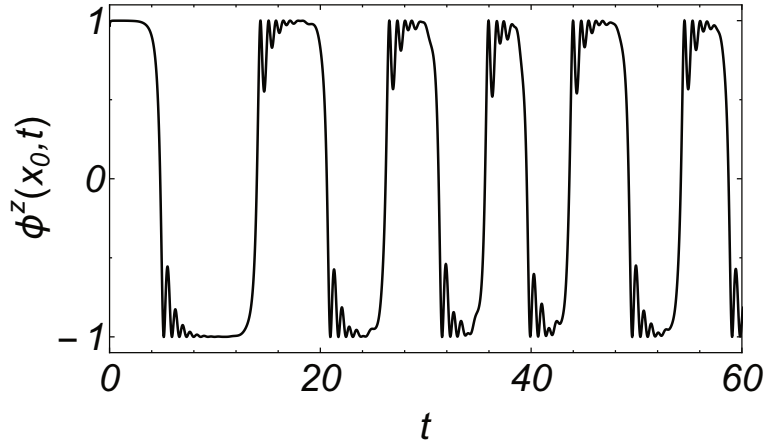


Figure 6.12 Time evolution of the order parameter field $\phi(x_0, t)$ at $D = 0.5, a = 0.01, J = 1, \alpha = 2, N = 400, x_0 = 150$ calculated with the coupled differential equations Eq. (6.37) for initial conditions close to the staggered antiferromagnetic state.

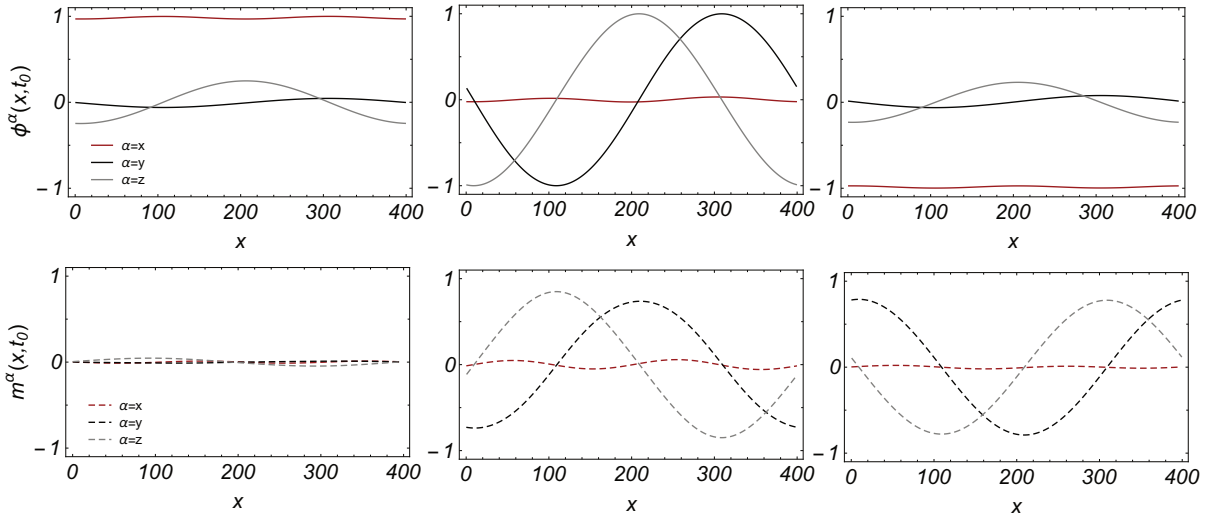


Figure 6.13 Spatial dependence of ϕ (upper row) and \mathbf{m} (lower row) at a time t_0 before (left), approximately at (middle) and after the transition (right). Parameters: $x_0 = 8, D = 0.5, a = 0.01, J = 1, \alpha = 2, N = 400$.

As an ansatz for ϕ we choose a linear combination of a constant field ϕ_0 and a spiral with the smallest possible non-zero momentum $|q| = 2\pi/L$ that varies periodically in the plane perpendicular to ϕ_0 . The relative strength between these two contributions is set by the phase $\varphi(t)$. For \mathbf{m} we make a simple long-wavelength spiral ansatz with $|q| = 2\pi/L$ and variable amplitude $m(t)$. This choice is motivated by the observation that the spatial dependence of $\phi(x, t_0)$ and $\mathbf{m}(x, t_0)$ presented in Fig. 6.13

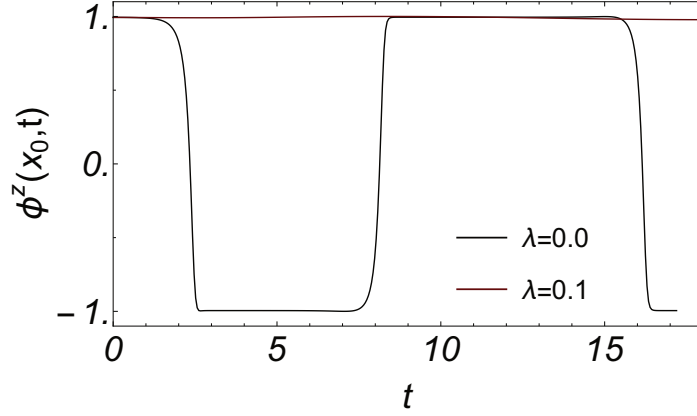


Figure 6.14 Time evolution of $\phi^z(x_0, t)$ including ($\lambda = 0.1$) and excluding ($\lambda = 0.0$) an explicit damping term in the equations of motion. Parameters: $x_0 = 1$, $D = 1.0$, $a = 0.01$, $J = 1$, $\alpha = 10$, $N = 100$.

contains only long-wavelength modes while $\mathbf{m}(x, t_0)$ has no constant contribution,

$$\begin{aligned}\boldsymbol{\phi}(x, t) &= \cos(\varphi(t))\mathbf{e}_z + \sin(\varphi(t))[\cos(qx)\mathbf{e}_x + \sin(qx)\mathbf{e}_y], \\ \mathbf{m}(x, t) &= m(t)[- \sin(qx)\mathbf{e}_x + \cos(qx)\mathbf{e}_y].\end{aligned}\quad (6.39)$$

Thus, we only consider two degrees of freedom $\varphi(t)$ and $m(t)$. The ansatz fulfills the constraints Eq. (6.30) by construction. Inserting Eq. (6.39) into the first differential equation yields

$$\partial_t m(t) = \alpha q \sin(\varphi(t)) \quad (6.40)$$

while the second differential equation simplifies to

$$\partial_t \varphi(t) = -4JSm(t). \quad (6.41)$$

Taking the derivative of Eq. (6.41) and using Eq.(6.40) yields the differential equation of a mathematical pendulum for the parameter φ ,

$$\ddot{\varphi}(t) + c \sin(\varphi(t)) = 0, \quad (6.42)$$

where we have set $c = 4JS\alpha q$. Eq. (6.42) can be solved exactly with the help of elliptic integrals or approximately in the small-angle approximation for small deviations from the stable state. Importantly, we obtain two solutions with $q = \pm 2\pi/L$. While for $\alpha > 0$ and $q > 0$ the configuration with $\varphi = 0$ is stable, the global minimum of the pendulum potential is at $\varphi = \pi$ for $q < 0$. The existence of these two solutions gives an explanation why we observe ongoing transitions in the numerical simulation of Eq. (6.37) at large system sizes.

Finally, we conclude with the numerical observation that including one of the possible explicit damping terms arising from the bath coupling does indeed remove the instability at $T = 0$ for certain parameters. The extended equations of motion then read

$$\begin{aligned}\dot{\mathbf{m}} &= S \partial_x \left(\left(J + \lambda \frac{d}{dt} m^2 \right) (\partial_x \boldsymbol{\phi} \times \boldsymbol{\phi}) \right) + \alpha \partial_x \boldsymbol{\phi} + D \partial_x^2 \mathbf{m}, \\ \dot{\boldsymbol{\phi}} &= 4S \left(J + \lambda \frac{d}{dt} m^2 \right) (\boldsymbol{\phi} \times \mathbf{m}).\end{aligned}\tag{6.43}$$

In Fig. 6.14 we show $\phi^z(x_0, t)$ for $\lambda = 0.0$ and $\lambda = 0.1$ where the system is, as before, initially prepared in a state with $\boldsymbol{\phi}(x, t) = \tilde{\boldsymbol{\phi}}_0(x)$ and $|\tilde{\boldsymbol{\phi}}_0(x) - \boldsymbol{\phi}_0| \ll 1$ for all x . While at $\lambda = 0.0$ the system shows transitions between the field configurations with $\boldsymbol{\phi} \approx \pm \boldsymbol{\phi}_0$, we find that at $\lambda = 0.1$ the initial state is stable.

There might be hope to observe the stabilization of long range order on the level of the field theoretical approach, which involves much less parameters than the full simulation, also at finite T .

Chapter 7

Conclusion and Outlook

In this thesis, we have shown that many-particle quantum systems can, by even small perturbations, be driven far out of equilibrium to highly exotic states hosting large currents. By pumping into degrees of freedom, which are approximately protected by symmetries, strong responses in the form of large steady state expectation values of the corresponding approximate conservation laws are induced.

We have developed a well-behaved perturbation theory for the steady state density matrix of weakly driven systems where we use a GGE defined by the balance of generalized heating and cooling processes as a zeroth order expansion point. We have validated the perturbative expansion for two fermionic models with two local conservation laws.

We have also applied the theory to weakly driven integrable systems that have an extensive set of local conserved quantities. We have given numerical and analytical evidence that the GGE ansatz indeed describes the steady state density matrix $\lim_{\varepsilon \rightarrow 0} \lim_{t \rightarrow \infty} \rho(t)$ correctly in the thermodynamic limit ($N \rightarrow \infty$) when all approximate conservation laws are included ($N_c \rightarrow \infty$). Even in the case of a truncated GGE with a moderate number of charges, we have found qualitatively good agreement with numerical exact calculations at small system sizes. However, due to strong finite size effects in the ED analysis, we have not been able to prove the validity of higher order corrections in ε rigorously. In a future study, such an analysis could be performed using more advanced methods such as DMRG. In this context, it would also be interesting to investigate whether the omission of conservation laws in the GGE ansatz is signaled by divergencies in the perturbation theory as pointed out in Sec. 2.3.2. Our numerical results also suggest that the time evolution of weakly open many-particle systems with approximate symmetries can be well captured by a time-dependent GGE at times $\tau \gtrsim 1$. However, a sophisticated analytical theory of the dynamics still has to be developed.

We have also used the concept of a GGE with space-dependent Lagrange parameters to describe inhomogeneous states in weakly open systems and derived a set of hydrodynamic equations for the simplified case in which conserved currents are forbidden by symmetry. Subsequently, we have presented two specific choices for Markovian Lindblad couplings, which can lead to such inhomogeneities. We believe that the investigation of phase transitions in weakly open quantum systems with approximate conservation laws is an interesting path for future research activities.

Eventually, a general theory is needed treating the time degree of freedom as well as perturbation strength and spatial variations on an equal footing. Such a theory is still missing.

We have made three suggestions of how the emergence of GGEs in weakly driven systems could be detected experimentally. Particularly, we have presented an idea of how to realize efficient spin and heat pumps in spin chain materials based on approximate integrability. As such pumps have not been realized yet, a future goal could be to find more candidates for spin chain materials whose lattice symmetries allow for finite spin and heat currents. Moreover, our analysis still has to be refined using a hydrodynamic approach to take account of the explicit spatial dependence of the problem.

Finally, we have addressed the question of how long range order can be stabilized in driven systems. Explicitly, we have considered the case where the order parameter is, by external driving, coupled linearly to the current of a conservation law that, in turn, is expected to stiffen the system. We have not observed such an effect in a classical simulation of our model but rather found an instability of the ordered state in the presence of the driving term. Nevertheless, we still think that the underlying physical motivation is reasonable and believe that the development of a minimal model, showing stabilization of long range order through a current, as well as further analysis of arising instabilities in this context, are of high interest and should be progressed in future research.

Bibliography

- [1] Sakurai, J. J. *Modern Quantum Mechanics* (Oxford University Press, New York, 2002).
- [2] Petruccione, F. & Breuer, H.-P. *The theory of open quantum systems* (Oxford Univ. Press, 2002).
- [3] Tong, D. Lectures on kinetic theory (2012). URL <http://www.damtp.cam.ac.uk/user/tong/kinetic.html>.
- [4] Auerbach, A. *Interacting Electrons and Quantum Magnetism* (Springer-Verlag, New York, 1994).
- [5] Hofstetter, W. & Qin, T. Master equations for coupled systems. *J. Phys. B: At. Mol. Opt. Phys.* **51**, 082001 (2018).
- [6] Weld, D. M. *et al.* Spin gradient thermometry for ultracold atoms in optical lattices. *Phys. Rev. Lett.* **103** (2009).
- [7] Hart, R. A. *et al.* Observation of antiferromagnetic correlations in the hubbard model with ultracold atoms. *Nature* **519**, 211–214 (2015).
- [8] Murmann, S. *et al.* Antiferromagnetic heisenberg spin chain of a few cold atoms in a one-dimensional trap. *Phys. Rev. Lett.* **115**, 215301 (2015).
- [9] Binder, F., Correa, L. A., Gogolin, C., Anders, J. & Adesso, G. *Thermodynamics in the Quantum Regime* (Springer-Verlag, New York, 2018).
- [10] Rigol, M., Dunjko, V. & Olshanii, M. Thermalization and its mechanism for generic isolated quantum systems. *Nature* **452**, 854–858 (2008).
- [11] Bocchieri, P. & Lionger, A. Spin gradient thermometry for ultracold atoms in optical lattices. *Phys. Rev.* **107**, 337–338 (1957).
- [12] Eberly, J. H., Narozhny, N. B. & Sanchez-Mondragon, J. J. Periodic spontaneous collapse and revival in a simple quantum model. *Phys. Rev.* **44**, 1323–1326 (1980).
- [13] Markov, M. A. *Group Theoretical Methods in Physics* (Harwood Academic Publishers, Volume 1, Chur, 1982).
- [14] Masoliver, J. & Ros, A. Integrability and chaos: the classical uncertainty. *Eur. J. Phys.* **32**, 431–456 (2011).
- [15] Bazhanov, V. & Burden, C. J. *Statistical Mechanics and Field Theory - Proceedings of the Seventh Physics Summer School* (World Scientific Publishing Company, Singapore, 1994).
- [16] Ilievski, E., Medenjak, M., Prosen, T. & Zadnik, L. Quasilocal charges in integrable lattice systems. *J. Stat. Mech.: Theory Exp.* **96**, 064008 (2016).

- [17] Larson, J. Integrability vs quantum thermalization. *J. Phys. B: At. Mol. Opt. Phys.* **46** (2013).
- [18] Sotiriadis, S., Calabrese, P. & Cardy, J. Quantum quench from a thermal initial state. *EPL* **87**, 20002 (2009).
- [19] Sotiriadis, S. & Martelloni, G. Equilibration and gge in interacting-to-free quantum quenches in dimensions $d > 1$. *J. Phys. A: Math. Theor.* **49**, 095002 (2016).
- [20] Iucci, A. & Cazalilla, M. A. Quantum quench dynamics of the luttinger model. *Phys. Rev. A* **80**, 063619 (2009).
- [21] Calabrese, P. & Cardy, J. Time dependence of correlation functions following a quantum quench. *Phys. Rev. Lett.* **96**, 136801 (2006).
- [22] Cardy, J. Thermalization and revivals after a quantum quench in conformal field theory. *Phys. Rev. Lett.* **112**, 220401 (2014).
- [23] Lieb, E. H. & Liniger, W. Exact analysis of an interacting bose gas. i. the general solution and the ground state. *Phys. Rev.* **130**, 1605–1616 (1963).
- [24] Lieb, E. H. Exact analysis of an interacting bose gas. ii. the excitation spectrum. *Phys. Rev.* **130**, 1616–1624 (1963).
- [25] Grabowski, M. P. & Mathieu, P. Structure of the conservation laws in integrable spin chains with short range interactions. *Annals of Physics* **243**, 299–371 (1995).
- [26] Vidmar, L. & Rigol, M. Generalized gibbs ensemble in integrable lattice models. *J. Stat. Mech.: Theory Exp.* **2016**, 064007 (2016).
- [27] Sachdev, S. *Quantum Phase Transitions, 2nd edition* (Camebridge University Press, Cambridge, 2011).
- [28] Shastry, B. S. Exact integrability of the one-dimensional hubbard model. *Phys. Rev. Lett.* **56**, 2453 (1986).
- [29] Lieb, E. H. & Wu, F. Y. Absence of mott transition in an exact solution of the short-range, one-band model in one dimension. *Phys. Rev. Lett.* **20**, 1445 (1968).
- [30] Levkovich-Maslyuk, F. Lectures on the bethe ansatz. *J. Phys. A* **49** (2016).
- [31] Braak, D. Integrability of the rabi model. *Phys. Rev. Lett.* **107**, 100401 (2011).
- [32] Casati, G. & Chirikov, V. Energy-level statistics of integrable quantum systems. *Phys. Rev. Lett.* **54**, 2626 (1985).
- [33] Scaramazza, J. A., Shastry, B. S. & Yuzbashyan, E. A. Integrable matrix theory: Level statistics. *Phys. Rev. E* **94**, 032106 (2016).
- [34] Uhrig, G. & Vollhardt, D. Drude weight and dc conductivity of correlated electrons. *Phys. Rev. B* **52**, 5617 (1995).
- [35] Herbrych, H., Prelovsek, P. & Zotos, X. Finite-temperature drude weight within the anisotropic heisenberg chain. *Phys. Rev. B* **84**, 155125 (2011).
- [36] Sirker, J., Pereira, R. G. & Affleck, I. Conservation laws, integrability and transport in one-dimensional quantum systems. *Phys. Rev. B* **83**, 035115 (2011).

- [37] Franchini, F. *An Introduction to Integrable Techniques for One-Dimensional Quantum Systems* (World Scientific Publishing Company, New York, 2017).
- [38] Sakai, K. & Klümper, A. The thermal conductivity of the spin-1/2 xxz chain at arbitrary temperature. *J. Phys. A: Math. Gen.* **34**, 8015 (2001).
- [39] Zotos, X. Finite temperature drude weight of the one-dimensional spin- 1/2 heisenberg model. *Phys. Rev. Lett.* **82**, 1764 (1999).
- [40] Prosen, T. Open xxz spin chain: Nonequilibrium steady state and a strict bound on ballistic transport. *Phys. Rev. Lett.* **106**, 217206 (2011).
- [41] Prosen, T. & Ilievski, E. Families of quasilocal conservation laws and quantum spin transport. *Phys. Rev. Lett.* **111**, 057203 (2013).
- [42] Jarzynski, C. Equalities and inequalities: Irreversibility and the second law of thermodynamics at nanoscale. *Seminaire Poicare* **77**, 102 (2010).
- [43] Evans, D. J., Cohen, E. G. D. & Morriss, G. P. Probability of second law violations in shearing steady states. *Phys. Rev. Lett.* **71**, 3616–3616 (1993).
- [44] Lux, J. Fluctuations in and out of equilibrium: Thermalization, quantum measurements and coulomb disorder. *PhD thesis* (2016).
- [45] Shannon, C. E. & Weaver, W. *Mathematical Theory of communication* (Combined Academic Publ., Harrogate, 1963).
- [46] Takahashi, K., Nishimori, H. & Martin-Mayor, V. Ensemble equivalence in spin systems with short-range interactions. *J. Stat. Mech.* **2011**, 08024 (2011).
- [47] Neill, C. *et al.* Ergodic dynamics and thermalization in an isolated quantum system. *Nature* **12**, 1037–1041 (2016).
- [48] Srednicki, M. Chaos and quantum thermalization. *Phys. Rev. E* **50**, 888 (1994).
- [49] Lieb, E. & Robinson, D. The finite group velocity of quantum spin systems. *Commun. Math. Phys.* **28**, 251–257 (1972).
- [50] Deutsch, J. M. Quantum statistical mechanics in a closed system. *Physical Review A*. **43**, 2046 (1991).
- [51] Srednicki, M. Chaos and quantum thermalization. *Phys. Rev. E*. **50**, 888 (1994).
- [52] Pal, A. Many-body localization. *PhD thesis* (2012).
- [53] D’Alessio, L., Kafri, Y., Polkovnikov, A. & Rigol, M. From quantum chaos and eigenstate thermalization to statistical mechanics and thermodynamics. *Advances in Physics* **65**, 239–362 (2016).
- [54] Pal, A. & Huse, D. A. Many-body localization phase transition. *Phys. Rev. B* **82**, 174411 (2010).
- [55] Altman, E. Many-body localization and quantum thermalization. *Nature Physics* **14**, 979–983 (2018).
- [56] Abanin, D. A., Altman, E., Bloch, I. & Serbyn, M. Colloquium: Many-body localization, thermalization, and entanglement. *Rev. Mod. Phys.* **91**, 021001 (2019).

- [57] Nandkishore, R. & Gopalakrishnan, S. Many body localized systems weakly coupled to baths. *Annalen der Physik* **529** (2017).
- [58] Kinoshita, T., T. W. & Weiss, D. S. A quantum newton's cradle. *Nature Physics* **440**, 900–903 (2006).
- [59] Rigol, M., Dunjko, V., Yurovsky, V. & Olshanii, M. Relaxation in a completely integrable many-body quantum system: An *Ab Initio* study of the dynamics of the highly excited states of 1d lattice hard-core bosons. *Phys. Rev. Lett.* **98**, 050405 (2007).
- [60] Essler, F. H. L. & Fagotti, M. Quench dynamics and relaxation in isolated integrable quantum spin chains. *J. Stat. Mech.: Theory Exp.* **2016**, 064002 (2016).
- [61] Moeckel, M. & Kehrein, S. Interaction quench in the hubbard model. *Phys. Rev. Lett.* **100**, 175702 (2008).
- [62] Kollar, M., Wolf, F. A. & Eckstein, M. Generalized gibbs ensemble prediction of prethermalization plateaus and their relation to nonthermal steady states in integrable systems. *Physical Review B* **84**, 054304 (2011).
- [63] Wouters, B. *et al.* Quenching the anisotropic heisenberg chain: Exact solution and generalized gibbs ensemble predictions. *Phys. Rev. Lett.* **113**, 117202 (2014).
- [64] Pozsgay, B. *et al.* Correlations after quantum quenches in the xxz spin chain: Failure of the generalized gibbs ensemble. *Phys. Rev. Lett.* **113**, 117203 (2014).
- [65] Mestyán, M., Pozsgay, B., Takács, G. & Werner, M. A. Quenching the xxz spin chain: quench action approach versus generalized gibbs ensemble. *J. Stat. Mech.: Theory and Exp.* **2015**, 04001 (2015).
- [66] Ilievski, E. *et al.* Complete generalized gibbs ensembles in an interacting theory. *Phys. Rev. Lett.* **115**, 157201 (2015).
- [67] Caux, J.-S. The quench action. *J. Stat. Mech.: Theory and Exp.* **2016**, 064006 (2016).
- [68] Caux, J.-S. & Essler, F. H. L. Time evolution of local observables after quenching to an integrable model. *Phys. Rev. Lett.* **110**, 257203 (2013).
- [69] Brockmann, M. *et al.* Quench action approach for releasing the néel state into the spin-1/2 xxz chain. *J. Stat. Mech.: Theory and Exp.* **2014**, 12009 (2014).
- [70] Langen, T. *et al.* Experimental observation of a generalized gibbs ensemble. *Science* **348**, 207–211 (2015).
- [71] Hinrichsen, H. Non-equilibrium phase transitions. *Physica A* **369**, 1–28 (2006).
- [72] Dittrich, T. *et al.* *Quantum Transport and Dissipation* (Wiley-VCH, Weinheim, 1998).
- [73] Eckardt, A. Colloquium: Atomic quantum gases in periodically driven optical lattices. *Reviews of Modern Physics* **89** (2017).
- [74] Genske, M. Periodically driven many-body quantum systems quantum ratchets, topological states and the floquet-boltzmann equation. *PhD thesis* (2017).
- [75] Abanin, D. A., De Roeck, W., Ho, W. W. & Huvneers, F. Effective hamiltonians, prethermalization, and slow energy absorption in periodically driven many-body systems. *Phys. Rev. B* **95**, 014112 (2017).

- [76] Genske, M. & Rosch, A. Floquet-boltzmann equation for periodically driven fermi systems. *Phys. Rev. A* **92**, 062108 (2015).
- [77] Hohenberg, P. C. & Halperin B., I. Theory of dynamic critical phenomena. *Rev. Mod. Phys.* **49** (1977).
- [78] Greiner, M., Mandel, O., Esslinger, T., Hänsch, T. W. & Bloch, I. Quantum phase transition from a superfluid to a mott insulator in a gas of ultracold atoms. *Nature* **415**, 39–44 (2002).
- [79] Dubi, Y., Meir, Y. & Avishai, Y. Nature of the superconductor–insulator transition in disordered superconductors. *Nature* **449**, 876–880 (2007).
- [80] Wolf, D. E., Schreckenberg, M. & Bachem, A. *Traffic and granular flow* (World Scientific, Singapore, 1996).
- [81] Barabási, A. L. & Stanley, H. *Fractal concepts in surface growth* (ambridge University Press, Cambridge, 1995).
- [82] Buchhold, M., Everest, M., B. Marcuzzi, Lesanovsky, I. & Diehl, S. Non-equilibrium effective field theory for absorbing state phase transitions in driven open quantum spin systems. *Phys. Rev. B* **95**, 014308 (2017).
- [83] Van den Broeck, C., Parrondo, J. M. R. & Toral, R. Noise-induced nonequilibrium phase transition. *Phys. Rev. Lett.* **73**, 3395 (1994).
- [84] Sandvik, A. W. Computational studies of quantum spin systems. *AIP Conf. Proc.* **1297** (2010).
- [85] Gardiner, C. W. *Handbook of Stochastic Methods* (Springer Verlag, 2nd Edition, Berlin, 1985).
- [86] Kunita, H. Effective hamiltonians, prethermalization, and slow energy absorption in periodically driven many-body systems. *Stochastic Processes and their Application* **120**, 622–652 (2010).
- [87] Lenarčič, Z., Lange, F. & Rosch, A. Perturbative approach to weakly driven many-particle systems in the presence of approximate conservation laws. *Phys. Rev. B* **97**, 024302 (2018).
- [88] Essler, F. H. L., Kehrein, S., Manmana, S. R. & Robinson, N. J. Quench dynamics in a model with tuneable integrability breaking. *Phys. Rev. B* **89**, 165104 (2014).
- [89] Calabrese, P. & Cardy, J. Quantum quenches in 1+1 dimensional conformal field theories. *J. Stat. Mech.: Theory and Exp.* **2016**, 064003 (2016).
- [90] Kawasaki, K. & Gunton, J. D. Theory of nonlinear transport processes: Nonlinear shear viscosity and normal stress effects. *Phys. Rev. A* **8**, 063604 (1973).
- [91] Robertson, B. Equations of motion in nonequilibrium statistical mechanics. *Phys. Rev.* **144**, 151 (1966).
- [92] Robertson, B. Equations of motion in nonequilibrium statistical mechanics. ii. energy transport. *Phys. Rev.* **160**, 206 (1968).
- [93] Ochiai, M. A new derivation of a kinetic equation in statistical-mechanical theory. *Phys. Rev. A* **44**, 145 (1973).
- [94] Willis, C. R. & Picard, R. H. Time-dependent projection-operator approach to master equations for coupled systems. *Phys. Rev. A* **9**, 1343 (1974).

- [95] Grabert, H. & Weidlich, W. Masterequation, h-theorem and stationary solution for coupled quantum systems. *Z. Phys.* **268**, 139 (1974).
- [96] Jung, P., Helmes, R. W. & Rosch, A. Transport in almost integrable models: Perturbed heisenberg chains. *Phys. Rev. Lett.* **96**, 067202 (2006).
- [97] Forster, D. *Hydrodynamic fluctuations, broken symmetry, and correlation functions*, vol. 47 (Reading, Mass., WA Benjamin, Inc.(Frontiers in Physics), 1975).
- [98] Mazur, P. Non-ergodicity of phase functions in certain systems. *Physica* **43**, 533–545 (1969).
- [99] Suzuki, M. Ergodicity, constants of motion, and bounds for susceptibilities. *Physica* **51**, 277–291 (1971).
- [100] Lange, F., Lenarčič, Z. & Rosch, A. Time-dependent generalized gibbs ensembles in open quantum systems. *Phys. Rev. B* **97**, 165138 (2018).
- [101] Calabrese, P., Essler, F. H. L. & Fagotti, M. Quantum quench in the transverse field ising chain: I. time evolution of order parameter correlators. *J. Stat. Mech.: Theory and Exp.* **2012**, 07016 (2012).
- [102] Calabrese, P., Essler, F. H. L. & Fagotti, M. Quantum quenches in the transverse field ising chain: II. stationary state properties. *J. Stat. Mech.: Theory and Exp.* **2012**, 07022 (2012).
- [103] Fagotti, M. & Essler, F. H. L. Reduced density matrix after a quantum quench. *Phys. Rev. B* **87**, 245107 (2013).
- [104] Sotiriadis, S. & Calabrese, P. Validity of the gge for quantum quenches from interacting to noninteracting models. *J. Stat. Mech.: Theory and Exp.* **2014**, 07024 (2014).
- [105] Bertini, B., Essler, F. H. L., Groha, S. & Robinson, N. J. Prethermalization and thermalization in models with weak integrability breaking. *Phys. Rev. Lett.* **115**, 180601 (2015).
- [106] Lange, F. Weakly driven many-particle quantum systems. *Master thesis* (2016).
- [107] Klaers, J., Schmitt, J., Vewinger, F. & Weitz, M. Bose-einstein condensation of photons in an optical microcavity. *Nature* **468**, 545–548 (2010).
- [108] Demokritov, S. *et al.* Bose–einstein condensation of quasi-equilibrium magnons at room temperature under pumping. *Nature* **443**, 430–433 (2006).
- [109] Butov, L. V. *et al.* Stimulated scattering of indirect excitons in coupled quantum wells: Signature of a degenerate bose-gas of excitons. *Phys. Rev. Lett.* **86**, 5608 (2001).
- [110] Kasprzak, J. *et al.* Bose-einstein condensation of exciton polaritons. *Nature* **443**, 409–414 (2006).
- [111] Lange, F., Lenarčič, Z. & Rosch, A. Pumping approximately integrable systems. *Nature communications* **8**, 15767 (2017).
- [112] Nojiri, H., Ajiro, Y., Asano, T. & Boucher, J. Magnetic excitation of $s = 1/2$ antiferromagnetic spin chain Cu benzoate in high magnetic fields. *New Journal of Physics* **8**, 218 (2006).
- [113] Kimura, S. *et al.* Collapse of magnetic order of the quasi one-dimensional ising-like antiferromagnet BaCo₂V₂O₈ in transverse fields. *Journal of the Physical Society of Japan* **82**, 033706 (2013).

- [114] Niesen, S. K. *et al.* Substitution effects on the temperature versus magnetic field phase diagrams of the quasi-one-dimensional effective ising spin- $\frac{1}{2}$ chain system $\text{BaCo}_2\text{V}_2\text{O}_8$. *Phys. Rev. B* **90**, 104419 (2014).
- [115] Oshikawa, M. & Affleck, I. Field-induced gap in $s=1/2$ antiferromagnetic chains. *Phys. Rev. Lett.* **79**, 2883 (1997).
- [116] Dender, D. C., Hammar, P. R., Reich, D. H., Broholm, C. & Aeppli, G. Direct observation of field-induced incommensurate fluctuations in a one-dimensional $s=1/2$ antiferromagnet. *Phys. Rev. Lett.* **79**, 1750 (1997).
- [117] Affleck, I. & Oshikawa, M. Field-induced gap in Cu benzoate and other $s = \frac{1}{2}$ antiferromagnetic chains. *Phys. Rev. B* **60**, 1038 (1999).
- [118] Kittel, C. *Introduction to Solid State Physics* (John Wiley & Sons, New York, 8 Auflage, 2004).
- [119] Temme, K., Pastawski, F. & Kastoryano, M. J. Hypercontractivity of quasi-free quantum semigroups. *J. Phys. A: Math. Theor.* **47**, 40 (2014).
- [120] Porras, D. & Cirac, J. I. Effective quantum spin systems with trapped ions. *Appl. Phys. Lett.* **92**, 207901 (2004).
- [121] Zalivako, I. *et al.* Nonselective paul ion trap loading with a light-emitting diode. *Appl. Phys. Lett.* **115**, 104102 (2019).
- [122] Britton, J. W. *et al.* Engineered two-dimensional ising interactions in a trapped-ion quantum simulator with hundreds of spins. *Nature* **484**, 489–492 (2012).
- [123] Graß, T. & Lewenstein, M. Trapped-ion quantum simulation of tunable-range heisenberg chains. *EPJ Quantum Technology* **1** (2014).
- [124] Reiter, F., Lange, F. & Lenarčič, Z. *arXiv:1910.01593* (2019).
- [125] Balescu, R. *Equilibrium and Non-equilibrium Statistical Mechanics* (John Wiley & Sons, New York, 1987).
- [126] Doyon, B. Emergent hydrodynamics in integrable systems out of equilibrium. *Cargèse, Corsica* (2017). URL https://indico.in2p3.fr/event/14018/images/1094-GHD_DoyonCargese2017.pdf.
- [127] Nardis, J. D., Bernard, D. & Doyon, B. Diffusion in generalized hydrodynamics and quasiparticle scattering. *SciPost Phys.* **6**, 49 (2019).
- [128] Doyon, B. & Yoshimura, T. A note on generalized hydrodynamics: inhomogeneous fields and other concepts. *SciPost Phys.* **2**, 014 (2017).
- [129] Castro-Alvaredo, O. A., Doyon, B. & Yoshimura, T. Emergent hydrodynamics in integrable quantum systems out of equilibrium. *Phys. Rev. X* **6**, 041065 (2016).
- [130] Bertini, B., Collura, M., De Nardis, J. & Fagotti, M. Transport in out-of-equilibrium xxz chains: Exact profiles of charges and currents. *Phys. Rev. Lett.* **117**, 207201 (2016).
- [131] Lam, C. Decomposition of time-ordered products and path-ordered exponentials. *J. Math. Phys.* **39**, 5543 (1998).
- [132] Mermin, N. D. & Wagner, H. Absence of ferromagnetism or antiferromagnetism in one- or two-dimensional isotropic heisenberg models. *Phys. Rev. Lett.* **17**, 1133 (1966).

-
- [133] Goldstone, J., Salam, A. & Weinberg, S. Broken symmetries. *Phys. Rev.* **127**, 965 (1962).
- [134] Manousakis, E. The spin-1/2 heisenberg antiferromagnet on a square lattice and its application to the cuprous oxides. *Rev. Mod. Phys.* **63**, 1 (1991).
- [135] Ivanov, N. B. & Sen, D. Spin wave analysis of heisenberg magnets in restricted geometries. *Lect. Notes Phys.* 195–226 (2004).
- [136] Vicsek, T., Czirók, A., Ben-Jacob, E., Cohen, I. & Shochet, O. Novel type of phase transition in a system of self-driven particles. *Phys. Rev. Lett.* **75**, 1226 (1995).
- [137] Kosterlitz, J. & Thouless, D. Ordering, metastability and phase transitions in two-dimensional systems. *J. Phys. C* **6**, 1181 (1973).
- [138] Toner, J. & Tu, Y. Long-range order in a two-dimensional dynamical xy model: How birds fly together. *Phys. Rev. Lett.* **75**, 4326 (1995).
- [139] Weiss, U. *Quantum Dissipative Systems* (World Scientific, Singapore, 1993).
- [140] Weigert, S. & Müller, G. Quantum integrability and action operators in spin dynamics. *Chaos, Solitons and Fractals* **5**, 1419–1438 (1995).
- [141] Bui, T. Explicit and implicit methods in solving differential equations. *Honors Scholar Theses* **119** (2010).
- [142] Hairer, E. Symmetric projection methods for differential equations on manifolds. *BIT* **40**, 726–734 (2000).
- [143] Tveten, E. G., Müller, T., Linder, J. & Brataas, A. Intrinsic magnetization of antiferromagnetic textures. *Phys. Rev. B.* **93**, 104408 (2016).
- [144] Haldane, F. D. M. Nonlinear field theory of large-spin heisenberg antiferromagnets: Semiclassically quantized solitons of the one-dimensional easy-axis néel state. *Phys. Rev. Lett.* **50**, 1153 (1983).

Appendix A

Zeroth order expansion point

Note that this appendix is taken from [87]. Here, we show that the condition (2.10),

$$\hat{P}(\hat{\mathcal{L}}_1 \hat{\mathcal{L}}_0^{-1} \hat{\mathcal{L}}_1 \rho_0) = 0, \quad (\text{A.1})$$

does give the correct reference point ρ_0 for situations where $\hat{P} \hat{\mathcal{L}}_1 \hat{P} = 0$. One way to show this is to use the perturbative analysis provided in Sec. 2.3.3 where the power counting of diagrams worked only if the correct reference point was chosen. Below we give a more direct argument. As described in the main text, Eq. (A.1) is obtained from the requirement that the dominant contribution to the time-averaged expectation value of conserved quantities must vanish,

$$\overline{\langle \hat{C}_i \rangle} = \text{Tr}[C_i \hat{P} \hat{\mathcal{L}}_1 (\rho_0 + \delta\rho)] = \text{Tr}[C_i \hat{P} \hat{\mathcal{L}}_1 \delta\rho] \stackrel{!}{=} 0, \quad (\text{A.2})$$

where \hat{P} is used to extract the non-oscillatory component and $\text{Tr}[C_i \hat{P} \hat{\mathcal{L}}_1 \rho_0] = 0$ due to the cyclicity of trace. As discussed in the main text, the starting point is the exact formula for $\delta\rho$, Eq. (2.4) and the formula Eq. (2.8) which directly leads to

$$\begin{aligned} \delta\rho &= \delta\rho^{(I)} + \delta\rho^{(II)} \\ &= -\hat{\mathcal{L}}_0^{-1} \hat{\mathcal{L}}_1 \rho_0 + \hat{\mathcal{L}}^{-1} \hat{\mathcal{L}}_1 \hat{\mathcal{L}}_0^{-1} \hat{\mathcal{L}}_1 \rho_0. \end{aligned} \quad (\text{A.3})$$

If we use only $\delta\rho^{(I)}$ in Eq. (A.2), then Eq. (A.1) follows immediately. Equivalently, the condition Eq. (A.1) implies that the contribution from $\delta\rho^{(I)}$ vanishes in Eq. (A.2). In the following we will show that Eq. (A.1) also implies that the contribution from $\delta\rho^{(II)}$ to Eq. (A.2) vanishes, which is less obvious, and a useful consistency check. Plugging $\delta\rho^{(II)}$ into Eq. (A.2) one finds

$$\begin{aligned} &\text{Tr}[C_i \hat{P} \hat{\mathcal{L}}_1 \delta\rho^{(II)}] \\ &= \text{Tr}[C_i \hat{P} \hat{\mathcal{L}}_1 \hat{\mathcal{L}}^{-1} \hat{\mathcal{L}}_1 \hat{\mathcal{L}}_0^{-1} \hat{\mathcal{L}}_1 \rho_0] \\ &= \text{Tr}[C_i \hat{P} \hat{\mathcal{L}}_1 \hat{\mathcal{Q}} \hat{\mathcal{L}}^{-1} \hat{\mathcal{Q}} \hat{\mathcal{L}}_1 \hat{\mathcal{L}}_0^{-1} \hat{\mathcal{L}}_1 \rho_0] = 0 \end{aligned} \quad (\text{A.4})$$

where the third line differs from the first one by two extra \hat{Q} super-operators enclosing $\hat{\mathcal{L}}^{-1}$. The first one can be inserted because we consider the case $\hat{P}\hat{\mathcal{L}}_1\hat{P} = 0$ and therefore $\hat{P}\hat{\mathcal{L}}_1 = \hat{P}\hat{\mathcal{L}}_1\hat{Q}$. The second one can be used as a consequence of Eq. (A.1), which states that the \hat{P} projection of the operator to the right of $\hat{\mathcal{L}}^{-1}$ vanishes. Finally, we can use that $\hat{Q}\hat{\mathcal{L}}^{-1}\hat{Q} = 0$, see Eq. (2.38), to prove that the whole expression vanishes. To finish our argument, we still have to show that $\delta\rho$ is small for $\varepsilon \rightarrow 0$ provided that Eq. (2.38) holds, which can be done using similar arguments as above. First, the combination $\hat{\mathcal{L}}_0^{-1}\hat{\mathcal{L}}_1\rho_0 = \hat{\mathcal{L}}_0^{-1}\hat{Q}\hat{\mathcal{L}}_1\rho_0$ is non-singular for $\hat{P}\hat{\mathcal{L}}_1\hat{P} = 0$ which implies that $\delta\rho^{(I)} \sim \mathcal{O}(\varepsilon)$. Second, we used already above that $\delta\rho^{(II)} = \hat{\mathcal{L}}^{-1}\hat{\mathcal{L}}_1\hat{\mathcal{L}}_0^{-1}\hat{\mathcal{L}}_1\rho_0 = \hat{\mathcal{L}}^{-1}\hat{Q}\hat{\mathcal{L}}_1\hat{\mathcal{L}}_0^{-1}\hat{\mathcal{L}}_1\rho_0$. As $\hat{Q}\hat{\mathcal{L}}^{-1}\hat{Q} = 0$ and $\hat{P}\hat{\mathcal{L}}^{-1}\hat{Q} \sim \mathcal{O}(1/\varepsilon)$ it follows immediately that also $\delta\rho^{(II)} \sim \mathcal{O}(\varepsilon)$ which concludes the derivation of Eq. (A.1).

Appendix B

Thermal state of the weakly open spin chain in the Ising limit

In this appendix we calculate the steady state density matrix $\rho_0 \sim e^{-\beta H_0}$, fulfilling $\mathcal{L}_1 \rho_0 = 0$, for the case described in Sec. 3.4. In the Ising limit ($J \rightarrow 0$) the Hamiltonian of the XXZ model simplifies to $H_0 = \Delta \sum_j \sigma_j^z \sigma_{j+1}^z$. We obtain

$$\hat{\mathcal{D}}^{(1)} \rho = \sum_j \sigma_j^x e^{-\beta H} \sigma_j^x - \frac{1}{2} \left(\sigma_j^x \sigma_j^x e^{-\beta H} + e^{-\beta H} \sigma_j^x \sigma_j^x \right) = e^{-\beta H} \sum_j \left(e^{2\beta \Delta \sigma_j^z (\sigma_{j-1}^z + \sigma_{j+1}^z)} - \mathbb{1} \right)$$

and

$$\begin{aligned} \hat{\mathcal{D}}^{(2)} \rho &= \sum_j P_j^\uparrow \sigma_{j+1}^+ e^{-\beta H} P_j^\uparrow \sigma_{j+1}^- - \frac{1}{2} \left\{ P_j^\uparrow P_j^\downarrow, e^{-\beta H} \right\} + \sum_j P_j^\downarrow \sigma_{j+1}^- e^{-\beta H} P_j^\downarrow \sigma_{j+1}^+ - \frac{1}{2} \left\{ P_j^\downarrow P_j^\uparrow, e^{-\beta H} \right\} \\ &= e^{-\beta H} \left(P_j^\uparrow P_{j+1}^\uparrow e^{2\beta \Delta \sigma_j^z (\sigma_{j-1}^z + \sigma_{j+1}^z)} - P_j^\uparrow P_{j+1}^\downarrow + P_j^\downarrow P_{j+1}^\downarrow e^{2\beta \Delta \sigma_j^z (\sigma_{j-1}^z + \sigma_{j+1}^z)} - P_j^\downarrow P_{j+1}^\uparrow \right). \end{aligned}$$

For the calculation of $\hat{\mathcal{D}}^{(i)} \rho$ ($i = 1, 2$), the following relations have been used

$$\begin{aligned} H \sigma_j^x &= \sigma_j^x H + [H, \sigma_j^x] = \sigma_j^x \left(H - 2\sigma_j^z (\sigma_{j-1}^z + \sigma_{j+1}^z) \right), \\ H \sigma_{j+1}^- &= \sigma_{j+1}^- H + [H, \sigma_{j+1}^-] = \sigma_{j+1}^- H + \frac{1}{2} \left([H, \sigma_{j+1}^x] - i[H, \sigma_{j+1}^y] \right) \\ &\quad \sigma_{j+1}^- (H - 2\sigma_j^z (\sigma_{j-1}^z + \sigma_{j+1}^z)), \end{aligned}$$

where the commutators of H with σ_j^x and σ_j^y are given by

$$\begin{aligned} [H, \sigma_j^x] &= \sum_k [\sigma_k^z \sigma_{k+1}^z, \sigma_j^x] = \sum_k \left(\underbrace{\delta_{jk} [\sigma_j^z, \sigma_j^x]}_{=2i\sigma_j^y} \sigma_{j+1}^z + \delta_{jk+1} \sigma_{j-1}^z \underbrace{[\sigma_j^z, \sigma_j^x]}_{=2i\sigma_j^y} \right) \\ &= 2i\sigma_j^y \sigma_{j+1}^z + 2i\sigma_{j-1}^z \sigma_j^y = -2\sigma_j^x (\sigma_j^z \sigma_{j+1}^z + \sigma_{j-1}^z \sigma_j^z), \end{aligned}$$

$$\begin{aligned}
[H, \sigma_j^y] &= \sum_k [\sigma_k^z \sigma_{k+1}^z, \sigma_j^y] = \sum_k \left(\underbrace{\delta_{jk} [\sigma_j^z, \sigma_j^y] \sigma_{j+1}^z}_{=-2i\sigma_j^x} + \delta_{jk+1} \sigma_{j-1}^z \underbrace{[\sigma_j^z, \sigma_j^y]}_{=-2i\sigma_j^x} \right) \\
&= -2i\sigma_j^x \sigma_{j+1}^z - 2i\sigma_{j-1}^z \sigma_j^x = -2\sigma_j^y (\sigma_j^z \sigma_{j+1}^z + \sigma_{j-1}^z \sigma_j^z).
\end{aligned}$$

In the steady state the time derivative of ρ is zero, therefore we have $\left[(1-\gamma)\hat{\mathcal{D}}^{(1)} + \gamma\hat{\mathcal{D}}^{(2)} \right] \rho = 0$. Using the ansatz $\beta(\gamma) = \frac{1}{4\Delta} \log(1-\gamma)$ the steady state equation is equivalent to

$$\sum_j \left[\gamma \left(P_j^\uparrow P_{j+1}^\uparrow + P_j^\downarrow P_{j+1}^\downarrow \right) + (1-\gamma) \right] e^{\frac{1}{2} \log(1-\gamma) \sigma_j^z (\sigma_{j-1}^z + \sigma_{j+1}^z)} = \sum_j \left[(1-\gamma) + \gamma \left(P_j^\downarrow P_{j+1}^\uparrow + P_j^\uparrow P_{j+1}^\downarrow \right) \right].$$

In the following we show that a thermal state with $\beta(\gamma) = \frac{1}{4\Delta} \log(1-\gamma)$ is indeed a steady state solution. Thus, we have to verify that the left and the right side of the equation are identical. To this end, we define

- number of parallel spin pairs with a left parallel neighbour: N_p^p
- number of parallel spin pairs with a left anti-parallel neighbour: N_p^a
- number of parallel spin pairs: $N_p = N_p^p + N_p^a$
- number of anti-parallel spin pairs with a left parallel neighbour: N_a^p
- number of anti-parallel spin pairs with a left anti-parallel neighbour: N_a^a
- number of parallel spin pairs: $N_a = N_a^p + N_a^a$

$$\underline{\text{left side:}} \quad (1-\gamma)N + \gamma N_a$$

$$\underline{\text{right side:}} \quad (1-\gamma)N_a^p + (1-\gamma)N_p^p + N_p^a + N_a^a$$

Due to the periodic boundary conditions, we have $N_a^p = N_p^a$. Therefore, the left side can be expressed as

$$\begin{aligned}
(1-\gamma)N_a^p + (1-\gamma)N_p^p + N_p^a + N_a^a &= (1-\gamma)(N_a^p + N_p^p + N_p^a + N_a^a) - (1-\gamma)(N_p^a + N_a^a) + N_a^a + N_p^a \\
&= (1-\gamma)N + \gamma(N_p^a + N_a^a) = (1-\gamma)N + \gamma N_a.
\end{aligned}$$

Appendix C

Phase transitions in weakly open spin chains

In the following, we consider a non-integrable spin chain, for example, a XXZ model with an additional next-nearest neighbor coupling term

$$H_0 = H_{XXZ} + J_\perp \sum_j \left(S_j^+ S_{j+2}^- + S_j^- S_{j+2}^+ \right) \quad (\text{C.1})$$

which is defined such that the total spin in z -direction is conserved. The spin chain is assumed to be weakly coupled to a Markovian bath that has been defined in Sec. 5.2.1. First, we simplify the expression for the generalized current J_{ij} ,

$$\begin{aligned} J_{ij}(r_0, t) &:= \int dr \int_{-\infty}^t dt' \frac{1}{\lambda_2(r_0, t')} \int_0^{\lambda_2(r_0, t')} d\tau \sigma_{ij}(r, r_0; t, t') \partial_r \lambda_j(r, t') \\ &= \int dr \int_0^\infty d\tilde{t} \frac{1}{\lambda_2(r_0, t - \tilde{t})} \int_0^{\lambda_2(r_0, t - \tilde{t})} d\tau \text{Tr} \left[j_j(r, \tau) j_i(r_0, \tilde{t}) \rho_{GGE, r_0}(t - \tilde{t}) \right] \partial_r \lambda_j(r, t - \tilde{t}) \\ &\approx \int dr \int_0^\infty d\tilde{t} \frac{1}{\lambda_2(r_0, t)} \int_0^{\lambda_2(r_0, t)} d\tau \text{Tr} \left[j_j(r, \tau) j_i(r_0, \tilde{t}) \rho_{GGE, r_0}(t) \right] \partial_r \lambda_j(r, t). \end{aligned} \quad (\text{C.2})$$

In the last line, we use the assumption that the time scales of the slow macroscopic and the fast microscopic dynamics are well separated and replace the time argument $t - \tilde{t}$ in $\nabla \lambda_j$, λ_j and ρ_{GGE, r_0} by t . For local current operators, we assume that the current-current correlation functions appearing in the formula for the conductivity are strongly peaked at $r = r_0$ meaning that $\langle j_j(r, \tau) j_i(r_0, \tilde{t}) \rangle_{GGE, r_0} \sim \delta(r - r_0)$ for $i, j = 1, 2$. Subsequently, this motivates to define

$$\tilde{L}_{ij} := \frac{1}{N} \int_0^\infty d\tilde{t} \frac{1}{\lambda_2(r_0, t)} \int_0^{\lambda_2(r_0, t)} d\tau \langle j_j(\tau) j_i(\tilde{t}) \rangle_{GGE, 0}.$$

Using this definition we obtain the following formulas for the generalized spin and heat current

$$\begin{aligned} J_1(r,t) &= \tilde{L}_{11} \partial_r \lambda_1(r,t) + \tilde{L}_{12} \partial_r \lambda_2(r,t), \\ J_2(r,t) &= \tilde{L}_{21} \partial_r \lambda_1(r,t) + \tilde{L}_{22} \partial_r \lambda_2(r,t), \end{aligned}$$

where the diagonal contributions are manifestations of Fick's law. Note that the different sign compared to the usual formulation of Fick's law is a consequence of the minus sign in the definition of the GGE, i.e. for an increasing value of the Lagrange parameter λ_i , the expectation value $\langle C_i \rangle_{GGE,0}$ decreases. Using Lehman representation we obtain for the real part of \tilde{L}_{ij} ,

$$\text{Re}[\tilde{L}_{ij}] = \frac{\pi}{N} \sum_{n,m} \langle n|j_j|m\rangle \langle m|j_i|n\rangle \delta(E_m - E_n) \langle n|\rho_{GGE,0}|n\rangle. \quad (\text{C.3})$$

Next, we reduce the analysis to mean-field level where the GGE ansatz simplifies to $\rho_{MF}(t) \sim \exp(-\lambda_1(t)S^\varepsilon)$. As mentioned in Sec. 5.2.1, we expect that stable configurations with domain walls exist. In order to investigate the typical length of a domain wall in dependence of the perturbation strength ε , we simulate the dynamics of the system by solving

$$\partial_t \lambda_1(r,t) - D \partial_r^2 \lambda_1(r,t) = F(\lambda_1) \quad (\text{C.4})$$

on a one-dimensional grid with periodic boundary conditions. We define the diffusion constant as $D := (\chi^{-1})_{11} \text{Re}[\tilde{L}_{11}]$ where we assume that $\text{Re}[\tilde{L}_{11}]$ is constant. Calculations of Eq. (C.3) for small system sizes show that this is a reasonable assumption in the considered regime with $-1 \lesssim \lambda_1 \lesssim 1$. In order to investigate the scaling behavior of the domain wall width, we initialize the system in an artificial box configuration

$$\lambda_1(x,0) = \begin{cases} \lambda_1^*(\gamma), & \frac{L}{4} < x < \frac{3L}{4} \\ -\lambda_1^*(\gamma), & \text{otherwise} \end{cases}$$

where $F_c(\pm\lambda_1^*(\gamma)) = 0$. In Fig. (C.1) the steady states for different values of ε are shown. The linear-log plot validates the expected scaling relation. As a prefactor, we obtain ~ 0.06 for the chosen parameters.

Next, we phenomenologically address the question of how fluctuations affect the dynamics of the system and whether transition can be triggered by noise. Heuristically, we expect two different kinds of noise: conservation preserving and conservation violating noise. While the first one originates from the coupling to a thermal bath, the second one is due to the Markovian bath coupling. We denote the stochastic contribution due to conservation preserving and violating fluctuations by ξ_J and ξ_L and

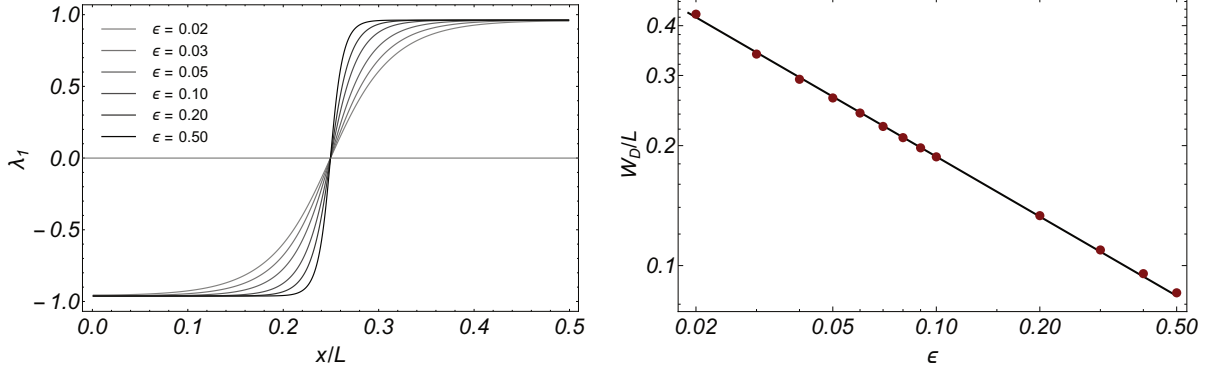


Figure C.1 Domain walls for different values of ϵ (left panel) and typical size of a domain wall as function of ϵ in a linear-log plot where the solid line displays $\epsilon^{-1/2}$ (right panel).

treat them effectively as Gaussian white noise

$$\begin{aligned}\langle \xi_\alpha(t, x) \rangle_\xi &= 0, \\ \langle \xi_\alpha(t, x) \xi_\beta(t', x') \rangle_\xi &= \sigma_\alpha^2 \delta(t - t') \delta(x - x') \delta_{\alpha, \beta}.\end{aligned}$$

In order to simplify the analysis further, we neglect the noisy component of the current ξ_J , which is conservation preserving, compared to the random force ξ_L . If we initialize the system homogeneously in one of the stable states, ξ_J does not contribute to the activation process at t_0 . Even though there is a quantitative influence of ξ_J at later times $t > t_0$. We finally arrive at a stochastic reaction-diffusion equation with additive noise

$$\partial_t \lambda_1(r, t) - D \partial_r^2 \lambda_1(r, t) = F(\lambda_1) + \xi_L. \quad (\text{C.5})$$

Starting from a homogeneous configuration where the system is prepared in one of the stable states, we gradually increase the noise strength. In Fig. C.2 the configuration of the system is shown in a x - t density plot. We observe the formation of domains when the noise strength σ is increased. Different regions are separated by domain walls which is depicted in Fig. C.3. On a short time scale, after approximate saturation, we observe a sharp transition of the order parameter, which is the total magnetization in z direction, as a function of σ , cf. Fig. C.4. Note that there is no phase transition in the limit $t \rightarrow \infty$.

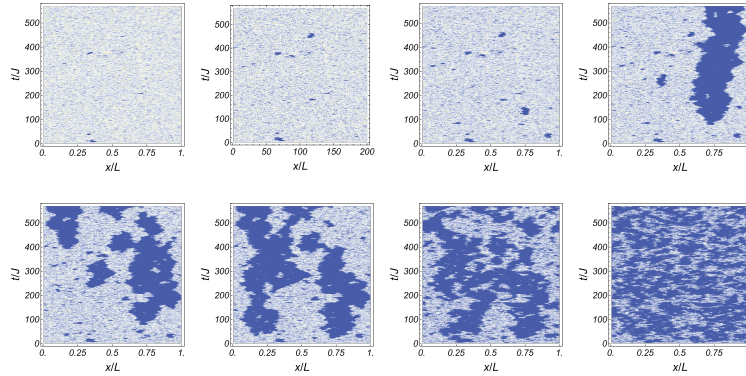


Figure C.2 The Lagrange parameter λ_1 is shown in the t - x plane for different noise strengths. Parameters: $\tilde{L}_{11} = 1, \varepsilon = 0.13, N = 200$.

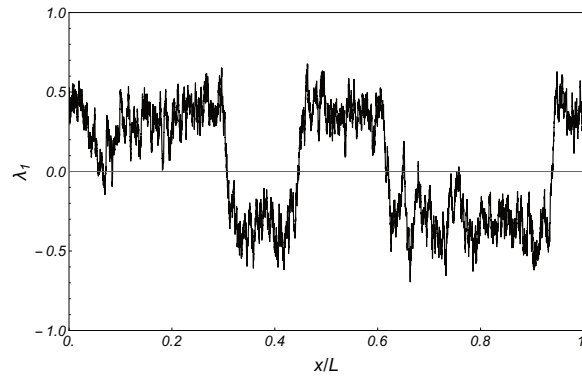


Figure C.3 Configuration of the chain at a fixed time for $\sigma/\varepsilon \approx 0.1$. We observe that domain walls form in the presence of noise. Parameters: $\tilde{L}_{11} = 1, \varepsilon = 0.13, N = 200$.

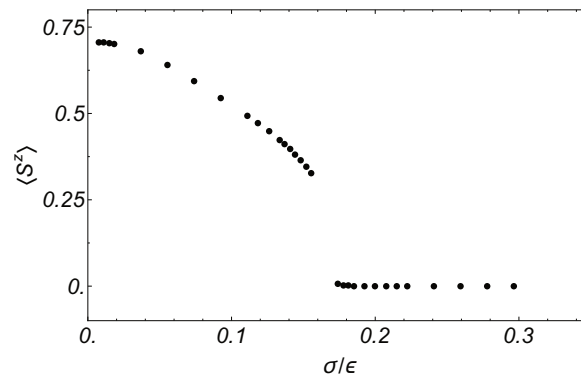


Figure C.4 Time-averaged total magnetization S^z as a function of the noise strength where we average over 10 noise realizations. We simulate the dynamics to times of order $t \sim \mathcal{O}(10^3)$ until we observe approximate saturation. On this time-scale we find a sharp transition between a partially ordered and a disordered state. Parameters $\tilde{L}_{11} = 1, \varepsilon = 0.13, N = 20000$.

Appendix D

Equations of motion of the two continuum fields m and ϕ

Starting from $\mathcal{L} = S \sum_j \mathbf{m}_j \cdot (\dot{\phi}_j \times \phi_j) - \mathcal{H}[\{\phi_j, \mathbf{m}_j\}]$ we calculate the equations of motion of the two continuum fields \mathbf{m} and ϕ . The variation of \mathcal{L} with respect to \mathbf{m} and ϕ reads

$$(1) \quad \frac{\delta \mathcal{L}}{\delta \mathbf{m}_j} = S (\dot{\phi}_j \times \phi_j) - \frac{\delta \mathcal{H}}{\delta \mathbf{m}_j} \stackrel{!}{=} \mathbf{0},$$

$$(2) \quad \frac{\delta \mathcal{L}}{\delta \phi_j} = S (\mathbf{m}_j \times \dot{\phi}_j) - S \frac{d}{dt} (\phi_j \times \mathbf{m}_j) - \frac{\delta \mathcal{H}}{\delta \phi_j} \stackrel{!}{=} \mathbf{0}.$$

We define $\boldsymbol{\omega}_{m,j} := -\frac{1}{S} \frac{\delta \mathcal{H}}{\delta \mathbf{m}_j}$ and $\boldsymbol{\omega}_{\phi,j} := -\frac{1}{S} \frac{\delta \mathcal{H}}{\delta \phi_j}$. Applying $\phi_j \times$ to both equation from the left, dividing by S and using the identity $\mathbf{A} \times (\mathbf{B} \times \mathbf{C}) = \mathbf{B}(\mathbf{A} \cdot \mathbf{C}) - \mathbf{C}(\mathbf{A} \cdot \mathbf{B})$ and the constraints Eq. (6.30), we obtain

$$\begin{aligned} \phi_j \times \frac{\delta \mathcal{L}}{\delta \mathbf{m}_j} &= \phi_j \times (\dot{\phi}_j \times \phi_j) + \phi_j \times \boldsymbol{\omega}_{m,j} \\ &= \dot{\phi}_j \underbrace{(\phi_j \cdot \phi_j)}_{=1} - \phi_j \underbrace{(\phi_j \cdot \dot{\phi}_j)}_{=0} - \boldsymbol{\omega}_{m,j} \times \phi_j \stackrel{!}{=} \mathbf{0} \end{aligned}$$

and for the second equation

$$\begin{aligned} \phi_j \times \frac{\delta \mathcal{L}}{\delta \phi_j} &= \phi_j \times (2 (\mathbf{m}_j \times \dot{\phi}_j) + (\dot{\mathbf{m}}_j \times \phi_j) + \boldsymbol{\omega}_{\phi,j}) \\ &= 2 \left(\underbrace{\mathbf{m}_j (\phi_j \cdot \dot{\phi}_j)}_{=0} - \underbrace{\dot{\phi}_j (\phi_j \cdot \mathbf{m}_j)}_{=0} \right) - \boldsymbol{\omega}_{\phi,j} \times \phi_j + \underbrace{\dot{\mathbf{m}}_j (\phi_j \cdot \phi_j)}_{=1} - \underbrace{\phi_j (\dot{\mathbf{m}}_j \cdot \phi_j)}_{=-\mathbf{m}_j \cdot \dot{\phi}_j} \stackrel{!}{=} \mathbf{0}. \end{aligned}$$

In the second line we can insert $\dot{\phi}_j = \boldsymbol{\omega}_{m,j} \times \phi_j$ into $\phi_j (\mathbf{m}_j \cdot \dot{\phi}_j)$ which yields the projection of $\mathbf{m}_j \times \boldsymbol{\omega}_{m,j}$ onto ϕ_j . In case of $\phi_j \parallel (\mathbf{m}_j \times \boldsymbol{\omega}_{m,j})$, one can replace the projection by the field itself and

we finally arrive at

$$\dot{\phi}_j = \boldsymbol{\omega}_{m,j} \times \phi_j \quad (\text{D.1})$$

$$\dot{\mathbf{m}}_j = \boldsymbol{\omega}_{\phi,j} \times \phi_j + \boldsymbol{\omega}_{m,j} \times \mathbf{m}_j. \quad (\text{D.2})$$

For the the Hamiltonian density of the Heisenberg model, we obtain to leading order that $\boldsymbol{\omega}_m \times \mathbf{m}_j = 0$. To obtain the contribution of the Heisenberg Hamiltonian to \mathcal{H} , we express H_0 in terms of ϕ_j and \mathbf{m}_j where we use the identity $2\phi_j\phi_{j+1} = \phi_j^2 + \phi_{j+1}^2 - (\phi_{j+1} - \phi_j)^2$,

$$\begin{aligned} \mathcal{H} &= JS^2 \sum_j \mathbf{S}_j \cdot \mathbf{S}_{j+1} \\ &\approx \frac{JS^2}{2} \sum_j \left[(-1)^j \phi_j + \mathbf{m}_j - \frac{m_j^2}{2} (-1)^j \phi_j \right] \left[(-1)^{j+1} \phi_{j+1} + \mathbf{m}_{j+1} - \frac{m_{j+1}^2}{2} (-1)^{j+1} \phi_{j+1} \right] \\ &\quad + \left[(-1)^{j-1} \phi_{j-1} + \mathbf{m}_{j-1} - \frac{m_{j-1}^2}{2} (-1)^{j-1} \phi_{j-1} \right] \left[(-1)^j \phi_j + \mathbf{m}_j - \frac{m_j^2}{2} (-1)^j \phi_j \right] \\ &= \frac{JS^2}{2} \sum_j \left[\mathbf{m}_j (\mathbf{m}_{j+1} + \mathbf{m}_{j-1}) - \phi_j (\phi_{j+1} + \phi_{j-1}) + \frac{1}{2} \phi_j (\phi_{j+1} (m_{j+1}^2 + m_j^2) + \phi_{j-1} (m_{j-1}^2 + m_j^2)) \right] \\ &= \text{const} + \frac{1}{2} \left[JS^2 \sum_j 2m_j^2 - (\mathbf{m}_{j+1} - \mathbf{m}_j)^2 + (\phi_{j+1} - \phi_j)^2 + 2m_j^2 - \frac{1}{2} (m_{j+1}^2 + m_j^2) (\phi_{j+1} - \phi_j)^2 \right]. \end{aligned}$$

With the discrete derivative $\partial_x \phi_j = \phi_{j+1} - \phi_j$, we obtain to leading order in \mathbf{m} and ∂_x Eq. (6.33).

Appendix E

Dedication and Declaration

E.1 Dedication

First, I would like to thank my supervisor Prof. Dr. Achim Rosch for his support and guidance. His genuine enthusiasm for physics is inspiring and highly contagious. I am very grateful for how much I could learn from his unique and intuitive way to approach physical problems.

I would also like to thank Dr. Zala Lenarčič and Dr. Jan Gelhausen, I worked together with on some of the projects covered in this thesis. It was a great pleasure for me to work not solely on my own but in a team.

I also thank Prof. Dr. Sebastian Diehl and Prof. Dr. Paul van Loosdrecht for reviewing this thesis. I am very grateful for the support I received from the Bonn-Cologne Graduate School of Physics and Astronomy, and to Dr. Petra Neubauer-Guenther

Moreover, I would like to thank all my colleagues for a pleasant working atmosphere and joint activities at conferences and beyond. Particularly, I would like to mention the ones I shared an office with: Jonathan Lux, Philipp Weiß, Vivek Lohani, Lukas Heinen, Jan Masell, Henry Legg, Emilio Torres, Zala Lenarčič, Jan Gelhausen, and Ankita Negi. I am also very thankful for many sports events we participated in as a group like the annual Unilauf, the Nikolauslauf or simply our weekly runs and Badminton matches. In this context, I would especially like to mention Christoph Berke, Carsten Bauer, Kai Meinerz, and Tim Eschmann. For reading parts of this manuscript I am indebted to Vatsal Dwivedi, Emilio Torres, Ankita Negi, Nina del Ser, Stefan Pols, Vivek Lohani, Henry Legg, Ciarán Hickey and Christian Lange. Thanks to Mariela Boevska, Ute Graffenberger and Yasemin Tieben for administrative and to Dr. Andreas Sindermann for technical support.

Finally, I would like to thank my family and friends for their patience and immeasurable support.

E.2 Declaration

Ich versichere, dass ich die von mir vorgelegte Dissertation selbständig angefertigt, die benutzten Quellen und Hilfsmittel vollständig angegeben und die Stellen der Arbeit - einschließlich Tabellen, Karten und Abbildungen -, die anderen Werken im Wortlaut oder dem Sinn nach entnommen sind, in jedem Einzelfall als Entlehnung kenntlich gemacht habe; dass diese Dissertation noch keiner anderen Fakultät oder Universität zur Prüfung vorgelegen hat; dass sie -abgesehen von unten angegebenen Teilpublikationen - noch nicht veröffentlicht worden ist sowie, dass ich eine solche Veröffentlichung vor Abschluss des Promotionsverfahrens nicht vornehmen werde. Die Bestimmungen der Promotionsordnung sind mir bekannt. Die von mir vorgelegte Dissertation ist von Prof. Dr. Achim Rosch betreut worden.

Florian Lange

Date

E.3 Teilpublikationen

- *Pumping approximately integrable systems*, F. Lange and Z. Lenarčič and A. Rosch, Nature communication **8**, 15767 (2017)
- *Perturbative approach to weakly driven many-particle systems in the presence of approximate conservation laws*, Z. Lenarčič and F. Lange and A. Rosch, Phys. Rev. B **97**, 024302 (2018)
- *Time-dependent generalized Gibbs ensembles in open quantum systems*, F. Lange and Z. Lenarčič and A. Rosch, Phys. Rev. B **97**, 165138 (2018)
- *Engineering generalized Gibbs ensembles with trapped ions*, F. Reiter and F. Lange and Z. Lenarčič, arXiv:1910.01593 (2019)